DRUG BINDING SITES ON $Na_V1.8$ SODIUM CHANNELS

Liam Edward Browne

Submitted in accordance with the requirements for the degree of Doctor of Philosophy

The University of Leeds

Institute of Membrane and Systems Biology

November 2008

Acknowledgments

First of all, I would like to thank Professor Dennis Wray for his supervision and encouragement during the last three years. I am also grateful to Dr. Jeff Clare for his advice and enthusiasm for the project. I would like to thank the past members of the Wray lab, Drs. Louisa Stevens, Min Ju, Kate Bracey and Moza Al-Owais for teaching me techniques and for the good company. I am also indebted to Drs. Lin-Hua Jiang and Malcolm Hunter for their technical advice and guidance.

I would like to thank the many people at GlaxoSmithKline that made me feel welcome during my time in Stevenage. I am particularly grateful to Drs. Andrew Powell and Shahnaz Yusaf for their technical advice, Tim Dale for advice with pulse protocols, and Dr. Frank Blaney who developed the homology model of the $Na_V1.8$ channel used in this thesis. I would also like to thank the Biotechnology and Biological Sciences Research Council and GlaxoSmithKline for their financial support during the course of this work.

Finally, I would like say a special thank you to Jenna, my family and my friends for the support, encouragement and understanding during three years of long hours and prolonged absences.

Abstract

The voltage-gated sodium channel, $Na_V1.8$, is known to play an important role in pain signalling. In this thesis, the functional properties and drug binding sites of wild type and mutant $Na_V1.8$ sodium channel currents were studied in mammalian sensory neuron-derived ND7/23 cells using whole-cell patch clamp.

While the voltage-dependence of activation was similar for wild type human and rat $Na_V1.8$ channels, the voltage-dependence of steady-state inactivation was more hyperpolarised for $hNa_V1.8$ compared to $rNa_V1.8$. Furthermore, as a consequence of the different time course for inactivation between human and rat channels, inhibition during frequent stimulation was less pronounced for $hNa_V1.8$ than for $rNa_V1.8$. Thus, this would imply that the human channel is more inactivated at normal resting potentials, and can support higher firing frequencies than the rat channel.

The action of tetracaine, ralfinamide, 227c89, V102862, and $Na_V1.8$-selective compound A-803467 on wild type $hNa_V1.8$ and $rNa_V1.8$ channels was studied. All compounds showed preferential block of inactivated channels rather than resting channels. Compound A-803467 showed greater affinity for inactivated $hNa_V1.8$ channels than for inactivated $rNa_V1.8$ channels. Unexpectedly, an increase in current was observed for V102862 and A-803467 during recovery from inactivation, likely due to "disinhibition" of resting block. For A-803467, rather than use-dependent inhibition, this disinhibition increased the current during frequent stimulation, while for V102862 it led to the absence of inhibition during low frequency stimulation. Thus while both V102862 and A-803467 are potent inhibitors of $Na_V1.8$, V102862, rather than A-803467 might be a more useful blocker where physiological firing frequencies are higher.

Alanine mutations at residues I381, N390, L1410, V1414, I1706, F1710 and Y1717 were made in the pore-lining S6 segments of the $hNa_V1.8$ channel, and at the corresponding positions in the $rNa_V1.8$ channel. Many of the mutations caused shifts in voltage-dependence of activation and inactivation, and gave a faster time course of inactivation, indicating that the native residues at these positions are important for both activation and inactivation in $Na_V1.8$ sodium channels.

The affinity of tetracaine for the resting and inactivated channels was reduced by $hNa_V1.8$ mutations I381A, F1710A and Y1717A (only inactivated state affinity was measured for the latter), and by mutation F1710A for A-803467. For mutation L1410A both compounds caused complete resting block at very low concentrations; this block was removed by further stimulation. While tetracaine did not show disinhibition for wild type channels during recovery from inactivation, it was seen particularly for mutants L1410 and F1710A. All mutations increased the extent of disinhibition of A-803467. These results suggest that the $Na_V1.8$-selective compound A-803467 acts within the pore S6 segments with a differing but partially overlapping site to that of the local anaesthetic tetracaine.

Contents

List of Figures

Chapter 1.

Chapter 2.

Chapter 3.

Chapter 4.

Chapter 5.

Chapter 6.

Chapter 7.

List of Tables

Chapter 1.

Chapter 2.

Chapter 4.

Chapter 5.

Chapter 6.

Chapter 7.

Abbreviations

μA	microamps
AS	anti-sense
bp	base pairs
°C	degrees centigrade
Ca_V	voltage-gated calcium channel
CD8	cluster of differentiation 8
cDNA	complementary DNA
cfu	colony-forming unit
CHO	chinese hamster ovary cells
CNS	central nervous system
cRNA	complimentary RNA
DMSO	dimethyl sulphoxide
DNA	deoxyribonucleic acid
dNTP	deoxyribonucleotides
DRG	dorsal root ganglion
EDTA	ethylene diamine tetraacetic acid
EGTA	ethylene glycol tetraacetic acid
E_{rev}	reversal potential
g	gram
μg	micrograms
GΩ	gigohm
G-V	conductance-voltage relationship
GFP	green fluorescent protein
G_{max}	maximum conductance
HEK293	human embryonic kidney 293 cells
HEPES	4-(2-hydroxyethyl)-1-piperazineethanesulfonic acid
$hNa_V1.8$	human $Na_V1.8$
Hz	hertz
I-V	current-voltage relationship
IC_{50}	half-maximal inhibitory concentration
I_{max}	maximum current amplitude
I_{Na}	peak current amplitude
k	slope factor
kb	kilobase
kDa	kilodalton
KcsA	potassium channel from *Streptomyces lividans*
K_D	apparent dissociation constant
kHz	kilohertz
K_i	inactivated state dissociation constant

K_r	resting state dissociation constant
K_V	voltage-gated potassium channel
L	litres
µl	microlitres
LB	luria broth
M	molar
µM	micromolar
MΩ	megohm
mg	milligrams
ml	millilitres
mM	millimolar
mm	millimetres
ms	milliseconds
MthK	potassium channel from *Methanobacterium thermoautrophicum*
mV	millivolts
nA	nanoamps
Na_V	voltage-gated sodium channel
ng	nanograms
nl	nanolitres
nm	nanometres
nM	nanomolar
nS	nano siemens
pA	picoamps
PBS	phosphate buffered saline
PCR	polymerase chain reaction
pF	picofarads
PKA	protein kinase A
PKC	protein kinase C
PNS	peripheral nervous system
pS	pico siemens
RNA	ribonucleic acid
$rNa_V1.8$	rat $Na_V1.8$
rpm	revolutions per minute
S	sense
s	seconds
TTX	tetrodotoxin
V	volts
$V_{1/2}$	voltage for half-maximal
V_h	holding potential

Amino Acid Abbreviations

Amino acid	One-letter abbreviation	Three-letter abbreviation
Alanine	A	Ala
Cysteine	C	Cys
Aspartic acid	D	Asp
Glutamic acid	E	Glu
Phenylalanine	F	Phe
Glycine	G	Gly
Histidine	H	His
Isoleucine	I	Ile
Lysine	K	Lys
Leucine	L	Leu
Methionine	M	Met
Asparagine	N	Asn
Proline	P	Pro
Glutamine	Q	Gln
Arginine	R	Arg
Serine	S	Ser
Threonine	T	Thr
Valine	V	Val
Tryptophan	W	Trp
Tyrosine	Y	Tyr

CHAPTER 1

GENERAL INTRODUCTION

1. Introduction

Action potentials are the rapidly propagating signals that underlie the ability for nerve, muscle and other electrically excitable cell types to process and transmit information. Ion channels are integral proteins that regulate these processes; they mediate the passive flux of ions, such as K^+, Na^+, Ca^{2+} and Cl^-, across the cell membrane down their electrochemical gradients. The classical studies on the giant squid axon in the 1950s by Hodgkin and Huxley established the role of Na^+ ion influx in the initiation of the action potential (Hodgkin and Huxley, 1952). Indeed, voltage-gated Na^+ channels are responsible for the generation and propagation of action potentials in excitable cells (Hille, 2001). Therefore they are important as the site of action for many therapeutically important drugs.

1.1 Voltage-gated Na^+ channel family

In 1984, the first voltage-gated Na^+ channel encoding cDNA was cloned from the electroplax organ of *Electrophorus electricus* (Noda et al., 1984). To date, nine mammalian Na_V α-subunit subtypes have been cloned, functionally expressed and classified as members of a single mammalian gene family according to sequence and their functional and pharmacological properties (Table 1.1). The voltage-gated Na^+ channel family members will be referred to using the widely accepted nomenclature of Goldin et al. (2000), where the prefix Na_V denotes the chemical symbol of the principle permeating ion (Na^+) and the predominant environmental regulator (gated by voltage). The first number indicates the gene subfamily, and the second number indicates the channel subtype (Goldin et al., 2000). For example, $Na_V1.8$ (previously named SNS1, PN3 and NaNG) is a voltage-gated ion channel principally selective for the conduction of Na^+ ions, which is the eighth subtype to be identified in the first subfamily (Na_V1 is currently the only subfamily). In addition to the nine mammalian Na_V1 subtypes identified and functionally expressed, atypical sodium channel-like proteins (Na_x) have been identified but not yet functionally expressed. The Na_x protein shows approximately 50% identity to the Na_V1 channel subfamily (Catterall et al., 2005).

TABLE 1.1

Voltage-gated sodium channel family

Subtype	Gene name	Chromosome location	TTX IC_{50} (nM)	Primary tissue
$Na_V1.1$	SCN1A	2q24	6	CNS
$Na_V1.2$	SCN2A	2q23-24	12	CNS
$Na_V1.3$	SCN3A	2q24	4	CNS
$Na_V1.4$	SCN4A	17q23-25	5	Skeletal muscle
$Na_V1.5$	SCN5A	3p21	2000	Heart
$Na_V1.6$	SCN8A	12q13	1	CNS, PNS
$Na_V1.7$	SCN9A	2q24	4	PNS
$Na_V1.8$	SCN10A	3p22-24	60,000	PNS (DRG)
$Na_V1.9$	SCN11A	3p21-24	40,000	PNS
Na_x	SCN7A	2q21-23	?	Widely expressed

1.1.1 Voltage-gated Na^+ channel family members and their distribution

The nine mammalian Na_V α-subunit subtypes share more than 50% identity between the amino acid sequence of transmembrane and extracellular domains (Catterall et al., 2005). The $Na_V1.1$, $Na_V1.2$, $Na_V1.3$ and $Na_V1.7$ channel amino acid sequences are closely related (Fig. 1.1); they all encode tetrodotoxin (TTX)-sensitive channels, and their genes are all located on human chromosome 2q23-24, consistent with a common evolutionary origin (Goldin, 2002). Furthermore, the $Na_V1.5$, $Na_V1.8$ and $Na_V1.9$ channel subtypes are also closely related in amino acid sequence (Fig. 1.1); they are insensitive to TTX to differing extents, and their genes are all located on human chromosome 3p21-24 (Goldin, 2002). The $Na_V1.4$ and $Na_V1.6$ channel genes are located on human chromosome 17q23-25 and 12q13 respectively, and they are TTX-sensitive (Table 1.1, Goldin, 2002). It seems likely that the single Na_V channel subfamily has arisen from gene duplications and chromosomal rearrangements (Goldin, 2002).

To understand the function of voltage-gated Na^+ channels in more detail, the expression pattern of specific subtypes has been determined. Seven of the cloned subtypes are expressed in the nervous system; $Na_V1.1$, $Na_V1.2$, $Na_V1.3$, and $Na_V1.6$ channels are predominantly expressed in the central nervous system (CNS), whereas $Na_V1.7$, $Na_V1.8$ and $Na_V1.9$ channels are principally found in the peripheral nervous system (PNS) (Catterall, 2005). In contrast, the $Na_V1.4$ channel is expressed in skeletal muscle cells, and the $Na_V1.5$ channel in cardiac muscle cells (Catterall, 2005).

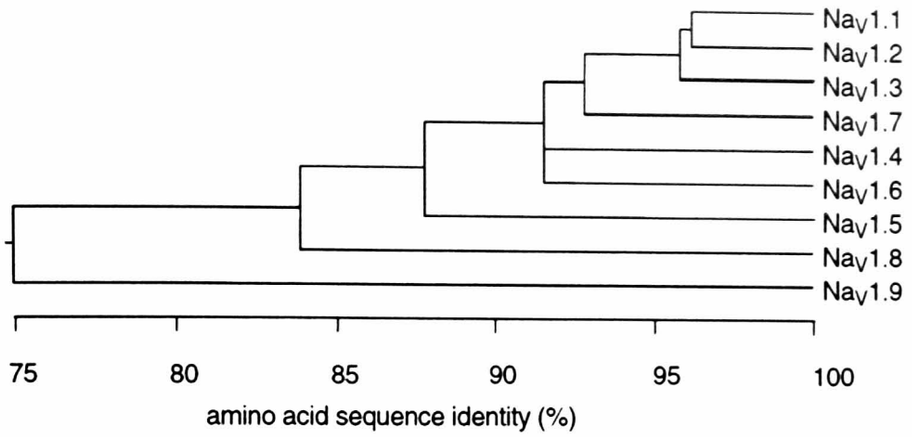

Figure 1.1 Amino acid sequence identity between voltage-gated Na^+ channel subtypes. This figure was adapted from Catterall et al. (2005).

1.1.2 Voltage-gated Na^+ channelopathies

The localised expression and functional diversity of ion channels is reflected by the variety of inherited disorders, known as channelopathies. Voltage-gated Na^+ channelopathies reflect their important role in action potential electrogenesis in a wide range of tissue types. The Na$_v$1.1 and Na$_V$1.2 channels have both been linked to different epilepsy syndromes (Escayg et al., 2000; Fujiwara et al., 2003; Kamiya et al., 2004; Kearney et al., 2001). These channelopathies are typical for channels predominantly expressed in the CNS, and illustrate the importance of Na$_V$1.1 and Na$_V$1.2 channels for normal brain function. In contrast to CNS channels, skeletal muscle Na$_v$1.4 channel channelopathies include paralytic disorders and myotonic disorders (hyperkalaemic periodic paralysis and paramyotonia congenitia; McClatchey et al., 1992; Ptacek et al., 1992; Ptacek et al., 1991; Rojas et al., 1991), and the cardiac channel Na$_v$1.5 channelopathies include arrhythmia disorders (long QT type 3 and Brugada syndrome; Bennett et al., 1995a; Chen et al., 1998; Wang et al., 1995). Remarkably, channelopathy of Na$_V$1.7, a channel expressed in sensory and sympathetic neurons, has been shown to cause congenital insensitivity to pain, indicating an important role for PNS-expressed Na$_V$ channels in pain signalling (Ahmad et al., 2007; Cox et al., 2006; Goldberg et al., 2007).

1.2 Voltage-gated Na^+ channel structure and function

Voltage-gated Na^+ channels are integral membrane heteromultimeric protein complexes. The principle structural component is a large highly glycosylated α-subunit (230-270kDa), which is alone sufficient to form a functional ion-conducting channel, but is usually associated with one

or more β-subunits (32-36kDa) (Catterall, 2000). The α-subunit (Fig. 1.2) contains four homologous domains (I-IV), each containing six membrane-spanning segments (S1-S6), presumably α-helical in structure (Catterall, 2000), assembled clockwise around the pore lumen (Dudley et al., 2000).

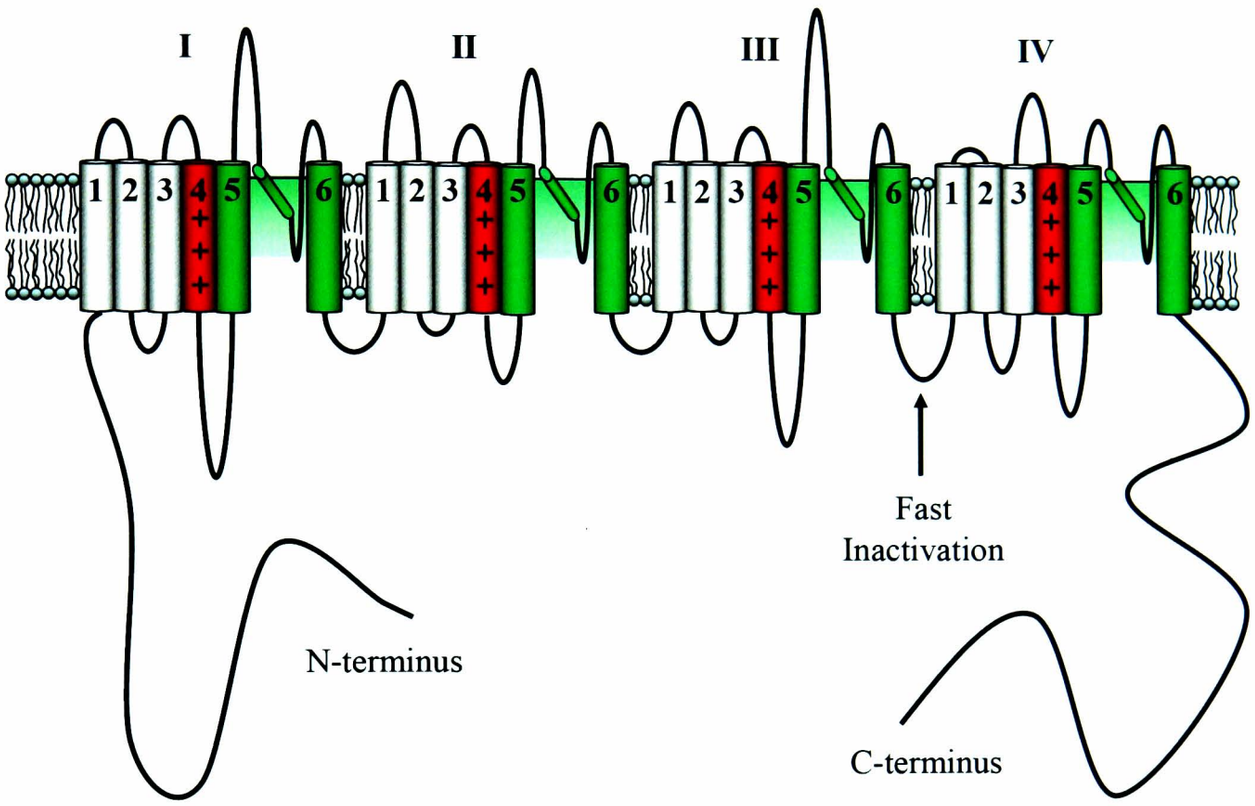

Figure 1.2 Schematic diagram of a voltage-gated Na^+ channel. The six segments of the four homologous domains, N- and C-terminals, and fast inactivation loop are labelled.

The three-dimension structure of the voltage-gated Na^+ channel from *Electrophorus electricus* was determined to a resolution of 19Å using cryppo-electron microscopy with single-particle analysis (Fig. 1.3A) (Sato et al., 2001). The latter authors showed that the voltage-gated Na^+ channel was 135Å in height and 100Å across with a diameter of 65Å. The channel was shown to be bell-shaped with one central and four peripheral cavities in the intracellular side of the channel, and four cavities on the extracellular side, which are connected by a large internal cavity (Fig. 1.3) (Sato et al., 2001).

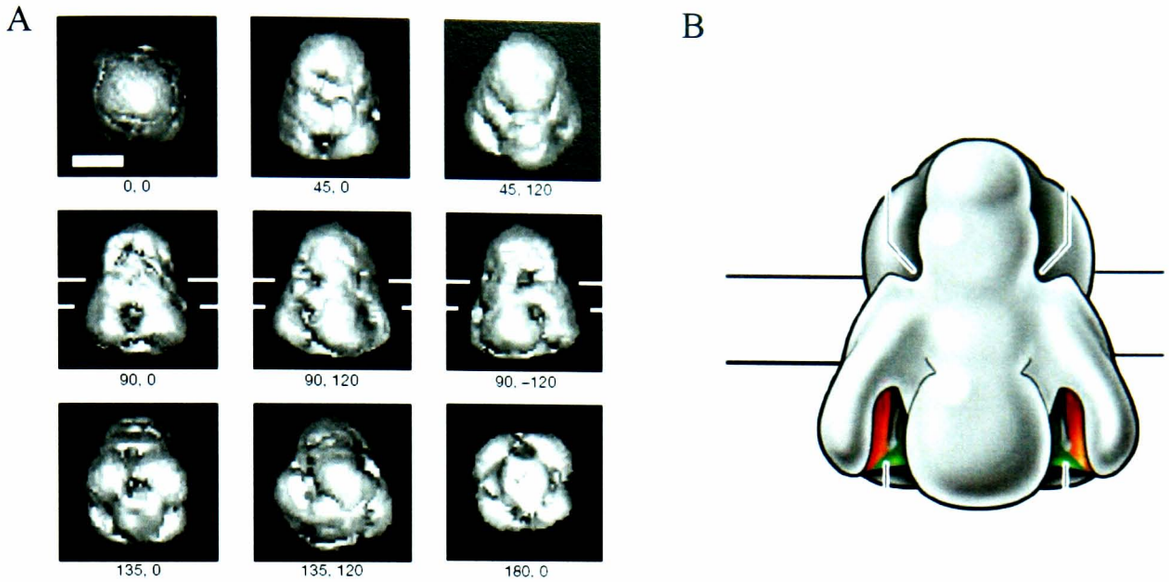

Figure 1.3. Three-dimensional structure of the voltage-gated sodium channel at 19Å resolution. A) Surface view of the Na_V channel structure from different angles. This figure was adapted from Sato et al., 2001. **B)** Side view of the Na_V channel. This figure was adapted from Yu and Catterall, 2003.

1.2.1 Voltage-gated Na^+ channel activation

Classical biophysical studies by Hodgkin and Huxley led to the identification of at least three functional states: closed, open and inactivated. These ion-conducting and non-conducting states are dependent upon voltage, where channels change conformation in response to the membrane potential (Fig. 1.4). The S4 segments contain a positively charged arginine or lysine residue every third or fourth position. In response to membrane depolarisation, the movement of the S4 segment charge dipoles ("voltage sensor") relative to the transmembrane electric field induces conformational changes in the pore through non-conducting resting states to a conducting open state ("gating") (Yang et al., 1996). The outward movement in the positive charges associated with channel activation is observed as a small outward "gating current". While the movements of the IS4, IIS4 and IIIS4 segments are essential for activation, the contribution of the IVS4 is not yet fully understood (Campos et al., 2004; Chanda and Bezanilla, 2002; Horn et al., 2000). The conformational changes induced by the S4 segment voltage-sensors during activation is likely to involve movements of the S6 segments through postulated glycine/serine hinges, as suggested by K^+ channel structures (Jiang et al., 2002; Perozo et al., 1999), and supported by Na_V mutagenesis studies (Wang et al., 2005; Yarov-Yarovoy et al., 2002; Zhao et al., 2004). Following the activation of Na_V channels, a maximum conductance of 19–22pS is typical (Catterall et al., 2005).

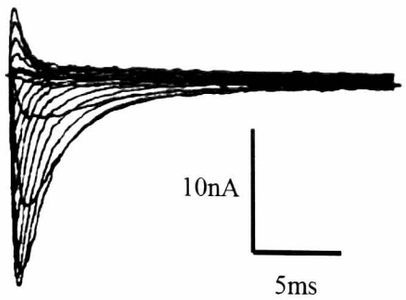

Figure 1.4. Voltage-gated Na^+ channel current. This current was recorded at a node of Ranvier in the presence of 6mM tetraethylammonium ion (TEA) to block potassium current. The initial increase in inward current occurs following the activation of the channel. The decay phase occurs following inactivation of the Na_V channel. This figure was adapted from Hille 1967.

1.2.2 Voltage-gated Na^+ channel selectivity filter

The linkers connecting segments S5 and S6 (P-loops) re-enter the membrane and line the narrow outer part of the pore to form the selectivity filter (Tikhonov and Zhorov, 2005). The selectivity filter is comprised of one amino acid residue from each of the four P-loops, forming rings of EEDD (glutamic acid, glutamic acid, aspartic acid, aspartic acid) and inner DEKA (aspartic acid, glutamic acid, lysine and alanine). These selectively allow Na^+ ions to pass through the ion-conduction pathway (Catterall, 2000; Favre et al., 1996; Vora et al., 2005). In fact, mutation of KA (of DEKA) to EE changes the selectivity from Na^+ ions to Ca^{2+} ions (Heinemann et al., 1992). The ability for Na_V channels to be permeable for Na^+ ions but generally not for others (such as K^+ ions) is largely a consequence of the size of the ion when it is hydrated or dehydrated. The KcsA K^+ channel permits the passage of mostly dehydrated K^+ ions by interactions with the carbonyl oxygens of the P-loops, which compensate energetically for the dehydration of K^+ ions, but not Na^+ ions (Doyle et al., 1998). For Na_V channels, the smaller Na^+ ion remains mostly hydrated (Hille, 1971) and is thought to interact with the flexible side chains of negatively and positively charged P-loop residues, compared to the more constrained main chain carbonyls of K^+ channels (Lipkind and Fozzard, 2008).

1.2.3 Voltage-gated Na^+ channel inactivation

Voltage-gated Na^+ channels open when the membrane is depolarised (activation), and close when the membrane is repolarised (deactivation). Prolonged depolarisation induces inactivation of channels, which prevents re-opening by activation for a period of time. In the inactivated state the non-conducting channel will remain refractory until the channel has recovered back to

the resting state. Recovery from inactivation may take the order of milliseconds to minutes depending on the inactivation state of the channel. Fast inactivation states are induced following short depolarisations and take milliseconds to recover. In contrast, voltage-gated Na^+ channels also enter multiple slow inactivated states following prolonged depolarisation, which may take seconds to minutes to recover from (Ulbricht, 2005). Fast and slow forms of inactivation are structurally and functionally different. Fast inactivation is abolished following the proteolytic treatment of the intracellular surface of Na_V channels (Armstrong, 1981; Armstrong et al., 1973). Indeed, fast inactivation is disturbed by site-directed antibodies and site-directed mutagenesis of the cytoplasmic linker connecting domains III and IV, indicating the role of this linker (Stuhmer et al., 1989; Vassilev et al., 1988). Mutation of the hydrophobic IFM (isoleucine, phenylalanine and methionine) motif in the DIII-IV linker removes fast inactivation (West et al., 1992), and peptides containing the IFM sequence are sufficient to restore fast inactivation (Eaholtz et al., 1994). The IFM residues in the DIII-IV linker are thought to form hydrophobic interactions with residues within or around the intracellular region of the pore (Eaholtz et al., 1994; West et al., 1992). This fast inactivation gate moves to occlude the ion-conducting pathway and immobilises gating charge (Cahalan and Almers, 1979; Hille, 2001). Fast inactivation contributes to action potential termination, spike frequency, and regulation of resting excitability (Nau and Wang, 2004).

The structural determinants of slow inactivation apparently involve residues within the P-loop, S4 segments, S6 segments, and residues adjacent to the IFM motif (Nau and Wang, 2004; Ulbricht, 2005), although it is not yet fully understood. Furthermore activation, fast inactivation and slow inactivation states are proposed to be coupled at the pore-lining S6 segments (Bai et al., 2003; Ulbricht, 2005; Wang et al., 2000; Yarov-Yarovoy et al., 2001). Slow inactivation is thought to be involved in the regulation of membrane excitability, spike frequency adaptation and firing properties (Nau and Wang, 2004).

Overall, the voltage-dependent properties of Na_V channels enable them to sequence through conducting and non-conducting states, thus sending rapid trains of action potentials, necessary for normal physiological functions (Clare et al., 2000).

1.2.4 Functional role of the β-subunits

The auxiliary β-subunits, despite not being necessary for ion conduction, play an important role in channel modulation and cellular localisation. Co-expression of β-subunits with the α-subunit has been shown to modify the voltage-dependence of activation, voltage-dependence of inactivation and the inactivation kinetics (Isom et al., 1995b; Patton et al., 1994). In addition, the β-subunits interact with adaptor proteins (such as contactin and ankyrin-G), for the localisation of the Na_V channel, for instance, at the nodes of Ranvier (Isom, 2001). To date, four

β-subunit gene family members have been cloned and functionally expressed; β_1-β_4 (with splice variants β_1 and β_{1A}) (Isom et al., 1992; Isom et al., 1995a; Kazen-Gillespie et al., 2000; Morgan et al., 2000; Wollner et al., 1987; Yu et al., 2003). The β-subunits are composed of a single membrane-spanning domain and an extracellular domain. The extracellular domain contains an immunoglobulin domain, which is likely to play a role in cell adhesion (Isom and Catterall, 1996; Isom, 2002). The β_1-, β_{1A}- and β_3-subunits associate with the α-subunit by non-covalent interactions, whereas the β_2-and β_4-subunits associate covalently (Isom, 2002; Yu et al., 2003).

1.2.5 Regulation of voltage-gated Na^+ channels

Regulation of neuronal action potential firing and conduction can be achieved by the modulation of voltage-gated Na^+ channels. In addition to modulation by β-subunits, Na_V channel α-subunits are also modulated by phosphorylation, G proteins, receptors, cytoskeletal elements and adaptor proteins. The Na_V channel α-subunit linkers connecting domains I and II, and linkers connecting domains II and III have been shown to be sites of phosphorylation (Chahine et al., 2005). Phosphorylation may occur following the activation of serine/threonine protein kinases PKA and PKC, and tyrosine kinase Fyn (Beacham et al., 2007; Cantrell et al., 2002; Murphy and Catterall, 1992; West et al., 1991). The linker connecting domains II and III is also important for the trafficking of most Na_V channel subtypes (Chahine et al., 2005). The linker contains a consensus sequence required for the binding of adaptor protein ankyrin-G to the Na_V channel α-subunit binding of actin-based cytoskeletons and other membrane proteins (Chahine et al., 2005; Cusdin et al., 2008). The C-terminus appears to be the principal site of interaction with cytoplamic modulatory proteins. It is comprises a highly conserved acidic (glutamic acid-rich) proximal half, and distal half with little conservation. The C-terminus contains motifs for the binding of G proteins, calmodulin and ubiquitin-ligase, and interacts directly with several cytoskeletal and adaptor proteins (Chahine et al., 2005). A carboxy-terminal α-helical segement of the C-terminus also appears to interact with the N-terminus in $Na_V1.4$ (Zhang et al., 2000).

1.3 Voltage-gated Na^+ channel pharmacology

Although voltage-clamp techniques were widely used in the studies of the giant squid axon during the 1940s and 1950s, it was not until 1959 that they were used to study ion channel pharmacology; cocaine and procaine were shown to block Na^+ and K^+ currents in the squid giant axon at clinically relevant concentrations (Shanes et al., 1959; Taylor, 1959). Considering

voltage-gated Na^+ channels are expressed throughout the nervous system, and cardiac and skeletal muscle tissues, it is not surprising that these drugs showed unwanted actions when used as local anaesthetics. Voltage-gated Na^+ channels are still highly studied targets for the development of compounds for use in local anaesthesia, cardiac arrhythmias, epilepsy, ischaemic events and other conditions (Clare et al., 2000).

1.3.1 Voltage-gated Na^+ channel neurotoxin receptor sites

Chemicals (neurotoxins and drugs) that act on the Na_V channel have been classified according to the receptor sites to which they bind (Table 1.2) (Catterall, 1992). Receptor site 1 binds the non-peptides tetrodotoxin and saxitoxin, and the peptide μ-conotoxins, which all selectively block Na_V channels by occluding the pore from the extracellular site (Catterall, 2000; Catterall et al., 2005; Fozzard and Hanck, 1996; Terlau and Stuhmer, 1998). Receptor site 2 binds the lipid-soluble toxins veratridine, batrachotoxin, aconitine and grayanotoxin, which all modulate the activation kinetics and inhibit inactivation of Na_V channels from a receptor within the pore (Catterall et al., 2005; Narahashi, 1998). Receptor site 3 binds the α-scorpion toxin (class 1) and sea anemone toxin peptides, which act extracellularly to prevent the outward movement of the IVS4 voltage sensor, slowing the coupling of activation and inactivation (Catterall et al., 2005; Clare et al., 2000; Narahashi, 1998). Receptor site 4 binds β-scorpion toxin peptides (class 2 and 3), which alter the voltage-dependence of activation (class 2), and additionally, the voltage-dependence of inactivation (class 3) by interacting with an extracellular receptor (Catterall et al., 2005; Narahashi, 1998). Receptor site 5 binds polyether brevetoxins and ciguatoxin, which alter activation kinetics and inhibit inactivation by acting on an intracellular receptor (Catterall et al., 2005; Narahashi, 1998). Receptor site 6 binds δ-conotoxins, which decrease the rate of inactivation, and perhaps actually bind to a similar site as the α-scorpion toxin (Catterall et al., 2005). In contrast to the lethal effects of many of these neurotoxins, voltage-gated Na^+ channel function may be subtly modulated by local anaesthetics and other structurally-related agents acting on the local anaesthetic receptor site, which will be discussed in detail in the next section.

TABLE 1.2

Receptor sites on sodium channels

Site	Neurotoxin or Drug	Source	Domains
1	Tetrodotoxin	Fish (Tetraodontiformes family)	IS2–S6, IIS2–S6
	Saxitoxin	Dinoflagellates and cyanobacteria	IIIS2–S6, IVS2–S6
	μ-conotoxins	Marine snails (Conus family)	
2	Veratridine	Plants (Liliaceae family)	IS6, IVS6
	Batrachotoxin	Frogs (Dendrobatidae family)	
	Grayanotoxin	Plants (Ericaceae family)	
3	α-scorpion toxin (class 1)		IS5–IS6, IVS3–S4
	Sea anemone toxins		IVS5–S6
4	β-scorpion toxins (class 2)		IIS1–S2, IIS3–S4
	β-scorpion toxins (class 3)		
5	Brevetoxins	Dinoflagellates	IS6, IVS5
	Ciguatoxin	Dinoflagellates	
6	δ-conotoxins	Marine snails (Conus family)	IVS3–S4
Local anaesthetic receptor	Local anaesthetic drugs		IS6, IIIS6 IVS6
	Anticonvulsant drugs		
	Antiarrythmic drugs		

1.3.2 Local anaesthetic, antiarrhythmic and anticonvulsant drugs acting on voltage-gated Na^+ channels

Local anaesthetic, antiarrhythmic and anticonvulsant drugs reversibly reduce the peak Na^+ current in a concentration-dependent manner during a single depolarisation known as "tonic block". Tonic block is voltage-dependent since more depolarised holding potentials increase the extent of block. Tonic block is a reduction of the open-probability at equilibrium of channel states. Block is also augmented by frequent depolarisation known as "use-dependent" or "phasic" block. These properties enable preferential inhibition of Na_V channels during periods of sustained depolarisation, repetitive firing or both, without inhibiting normal physiological function.

Common structural features of clinically useful local anaesthetics include a hydrophobic aromatic group, an intermediate linker containing an ester or amide group, and a hydrophilic tertiary amine group. Local anaesthetic drugs include ester-containing tetracaine, benzocaine and procaine, and amide-containing lidocaine, etidocaine, and the derivatives bupivacaine, mepivacaine, and ropivacaine.

Anticonvulsant drugs are compounds that effectively reduce the occurrence of seizure activity without causing sedation or diminishing normal brain activity (Clare et al., 2000). These include lidocaine, phenytoin and lamotrigine. All classes of clinically effective anticonvulsants are lipid-soluble compounds, a number of which act to selectively block Na_V channels. Many anticonvulsants (such as lidocaine and phenytoin) are also used as antiarrythmics. Class I antiarrhythmic drugs are compounds that reduce the occurrence of cardiac arrhythmia at clinical concentrations by acting on voltage-gated Na^+ channels. Antiarrythmic drugs, such as quinidine, primarily inhibit Na_V channels in the heart.

Improvements in both depressive and manic phases of bipolar disorder were also observed in patients taking anticonvulsants carbamazepine, valproate, lamotrigine or oxycarbazepine (Perez-Ceballos et al., 2006). Moreover, the symptoms of neuroleptic-resistant schizophrenia have been reported to be reduced by anticonvulsants lamotrigine, carbamazepine, and particularly valproate (Rogawski and Loscher, 2004). Voltage-gated Na^+ channels are also thought to be involved in excitotoxic damage following ischaemic events. Indeed, sipatrigine, crobenetine, and compound 202W92 have been shown to inhibit Na_V channels in a use-dependent manner, preventing neuronal degradation (Carter et al., 2000; Clare et al., 2000; Liu et al., 2003; Yarov-Yarovoy et al., 2001; Yarov-Yarovoy et al., 2002). In addition, Na_V channel inhibitors have been reported to treat a variety of other conditions. For example, phenytoin and carbamazepine have been shown to effectively reduce neuromuscular disorders (myotonia, myokymia and dystonia) and pain conditions (neuropathic pain and trigeminal neuralgia) (Rogawski and Loscher, 2004). This range of conditions is likely the consequence of the distribution of different Na_V channel subtypes and differences between the actions of these drugs.

1.3.3 Mechanism of action of drug block

Almost all clinically useful local anaesthetics are tertiary amine compounds and are uncharged (lipid-soluble) at high pH and charged (lipid-insoluble) at low pH. Quaternary local anaesthetics (such as QX-314) are permanently charged, and only inhibit Na_V channel current when applied internally, suggesting the local anaesthetic drug may only access the binding site from the intracellular side of the channel (Fig. 1.5) (Frazier et al., 1970). Following internal application of a quaternary local anaesthetic, drug block and drug dissociation may only occur when the channel is open (Strichartz, 1973). The dissociation of quaternary local anaesthetic drugs from the open channel is increased with a higher concentration of external Na^+ ions. In contrast, tertiary amine local anaesthetics do not require the channel to be open in order to dissociate; they can "leak" from closed channels. The leak of tertiary local anaesthetics from closed channels is slower in the presence of a low external pH, suggesting protons have access to the bound drug from the external side. In contrast, low internal pH has little effect on drug

leak, indicating protons do not have access to the bound drug from the internal side (Hille, 2001). Taken together, the local anaesthetic binding site appears to be located within the pore between the external selectivity filter and the internal inactivation gate (Hille, 2001). Furthermore, while lipid-insoluble quaternary local anaesthetics only enter the Na_V channel pore through the open channel from the intracellular hydrophilic pathway, lipid-soluble tertiary local anaesthetics may additionally access the Na_V channel pore from within the membrane using a hydrophobic pathway (Fig. 1.5) (Hille, 1977).

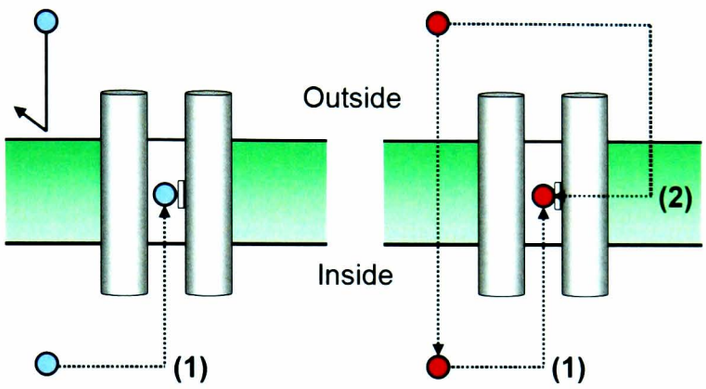

Figure 1.5. Schematic diagram of hydrophobic and hydrophilic pathways. Lipid-insoluble quaternary local anaesthetics (•) may only access the drug binding site from inside the cell using the hydrophilic pathway (1). Lipid-soluble tertiary local anaesthetics (•) may access the drug binding site using the hydrophilic (1) or hydrophobic (2) pathways.

The voltage-dependent action of drugs acting on Na_V channels may be explained by the "modulated receptor" hypothesis (Hille, 1977; Hondeghem and Katzung, 1977). This model proposes that blockers bind to a specific binding site coupled to the channel, where their binding affinity and the onset and offset rate constants are different between at least three channel states (resting, open, inactivated). In this model, blocking properties are the consequence of the state-dependent properties, whereby higher affinity states might be induced at more depolarised potentials (Fig. 1.6). For instance, channels with a low affinity for a drug (resting channels) are present at hyperpolarised potentials, but following sustained depolarisation or repetitive depolarisation, channels with a high affinity for a drug (open or inactivated channels) are induced. A perhaps less established model is the "guarded receptor" hypothesis, which proposes that the voltage-dependent blocking properties are caused by the voltage-dependent alteration in the access pathways to a binding site with a single drug binding affinity (Starmer et al., 1984).

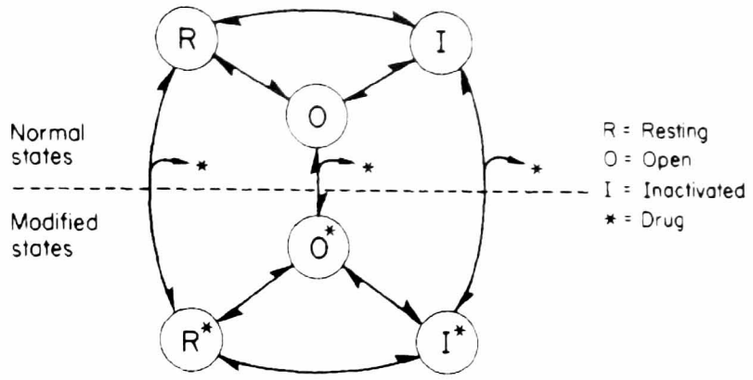

Figure 1.6. Modulated receptor hypothesis model. This scheme from Hille (1977) shows the normal sodium channel states (R, O, I) and drug modified sodium channel states (R*, O*, I*).

Once drugs reach the drug receptor and bind (in a 1:1 stoichiometry), local anaesthetic drugs generally stabilise the inactivated channel state, showing hyperpolarising shifts in the inactivation curve and slowing recovery from inactivation. Local anaesthetics act to inhibit Na^+ current and immobilise gating charge; by "locking" the IIIS4 and IVS4 segments (but not the IS4 or IIS4 segments) in the outward position (Sheets and Hanck, 2003). More recently, findings by Sheets & Hanck support the modulated receptor model; they showed that if they stabilised a depolarised conformational state, by locking the IIIS4 and IVS4 segments in the outward position, lidocaine would bind with high-affinity (Sheets and Hanck, 2007).

As McPhee et al. (1995) pointed out, the actions of drugs on Na_V channels are similar to the action of the fast inactivation gate; they both act intracellularly to inhibit current and immobilise gating charge, and local anaesthetics generally appear to stabilise the inactivated state (McPhee et al., 1995). Indeed, in fast inactivation-deficient Na_V channels (IFM motif mutated to QQQ), the high-affinity block of lidocaine was reduced (Bennett et al., 1995b). However, in contrast, following the removal of fast inactivation, mexiletine, flecainide, disopyramide, QX-314, and lidocaine derivative RAD-243 retained many blocking properties (Grant et al., 2000; Grant et al., 1996; Wang et al., 1987; Wang et al., 2003, 2004). Rather, use-dependent block of some drugs appears to result from an interaction between local anaesthetics and slow inactivation states (Ong et al., 2000). This is supported by the finding that lacosamide enhances the slow inactivation state, without interacting with the fast inactivation state (Errington et al., 2008). Furthermore, lidocaine and carbamazepine have also shown greater potency for slow inactivated states than other states (Cardenas et al., 2006; Leffler et al., 2007).

1.3.4 Molecular determinants of local anaesthetic drugs acting on voltage-gated Na^+ channels

Characterisation of the structural determinants involved in the action of Na_V channel pore-blocking drugs has long been an active area of research. Photoaffinity labelling studies indicated that phenylalkylamine interacts with the IVS6 segment of Ca_V1 (L-type) channels within the pore (Striessnig et al., 1990). Since this interaction was thought to be similar to local anaesthetics binding to Na_V channel, the involvement of pore-lining S6 segment amino acid residues were studied. Figure 1.7, shows the homology between the S6 segments of different human Na_V subtypes. The corresponding residues between subtypes have different numbering, thus, for ease of understanding, the residue position numbering of $Na_V1.8$ will be used. Mutation of IVS6 segment phenylalanine (F1710) or tyrosine (Y1717) residues were shown to significantly reduce the inactivated state affinity of local anaesthetics (etidocaine, tetracaine, benzocaine and cocaine) for $Na_V1.2$-1.5 channels (Li et al., 1999; Nau et al., 2000; Ragsdale et al., 1994; Wright et al., 1998). The same two aromatic residues also showed less pronounced use-dependent block by local anaesthetics when mutated (Li et al., 1999; Ragsdale et al., 1994; Wang et al., 1998a). In addition, mutation of a IVS6 segment isoleucine residue (I1706) did not show use-dependent block (Ragsdale et al., 1994; Wang et al., 1998a). For the latter mutation only, lipid-insoluble quaternary local anaesthetics were shown to access the binding site from the external side. It was proposed that the I1706A mutation reduced use-dependent block of etidocaine by increasing drug dissociation through an external access pathway (Ragsdale et al., 1994; Wang et al., 1998a).

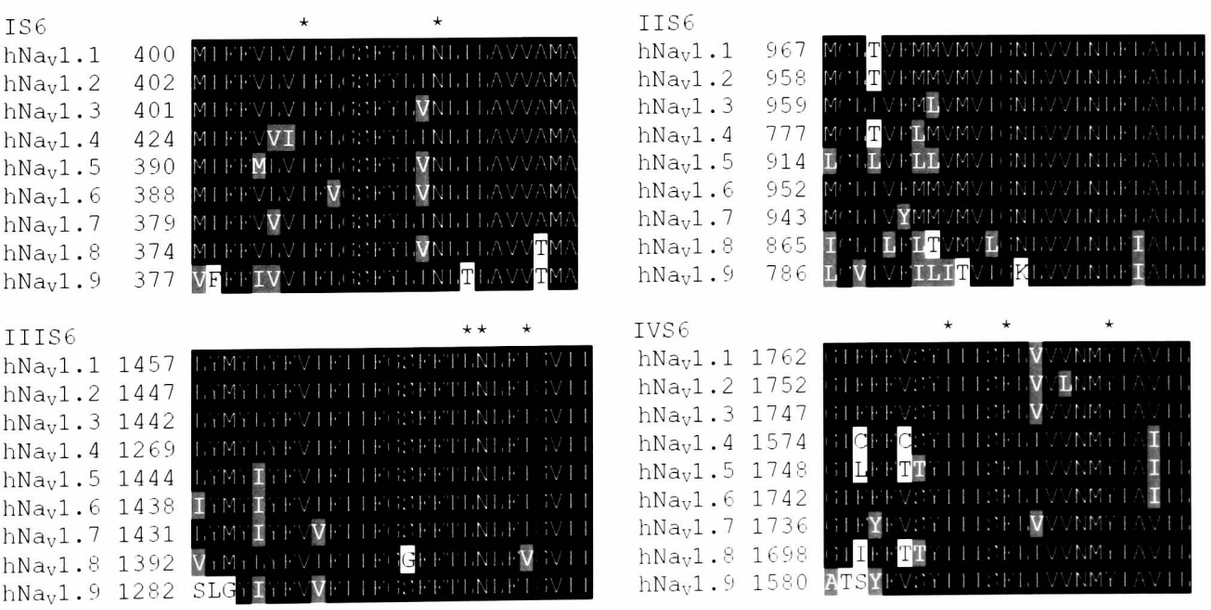

Figure 1.7. Amino acid sequence similarity between human Na_V channel S6 segments from domains I-IV. The residues proposed to be involved in local anaesthetic binding are indicated with *asterisks*. Sequences were aligned using ClustalW and visualised using BoxShade.

In order to determine whether other S6 segments are also involved in drug interactions, mutagenesis studies of the other three domains was carried out. The inactivated state affinity of a number of local anaesthetics was reduced by mutation of IS6 isoleucine residue (I381) in $Na_V1.2$ and $Na_V1.4$ channels, as was the use-dependent block (Wright et al., 1998; Yarov-Yarovoy et al., 2001). The IS6 asparagine residue (N390) also showed a reduction in the inactivated state affinity for local anaesthetics when mutated to lysine in $Na_V1.4$, $Na_V1.5$ and $Na_V1.7$ channels (Nau et al., 1999, 2000; Sheets et al., 2007; Wang et al., 1998b). Furthermore, the latter residue showed less pronounced use-dependent block when mutated to lysine or alanine (Sheets et al., 2007; Wang et al., 1998b; Yarov-Yarovoy et al., 2002). For the IIIS6 segment, mutation of the leucine or isoleucine residues (at positions 1410 and 1414 respectively) reduced the inactivated state affinity of local anaesthetics for Na_V channels, and gave less use-dependent block (Nau et al., 2003; Wang et al., 2000; Yarov-Yarovoy et al., 2001). The IIIS6 asparagine residue (N1411) also reduced the affinity of local anaesthetics for inactivated Na_V channels, but in contrast to other mutations, did not show altered use-dependent block (Nau et al., 2000; Yarov-Yarovoy et al., 2001). The IIS6 segment does not appear to be involved in local anaesthetic binding, which may perhaps be understood since it is orientated directly opposite the IVS6 segment (the principle site of action) (Wang et al., 2001; Yarov-Yarovoy et al., 2002), and so the drugs may be "drawn away" from IIS6.

It is also of note that while asparagine (N390) is proposed to be oriented towards the pore lumen in the $Na_V1.4$ channel (Nau et al., 2003), apparently contradictory orientations have been suggested in the same channel (Kondratiev and Tomaselli, 2003) and the $Na_V1.2$ channel (Yarov-Yarovoy et al., 2002). Interestingly, NMR spectroscopy of a 12 residue peptide analogous to part of the $Na_V1.2$ channel IS6 segment (amino acid residues G384 to V495) suggested it was 3_{10}-helcial in structure and molecular modelling suggested that the asparagine (N390) is a molecular determinant for drug block (Lou et al., 2005).

Additional residues with less established roles in the binding of local anaesthetics include the IS6 isoleucine, serine, phenylalanine and leucine residues (positions 330, 385, 386 and 393, respectively), the IIS6 isoleucine and valine residues (positions 876 and 880, respectively), and the IVS6 asparagine residue (position 1715) (Kondratiev and Tomaselli, 2003; Nau et al., 2000; Wang et al., 1998b; Wang et al., 2007)

1.3.5 Structural determinants of anticonvulsant and antiarrhythmic drugs acting on voltage-gated Na^+ channels

Remarkably, the phenylalanine and tyrosine residues of the IVS6 segment (F1710 and Y1717) are also important for the voltage- and use-dependent properties of a number of other

Na_V channel inhibitors including anticonvulsants (lidocaine, phenytoin and lamotrigine), antiarrhythmics (quinidine, flecainide and mexiletine), anti-ischaemic drugs (sipatrigine and crobenetine), and tricyclic antidepressant drugs (amitriptyline) (Carter et al., 2000; Liu et al., 2003; Ragsdale et al., 1996; Wang et al., 2004; Weiser et al., 1999), perhaps by means of an overlapping but non-identical binding site. Indeed, the phenylalanine residue (F1710) appears to be the primary determinant of drug binding, since no voltage-dependent pore-blocking drug has been unaffected by its mutation to alanine.

Anticonvulsant and antiarrhythmic drugs generally have more complex structures than local anaesthetics, thus, it was hypothesised that they may interact with additional residues. Mutation of IIIS6 segment leucine and isoleucine residues (at positions 1410 and 1414, respectively) reduced the affinity of lamotrigine derivatives sipatrigine (an anti-ischaemic), 227c89 (an analgesic), and 4030w92 (an analgesic and anticonvulsant) (Yarov-Yarovoy et al., 2001). Mutation of the asparagine residue (N1411) did not affect the affinity of inactivated $Na_V1.2$ channels for sipatrigine or 227c89 as it did with 4030w92 (Yarov-Yarovoy et al., 2001). Furthermore, mutations in the IS6 and IIS6 segments did not appear to affect the inactivated state binding affinity or the extent of use-dependent block of lamotrigine derivative, sipatrigine, suggesting it may not directly interact with these segments (Yarov-Yarovoy et al., 2002).

The IS6 asparagine (N390), and IVS6 isoleucine (I1706), phenylalanine (F1710), tyrosine (Y1717) residues have been shown to be important for both fast and slow inactivation properties of the Na_V channel (Bai et al., 2003; Carboni et al., 2005; Wang and Wang, 1997). In fact in the absence of drug almost all mutations at sites involved in drug binding affect the activation properties, inactivation properties or both (Nau and Wang, 2004). While this has led to concerns to whether these residues are really involved in drug interactions, it seems likely that the S6 segments are required for both gating processes and drug binding. Since the effect of the S6 segment residues on drug binding is state-dependent, conformational changes in the S6 segment are expected to expose these residues to the conduction pathway where pore-blocking drugs may bind with greater affinity (Liu et al., 2003). Indeed, the S6 segments of K^+ and Ca^{2+} channels are also essential for the state-dependent action of drugs (Chen et al., 2002; Hockerman et al., 1997).

Functional studies have demonstrated that although the local anaesthetic binding site may predominantly involve S6 segments, it is not exclusive to them. The $Na_V1.4$ channel residue K1237 (of the selectivity filter DEKA motif) is involved in interactions with lidocaine, suggesting the selectivity filter may be adjacent to the drug binding site (Sunami et al., 1997). Mutation of the rat $Na_V1.4$ channel residue W1531 (located in the external pore vestibule) was found to reduce local anaesthetic block (Tsang et al., 2005). Furthermore, the intracellular IVS4/S5 linker has also shown to make interactions with local anaesthetics (Fraceto et al., 2006).

Taken together, the literature suggests that the IVS6 segment phenylalanine (F1710) residue is a principal determinant of drug action, while other IS6, IIIS6 and IVS6 segment residues and other regions of the channel are involved in a differential manner between drugs. In particular, the IS6 isoleucine (I381) and asparagine (N390) residues, the IIIS6 leucine (L1410), asparagine (N1411), and the IVS6 isoleucine (I1706) and tyrosine (Y1717) residues appear to be important for the action of a variety of drugs (Fig. 1.6).

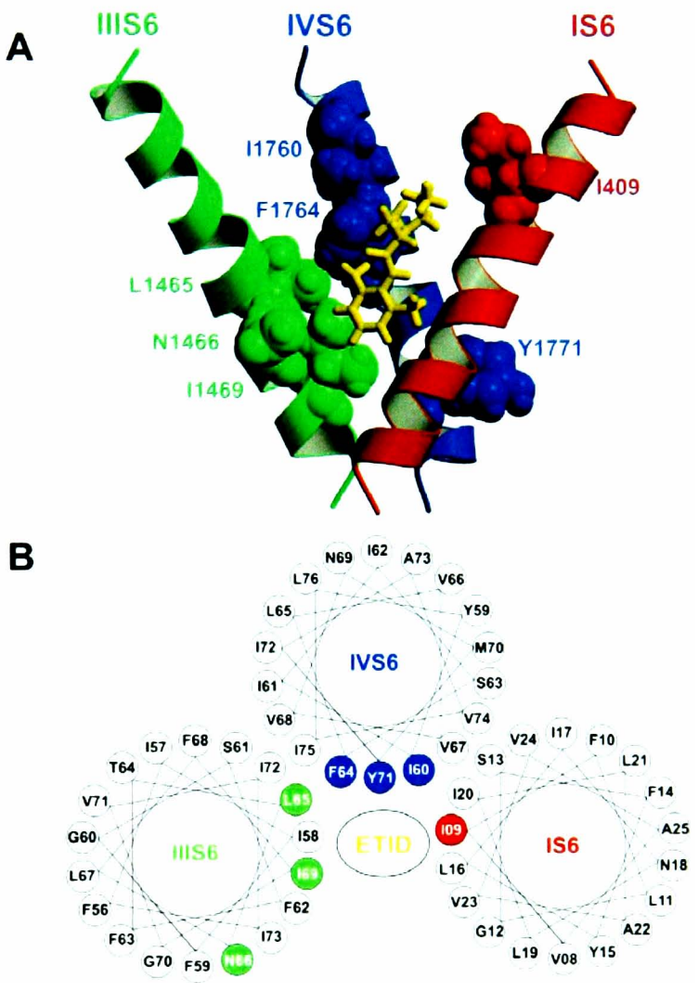

Figure 1.8. Model of the rat $Na_V1.2$ channel with etidocaine binding to the S6 segments. A) The model shows the IS6 (*red*), IIIS6 (*green*) and IVS6 (*blue*) transmembrane segments. The residues involved in the binding of local anaesthetic etidocaine (*yellow*), are shown in *space-fill*. Residues I409, L1465, N1466, I1469, I1760, F1764 and Y1771 correspond to the $Na_V1.8$ channel residues I381, L1410, N1411 I1706, F1710 and Y1717 respectively. **B)** Helical-wheel representation of the IS6, IIIS6 and IVS6 segments, with the residues involved in etidocaine binding indicated. The N390 residue is not indicated on the model, as this model suggests it faces away from the pore lumen. This figure is from Yarov-Yarovoy et al. (2002).

It is noteworthy that some studies have reported apparently contradictory findings. Anticonvulsants phenytoin, carbamazepine and lamotrigine were not effective in inhibiting Na_V channel current internally, suggesting an external drug binding site for these drugs (Kuo, 1998). Furthermore, it was reported that batrachotoxin (binding site 2) and brevetoxin toxins (binding site 5) acting on their intracellular binding sites did not affect the binding of radiolabelled lamotrigine derivative, 202W92. However, extracellular binding of α-scorpion (binding site 3) and β-scorpion (binding site 4) significantly impaired 202W92 binding. These findings suggest the presence of more than one drug receptor on Na^+ channels where 202W92 binds to a novel extracellular binding site on rat brain Na^+ channels (Riddall et al., 2006). Therefore, work in the future is required to understand these more controversial findings.

1.3.6 Mechanism of action of pore-blocking drugs at the S6 segments

In order to understand the detailed mechanisms for drug block at the IVS6 segment, a number of structure-function studies have been carried out. The phenol derivative, 2,6-dimethylphenol (resembling the aromatic tail of a local anaesthetic), was reported to show similar properties to lidocaine (Haeseler et al., 2002). Indeed, the voltage- and use-dependent effects of toluene (methylbenzene) are dependent on the IVS6 segment phenylalanine residue (F1710) in the $Na_V1.4$ channel (Gauthereau et al., 2005). Structure-function studies indicate that both the amine head and aromatic tail groups interact with the Na_V channel (Li et al., 1999). These findings suggest that while the aromatic head group is sufficient for state-dependent block, the hydrophilic tertiary amine is not necessary but it can also interact with the channel.

The hydrophobic and aromatic properties of the phenylalanine residue (F1710) were found to be important for local anaesthetic binding to open/inactivated states, by either cation-π interaction or π-π stacking while the contribution of tyrosine residue (Y1717) to the drug receptor was unclear (Li et al., 1999). Furthermore, mutation of the phenylalanine residue reduced the open/inactivated state affinity by a greater percentage compared to the reduction in the resting state affinity. The greater effect on the inactivated state affinity indicates that the phenylalanine residue (F1710) may contribute to the preference of drugs for the open/inactivated states (Li et al., 1999). More recently, the phenylalanine (F1710) and tyrosine (Y1717) residues were substituted with a number of unnatural derivatives with reduced electrostatic potentials (Ahern et al., 2008). This study suggests that phenylalanine interacts with lidocaine by cation-π interactions, while tyrosine does not appear to interact with lidocaine by either cation-π interactions or π –π stacking.

1.3.7 Molecular modelling of drug binding

Molecular modelling studies of drugs bound to Na_V channels have been used more extensively to support the mutagenesis studies and have important uses for predicting the physicochemical mechanisms of block. By homology with the crystallographic structure of the closed KcsA channel, Lipkind and Fozzard (2005) used the structure of the open MthK channel to develop an open channel model of a Na_V channel P-loops and S5 and S6 segments (characterised by bends at the S6 segment glycine or serine residues). After docking a number of local anaesthetics, they proposed that the amine head group of local anaesthetic drugs interacts with the IVS6 phenylalanine (F1710) and IIIS6 leucine (L1410) residues, while the aromatic tail group interacts with IVS6 tyrosine (Y1717) and asparagine (N390) residues (Lipkind and Fozzard, 2005). Molecular modelling of the human $Na_V1.8$ channel by homology with the structure of the open MthK channel, suggested that tetracaine interacts with selectivity filter residues D356 and E849, IVS6 phenylalanine (F1710) and tyrosine (Y1717) residues, the IIIS6 segment asparagine (N1411) residues, and inactivation gate residues I1433 and F1434 of the IFM motif (Scheib et al., 2006). Importantly, these two studies are both consistent with the findings of the mutagenesis studies. The docked local anaesthetic drug appeared to be too small to completely physically occlude the ion conduction pathway, suggesting ion conduction may be reduced by an electrostatic barrier (Lipkind and Fozzard, 2005). In order to experimentally test this, the phenylalanine residue was substituted for a cationic amino acid (lysine or arginine) or an anionic amino acid (aspartic acid or glutamic acid) (McNulty et al., 2007). The latter authors showed that the unitary conductance was reduced by the cationic amino acid and conversely, increased by the anionic amino acid. Taken together, local anaesthetic drugs appear to reduce Na^+ permeation by partly physically blocking the ion conduction pathway, while the charged amine produces an electrostatic barrier (McNulty et al., 2007).

The molecular models described above have been based on bacterial potassium channel structures. More recently however, Frank Blaney (GlaxoSmithKline, Harlow) developed a model of the human $Na_V1.8$ sodium channel based on its homology with structure of the mammalian $K_V1.2$ potassium channel (Fig. 1.9). Hydropathy plots of the $hNa_V1.8$ and $rK_V1.2$ channel sequences were used to identify the S5-P-loop-S6 region of each domain and alignment of the S6 regions was based on the conserved S6 glycine and serine residues (Fig. 1.9A). The model (Fig. 1.9B) was used for comparison with the findings of this thesis.

A

S5

$K_V1.2$	LQILGQTLKASMRELGLLIFFLFIGVILFSSAVY
$Na_V1.8$ Domain I	PGLKVIVGALIHSVKKLADVTILTIFCLSVFALV
$Na_V1.8$ Domain II	PTLNTLIKIIGNSVGALGNLTIILAIIVFVFALV
$Na_V1.8$ Domain III	EGMRVVVDALVGAIPSIMNVLLVCLIFWLIFSIM
$Na_V1.8$ Domain IV	KGIRTLLFALMMSLPALFNIGLLLFLVMFIYSIF

P-loop

$K_V1.2$	AFWWAVVSMT**T**VGYGD
$Na_V1.8$ Domain I	FLSLFRLMTQ**D**SWERL
$Na_V1.8$ Domain II	FLIVFRILCG**E**WIENM
$Na_V1.8$ Domain III	YLALLQVATF**K**GWMDI
$Na_V1.8$ Domain IV	MLCLFQITTS**A**GWDGL

S6

$K_V1.2$	GKIVGSLCAIA**G**VLTIALPVPVIVSNFNYFYHRET
$Na_V1.8$ Domain I	YMIFFVLVIFL**G**SFYLVNLILAVVTMAYEEQNQAT
$Na_V1.8$ Domain II	CLILFLTVMVL**G**NLVVLNLFIALLLNSFSADNLTA
$Na_V1.8$ Domain III	MYLYFVIFIIF**G**GFFTLNLFVGVIIDNFNQQKKKL
$Na_V1.8$ Domain IV	GIIFFTTYIII**S**FLIVVNMYIAVILENFNVATEES

B

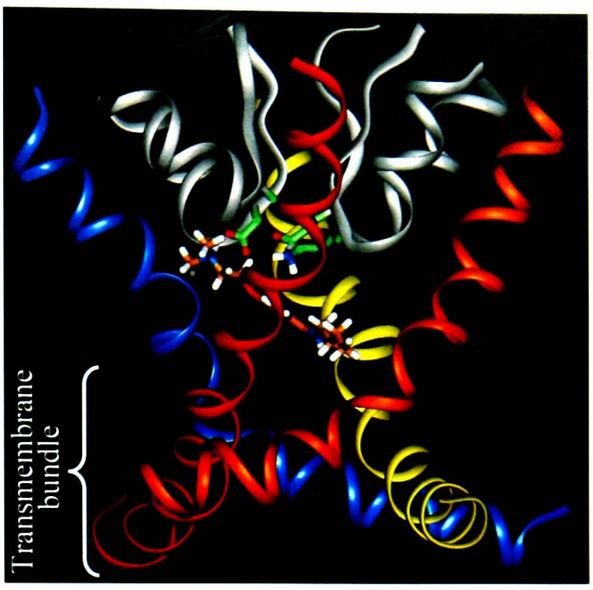

Figure 1.9. A model of the human $Na_V1.8$ channel with tetracaine docked. A) Sequence alignments used in the model. The S5 segments, P-loops and S6 segments are aligned with the rat $K_V1.2$ channel. **B)** A side view of a three-dimensional model of the human $Na_V1.8$ channel, shown with the P-loops for domains I and IV and S6 helices for all four domains. The alpha carbon ribbons are for pore loops (grey), IS6 (blue), IIS6 (yellow), IIIS6 (orange), IVS6 (red). This model was constructed by Frank Blaney (GlaxoSmithKline).

1.3.8 Subtype-specific drug action

Despite sharing nearly identical S6 segments (Fig. 1.7), block by a number of drugs appears to be different between Na_V subtypes. While the $Na_V1.2$, $Na_V1.4$ and $Na_V1.6$ channels are inhibited by the anaesthetic isoflurane, its block is significantly smaller for the $Na_V1.8$ channel (Shiraishi and Harris, 2004). Furthermore, use-dependent inhibition by lidocaine and benzocaine was significantly more effective for $Na_V1.2$ than for TTX-resistant Na^+ currents (Weiser, 2006). Conversely, ambroxol blockade was much more effective in TTX-resistant Na^+ currents (Weiser, 2006). Compared to other TTX-sensitive channels, use-dependent block by lidocaine was more pronounced for $Na_V1.8$ (Leffler et al., 2007; Roy and Narahashi, 1992). In addition, μO-conotoxin MrVIB was demonstrated to block $Na_V1.8$ channels 10-fold more potently than for several other Na_V channels (Ekberg et al., 2006).

Of particular note, tonic block by compound A-803467 was >100-fold more selective for inactivated human $Na_V1.8$ channels that for several other Na_V channel subtypes (Jarvis et al., 2007). Further, inactivated state block of the human $Na_V1.8$ channel by compound A-803467 was greater than for rat TTX-resistant Na^+ currents (Jarvis et al., 2007). The high selectivity of compound A-803467 has led to the speculation that it may not bind to the local anaesthetic binding site (Cummins and Rush, 2007).

1.4 Voltage-gated Na^+ channel – $Na_V1.8$

In 1960, the puffer fish poison tetrodotoxin (TTX) was shown to selectively and potently inhibit Na^+ currents in the squid giant axon, which led to the extensive use of TTX to study ion channels. Experiments demonstrated that Na_V channels of some cardiac muscle tissues were less sensitive to TTX (Narahashi, 1974). Furthermore, in addition to the fast-inactivating Na^+ currents that are TTX-sensitive, the peripheral nervous system also expresses slowly inactivating and persistent Na^+ currents that are TTX-resistant (Fig. 1.10) (Cummins et al., 1999). The channels responsible for the TTX-resistant Na^+ current were identified when the $Na_V1.8$ channel was cloned in 1996, and the $Na_V1.9$ channel was cloned two years later (Akopian et al., 1996; Dib-Hajj et al., 1998; Sangameswaran et al., 1996; Tate et al., 1998). Both of these Na_V subtypes are selectively expressed in damage-sensing (nociceptive) neurons; however, the $Na_V1.8$ channel contributes to the majority (>60%) of the action potential upstroke in small diameter DRG cells in rat (Blair and Bean, 2002; Renganathan et al., 2001).

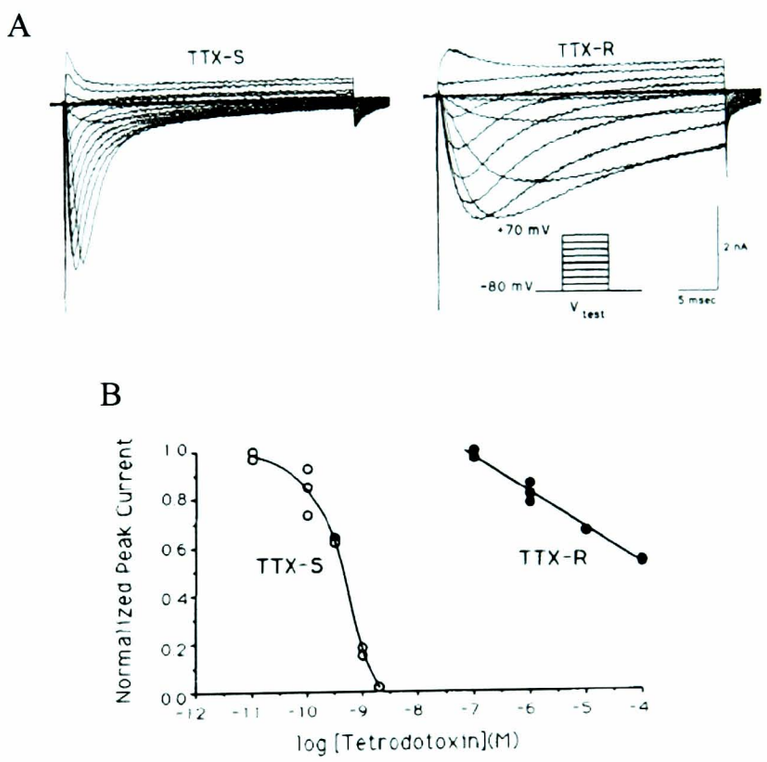

Figure 1.10. TTX-sensitive and TTX-resistant Na^+ channel currents. A) Current traces recorded from rat DRG cells expressing TTX-sensitive (TTX-S) and TTX-resistant (TTX-R) Na^+ channel currents. **B)** This graph shows the effect of TTX on TTX-resistant and TTX-sensitive channel currents. This figure was adapted from Roy and Narahashi (1992).

1.4.1 Functional properties of $Na_V1.8$ sodium channels

In comparison to other Na_V channel subtypes, the $Na_V1.8$ channel has distinct biophysical properties. The $Na_V1.8$ channel shows both slower kinetics and more depolarised voltage-dependent activation and inactivation in rat DRG or when expressed in *Xenopus* oocytes than the other Na_V channel subtypes (Akopian et al., 1996; Elliott and Elliott, 1993; Sangameswaran et al., 1996). The $Na_V1.8$ channel recovers from inactivation with a fast and slow component. Recovery from fast inactivation is rapid, and suitable for high action potential firing frequencies (Cummins and Waxman, 1997; Elliott and Elliott, 1993). The $Na_V1.8$ channel has more pronounced slow inactivation than other Na_V subtypes (Leffler et al., 2007), and its recovery is slower even during short depolarising pulses from normal resting membrane potentials (Blair and Bean, 2003).

1.4.2 Role of the $Na_V1.8$ sodium channel in pain pathways

$Na_V1.8$ channels are predominantly expressed in dorsal root, trigeminal and nodose ganglia (Akopian et al., 1996; Sangameswaran et al., 1996). Following nerve damage, the functional expression of $Na_V1.8$ channels is reduced in injured neurons but increased in uninjured axons, indicating that the activity of uninjured neurons might be important for neuropathic pain (Gold et al., 2003). Intrathecal administration of $Na_V1.8$-specific antisense oligodeoxynucleotides was found to reverse hyperalgesia and allodynia in nerve-injured animal models, without influencing non-noxious sensation or response to acute pain (Joshi et al., 2006; Lai et al., 2002; Porreca et al., 1999). Similarly, mechanical allodynia in rat models of neuropathic pain was attenuated by siRNA-mediated selective knockdown of $Na_V1.8$ channels (Dong et al., 2007). In contrast, $Na_V1.8$ null mice do not have a significant neuropathic pain phenotype though they do show resistance to noxious mechanical stimuli, nerve growth factor-induced thermal hyperalgesia and visceral pain (Akopian et al., 1999; Kerr et al., 2001; Laird et al., 2002; Nassar et al., 2005). More recently, neurons expressing $Na_V1.8$ were shown to be necessary for the sensations of noxious mechanical and cold stimuli, thermal and mechanical allodynia following inflammation, but not neuropathic pain or heat sensing (Abrahamsen et al., 2008). Indeed, due to the cold-resistant properties of the $Na_V1.8$ channel, $Na_V1.8$ is critical for the perception of pain at low temperatures (Zimmermann et al., 2007).

Pharmacological agents that block $Na_V1.8$ channels have also been shown to be anti-hyperalgesic and anti-allodynic in animal models of inflammatory and neuropathic pain. For instance, the anti-nociceptive properties of ralfinamide (NW-1029) are proposed to result from a pronounced inhibition of TTX-resistant Na^+ currents (Stummann et al., 2005). The $Na_V1.8$-

selctive μO-conotoxin MrVIB, and small-molecule compound A-803467, have both been shown to effectively reduce pain in animal models; MrVIB reduced allodynia and hyperalgesia in both neuropathic and chronic inflammatory pain models (Ekberg et al., 2006), and A-803467 reduced thermal hyperalgesia in inflammatory models of pain and mechanical allodynia in neuropathic models of pain (Jarvis et al., 2007). Furthermore, consistent with the findings of Zimmerman et al. (2005) and Abrahamsen et al. (2008), the latter compound reduced acute mechanical pain and cold allodynia, but not acute thermal pain (Jarvis et al., 2007).

1.4.3 Role of the inactivation properties of $Na_V1.8$ channels

The generation and propagation of action potentials in excitable cells is largely influenced by the voltage-dependent gating mechanisms of voltage-gated Na^+ channels. Compared with other Na_V channel subtypes, the relatively depolarised inactivation of $Na_V1.8$ indicates that fewer channels will be inactivated at normal sensory neuron resting membrane potentials (Harty and Waxman, 2007). Therefore, a greater proportion of $Na_V1.8$ channels are available to activate; indeed, the $Na_V1.8$ channel contributes significantly to the action potential upstroke, even at depolarised sensory neuron resting potentials (Harty and Waxman, 2007).

The more pronounced slow inactivation of the $Na_V1.8$ channel has both physiological and pharmacological significance. At normal physiological action potential firing frequencies, a large proportion of $Na_V1.8$ channels enter slow inactivation states (Tripathi et al., 2006). The extent of current inhibition at a known firing frequency depends on the rate of entry into inactivated states and the rate of recovery from inactivated states. While the extent of slow inactivation is greater for $Na_V1.8$ channels, the TTX-sensitive Na^+ channels fully recover between depolarisations at normal frequencies. Recently the use-dependent properties of TTX-resistant Na^+ (likely $Na_V1.8$) channels were shown to cause a decrease in the speed of action potential conduction along axons following activity ("activity-dependent slowing of conduction velocity") (De Col et al., 2008). In addition to the physiological importance, the more pronounced slow inactivation of $Na_V1.8$ has important implications for its pharmacology. As discussed above, drugs such as lidocaine, carbamezipine and lacosamide bind with a greater preference for slow inactivation states over other states (Cardenas et al., 2006; Errington et al., 2008; Leffler et al., 2007). Thus, this dependence on the type of inactivation state provides a basis for subtype-specific selectivity of these drugs between Na_V channels; indeed, lidocaine and carbamezipine have a greater potency for $Na_V1.8$ channels, than for other Na_V channel subtypes (Cardenas et al., 2006; Leffler et al., 2007). The different functional properties of $Na_V1.8$ might also be responsible for the highly selective block of compound A-803467,

although it seems likely that differences in the protein sequence and conformation also contribute.

1.4.4 Heterologous expression of human and rat $Na_V1.8$ channels

The cloning of rat $Na_V1.8$ channel enabled its functional expression in *Xenopus laevis* oocytes (Akopian et al., 1996; Sangameswaran et al., 1996). Both of the latter authors showed rat $Na_V1.8$ channel currents that were small in amplitude, suggesting low levels of expression. The rat $Na_V1.8$ channel has been functionally expressed in a number of mammalian cell lines; chinese hamster ovary (CHO), African green monkey kidney (COS-7), human embryonic kidney (HEK-293) cells (Okuse et al., 2002). More recently, the dorsal root ganglion neuroblastoma ND7/23 cell line was shown successfully to express rat $Na_V1.8$ channels (Choi et al., 2004; John et al., 2004; Leffler et al., 2007).

For the human $Na_V1.8$ channel, the functional properties were also first examined in *Xenopus laevis* oocytes (Rabert et al., 1998). In addition, human $Na_V1.8$ channels have been functionally expressed in mammalian CHO and neuroblastoma SH-SY5Y cells (Akiba et al., 2003; Dekker et al., 2005). It is noteworthy that authors have noted the difficulty in expressing both human and rat $Na_V1.8$ channels in mammalian cell lines (Dekker et al., 2005; Leffler et al., 2007); this has hindered the number of functional studies of $Na_V1.8$ channels.

It is important to consider whether the heterologous expression of $Na_V1.8$ shows functional properties which are similar to those in native neurons. The heterologous expression of rat $Na_V1.8$ channels in ND7/23 cells showed that steady-state inactivation was half-maximal at -54mV (John et al., 2004). The latter authors showed that using the same steady-state inactivation protocol the TTX-resistant Na^+ current of rat DRG neurons were also half-maximal at -54mV. Thus, John et al. (2004) suggest that the rat $Na_V1.8$ channel expressed in the ND7/23 cell line showed functional properties that closely resemble the native TTX-resistant Na^+ currents in DRG neurons. The values for half-maximal inactivation in TTX-resistant DRG neurons are reported to be more depolarised in other studies. For instance, the voltage for half-maximal inactivation for TTX-resistant currents in rat DRG was shown to be -29mV (Elliott and Elliott, 1993) and -43mV (Choi et al., 2006). It seems likely that the different values are a consequence of the range of experimental conditions, such as the pulse protocols and solutions used.

In the recordings from two-electrode voltage-clamped oocytes the value for half-maximal inactivation was more hyperpolarised for the human channel (Rabert et al., 1998) as compared with the value for the rat channel (Akopian et al., 1996). Moreover, Akiba et al. (2003) also noted that human $Na_V1.8$ channels expressed in CHO cells appear to have more hyperpolarised inactivation than the rat $Na_V1.8$ channel observed by Akopian et al. (1996). However, no direct

comparison of the human and rat $Na_V1.8$ channel properties has been carried out in mammalian cells (or indeed between any two Na_V channel orthologues), and comparison of values for inactivation is not easy because of the wide range of experimental conditions used.

1.4.5 Modulation of the $Na_V1.8$ sodium channel

As discussed above, the β-subunits alter both the functional properties and cellular localisation. *In situ* hybridisation and immunochemistry have shown that the small and large fibers of DRG neurons express β_1-, β_2- and β_3-subunits; functional expression of the $Na_V1.8$ α-subunit is increased by β_1, and its voltage-dependence of inactivation is shifted to more hyperpolarised potentials by β_1 and β_3, and to more depolarised potentials by β_2 (Vijayaragavan et al., 2004b). The β_3 subunit also appears to be important in cellular localisation since a significant increase in β_3-subunit:neurofilament ratio was observed after injury of human sensory neurons (Casula et al., 2004).

A variety of proteins have also been shown to interact with the intracellular linkers of the $Na_V1.8$ channel, and in particular, the C-terminus. The proximal (conserved) half of the C-terminus of $Na_V1.8$ has been shown to associate with cytoskeletal and adaptor proteins (such as dynein intermediate chain, α-tubulin, and moesin), enzymes (inositol polyphosphate 5-phosphate and thousand and one protein kinase) and membrane proteins (voltage-dependent anion channel VDAC3V, tetraspanin and connexin 43) (Malik-Hall et al., 2003). The distal (non-conserved) half of the C-terminus of $Na_V1.8$ interacts with calmodulin, which has been been shown to regulate current density and functional properties of several Na_V channel subtypes in a subtype-specific manner (Choi et al., 2006). For the $Na_V1.8$ channel, calmodulin interacts with channels in native neurons and significantly increases current density, slows the second component of recovery from inactivation, and increases use-dependent current inhibition (Choi et al., 2006).

Other intracellular regions also appear to be important sites of $Na_V1.8$ channel regulation. The N-terminus of the $Na_V1.8$ channel binds to the light chain of annexin II (p11), which is a cytoskeletal (F-actin) receptor that associates with the membrane in a Ca^{2+}-dependent manner (Okuse et al., 2002; Poon et al., 2004). The interaction of p11 with $Na_V1.8$ appears to promote its translocation to the cell membrane of small fibers of DRG neurons, while it does not appear to interact with several other Na_V channel subtypes (Okuse et al., 2002; Poon et al., 2004). Further, deletion of pII causes deficits in acute and neuropathic pain (Foulkes et al., 2006). Activation of G proteins by GTPγS has also been reported to increase $Na_V1.8$ channel current amplitude (Saab et al., 2003). More recently it was shown that $Na_V1.8$ current density was increased after phosphorylation of two serine residues in the DI-II linker (S551 and S556) by

p38 mitogen-activated protein kinase, which is activated following nerve injury and inflammation (Hudmon et al., 2008).

1.5 Summary of aims of this thesis

This thesis aims to describe the structural determinants for drugs acting on the $Na_V1.8$ channel. For this work, owing to reported difficulties with the expression of $Na_V1.8$ channels, an appropriate expression system was first required. Therefore the expression of $Na_V1.8$ channels was compared in the *Xenopus laevis* oocyte expression system and the transient transfected mammalian sensory neuron-derived cell line, ND7/23.

Using ND7/23 cells, it was possible to carry out a detailed analysis and comparison of the electrophysiological properties of the wild type human and rat $Na_V1.8$ channels using whole-cell patch clamp. This is the first time a direct, cross-species comparison of the functional properties of a Na_V subtype has been carried out in the same mammalian background.

The pharmacological actions of drugs were then compared in the human and rat $Na_V1.8$ channels, using tetracaine (a local anaesthetic), ralfinamide (an analgesic), 227c89 (a lamotrigine derivate with analgesic properties), V102862 (an anticonvulsant), and A-803467 (a potent and selective inhibitor of $Na_V1.8$). The resting and inactivated state affinities were studied as well as the effects on use-dependent inhibition and recovery from inactivation.

Seven alanine mutations (I381A, N390A, L1410A, V1414A, I1706A, F1710A and Y1717A) were generated in the human and rat $Na_V1.8$ channel corresponding to positions in other Na_V channel subtypes where local anaesthetics have been found to act in the S6 segments of domains I, III and IV. The effect of these mutations of the S6 segment on the activation and inactivation of human and rat $Na_V1.8$ was examined.

Finally, the effects of these same S6 segment mutations on the action of tetracaine and the $Na_V1.8$-selective blocker A-803467, were studied. Here the sites of action of tetracaine and compound A-803467 were determined in the $Na_V1.8$ channel. The resting and inactivated state affinities were investigated, as were and the effects on use-dependent inhibition and recovery from inactivation.

Much of the work in this thesis has already been submitted for publication, as described below.

1.6 Publications

1.6.1 Full Papers

Browne, L. E., Clare, J. J., Wray, D. Functional and pharmacological properties of human and rat $Na_V1.8$ channels. *Neuropharmacology.* (submitted)

Browne, L. E., Blaney, F. E., Yusaf, S. P., Clare, J. J., Wray, D. Structural determinants of drugs acting on the $Na_V1.8$ channel. *J. Biol. Chem.* (submitted)

1.6.2 Abstracts

Browne, L. E., Yusaf, S. P., Clare, J. J., Wray, D. Effects of human and rat $Na_V1.8$ channel S6 segment mutations on channel function. British Pharmacological Society Winter Meeting 2007.

Browne, L. E., Yusaf, S. P., Clare, J. J., Wray, D. Human and rat $Na_V1.8$ channel gating and the effects of S6 segment mutations. Biophysical Society 52nd Meeting 2008.

CHAPTER 2

MATERIALS AND METHODS

2.1 Materials

2.1.1 Chemicals and reagents

Collagenase Type 1A, ethidium bromide, tricaine (3-aminobenzoic acid ethyl ester), kanamycin, penicillin-streptomycin and sigmacote® were all obtained from Sigma (Poole, UK). Ampicillin was obtained from Stratagene (La Jolla, CA). EZ-Glass milk™ was purchased from Qbiogene (Cambridge, UK). Agarose and dynabeads® CD8 were purchased from Invitrogen (San Diego, CA). *Escherichia coli* MAX efficiency® Stbl2™ competent cells were obtained from Invitrogen and XL10-Gold® competent cells from Stratagene (La Jolla, CA). Transfection reagent Lipofectamine™ 2000 was purchased from Invitrogen (San Diego, CA). Tetrodotoxin citrate was obtained from Tocris Bioscience (Bristol, UK).

2.1.2 Voltage-gated sodium channel blocking drugs

Tetracaine (4-(Butylamino)benzoic acid 2-(dimethylamino)ethyl ester), compound A-803467 (5-(4-Chlorophenyl)-N-(3,5-dimethoxyphenyl)-2-furancarbo xamide), compound V102862 (4-(4-Fluorophenoxy)benzaldehyde semicarbazone), ralfinamide ((S)-(-i-)-2-(4-(2-fluorobenzoxy)-benzylamino)-propanamide) and 227c89 (5-(2,6-dichlorophenyl)-6-methylpyrimidine-2,4-diamine) were all synthesised at GlaxoSmithKline.

2.1.3 Enzymes and kits

Restriction enzymes were obtained from Roche (Mannheim, Germany), unless otherwise stated. The restriction enzyme buffers were supplied with the enzymes. For the generation of point mutations, the QuikChange® XL Site-Directed Mutagenesis Kit was purchased from Stratagene (La Jolla, CA). Calf Alkaline Phosphatase and T4 DNA Ligase were obtained from Roche (Mannheim, Germany). The MEGAscript® SP6 Transcription Kit was obtained from Ambion (Huntingdon, UK). The QIAquick® Gel Extration Kit, QIAprep® Miniprep Kit, HiSpeed® Plasmid Maxi Kit and Robot QIAprep® 8 Turbo Kit were all obtained from Qiagen (Crawley, UK).

2.1.4 Oligonucleotides and sequencing

Mutagenesis and sequencing primers were designed using Vector NTI (Invitrogen), and synthesised by Invitrogen. Sequencing primers for the entire $Na_V1.8$-encoding cDNA were designed 400bp apart, for the contiguous defragmentation of sequences (showing a typical overlap of three fragments). Sequencing and mutagenesis primers are shown in Tables 2.1a and 2.1b. Oligonucleotide primers were resuspended in Tris-EDTA, briefly centrifuged and gently vortexed to give 0.1mM of each primer. Sequencing of plasmid DNA was carried out at GlaxoSmithKline Harlow.

TABLE 2.1a

Sequences of oligonucleotide primers for sequencing

Primer Name	Primer Sequence (5' to 3')
hNa V1.8 seq1	TAATACGACTCACTATAGGG
hNa V1.8 seq2	GGTTTAGTGCCACTCGGGC
hNa V1.8 seq3	CCCTGATTCACTCAGTGAAG
hNa V1.8 seq4	CTATATGATCTTTTTTGTGCTCG
hNa V1.8 seq5	GTTCCATTTCCGGTCCCC
hNa V1.8 seq6	GTCTCAGAAGTATCTGATCTGG
hNa V1.8 seq7	CCCACCTTAAACACACTCATC
hNa V1.8 seq8	GATGGGGAGGTGAACAACCTG
hNa V1.8 seq9	GGTGTGGGGACCACCTGAC
hNa V1.8 seq10	CTTTGAAGACTATTACCTGGAC
hNa V1.8 seq11	CTTCGCAGGGAAGTTTTGG
hNa V1.8 seq12	GCAGAAGAAATACTACAATGCC
hNa V1.8 seq13	CTCTTCAGAGTCATCCGCC
hNa V1.8 seq14	CCTACATCATCATCTCCTTCC
hNa V1.8 seq15	CATCCTATGAACCAATAGCAAC
hNa V1.8 seq16	GCCCTATTCTATAGTGTCACC
rNa V1.8 seq1	TGGCGGCCGCATCACGAAGC
rNa V1.8 seq2	CTGTCCATTCCTGGTTCTCC
rNa V1.8 seq3	TGCCTGAGCGTCTTCGCCTT
rNa V1.8 seq4	GGTCACCATGGCGTATGAAG
rNa V1.8 seq5	CAGGAAAGCCGTCGAGGTTC
rNa V1.8 seq6	TGACTGACCCCTTCGCAGAG
rNa V1.8 seq7	CTTTATCCTGGCCATCATCG
rNa V1.8 seq8	TACATCAGCAGCCACTGCCG
rNa V1.8 seq9	GGGTGAGAGCTGGAAGAGGA
rNa V1.8 seq10	CATCTTCGTCTTTGAGATGCTGC
rNa V1.8 seq11	GTCCGAGTGTCACAATCAAAACAG
rNa V1.8 seq12	GAATAAGTACCAAGGCTTCGTGTTTG
rNa V1.8 seq13	GCTCTTTGCCCTCATGATGTCCC
rNa V1.8 seq14	TCAACGTAGCCACCGAGGAGAGCAC
rNa V1.8 seq15	GAGCTACATGCTGCACCGCT
rNa V1.8 seq16	CATTAACCCATCTAGCTCAATGC

TABLE 2.1b

Sequences of oligonucleotide primers for mutagenesis

Primer Name	Primer Sequence (5' to 3')
hNa$_V$1.8 I381A S	GTGCTCGTAGCCTTCCTGGGATC
hNa$_V$1.8 I381A AS	GATCCCAGGAAGGCTACGAGCAC
hNa$_V$1.8 N390A S	CTACCTGGTCGCCTTGATCTTGGC
hNa$_V$1.8 N390A AS	GCCAAGATCAAGGCGACCAGGTAG
hNa$_V$1.8 L1410A S	GGCTTCTTCACAGCGAATCTCTTTG
hNa$_V$1.8 L1410A AS	CAAAGAGATTTCGCTGTGAAGAAGCC
hNa$_V$1.8 V1414A S	GAATCTCTTTGCTGGGGTCATAATTG
hNa$_V$1.8 V1414A AS	CAATTATGACCCCAGCAAAGAGATTC
hNa$_V$1.8 I1706A S	CACCACCTACGCCATCATCTCCTTC
hNa$_V$1.8 I1706A AS	GAAGGAGATGATGGCGTAGGTGGTG
hNa$_V$1.8 F1710A S	CATCATCTCCGCCCTCATCGTGG
hNa$_V$1.8 F1710A AS	CCACGATGAGGGCGGAGATGATG
hNa$_V$1.8 Y1717A S	GGTCAACATGGCCATTGCAGTGATTC
hNa$_V$1.8 Y1717A AS	GAATCACTGCAATGGCCATGTTGACC
rNa$_V$1.8 I380A S	CGTGCTGGTTGCTTTCCTTGGATCG
rNa$_V$1.8 I380A AS	CGATCCAAGGAAAGCAACCAGCACG
rNa$_V$1.8 N389A S	CTACCTGGTCGCTTTGATCTTGGC
rNa$_V$1.8 N389A AS	GCCAAGATCAAAGCGACCAGGTAG
rNa$_V$1.8 L1411A S	GCTTCTTCACGGCGAATCTCTTTG
rNa$_V$1.8 L1411A AS	CAAAGAGATTCGCCGTGAAGAAGC
rNa$_V$1.8 V1415A S	CTGAATCTCTTTGCTGGGGTCATAATC
rNa$_V$1.8 V1415A AS	GATTATGACCCCAGCAAAGAGATTCAG
rNa$_V$1.8 I1707A S	CACCACCTACGCCATCATCTCCTTC
rNa$_V$1.8 I1707A AS	GAAGGAGATGATGGCGTAGGTGGTG
rNa$_V$1.8 F1711A S	CATCATCTCCGCCCTCATCGTGGTC
rNa$_V$1.8 F1711A AS	GACCACGATGAGGGCGGAGATGATG
rNa$_V$1.8 Y1718A S	GGTCAACATGGCCATCGCAGTGATTC
rNa$_V$1.8 Y1718A AS	GAATCACTGCGATGGCCATGTTGACC

The codon encoding the substituted residue is *underlined* and the bases which differ from wild type sequence are shown in *red*.

2.1.5 Human and rat Na$_V$1.8 cDNA clones

The human $Na_V1.8$ ($hNa_V1.8$) and rat $Na_V1.8$ ($rNa_V1.8$) channel α-subunits were cloned at GlaxoSmithKline. The α-subunit cDNAs used were human $Na_V1.8$ (Accession number Q9Y5Y9, polymorph 1073V), and rat $Na_V1.8$ (Accession No. Q62968, polymorph 1896I and 1901D). The pFastBacMam1-$hNa_V1.8$, pSP64T-$hNa_V1.8$ and pCIN5-$rNa_V1.8$ constructs were from GlaxoSmithKline. The pFastBacMam1-$h\beta_1$ and pFastBacMam1-$h\beta_3$ subunits were a gift from Fiona Cusdin (University of Cambridge). The pFastBacMam1 vector (Condreay et al.,

1999), EBO-pCD-Leu2 plasmid (American Type Culture Collection) and pEGFP-N1 plasmid (Clontech) were also used.

2.1.6 Growth media, solutions and buffers

TABLE 2.2a

Growth media for E. coli cells	
Luria Broth (LB) Media	Bacto-Tryptone (10g/L), Bacto-Yeast extact (5g/L) and NaCl (5g/L)
LB-Agar Plate	Agar (1.5%), LB media and antibiotic

TABLE 2.2b

Preparation and analysis of DNA and RNA	
Tris-Acetate-EDTA (TAE) Buffer (50x)	Tris (252g/L), Na_2EDTA (pH 8.0, 50mM) and glacial acetic acid (5.71%)
RNA New Wash	Ethanol (50%), Tris-HCl (pH 8.0, 10mM), NaCl (100mM) and EDTA (pH 8.0, 2.5mM)
Denaturing Solution	Guanidine thiocyanate (5mM), N-lauryl sarcosine (0.05%), sodium citrate (125mM) and 2-mercaptoethanol (0.007%)

TABLE 2.2c

Media for ND7/23 mammalian cells	
Growth Media	Dulbecco's modified Eagle medium (DMEM, 4500mg/L glucose, 89%), heat-inactivated foetal bovine serum (HI-FBS, 10%) and non-essential amino acids (NEAA, 1x, 1%). Filter sterilised.
Freezing Media	Dulbecco's modified Eagle medium (DMEM, 4500mg/L glucose, 40%), heat-inactivated foetal bovine serum (HI-FBS, 50%) and DMSO (10%).

TABLE 2.2d

Electrophysiological recording solutions	
OR2 (Calcium-free Ringer) Solution	NaCl (82mM), KCl (2mM), HEPES (5mM) and $MgCl_2$ (1mM), pH adjusted to 7.2 with NaOH.
Barth's Solution	NaCl (88mM), KCl (1mM), $NaHCO_3$ (2.4mM), $MgCl_2$ (0.82mM), $Ca(NO_3)_2$ (0.33mM), penicillin (10μg/ml), streptomycin (10μg/ml), Tris-HCl (pH 7.6, 7.25mM) and $CaCl_2$ (0.41mM)
Frog Ringer Solution	NaCl (90mM), KCl (2mM), $CaCl_2$ (1.8mM), $MgCl_2$ (2mM), HEPES (5mM), adjusted to pH 7.6 using NaOH.
Patch Clamp Internal Solution	CsF (120mM), HEPES (10mM) EGTA (10mM) and NaCl (15mM), adjusted to pH 7.2 with CsOH. Filter steriled
Patch Clamp External Solution	NaCl (140mM), HEPES (5mM), $MgCl_2$ (1.3mM), $CaCl_2$ (1mM), Glucose (11mM) and KCl (4.7mM), adjusted to pH 7.4 with NaOH. Filter sterilised or used within 48hrs.

2.2 General Molecular Biology Methods

2.2.1 Transformation of plasmid DNA into competent bacterial cells

Due to the size and instability of the constructs, plasmid DNA was transformed into *E. coli* MAX Efficiency® Stbl2™ (>1x10^9 cfu/μg; Invitrogen) or XL10-Gold® (≥5x10^9 cfu/μg; Stratagene) competent cells (Table 2.3). The competent cells were thawed on ice for 10 minutes and transferred to a pre-chilled 1.5ml microcentrifuge tube. Plasmid DNA was added to the cells, and the mixture was incubated on wet ice for 30 minutes. The cells were heat-shocked at 42°C for 25–30 seconds and then returned to ice for 2 minutes. Pre-warmed media was then added to the mixture and incubated at 28°C for 90 minutes while shaking at 225-250rpm. After this recovery period, the cell culture was centrifuged for 3 minutes at 4,000rpm. The supernatant was removed and the cell pellet resuspended in 150μl fresh media. Cell culture (50μl and 100μl) was spread out on LB agar plates (Table 2.2a) containing antibiotic (100μg/ml ampicillin or 50μg/ml kanamycin depending on the antibiotic resistance gene present in the transformed plasmid DNA) and incubated at 28°C for 24–48 hours.

TABLE 2.3

Escherichia coli competent cells for plasmid DNA transformations

Experiment	Cells
Plasmid DNA grow up	Stbl2 (16μl)
Following ligation (*2.3.6*)	Stbl2 (100μl)
Following site-directed mutagenesis (*2.2.7*)	XL10-Gold (45μl)

2.2.2 Inoculation of LB media for small-scale growth of a single bacterial colony

In order to gain a sufficient quantity of transformed cells for DNA extraction, a randomly selected individual colony was removed from the plate with a 200μl micropipette tip and introduced to 2ml LB media (Table 2.2a) containing antibiotic (100μg/ml ampicillin or 50μg/ml kanamycin depending on the antibiotic resistance gene). The culture was incubated overnight at 28°C while shaking at 225-250 rpm.

2.2.3 Mini-prep extraction of plasmid DNA from transformed bacterial cell culture

The overnight culture was transferred into a 1.5ml microcentrifuge tube and the cells were harvested by centrifugation at 8,000rpm for 3 minutes at room temperature. Remaining culture (approx. 500ml) was stored at 4°C for large-scale culture of cells. Plasmid DNA was extracted and purified using the QIAprep® Miniprep Kit (Qiagen) according to the manufacturer's protocol or using a QIAprep® 8 Turbo Kit (Qiagen) on a Qiagen BioRobot 9600.

2.2.4 Restriction digest of plasmid DNA

Following manipulation of plasmid DNA (e.g. small-scale amplification of DNA), restriction mapping of DNA was carried out on an agarose gel. Restriction digest of plasmid DNA was carried out for both subcloning and RNA synthesis according to manufacture's instructions. The plasmid DNA, appropriate enzyme buffer, one or more restriction enzymes and DNA-grade water (to give final reaction volume) were mixed in a 0.5ml tube and incubated at optimum temperature for the enzyme. For verification of plasmid DNA a small volume of DNA (typically 250ng) and two enzymes were mixed in a total volume of 10µl for incubation for 2 hours. In contrast, subcloning and RNA synthesis required larger amounts of DNA (3µg and 0.5µg respectively) incubated overnight in reaction volumes of 30µl and 50µl respectively.

2.2.5 Agarose gel electrophoresis to confirm DNA

The semi-quantitative analysis of linear and non-linear DNA was carried out on a 0.7% or 1% agarose gel with ethidium bromide (6µl, 10mg/ml). The agarose gel was transferred to an Anachem Origo H2SET electrophoresis gel tank, containing 1x TAE (Table 2.2b). To the DNA samples, 6x gel loading solution (Sigma) was added and the mixture was loaded into separate lanes alongside a DNA ladder. The gels were run for 30–45 minutes at 80V and visualised using Quantity One 4.4.1 Imaging Software on a BioRad Gel Doc 1000.

2.2.6 Preparation of cRNA for microinjection

The DNA preparation was purified to RNA grade with the addition of 200µl denaturing solution (see Table 2.2b) and 15µl glass milk and incubating on ice for 5 minutes and centrifuging and washing the pellet in RNA New Wash (Table 2.2b) 3 times before

resuspending the dry pellet in 20µl RNA grade water. A 1µl aliquot was run on a 0.7% agarose gel to confirm the presence of DNA. Wild type $hNa_V1.8$ cRNA was synthesised *in vitro* using SP6 polymerase with the MEGAscript® transcription kit (Ambion) according to the manufacturer's protocol. A 1µl aliquot was run on a 0.7% agarose gel for 15 minutes and visualised on a BioRad Gel Doc 2000 to estimate the cRNA concentration. The remaining cRNA was stored at -20°C.

2.2.7 Site-directed mutagenesis

The role of a single amino acid residue in protein structure and function may be studied by its substitution to a residue with different properties. Point mutations to alanine were generated using the QuikChange® method (Fig. 2.1) developed by Stratagene (La Jolla, CA). Due to the size (13kb) of the plasmid DNA, the XL version of the QuikChange® Mutagenesis Kit (Stratagene) was used to substitute nucleotides. To a 0.2ml PCR tube, reaction buffer (5µl, 10x), plasmid DNA (1µl, 50ng), sense mutagenic primer (0.5µl, 0.1mM), antisense mutagenic primer (0.5µl, 0.1mM), dNTP mix (1µl), DMSO (2.5µl) and water (39.5µl) were added. Thermal cycling was carried out in a PTC-200 (MJ Research) PCR machine as shown in Table 2.4, where *PfuTurbo*® DNA polymerase (1µl) was added after *Segment 1*.

TABLE 2.4

General thermal cycling parameters for site-directed mutagenesis

Segment	Cycles	Temperature	Time
1	1	95°C	5m
2	15	95°C	50s
		50°C - 60°C	1m
		68°C	14m
3	1	68°C	7m

After thermal cycling the non-mutated *dam*-methylated parental DNA was digested by adding *Dpn*I endonuclease (1µl) and incubating overnight at 37°C. The remaining plasmid DNA was then transformed into XL10-Gold® competent cells (see *Section 2.2.1*).

2.2.8 Inoculation of LB media for large-scale growth of a single bacterial colony

While the small-scale *E.coli* culture was sufficient for preparation of <10µg of plasmid DNA, preparation of >200µg plasmid DNA required a large-scale growth of the transformed *E.coli* culture. Small-scale *E.coli* culture (50-100µl) was introduced to a 2L flask containing

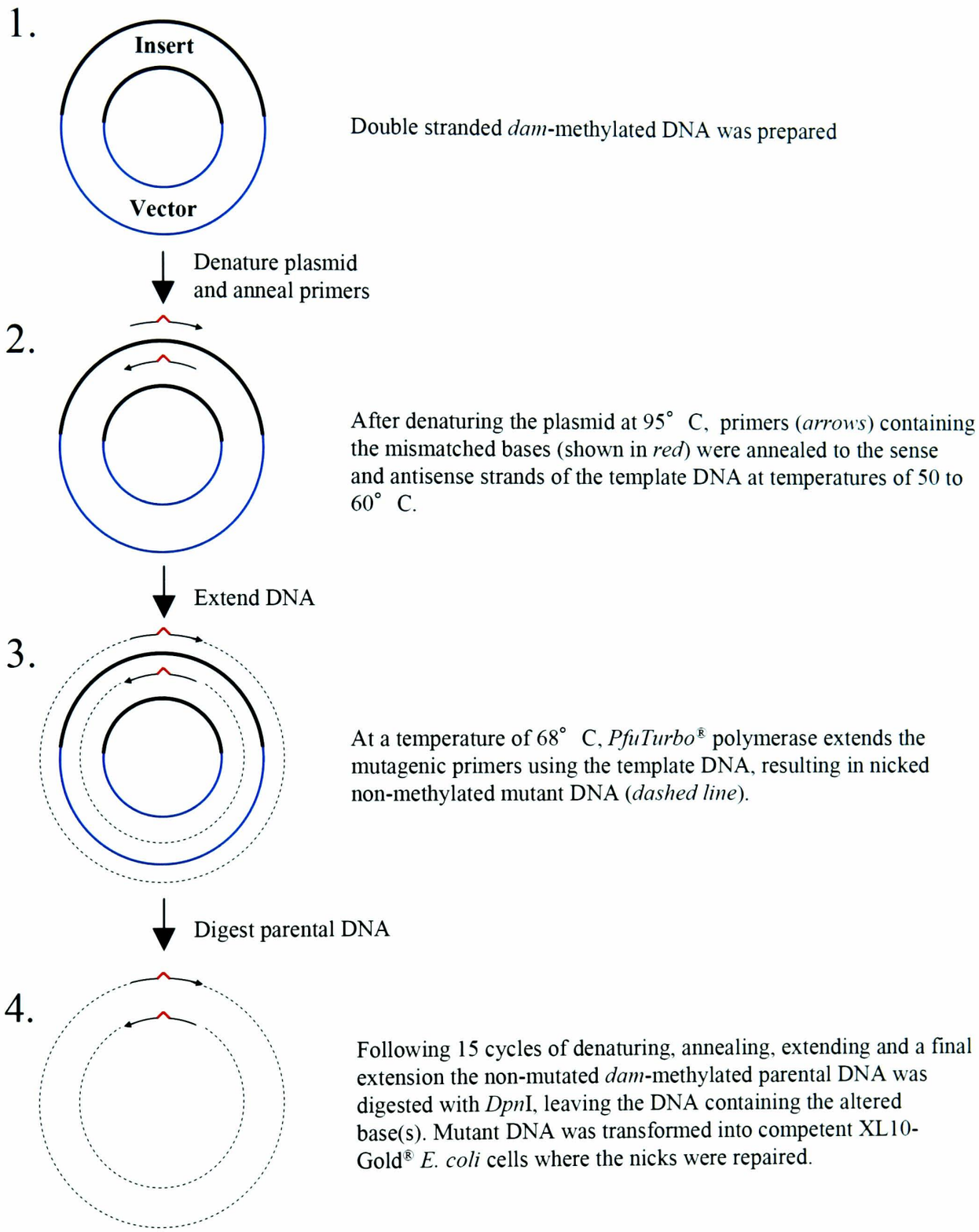

Fig. 2.1. Overview of the QuikChange® site-directed mutagenesis method. The diagram was adapted from the Stratagene protocol.

200ml LB media and 100μg/ml ampicillin. The flask was incubated for 18 hours at 28°C while shaking at 225rpm.

2.2.9 Maxi-prep extraction of plasmid DNA from transformed bacterial cell culture

Overnight large-scale culture was transferred to 1L centrifuge tube and bacterial cells were harvested by centrifugation at 4,000rpm for 10 minutes at 4°C. Plasmid DNA was extracted and purified using the HiSpeed® Plasmid Purification Kit (Qiagen) according to the manufacturer's protocol. The plasmid DNA was eluted with Tris-EDTA (1ml) and the concentration was determined by measuring the absorbance at 260nm using a GeneQuant RNA/DNA Calculator (Pharmacia Biotech).

2.2.10 Glycerol Stocks

In order to store transformed *E.coli* cells for long periods of time, 700μl was vortexed with 300μl sterile glycerol in a 2ml cryotube and frozen at -80°C. When the cells were required the culture was thawed and 2μl inoculated (see *Section 2.2.2*)

2.3 Specific Molecular Biology Methods

2.3.1 Purification of a DNA digest

Following the incubation of DNA with a restriction enzyme, the buffer and enzyme must be removed before incubation with a different enzyme. The purification of DNA was carried out using the QIAquick® Gel Extraction Kit (QIAGEN) according to the manufacturer's protocol; the Buffer QG (300μl) was added directly to the 30μl reaction volume containing the DNA.

2.3.2 Blunting of "sticky" ends

Many restriction enzymes cut double stranded DNA leaving an "overhang" or "sticky" end. Therefore, in order to enable a sticky end to ligate to another blunt end, it should be blunted with a DNA polymerase. A 0.2ml PCR reaction tube containing DNA (28μl), dNTP (1μl,

10mM) and buffer (5µl, 10x) was incubated in a PTC-200 (MJ Research) PCR machine as shown in Table 2.5, where *PfuTurbo*® DNA polymerase (1µl) was added after *Segment 1*.

TABLE 2.5

Thermal cycling parameters for blunting of "sticky" ends

Segment	Temperature	Time
1	95°C	2m
2	75°C	30m

2.3.3 Dephosphorylation of a DNA fragment

To ensure that the vector fragment or insert fragment do not ligate to themselves during subcloning, the vector fragment was dephosphorylated. To the vector fragment (30µl), alkaline phosphatase (1µl, Roche) was added and incubated at room temperature for 2 hours. The vector and insert fragments were validated and purified by running them on a 1% agarose gel, excising the bands, and extracting DNA fragments from each band.

2.3.4 Excision and purification of a DNA fragment

A DNA fragment of interest can be excised directly from an agarose gel and purified. Following the separation of DNA fragments on an agarose gel, the band of interest was removed using a sterile scalpel blade. The QIAquick® Gel Extraction Kit (QIAGEN) was used to extract the DNA from the agarose gel, according to the manufacturer's protocol. The purified DNA fragment was eluted in 30µl DNA-grade water, and 1µl run on a 1% agarose gel to estimate the DNA concentration.

2.3.5 Ligation of DNA fragments

In order to ligate the vector and insert DNA fragments, an approximate 10:1 concentration ratio of insert to vector was added to a 0.5ml tube containing T4 DNA ligase buffer (2µl), T4 DNA ligase (1µl) and DNA-grade water (to give a total reaction tube volume of 10µl). The reaction tube was incubated at 16°C overnight.

2.3.6 Construction of pFastBacMam1-rNa$_V$1.8 plasmid DNA

The subcloning of rNa$_V$1.8 into the pFastBacMam1 vector is shown in Figure 2.2. The pCIN5-rNa$_V$1.8 plasmid was restricted first with *Hpa*I (blunt end) and then with *Not*I. The pFastBacMam1 vector was restricted with *Xba*I, the sticky ends blunted with *Pfu* DNA polymerase and then cut a second time with *Not*I. For both pCIN5-rNa$_V$1.8 and pFastBacMam1, the DNA was purified after each reaction and visualised using agarose gel electrophoresis. The double cut pFastBacMam1 vector was then dephosphorylated, and run on a separate agarose gel to the rNa$_V$1.8 insert for fragment extraction and purification. The rNa$_V$1.8 insert and pFastBacMam1 fragments were ligated and transformed into *E. coli* Stbl2 competent cells for small-scale amplification and mini-prep extraction of DNA and a subsequent large-scale amplification and maxi-prep extraction of DNA. The pFastBacMam1-rNa$_V$1.8 construct was confirmed using agarose gel visualisation of multiple restriction digests and sequencing of the insert-vector overlap and then the entire rNa$_V$1.8 sequence. The pFastBacMam1-rNa$_V$1.8 and pFastBacMam1-hNa$_V$1.8 plasmid DNA maps are shown in Figure 2.3.

2.4 Tissue culture

2.4.1 ND7/23 mammalian cell line

ND7/23 cells are a hybrid cell line derived from the fusion of rat DRG neurons with mouse N18Tg2 neuroblastoma cells (Wood et al., 1990) acquired from ECACC (Salisbury, UK). The number of cells was normally determined using a Vi-CELL XR (Beckman Coulter).

2.4.2 Reviving mammalian cells

Cells were rapidly thawed after warming the cryotube (containing $1x10^7$ cells) in a water bath at 37°C for 5 minutes. The cells were carefully transferred to a sterile 14ml Falcon tube, to which pre-warmed growth media (see Table 2.2c) was slowly added to make up to 10ml. The cell suspension was mixed and centrifuged at 1,000rpm for 5 minutes. The media was removed, the cell pellet gently resuspended in 5ml fresh growth media, and the mixture transferred to a T75 flask containing 7ml pre-warmed growth media. The cells were incubated at 37°C (5% CO_2).

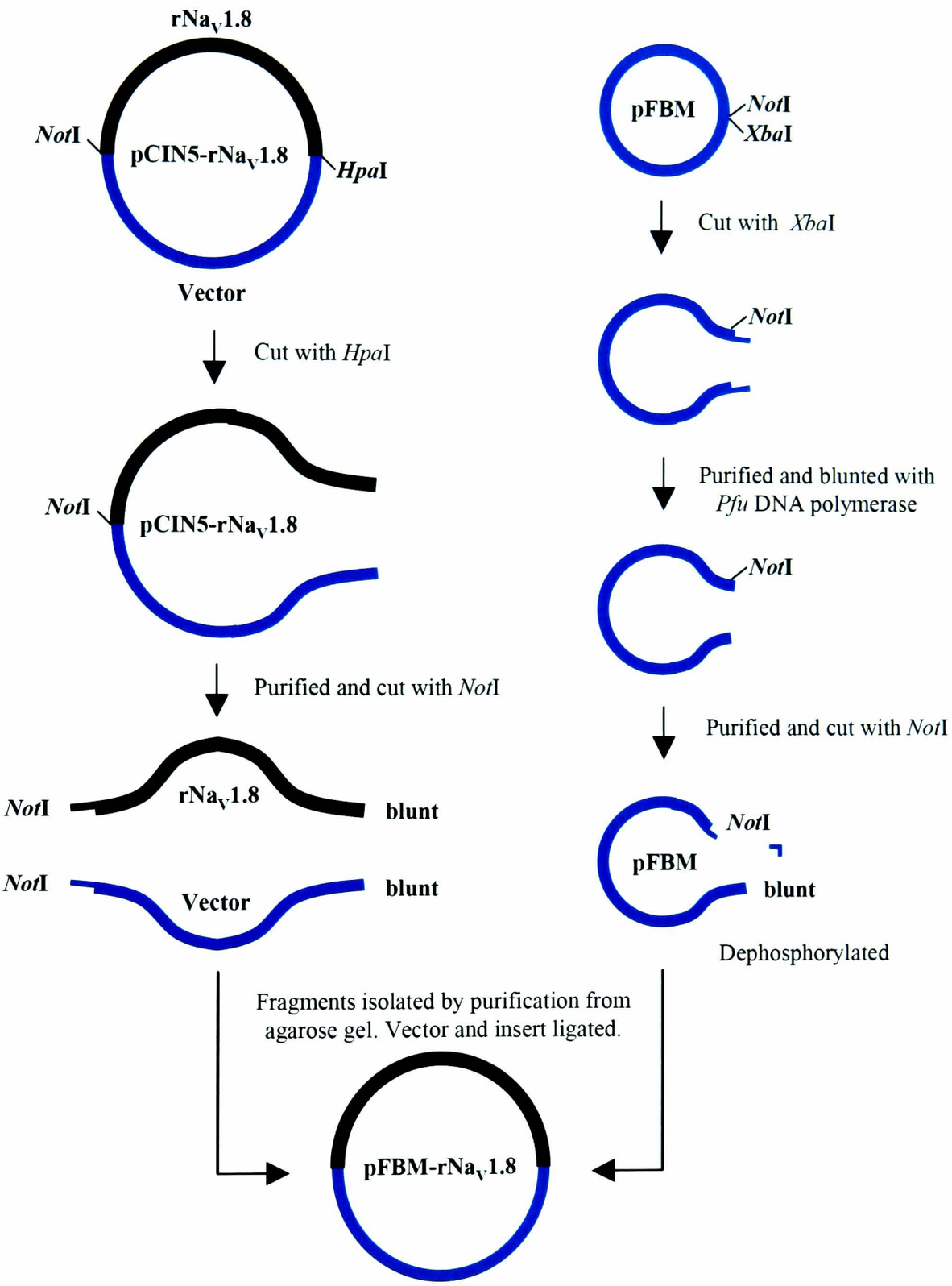

Fig. 2.2. Schematic diagram of the construction of pFastBacMam-rNa$_V$1.8 plasmid DNA. The restriction sites used are labelled. The diagram is not to scale.

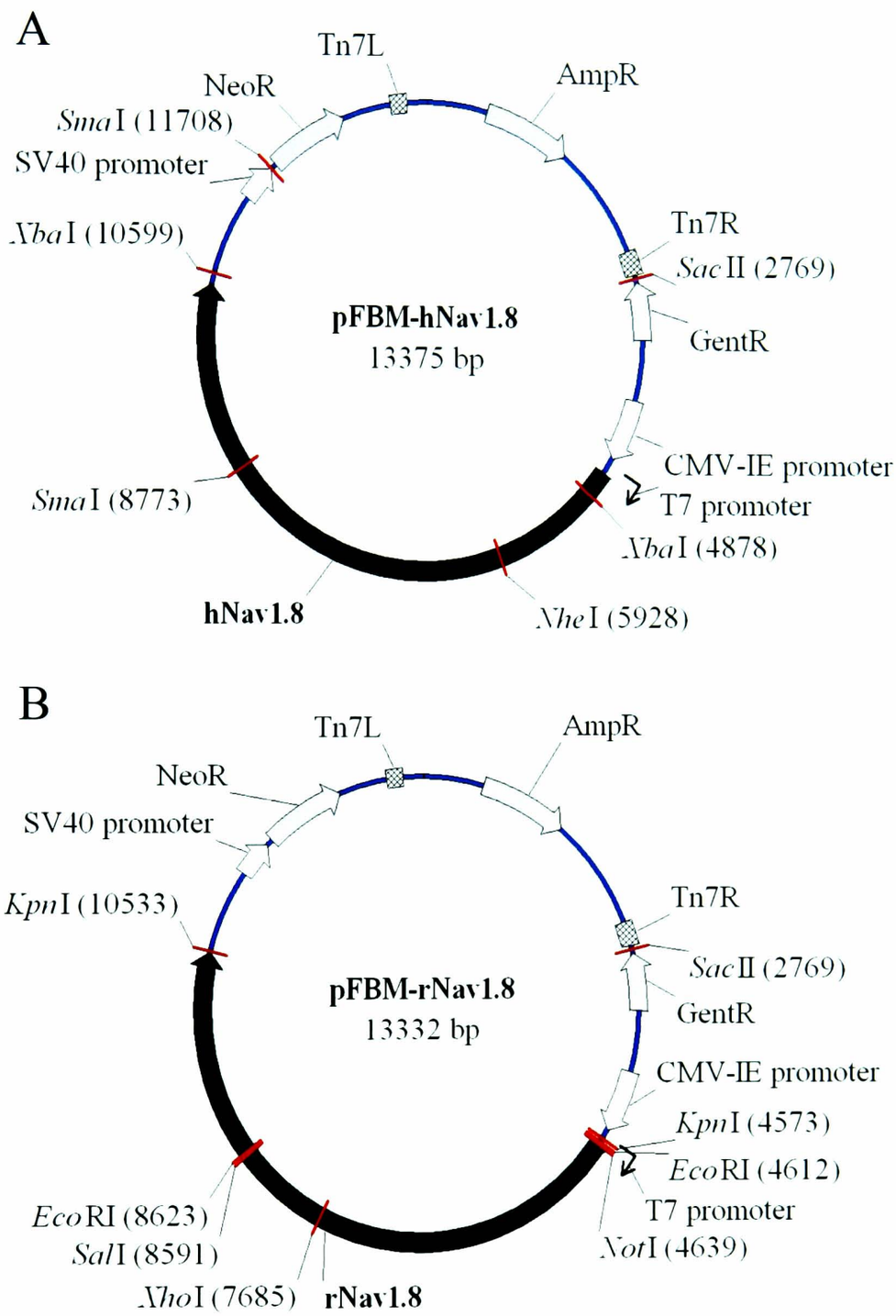

Fig. 2.3. Plasmid DNA maps for human and rat $Na_V1.8$ channel cDNAs in pFastBacMam1 vectors. The pFastBacMam1-h$Na_V1.8$ (**A**) and pFastBacMam1-r$Na_V1.8$ (**B**) plasmid diagrams show antibiotic resistance genes for neomycin (*NeoR*), ampicillin (*AmpR*) and gentamicin (*GentR*), simian virus 40 (*SV40*) promoter, cytomegalovirus intermediate/early (*CMV-IE*) promoter and the T7 promoter, and Tn7 transposons (*Tn7R* and *Tn7L*). Restriction sites used and their respective base numbers are shown.

2.4.3 Maintaining mammalian cells

Mammalian cells were passaged when they reached approximately 90% confluence (every 2–3 days). Old growth media was removed and the cells were washed with PBS (GIBCO). In order to detach the cells from the T75 flask, 2ml pre-warmed versene was introduced and the flask incubated at 37°C (5% CO_2) for 4 minutes. Growth media (4ml) was added and the cells were gently resuspended. To a T75 flask containing 11ml growth media, 1ml of the resuspended cells were added to give a 1:6 dilution. Rather than the 1:6 dilution described, a 1:8 dilution is more appropriate at later passage numbers, when cells grow faster. Cells with a passage number greater than 30 were discarded.

2.4.4 Storing mammalian cells

In order to store ND7/23 cells for later use, cells at approximately 80% confluence were washed with versene and detached from the T75 flask. Following resuspension of cells in pre-warmed growth media, the cells were centrifuged at 1,000rpm for 5 minutes. The media was removed and cells carefully resuspended in 1ml fresh cell freezing media (Table 2.2c) and transferred to a cryotube. Cells were frozen overnight at -80°C in a freezing container (Nalgene) and then transferred to -140°C for storage.

2.4.5 Transfection of mammalian cells

Cells were seeded in a 35mm dish at 60% confluence and incubated at 37°C (5% CO_2) overnight. Cells were co-transfected the following day with 3.0μg $Na_V1.8$ channel DNA in the pFastBacMam1 vector and 0.3μg EBO-pCD-Leu2 plasmid DNA (encoding Leu2, for selection with anti-CD8 beads) or pEGFP-N1 DNA (encoding EGFP, for selection with fluorescence) with 5.5μg Lipofectamine™ 2000 (Invitrogen).

2.5 Electrophysiology

2.5.1 Xenopus laevis oocyte preparation

Mature female *Xenopus laevis* frogs were obtained from Blades (UK) and killed by schedule 1 methods; frogs were anaesthetised by immersion in 0.2% (w/v) tricaine for approximately 40 minutes and killed by destruction of the spinal cord and brain. Ovarian lobes were removed and washed in sterile OR2 solution (see Table 2.2d). Connective tissue was removed by collagenase treatment on a gyro mixer for 40 minutes in 20ml OR2 solution and 2mg/ml type IA collagenase. The dissociated oocytes were washed in OR2 solution and stage V and VI oocytes were defolliculated with watchmaker's forceps (Dumont, size 5, Agar Scientific), and stored in OR2 until cRNA injection the same day.

2.5.2 Preparation of cRNA for microinjection

Micropipettes were pulled from borosilicate glass (Drummond Scientific Company) using a Model P-87 Flaming/Brown micropipette puller (Sutter Instrument) and the tip manually broken using forceps. The micropipette was backfilled with mineral oil and mounted on a Drummond microinjection syringe on a Micro-instruments manipulator. The cRNA (1µl, 125ng/µl) was drawn up into the micropipette from a microscope slide covered with nescofilm (VWRI). Dumont stage V and VI oocytes were injected with cRNA (50nl, 5ng). After injection, oocytes were incubated at 19.6°C in 96 well culture plates containing Barth's solution (see Table 2.2d) with solution changes daily. Electrophysiological recordings of oocytes were carried out 3-4 days after injection.

2.5.3 Two-electrode voltage clamp

Macroscopic currents were recorded using a GeneClamp 500 amplifier (Axon Instruments), filtered at 2kHz and sampled at 4kHz. CED analysis software was used to design protocols and a CED 1401 interface (Cambridge Electronic Design, UK) was used to supply command potentials to the amplifier and to record elicited currents. Microelectrodes were made with 1.0mm x 0.58mm thin borosilicate glass (Harvard Apparatus), pulled by a custom-built vertical two-stage puller. The microelectrodes were filled with 3M KCl and mounted on the headstages (Axon Instruments) using a holder containing a silver-silver chloride wire. The headstages were

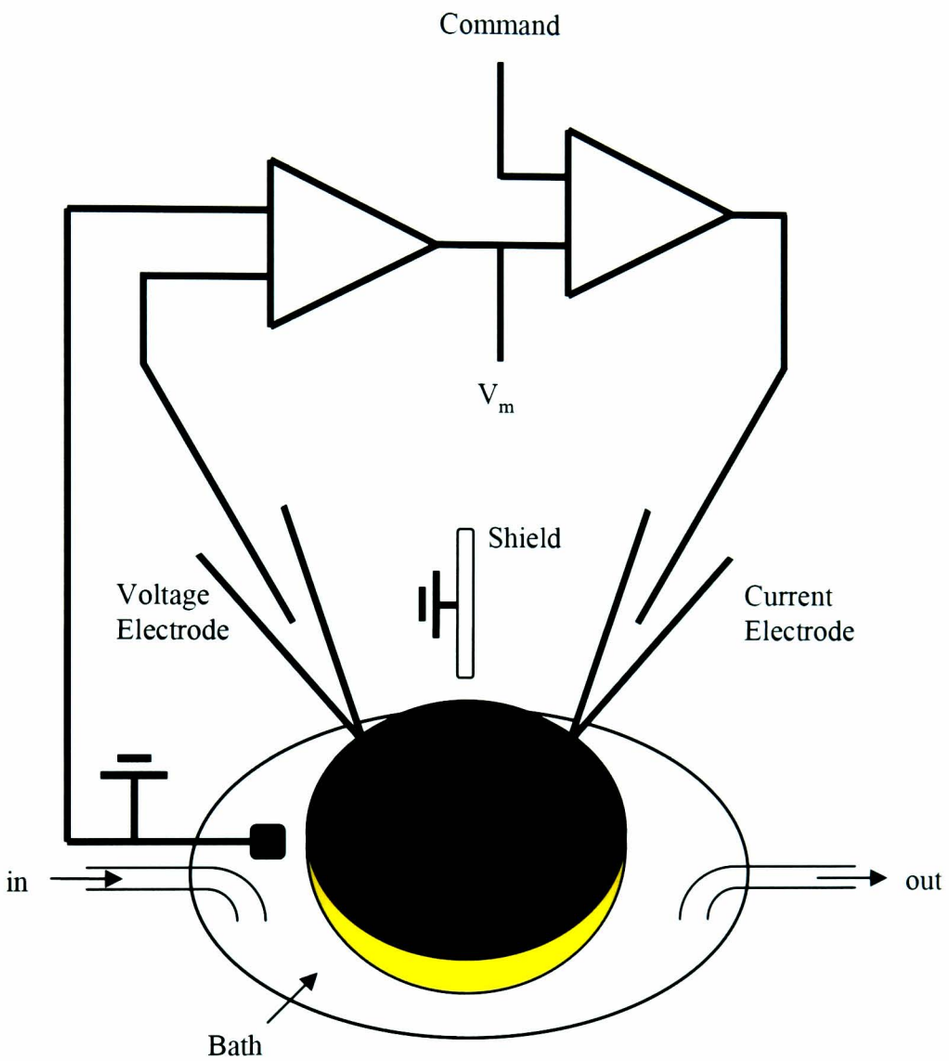

Fig. 2.4. Schematic diagram of the two-electrode voltage-clamp chamber. The *Xenopus* oocyte is impaled by the voltage and current electrodes. The animal pole is shown in *brown* and the vegetal pole is shown in *yellow*.

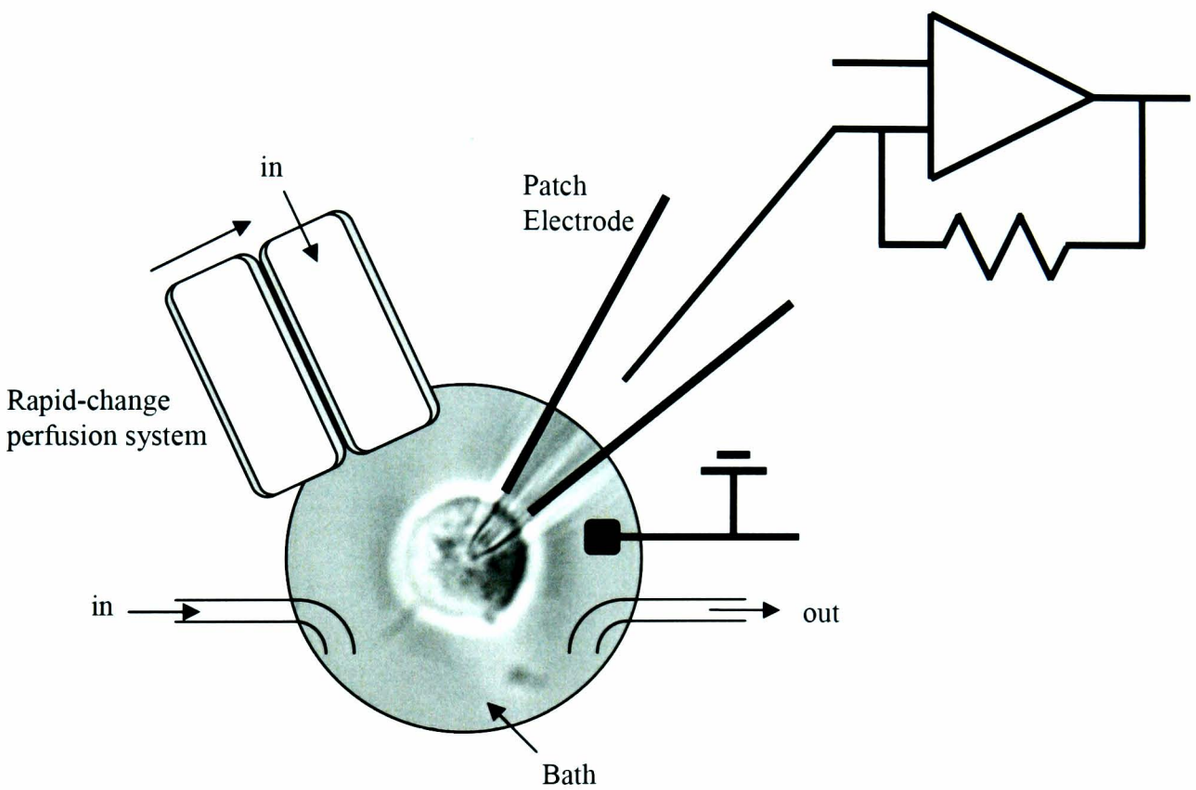

Fig. 2.5. Schematic diagram of the whole-cell patch clamp chamber. A GΩ seal is formed between the patch electrode and the mammalian cell in the whole-cell configuration. The rapid-change perfusion system was controlled externally. The experiments were carried out on an air table to reduce vibration.

controlled using a Micro-instruments manipulator. The voltage microelectrodes showed resistances between 1.0 and 2.5MΩ and the current microelectrode showed resistances between 0.5 and 1.0MΩ. A silver-silver chloride wire or pellet was used for the bath electrode. Experiments were carried out at room temperature (20–22°C) in an oocyte chamber (Fig. 2.4) continuously perfused (2ml/min) with Frog Ringer's solution (Table 2.2d). Oocytes were impaled with both microelectrodes and allowed to stabilise for 5 minutes. The resting membrane potential was measured, to which the initial voltage clamp offset was set, and the amplifier was switched to voltage clamp mode. The gain and stability were increased during repetitive depolarising pulses (10mV step at 0.1Hz) of the oocyte membrane until the oscilloscope showed a square wave trace. The membrane potential was then held at -100mV, from which currents were elicited for 25ms pulses with voltage steps from -90mV to +60mV in 10mV increments in order to construct current-voltage (*I-V*) relationships.

2.5.4 Preparation of transfected mammalian cells

Transfected cells were seeded on sterile 100mm diameter glass coverslips >12 hours before use. For the selection of cells with CD8 beads, the beads (20µl) were prepared by pelleting with a magnet and resuspending in PBS three times. The beads were then suspended in 2ml PBS and introduced to the PBS-washed cells, and incubated at 37°C (5% CO_2) for 30 minutes. The unassociated beads were removed and the cells washed in PBS and allowed to recover at 37°C (5% CO_2) for 30 minutes before use.

2.5.5 Whole-cell patch clamp technique

Transfection-positive cells were analysed 2–4 days after transfection and identified with immunobeads (anti-CD8 Dynabeads; Invitrogen) or green fluorescence using a Nikon super high pressure mercury lamp. Recordings of currents were obtained in the whole-cell configuration of the patch clamp technique (Fig. 2.5) at room temperature (20–22°C) on an air table using an Axopatch-1C or Axopatch 200B amplifier (Axon Instruments). Patch pipettes were fabricated from thin-walled borosilicate glass capillaries (GC150TF-10; Harvard Apparatus) using a Model P-87 or P-97 Flaming/Brown micropipette puller (Sutter Instrument) and usually fire polished using a Micro Forge (MF-830; Narishige). Patch pipettes were filled with internal solution (see Table 2.2d), which contains fluoride as in many previous studies of $Na_V1.8$ channel currents in cultured cells and TTX-resistant Na^+ currents in DRG cells (John et al., 2004; Leffler et al., 2007; Zhao et al., 2007; Elliott and Elliott, 1993; Choi et al., 2006; Dekker et al., 2005; Cardenas et al., 2006). Patch pipettes were coated with Sigmacote (Sigma-

Aldrich) and allowed to air dry. The patch pipette was inserted into an electrode holder containing a silver-silver chloride wire, which in turn was fixed into the headstage (CV-203 BU; Axon Instruments). The headstage was mounted and controlled with a coarse manipulator (TS-5000-300; Burleigh), and also controlled remotely with a fine manipulator (PC-5000 series; Burleigh). A silver-silver chloride wire or pellet was used for the bath electrode. During experiments, cells were continuously perfused with an external solution (Table 2.2d) containing TTX (200nM, Tocris) in order to completely inhibit endogenous Na^+ currents. Patch pipettes typically showed tip resistances of 1.5–2.5MΩ, and while in solution (<1 minute) the pipette offset was used to zero the current at 0mV. Using the coarse and fine manipulators the patch pipette tip was positioned against the cell membrane, negative pressure was applied until the resistance increased to >1GΩ ("cell-attached mode"), and pipette capacitance was compensated. The command voltage was changed to -40mV and further negative pressure was applied until the patched membrane was ruptured ("whole-cell mode"), and whole-cell capacitance was compensated. Series resistance was compensated by 80-85%. Cells were allowed to equilibrate for 10 minutes in the whole-cell configuration before voltage pulses were applied, and currents were filtered at 5kHz and sampled at 10kHz using pClamp8 or pClamp9 software (Clampex; Axon Instruments). Cells which showed an I_{max} of <200pA were discarded. Voltage pulses were adjusted by -8mV to correct for liquid junction potentials. The membrane potentials were then corrected offline +8mV accordingly.

2.5.6 Application of drugs

All compounds were prepared in dimethyl sulphoxide (DMSO) and x100 stocks stored at -20°C. The desired concentration in the external solution gave a final concentration of 1% DMSO. Compounds were applied during a 3–4 minute incubation period using a six-channel valve controller (VC-6; Warner Instruments) and rapid solution changer (SF-77B; Warner Instruments). The drug-free external control solution also contained 1% DMSO in the drug experiments.

2.6 Electrophysiological protocols and analysis

2.6.1 Software

For offline data analysis, current traces were measured using Signal v2.05 (Cambridge Electronic Design, UK) for two-electrode voltage clamp recordings, or using Clampfit v9 or 10 (Molecular Devices) for whole-cell patch clamp recordings. Data handling and statistical testing were done using Microsoft Excel, and Origin v5.0 (MicroCal Inc.) was used to present the data.

2.6.2 Voltage-dependence of activation

In order to construct current-voltage curves, test pulse voltages of -100mV to +60mV (Fig 2.6) were used to elicit Na^+ currents from a holding potential of -120 or -80mV.

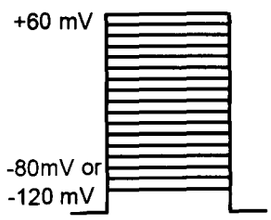

Figure 2.6. Voltage-dependence of activation pulse protocol.

The peak current amplitude (I_{Na}) was measured and plotted against the test pulse voltage from which it was elicited. Conductance (G) was calculated from the peak sodium current (I_{Na}), using the equation:

$$G = \frac{I_{Na}}{V - E_{rev}} \qquad \text{Eq. 1}$$

where V is the membrane potential and E_{rev} is the reversal potential obtained from the I-V curve for each cell. These curves were fitted with the Boltzmann equation:

$$G = \frac{G_{max}}{1 + \exp\left(\frac{V_{1/2} - V}{k}\right)} \qquad \text{Eq. 2}$$

where G_{max} is maximum conductance, $V_{1/2}$ is the voltage for half-maximal activation, V is the membrane potential and k is the slope factor. Conductance values were normalised to G_{max} and plotted against the membrane potential.

2.6.3 Voltage-dependence of steady-state inactivation

In order to determine the voltage-dependence of steady-state inactivation, a 4 second conditioning pulse was used to inactivate channels and a test pulse to 0mV was used to measure the proportion of non-inactivated channels. This protocol (Fig. 2.7) was carried out from holding potentials of -120mV or -80mV.

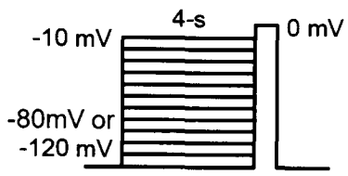

Figure 2.7. Voltage-dependence of inactivation pulse protocol.

Inactivation curves were fitted with the Boltzmann equation:

$$I = \frac{B - A}{1 + \exp\left(\frac{V - V_{1/2}}{k}\right)} + A \qquad \text{Eq. 3}$$

where B is the maximum current and A is the amplitude of a non-inactivating component, V is the membrane potential, $V_{1/2}$ is the voltage of half-maximal inactivation and k is the slope factor. Current was normalised to the maximum current (B) and plotted against the membrane potential.

2.6.4 Time course for inactivation

In order to determine the inactivation time course, two approaches were used to measure the time constants. For the first approach, the decay phase of the current during the 15ms depolarising pulse was fitted with the exponential equation:

$$I = I_0 + I_i \exp^{\left(\frac{-t}{\tau_i}\right)} + I_2 \exp^{\left(\frac{-t}{\tau_2}\right)} \qquad \text{Eq. 4}$$

where I_0 is the steady-state current asymptote, τ_1 is the time constant of the initial component with amplitude I_1, and τ_2 is the time constant of the second component with amplitude I_2. However, since the kinetics were examined over relatively short 15ms depolarising pulses, any slow component was generally too small in magnitude to be measured. Therefore, another approach was also employed to study the time course of development of inactivation, whereby the current amplitude was measured following a 0mV control pulse of varying length and a 4ms recovery period (Fig. 2.8).

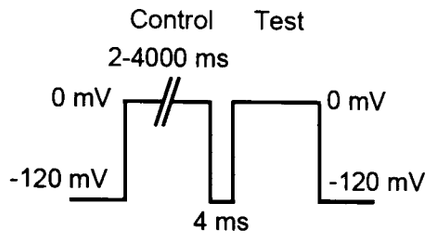

Figure 2.8. Development of inactivation pulse protocol.

Development of inactivation showed two components. The current amplitude during the test pulse was fitted with the following exponential equation:

$$I = I_0 + I_{fast} \exp^{\left(\frac{-t}{\tau_{fast}}\right)} + I_{slow} \exp^{\left(\frac{-t}{\tau_{slow}}\right)} \qquad \text{Eq. 5}$$

where I_0 is the steady-state current asymptote, I_{fast} is the amplitude of the first component decaying with time constant τ_{fast}, and I_{slow} is the amplitude of the second component decaying with time constant τ_{slow}.

2.6.5 Time course of recovery from inactivation

Recovery from inactivation was investigated using a similar protocol as in *Section 2.6.4* but with varying time between control pulse and test pulse (Fig. 2.9).

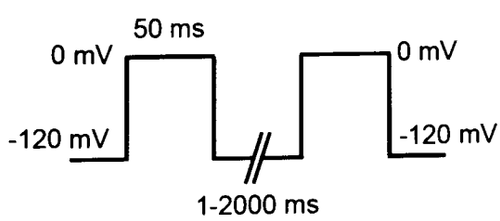

Figure 2.9. Recovery from inactivation pulse protocol.

At least two components were shown for the recovery from inactivation time course. Where two components were observed, the curve was fitted with the equation:

$$I = I_0 + I_{fast} \exp^{\left(\frac{-t}{\tau_{fast}}\right)} + I_{slow} \exp^{\left(\frac{-t}{\tau_{slow}}\right)} \qquad \text{Eq. 6}$$

where I_0 is the steady-state current asymptote, I_{fast} is the amplitude of the first component decaying with time constant τ_{fast}, and I_{slow} is the amplitude of the second component decaying with time constant τ_{slow}. However, when an additional third component was observed, the curve was fitted with the equation:

$$I = I_0 + I_{fast} \exp^{\left(\frac{-t}{\tau_{fast}}\right)} + I_{slow} \exp^{\left(\frac{-t}{\tau_{slow}}\right)} + I_3 \exp^{\left(\frac{-t}{\tau_3}\right)} \qquad \text{Eq. 7}$$

where I_0 is the steady-state current asymptote and τ_{fast}, τ_{slow} and τ_3 are the time constants of the first, second, and third components with their respective amplitudes I_{fast}, I_{slow} and I_3.

2.6.6 Use-dependent current inhibition

The effects of frequent depolarisation on the channels results in the accumulation of inactivated channels. This effect ("use-dependent current inhibition") was studied by measuring the peak current amplitude (I_{Na}) during a train of 10ms depolarising pulses to 0mV from a holding potential of -120mV or -80mV (Fig 2.10). A train of 60 pulses at a range of frequencies (2-50Hz) was used.

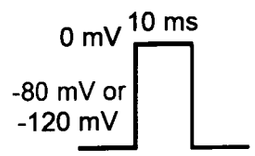

Figure 2.10. Use-dependent inhibition pulse protocol.

2.6.7 Determination of resting state dissociation constants

Local anaesthetics and other drugs show a greater extent of block at more depolarised membrane potentials. Indeed, voltage-gated Na^+ channels open and become inactivated at more depolarised potentials and these drugs show a significantly greater affinity for open/inactivated voltage-gated Na^+ channels compared to the resting channels. This finding is consistent with the

modulated-receptor hypothesis (Hille, 1977; Hondeghem and Katzung, 1977). Thus the simplified modulated-receptor model was proposed by Kuo and Bean (1994):

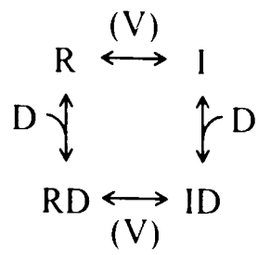

Figure 2.11. Simplified modulated-receptor model

where the transition between resting (*R*) and inactivated (*I*) channels is dependent on the voltage (*V*), and the association of drug (*D*) to either the resting channel or the inactivated channel gives drug bound (and blocked) states *RD* and *ID* respectively (Kuo and Bean, 1994). According to the modulated receptor hypothesis, the apparent dissociation constant (K_D) is the combination of the binding to resting and inactivated states:

$$K_D = \frac{1}{\frac{h}{K_r} + \frac{1-h}{K_i}} \qquad \text{Eq. 8}$$

where K_r and K_i are the dissociation constants for resting and inactivated channels respectively, and h is the proportion of resting channels (i.e. non-inactivated channels). Thus the K_r may be determined when h approaches 1; when virtually all channels are in the resting state at hyperpolarised potentials the apparent dissociation constant is equal to the resting state dissociation constant (K_r). The resting state dissociation constant may then be calculated using the equation:

$$K_r = \frac{[R][D]}{[RD]} \qquad \text{Eq. 9}$$

where [X] represents the concentration of each state. Furthermore, the total channels (R_T) is given by:

$$R_T = [R] + [RD] \qquad \text{Eq. 10}$$

Combining equations 9 and 10 gives the following:

$$K_r = \frac{[D]}{\frac{R_T}{[R]} - 1} \qquad \text{Eq. 11}$$

In this model, the current amplitude is proportional to the number of unoccupied channels ($I \propto [R]$). The ratio of $[R]/R_T$ (Fig. 2.12) is equal to the current amplitude after drug application expressed as a fraction of the current amplitude before drug application (I_{Dr}).

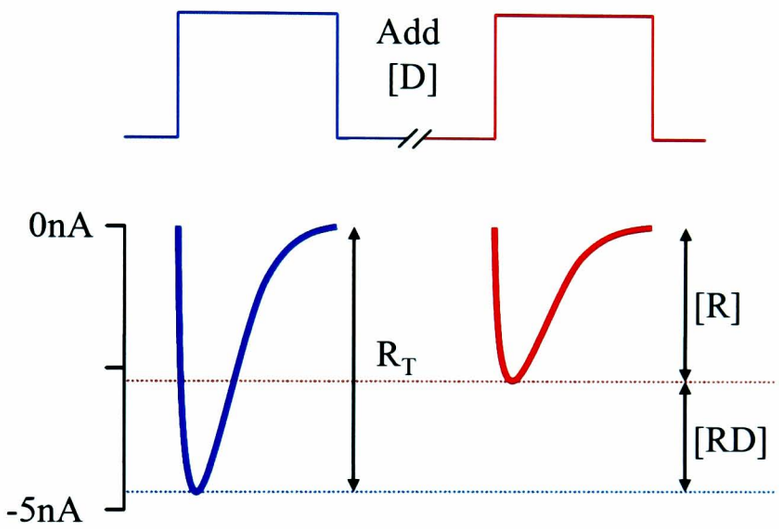

Figure 2.12. Test currents before (*blue*) and after (*red*) drug application used for the calculation of K_r.

The K_r value may be calculated using the following equation:

$$K_r = \frac{[D]}{\frac{1}{I_{Dr}} - 1} \qquad \text{Eq. 12}$$

2.6.8 Determination of the inactivated state dissociation constants

For the determination of the inactivated state dissociation constant (K_i) from Equation 8, drugs which preferentially block inactivated channels ($K_r \gg K_i$) give the following:

$$K_D \cdot (1 - h) \approx K_i \qquad \text{Eq. 13}$$

where the apparent dissociation constant (K_D) is practically equal to the K_i when h is small (i.e. inactivated channels approach 100%). However, experimentally h cannot be altered to be too small, as no current will be observed from the non-conducting inactivated channels. Therefore, the voltage of a pulse (4 seconds) was chosen so as to give 60-80% inactivation (h = 0.4-0.2) as shown in Figure 2.13.

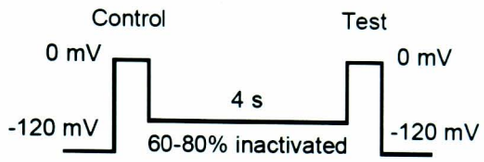

Figure 2.13. Inactivated state dissociation constant pulse protocol.

Before the application of drug, the ratio of the amplitude at the test pulse to the amplitude of the control pulse gives h. The value for h therefore determines the total number of inactivated channels (I_T). Similarly for the calculation of the resting state dissociation constant, the current amplitude is proportional to the number of unoccupied channels ($I \propto [R]$) and the ratio of $[R]/R_T$ (Fig. 2.14) is equal to the current amplitude after drug application expressed as a fraction of the current amplitude before drug application (in this case, I_{Di}).

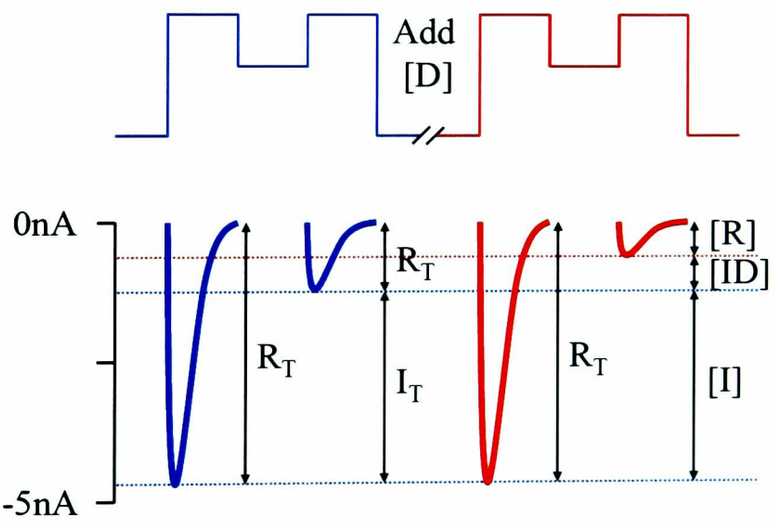

Figure 2.14. In the absence of drug (*blue*) the extent of inactivation is determined. Test currents before and after (*red*) drug application used for the calculation of K_i. The control pulse in the presence of drug is not required for this calculation.

The K_i value may be calculated using the following equation:

$$K_i = \frac{[D]}{\frac{1}{I_{Di}} - 1} \cdot (1 - h) \qquad \text{Eq. 14}$$

where D is the drug concentration and I_{Di} is the fraction of inactivated sodium channels not blocked by a drug (corrected for the effects on the inactivated current amplitude over time, see *Section 5.2.3*), where the fraction of non-inactivated sodium current following the 4 second depolarisation before drug application is h.

2.6.9 Leak subtraction

For two-electrode voltage clamp data, pulse protocols were followed by twenty hyperpolarising pulses at 2 second intervals to -110mV for subsequent leak and capacity subtraction.

For whole-cell patch clamp data, for protocols using test pulses to various membrane potentials (voltage-dependence of activation and inactivation, Fig 2.6, 2.7), leak and capacitance currents were minimised online using the P/4 protocol. In P/4 subtraction, four pulses at a 1/4 of value of the command potential are applied before each test pulse. The elicited currents are summated and subtracted from the data. For protocols that only used test pulses to 0mV, since linear leak current would be practically equal between pulses and holding current is of small amplitude with a high-resistance seal (greater than 1GΩ), leak subtraction was not carried out.

2.6.10 Statistical analysis of data

Data are presented as mean ± standard error, and Student's *t* test was used to determine the significance of changes in mean values. *p* values of less than 0.05 were considered statistically significant.

CHAPTER 3

GENERATION OF MUTANT $Na_V1.8$ SODIUM CHANNELS

3.1. Introduction

The size and instability of voltage-gated Na^+ channel cDNA can make manipulation using standard techniques difficult. Furthermore, expression of the $Na_V1.8$ channel in *Xenopus laevis* oocytes or in mammalian cell lines has shown limited success. For these reasons structure-function studies of the $Na_V1.8$ channel are rare.

In this chapter, cRNA was prepared for the expression of the human $Na_V1.8$ channel in *Xenopus laevis* oocytes. For the expression of $Na_V1.8$ channels in mammalian cells, cDNA encoding the rat $Na_V1.8$ channel was subcloned into the pFastBacMam1 vector, to reduce any assumptions made during the comparison of human and rat channels since the human $Na_V1.8$ was already in the pFastBacMam1 vector. The pFastBacMam1 vector also enables the generation of baculovirus particles for the transduction of mammalian cells, should the normal transfection methods be unsuccessful. In the pFastBacMam1 vector, site-directed mutagenesis was used to substitute cDNA bases to encode alanine at seven positions in the S6 segments of the human and rat $Na_V1.8$ channels. Alanine is commonly located in α-helical transmembrane regions and due to its small side chain has little effect on the protein secondary structure (McPhee et al., 1995). Therefore, alanine substitutions were used to alter the size and hydrophobicity of amino acids, without causing severe distortion of the molecular structure. The mutations of the S6 segments in the human $Na_V1.8$ channel were at residue positions I381, N390 in domain I, L1410, V1414 in domain III and I1706, F1710, Y1717 in domain IV, and the corresponding seven positions in the rat $Na_V1.8$ channel. The alanine mutations were chosen at these positions, as they correspond to positions found in other Na_V channel subtypes that alter the functional properties and where a number of drugs have been found to act.

3.2 Results

3.2.1 Preparation of human $Na_V1.8$ cRNA

The cDNA encoding the human $Na_V1.8$ channel was in the pSP64T *Xenopus* oocyte expression vector. The human $Na_V1.8$ channel sequence was flanked either side by globin gene sequences in the pSP64T vector, which has been shown to increase the stability of the injected cRNA (Krieg and Melton, 1984). A prominent band was observed by agarose gel electrophoresis of the pSP64T-h$Na_V1.8$ plasmid DNA, corresponding to the supercoiled DNA (Fig. 3.1A, lane 2) The pSP64T-h$Na_V1.8$ plasmid DNA was linearised by cutting once in the vector sequence using the *Sal*I enzyme. Agarose gel electrophoresis (Fig. 3.1A; lane 3) shows

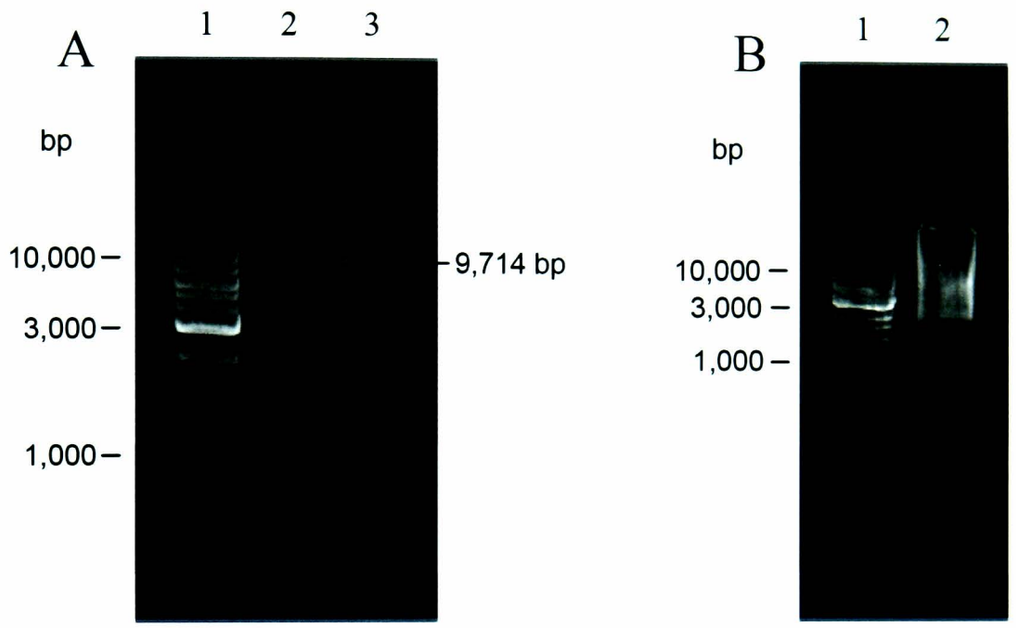

Fig. 3.1. Preparation of human $Na_V1.8$ cRNA. A) An agarose gel showing the circular and linearised pSP64T-$hNa_V1.8$ DNA. Lane 1 contains the 1 Kb DNA ladder, lane 2 contains the undigested pSP64T-$hNa_V1.8$ plasmid DNA and lane 3 contain the pSP64T-$hNa_V1.8$ plasmid DNA linearised with *Sal*I (9,714bp). **B)** An agarose gel showing the cRNA preparation. Lane 1 contains the 1 Kb DNA ladder, lane 2 contains the $hNa_V1.8$ cRNA.

the presence of a 9.7kb fragment corresponding to the linearised plasmid DNA. The linearised DNA was purified to RNA grade and human $Na_V1.8$ cRNA was synthesised *in vitro* using SP6 polymerase (see *Section 2.2.6*). The presence of RNA can been seen from agarose gel electrophoresis (Fig. 3.1B, lane 2). The cRNA concentration was estimated from the band intensity as 125ng/μl, which is sufficient for injection in oocytes.

3.2.2 Subcloning of rNa$_V$1.8 into the pFastBacMam1 vector

Here the cDNA encoding the rat $Na_V1.8$ channel was subcloned into the pFastBacMam1 vector. This vector enables a number of possible means for expressing channels in a mammalian cell line. In addition to ampicillin and gentamicin antibiotic resistance genes, the pFastBacMam1 vector (Condreay et al., 1999) enables transient or stable expression of $Na_V1.8$ in mammalian cells or the generation of baculovirus for the transduction of mammalian cell lines. In addition, it is important that both the human and rat $Na_V1.8$ channels are in the same vector to reduce variation between experiments.

The pFastBacMam1 vector multiple cloning site contains single recognition site for *Xba*I and *Not*I restriction enzymes. The $rNa_V1.8$ channel cDNA was subcloned into the pFastBacMam1 vector using the procedure shown in Figure 2.2. The pFastBacMam1 vector was first cut once using the *Xba*I enzyme and then purified. Agarose gel electrophoresis (Fig. 3.2A; lanes 2 and 3) shows the presence of a 7.4kb fragment corresponding to the linearised vector. The sticky ends were blunted with *Pfu* DNA polymerase, the DNA was purified and cut a second time with the *Not*I enzyme, and then the vector was dephosphorylated. In order to isolate the 7,4kb vector from the small 18bp fragment, the DNA was visualised on an agarose gel (Fig. 3.2B; lane 3), and the large fragment was gel extracted.

For the cDNA encoding the $rNa_V1.8$ channel, the cDNA must first be removed from the pCIN5 vector. The pCIN5-$rNa_V1.8$ construct contains single recognition sites for the *Hpa*I and *Not*I enzymes flanking the 3' and 5' of the $rNa_V1.8$ insert, respectively. The plasmid DNA was first restricted with the *Hpa*I enzyme and then purified. The presence of a 10.8kb band (Fig. 3.2C; lanes 2 and 3) indicates that the pCIN5-$rNa_V1.8$ plasmid DNA was linearised. Restriction enzyme *Not*I was used to cut the pCIN5-$rNa_V1.8$ DNA a second time and the preparation was purified after restriction. The 5,9kb fragment corresponding to the $rNa_V1.8$ insert was gel extracted (Fig. 3.2D; lane 2).

Following ligation of the insert and vector, the pFastBacMam1-$rNa_V1.8$ DNA was transformed into *E. coli* Stbl2 competent cells for the mini-prep for small-scale preparation of plasmid DNA. A subsequent large-scale grow up in duplicate achieved greater yields (200 to 2000μg) after maxi-prep extraction. A prominent band was observed by agarose gel

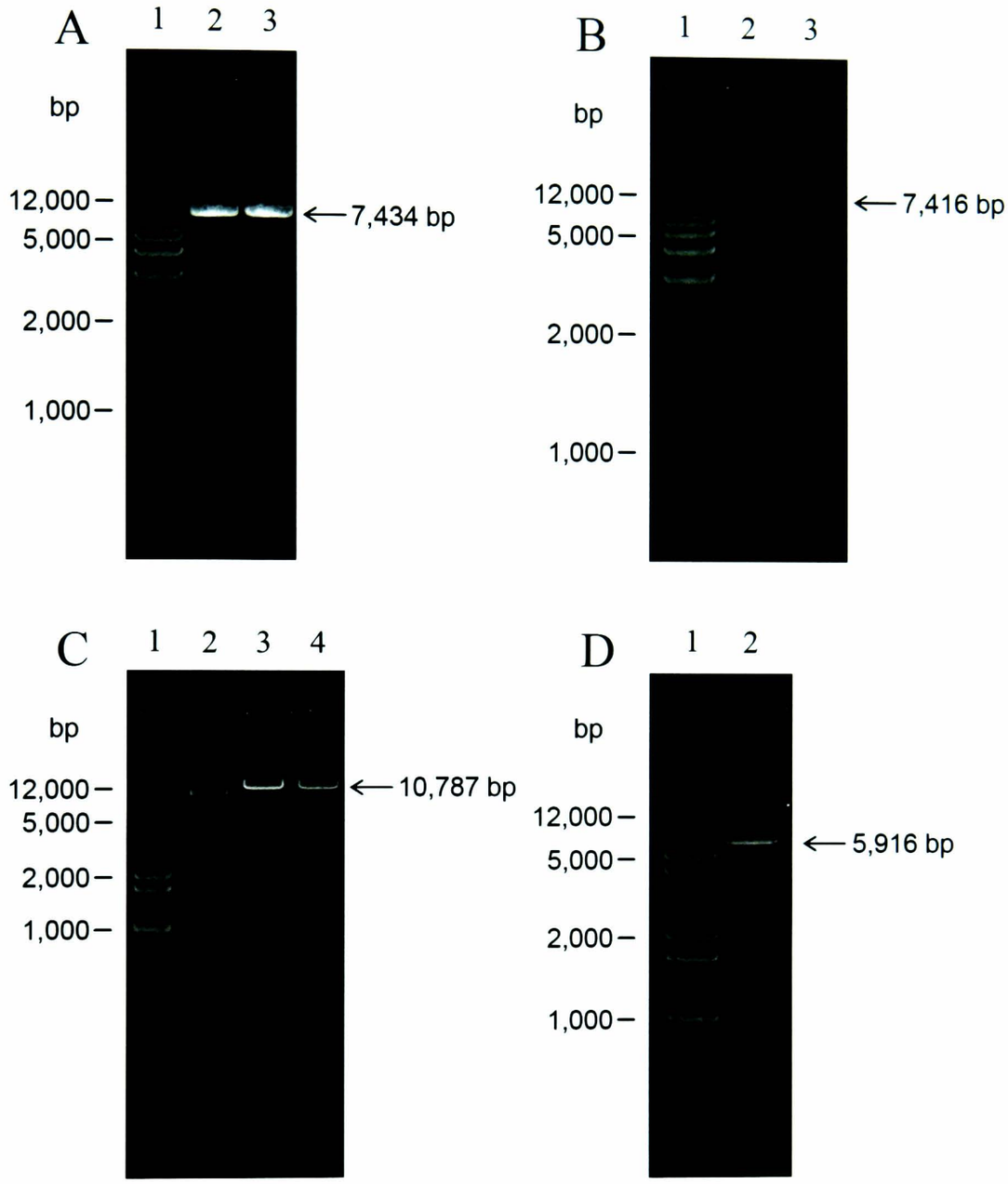

Fig. 3.2. Digestion of the pFastBacMam1 vector and the pCIN5-rNa$_V$1.8 plasmid. A) An agarose gel showing the pFastBacMam1 vector following *Xba*I digestion and purification. Lane 1 contains the Track-It 1 Kb Plus DNA ladder, lanes 2 and 3 contain the linearised vector (7434bp). **B)** An agarose gel showing the *Xba*I linearised and *Pfu* blunted pFastBacMam1 vector following *Not*I digestion. Lane 1 contains the Track-It 1 Kb Plus DNA ladder, lanes 2 and 3 contain the double cut vector (7416bp). The band is very faint in lane 2. **C)** An agarose gel showing the pCIN5-rNa$_V$1.8 plasmid following *Hpa*I digestion and purification. Lane 1 contains the Track-It 1 Kb Plus DNA ladder, lane 2 contains the undigested plasmid, and lanes 3 and 4 contain the linearised plasmid (10787bp). **D)** An agarose gel showing the *Hpa*I linearised and *Pfu* blunted pCIN5-rNa$_V$1.8 plasmid following *Not*I digestion. Lane 1 contains the Track-It 1 Kb Plus DNA ladder and lane 2 contains the double cut plasmid, where the 5916bp band represents the rNa$_V$1.8 insert.

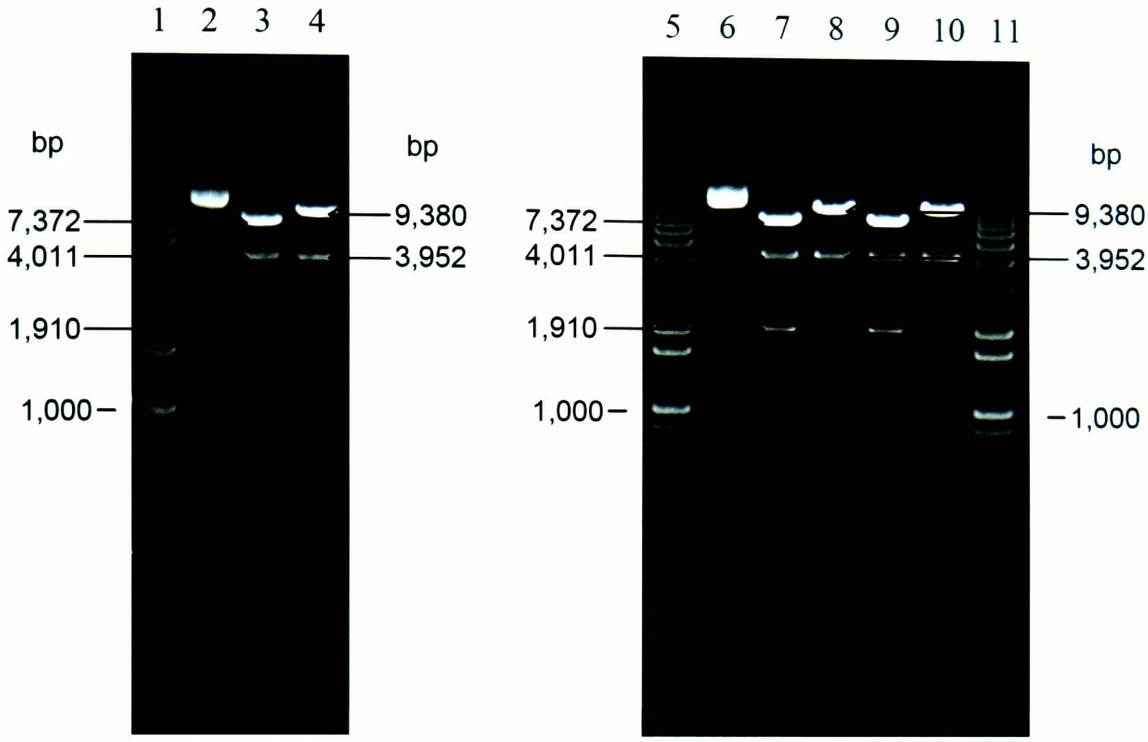

Fig. 3.3. Restriction of ligated pFastBacMam1-rNa$_V$1.8 DNA. Agarose gels are shown the ligated pFastBacMam1-rNa$_V$1.8 plasmid following double restriction with *Eco*RI and *Kpn*I or *Sal*I and *Not*I. Lanes 1, 5 and 11 contain the Track-It 1 Kb Plus DNA ladder, lanes 2 and 6 contain the undigested pFastBacMam1-rNa$_V$1.8 plasmid (samples 1 and 2 respectively). Lanes 3, 7 and 9 contain the plasmid double digest by *Eco*RI and *Kpn*I (7372, 4011 and 1910bp fragments) for samples 1, 2 and 3 respectively. Lanes 4, 8 and 10 contain the plasmid double digest by *Sal*I and *Not*I (9380 and 3952bp fragments) for samples 1, 2 and 3 respectively.

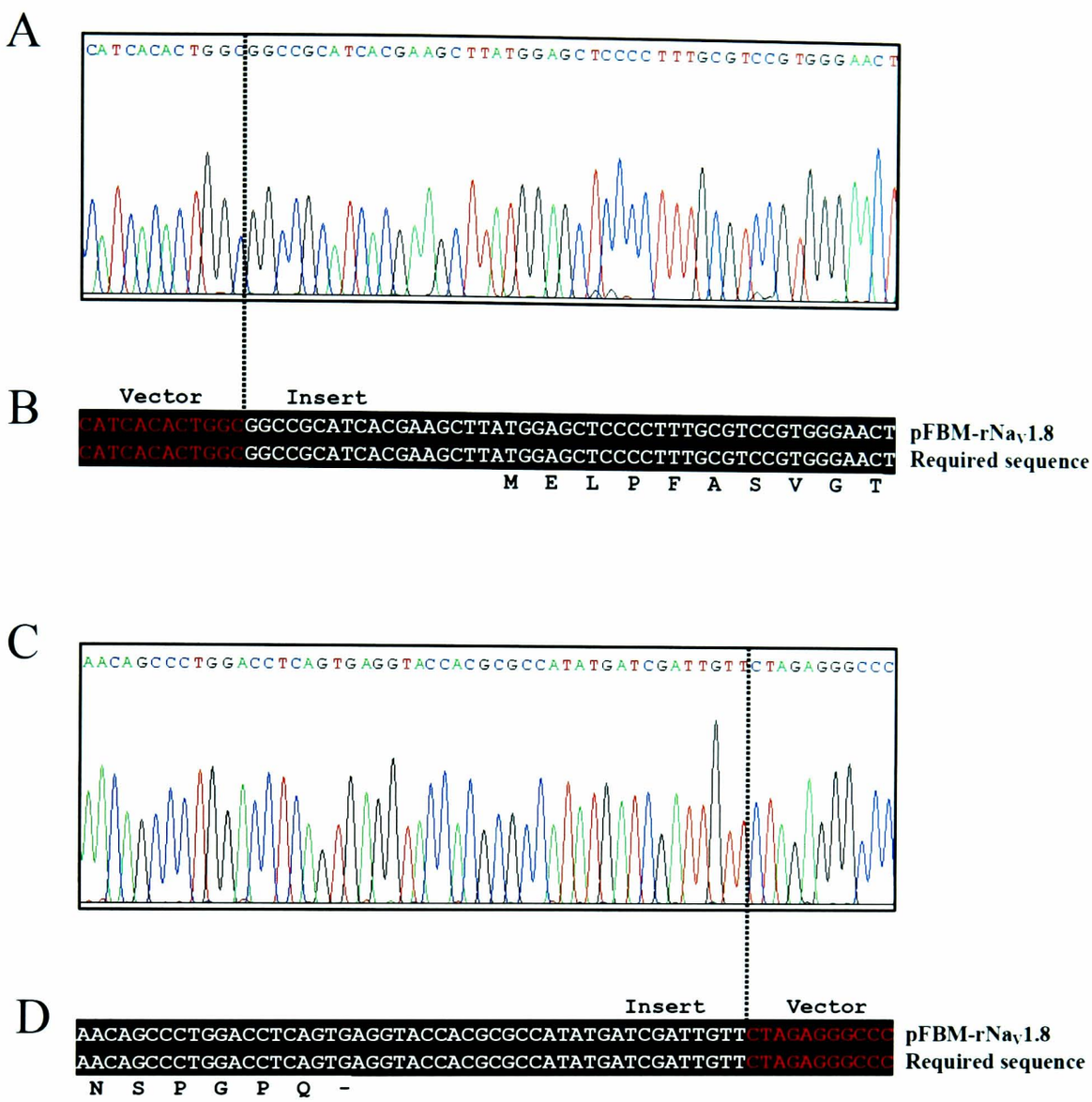

Fig. 3.4. Sequencing of pFastBacMam1-rNa$_V$1.8 plasmid DNA. A) An electrophoretogram is shown for the pFastBacMam1-rNa$_V$1.8 construct (sample 3) at the interface between the vector ('3 end) and insert (5' end). **B)** The sequence alignment is shown for the pFastBacMam1-rNa$_V$1.8 construct (sample 3) corresponding to the bases in A. **C)** An electrophoretogram is shown for the pFastBacMam1-rNa$_V$1.8 construct (sample 3) at the interface between the vector (5') and insert (3'). **D)** The sequence alignment is shown for the pFastBacMam1-rNa$_V$1.8 sequence (sample 3) corresponding to the bases shown in C. For C and D, it can been seen that the pFastBacMam1-rNa$_V$1.8 construct (sample 3) is identical to the required sequence. The amino acid residues are also shown. Sequences were aligned using ClustalW and visualised using BoxShade.

electrophoresis, corresponding to the supercoiled DNA (Fig. 3.3B; lane 2). Restriction digest of the pFastBacMam1-rNa$_V$1.8 plasmid DNA was carried out using *Eco*RI and *Kpn*I or *Sal*I and *Not*I. These restriction enzymes were chosen so that both the vector and insert were cut to give fragments with a range of sizes (see Figure 2.3B). The agarose gels for *Eco*RI and *Kpn*I (Fig 3.3; lanes 3, 7 and 9) gave bands of the expected sizes (7.4kb, 4.0kb and 1.9kb). Furthermore, restriction with *Sal*I and *Not*I (Fig 3.3; lanes 4, 8 and 10) also gave bands of the expected sizes (9.4kb and 4.0kb). These restriction digests therefore indicate that the pFastBacMam1-rNa$_V$1.8 channel DNA has been inserted into the plasmid. In order to further confirm that there were no rearrangements or deletions in the cDNA encoding the rNa$_V$1.8 channel, the entire insert was sequenced. The sequence correctly matched the known rNa$_V$1.8 sequence, and the 5' end of the insert joined the vector with the predicted sequence (Fig. 3.4A,B), as did the 3' end of the insert (Fig. 3.4C,D). Therefore, the cDNA encoding the rNa$_V$1.8 channel was successfully subcloned into the pFastBacMam1 vector (Fig. 2.3).

3.2.3 Generation of rat and human Na$_V$1.8 channel mutations

While the mutagenesis of sodium channels is normally carried out in a small DNA plasmid, and then subcloned back into the expression vector, here it was necessary to keep manipulations of the Na$_V$1.8 channel DNA to a minimum. Thus, site-directed mutagenesis was carried out in the pFastBacMam1 vector. However, due to the size of the plasmid DNA (13kb), certain conditions were required. Site-directed mutagenesis was carried out with the *PfuTurbo*® DNA polymerase, which has a lower error rate than *Taq* DNA polymerase, and requires shorter DNA extension times, fewer thermal cycles, and lower DNA template concentrations than *Pfu* DNA polymerase. The properties of the DNA polymerase reduce the potential for random mutations. For the mutagenic oligonucleotide primers it was expected that longer mutagenic primers would be necessary to prevent unspecific binding. However, they resulted in very few, if any viable colonies; thus, shorter (23-27 bases) mutagenic primers were used despite a reduced mutagenesis efficiency. For the transformation of the DNA it was important to use recombination-deficient competent cells (Stbl2 or XL10-Gold cells), which show high transformation rates ($\geq 5 \times 10^9$ cfu/μg). Finally, the competent cells were incubated at a reduced temperature of 28°C, in order to reduce the likelihood of recombination events. The mutated DNA was checked by restriction with at least two enzymes and visualised on an agarose gel, and when a sufficient volume of DNA had been prepared the entire rNa$_V$1.8 cDNA was sequenced.

Following site-directed mutagenesis of human and rat Na$_V$1.8 channels, the plasmid DNA was extracted by mini-prep, and purified from 8 to 10 cultures of transformed single *E. coli*

colonies. Sequencing of the mutated region with a single sequencing primer, showed a mutagenesis efficiency of approximately 50%. It is noteworthy that generation of the N1411 mutation in $hNa_V1.8$ or the corresponding mutation in $rNa_V1.8$ was not successful. For each successful mutation, two of the correct DNA preparations were extracted by maxi-prep, and visualised by agarose gel electrophoresis (for $rNa_V1.8$, Figs. 3.5 and 3.6; for $hNa_V1.8$, Figs. 3.7). The gels indicate that undigested DNA was of a sufficient concentration (200 to 500μg/μl), and supercoiled DNA showed a prominent band in all samples (for $rNa_V1.8$, Figs. 3.5 and 3.6; not all shown for $hNa_V1.8$). For rat $Na_V1.8$ mutant preparations, restriction of plasmid DNA with *Eco*RI and *Kpn*I showed 7.4kb, 4.1kb and 1.9kp bands for all mutations, as expected for the pFastBacMam1-$rNa_V1.8$ channel (Fig. 2.3, Figs. 3.5 and 3.6). This was further supported by the restriction of a number of mutations I380A, N389A, I1707A, F1711A and Y1718A with *Eco*RI and *Sac*II enzymes, with 7.5kb, 4.0kb and 1.8kb bands (Fig 3.5). For human $Na_V1.8$ mutant preparations, restriction of plasmid DNA with *Sma*I and *Sac*II showed 6.0kb, 4.4kb and 2.9kb bands for mutation I381A as expected (Fig. 3.7A). Restriction by *Xba*I and *Nhe*I showed 7.7kb and 4.7kb bands for N390A, L1410A, V1414A, I1706A, F1710A and Y1717A preparations, as expected for the pFastBacMam1-$hNa_V1.8$ channel (Fig. 2.3, Fig. 3.7). The *Xba*I and *Nhe*I restriction of L1410A (sample 1, lane 5) was incomplete. These results suggest that large rearrangements or deletions did not occur in the preparations corresponding to the mutated pFastBacMam1-$rNa_V1.8$ and pFastBacMam1-$hNa_V1.8$ channel DNA plasmids. Thus the DNA was of a sufficient quality and quantity for sequencing of the entire human and rat $Na_V1.8$ channel encoding sequence.

Sequencing of the entire insert confirmed that the correct mutations in the human and rat $Na_V1.8$ channel DNA were present (Figs. 3.8 to 3.11), while the remainder of the sequences were confirmed as identical to the wild type channel sequence. Indeed, the entire cDNAs encoding rat $Na_V1.8$ mutations I380A sample 2, N389A sample 2, L1411A sample 1, V1415A samples 1 and 2, I1707A samples 1 and 2, F1711A samples 1 and 2, and Y1718A sample 1 were correct (the mutated region is shown in Figures 3.8 and 3.9). Furthermore, the entire cDNA encoding human $Na_V1.8$ mutations I381A samples 1 and 2, N390A samples 1 and 2, L1410A sample 1 and 2, V1414A samples 1 and 2, I1706A sample 1, F1710A samples 1 and 2, and Y1717A samples 1 and 2 were correct (the mutated region is shown in Figures 3.10 and 3.11). The translated protein sequence (Figs. 3.8 to 3.11) of the successful DNA preparations confirm that the seven key amino acid S6 residues were substituted to alanine in both human and rat $Na_V1.8$ channels.

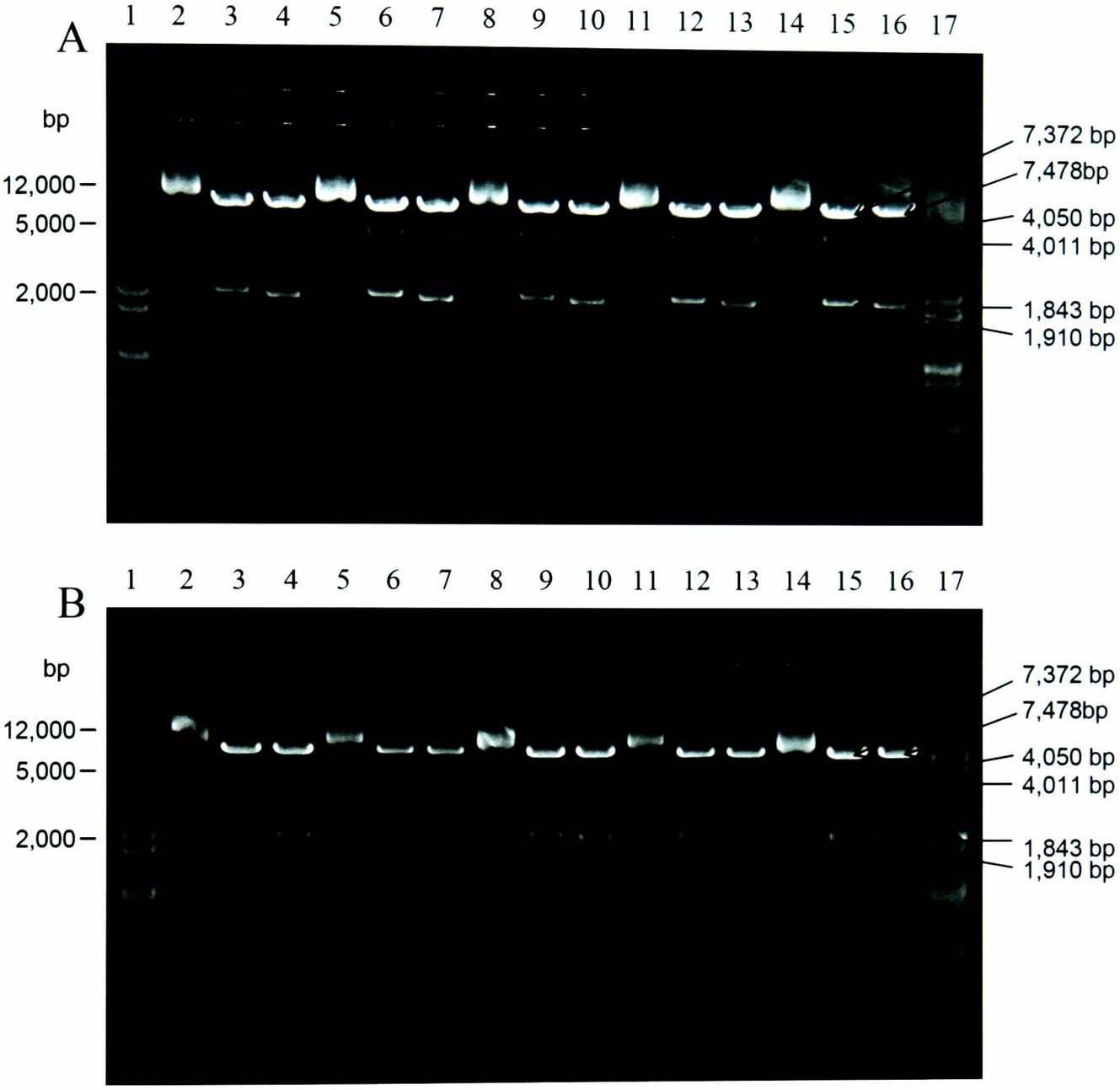

Fig. 3.5. Restriction of pFastBacMam1-rNa$_V$1.8 mutant plasmids. The agarose gels show the pFastBacMam1-rNa$_V$1.8 mutant DNA undigested (U) and double restriction by *Kpn*I and *Eco*RI (KE) or *Eco*RI and *Sac*II (ES). Lanes 1 and 17 contain the Track-It 1 Kb Plus DNA ladder in both agarose gels. **A)** The agarose gel shows I380A sample 1 (lane 2, U; lane 3, KE; lane 4, ES), I380A sample 2 (lane 5, U; lane 6, KE; lane 7, ES), N389A sample 1 (lane 8, U; lane 9, KE; lane 10, ES), N389A sample 2 (lane 11, U; lane 12, KE; lane 13, ES), I1707A sample 1 (lane 14, U; lane 15, KE; lane 16, ES). **B)** The agarose gel shows I1707A sample 2 (lane 2, U; lane 3, KE; lane 4, ES), F1711A sample 1 (lane 5, U; lane 6, KE; lane 7, ES), F1711A sample 2 (lane 8, U; lane 9, KE; lane 10, ES), Y1718A sample 1 (lane 11, U; lane 12, KE; lane 13, ES), Y1718A sample 2 (lane 14, U; lane 15, KE; lane 16, ES). The KpnI and EcoRI (KE) digests show 7372, 4050 and 1910bp fragments, and the EcoRI and SacII (ES) digests show 7478, 4011 and 1843bp fragments.

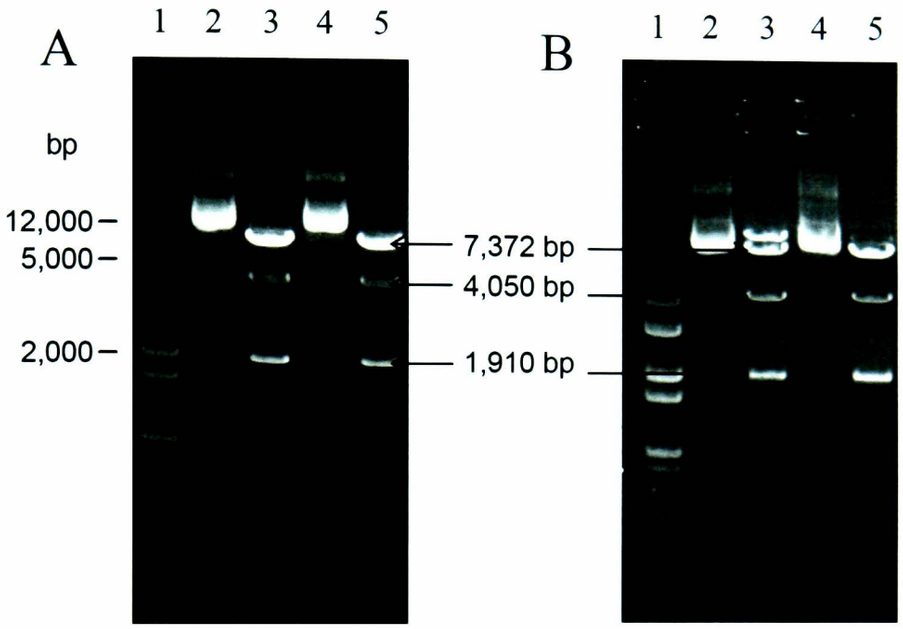

Fig. 3.6. Restriction of pFastBacMam1-rNa$_V$1.8 mutant plasmids. The agarose gels show the pFastBacMam1-rNa$_V$1.8 mutant DNA undigested (U), and double restricted by *Kpn*I and *Eco*RI (KE). Lane 1 in both agarose gels contains the Track-It 1 Kb Plus DNA ladder. **A)** The agarose gel shows L1411A sample 1 (lane 2, U; lane 3, KE), L1411A sample 2 (lane 4, U; lane 5, KE). **B)** The agarose gel shows V1415A sample 1 (lane 2, U; lane 3, KE), V1415A sample 2 (lane 4, U; lane 5, KE). The *Kpn*I and *Eco*RI (KE) digests show 7372, 4050 and 1910bp fragments.

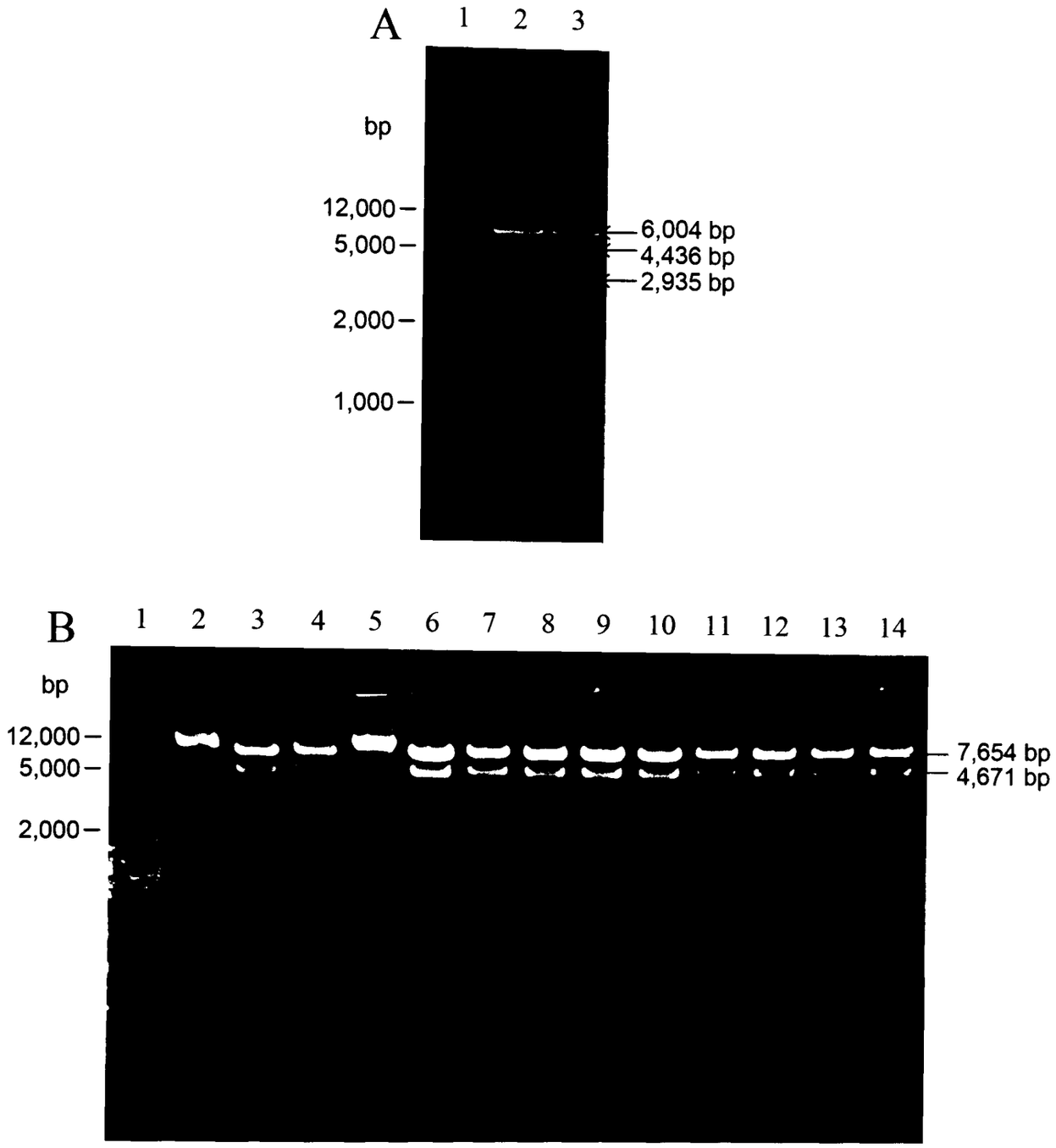

Fig. 3.7. Restriction of pFastBacMam1-hNa$_V$1.8 mutant plasmids. A) Lane 1 contains the Track-It 1 Kb Plus DNA ladder, lane 2 contains I381A sample 1 following double restriction with *Sma*I and *Sac*II and lane 3 contains I381A sample 2 following double restriction with *Sma*I and *Sac*II. The *Sma*I and *Sac*II digests show 6004, 4436 and 2935bp fragments. **B)** Lane 1 contains the Track-It 1 Kb Plus DNA ladder and lane 2 contains an example pFastBacMam1-hNa$_V$1.8 mutant DNA preparation (V1414A sample 1). The agarose gel shows samples following double restriction with *Xba*I and *Nhe*I for N389A sample 1 (lane 3), N389A sample 2 (lane 4), L1410A sample 1 (lane 5), L1410A sample 2 (lane 6), V1414A sample 1 (lane 7), V1414A sample 2 (lane 8), I1706A sample 1 (lane 9), I1706A sample 2 (lane 10), F1710A sample 1 (lane 11), F1710A sample 2 (lane 12), Y1717A sample 1 (lane 13), and Y1717A sample 2 (lane 14). The *Xba*I and *Nhe*I digests show 7654 and 4671bp fragments (the 1050bp fragment is too faint to be seen).

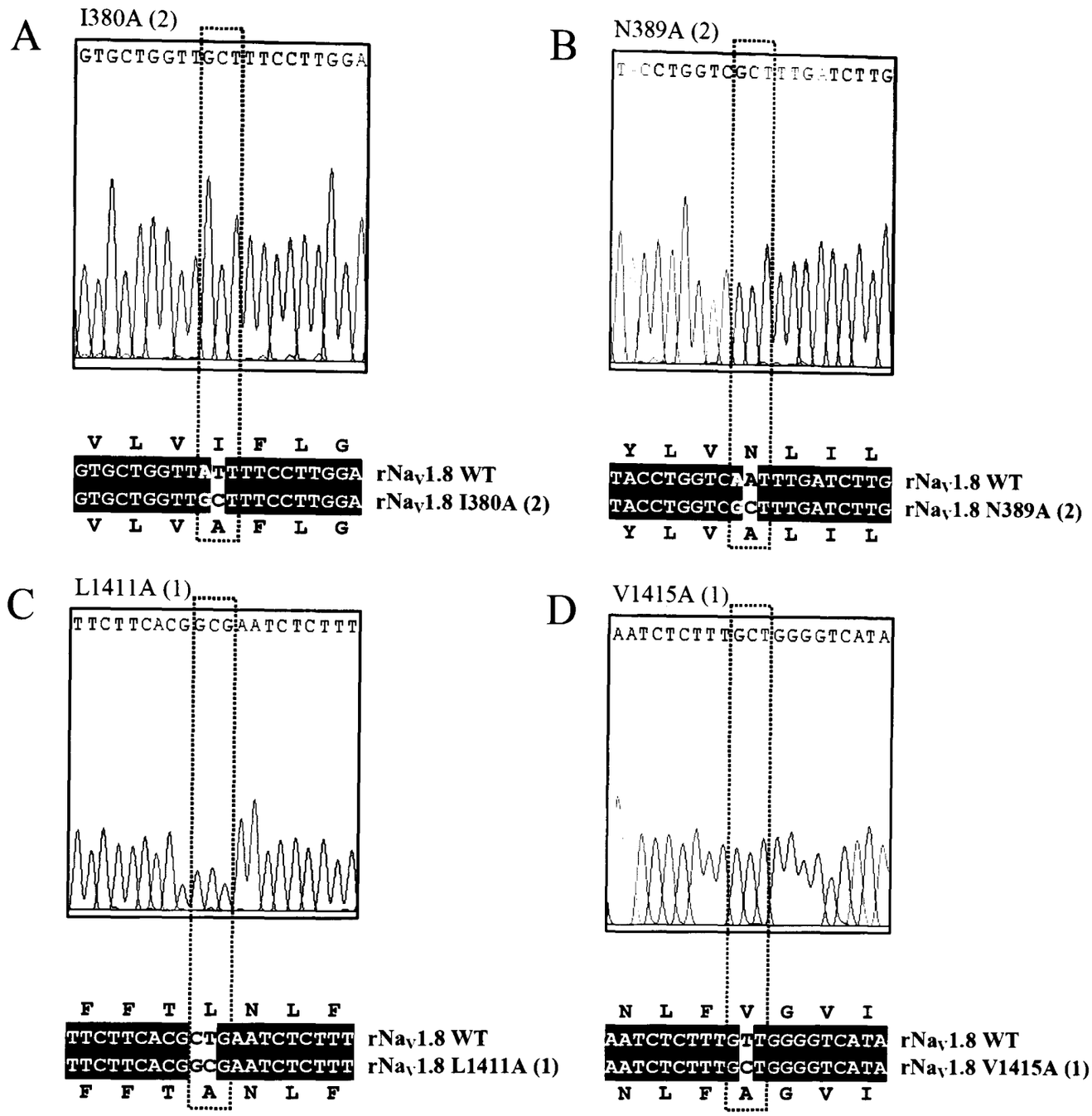

Fig. 3.8. Sequencing of $rNa_V1.8$ mutant DNA. Electrophoretograms are shown for $rNa_V1.8$ alanine mutations with the mutated codon indicated and alignment of mutant and wild type DNA sequences (the relevant codon indicated with a *dotted line* box). **A)** The I380A mutation (sample 2) with the ATT codon changed to GCT. **B)** The N389A mutation (sample 2) with the AAT codon changed to GCT. **C)** The L1411A mutation (sample 1) with the CTG codon changed to GCG. **D)** The V1415A mutation (sample 1) with the GTT codon changed to GCT. The amino acid residues are also shown. Sequences were aligned using ClustalW and visualised using BoxShade.

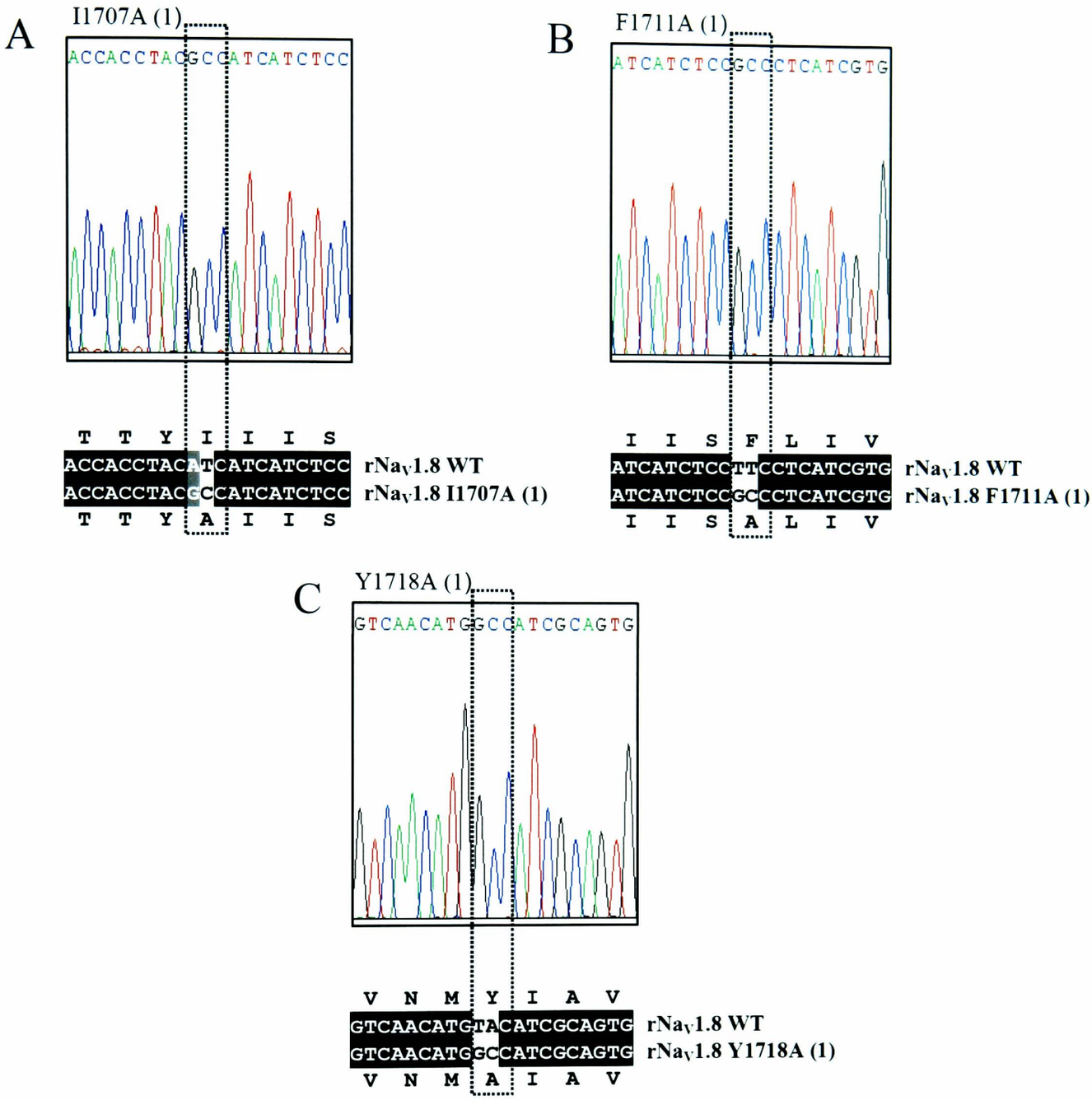

Fig. 3.9. Sequencing of rNa$_V$1.8 mutant DNA. Electrophoretograms are shown for rNa$_V$1.8 alanine mutations with the mutated codon indicated and alignment of mutant and wild type DNA sequences (the relevant codon indicated with a *dotted line* box). **A)** The I1707A mutation (sample 1) with the ATC codon changed to GCC. **B)** The F1711A mutation (sample 1) with the TTC codon changed to GCC. **C)** The Y1718A mutation (sample 1) with the TAC codon changed to GCC. The amino acid residues are also shown. Sequences were aligned using ClustalW and visualised using BoxShade.

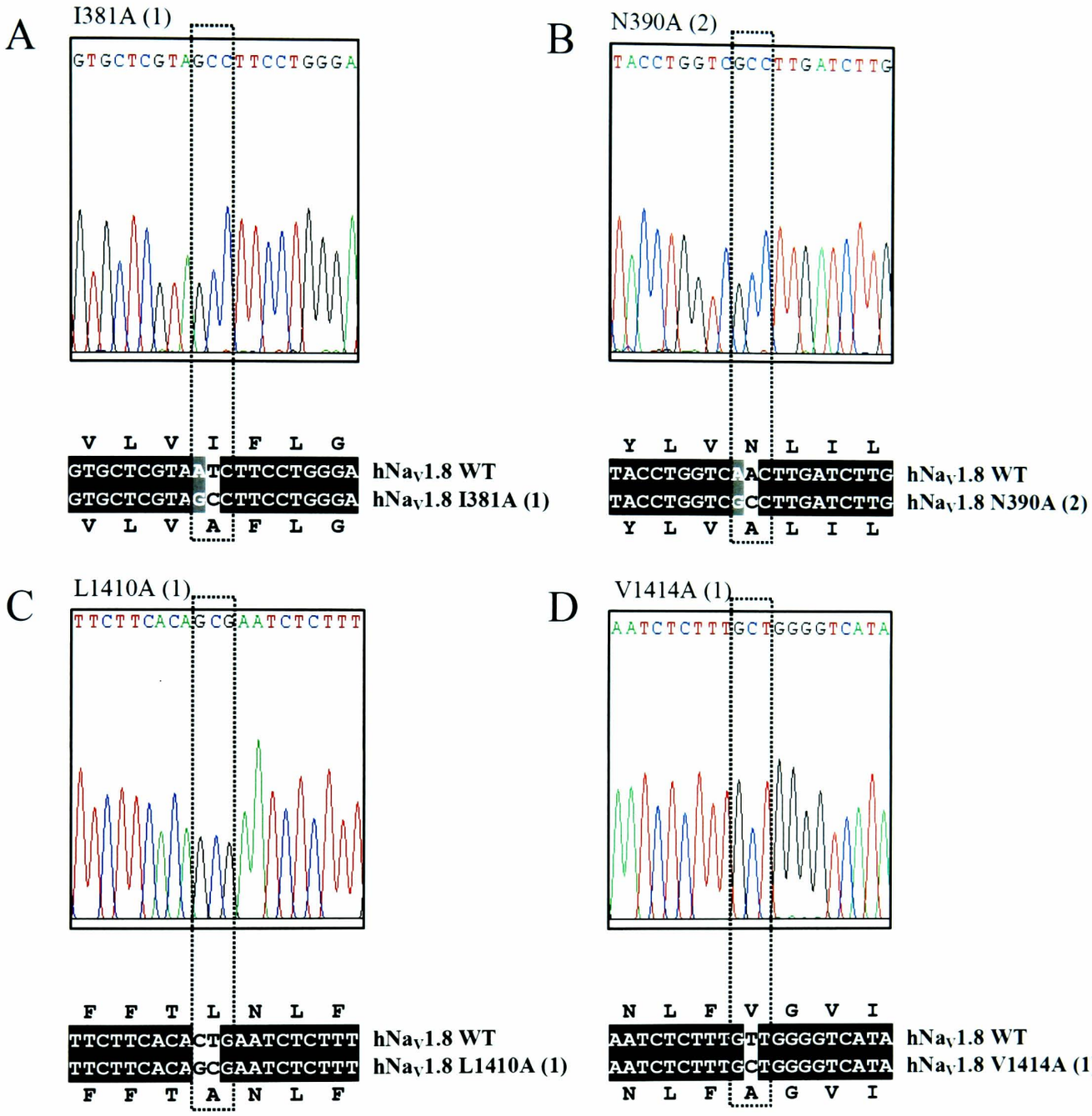

Fig. 3.10. Sequencing of $hNa_V1.8$ mutant DNA. Electrophoretograms are shown for $hNa_V1.8$ alanine mutations with the mutated codon indicated and alignment of mutant and wild type DNA sequences (the relevant codon indicated with a *dotted line* box). **A)** The I381A mutation (sample 1) with the ATC codon changed to GCC. **B)** The N390A mutation (sample 2) with the AAC codon changed to GCC. **C)** The L1410A mutation (sample 1) with the CTG codon changed to GCG. **D)** The V1414A mutation (sample 1) with the GTT codon changed to GCT. The amino acid residues are also shown. Sequences were aligned using ClustalW and visualised using BoxShade.

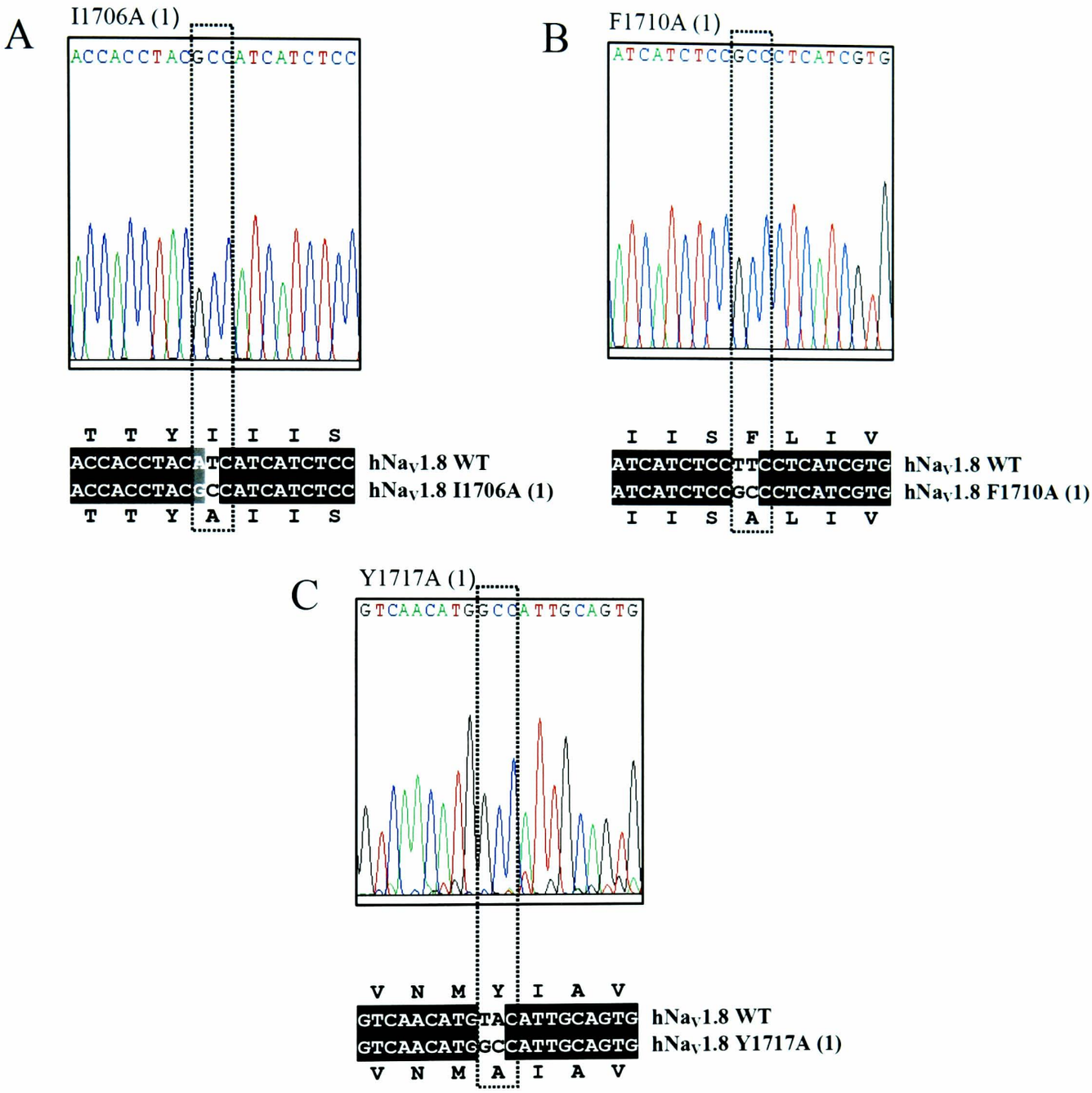

Fig. 3.11. Sequencing of $hNa_V1.8$ mutant DNA. Electrophoretograms are shown for $hNa_V1.8$ alanine mutations with the mutated codon indicated and alignment of mutant and wild type DNA sequences (the relevant codon indicated with a *dotted line* box). **A)** The I1706A mutation (sample 1) with the ATC codon changed to GCC. **B)** The F1710A mutation (sample 1) with the TTC codon changed to GCC. **C)** The Y1717A mutation (sample 1) with the TAC codon changed to GCC. The amino acid residues are also shown. Sequences were aligned using ClustalW and visualised using BoxShade.

3.3 Discussion

In this chapter, the human $Na_V1.8$ channel cRNA was prepared for *Xenopus* oocyte expression. For the expression of $Na_V1.8$ channels in mammalian cells, the rat $Na_V1.8$ channel cDNA was subcloned into the pFastBacMam1 vector, and the codons encoding seven key S6 segment amino acid residues of both cDNAs encoding human and rat $Na_V1.8$ channels were altered to encode alanine.

The instability of cDNA for some ion channels can make manipulation using standard techniques difficult, and heterologous expression of some can also prove challenging. The cDNA encoding the rat $Na_V1.8$ channel was subcloned into the pFastBacMam1 vector for consistency of experiments, since the human $Na_V1.8$ channel cDNA was already in the pFastBacMam1 vector. The pFastBacMam1 vector also enables baculovirus transduction of mammalian cells, if the normal transfection methods were shown to be unsuccessful. The $rNa_V1.8$ channel cDNA was removed from the pCIN5 vector using *Hpa*I and *Not*I restriction enzymes, and the vector was prepared by restriction with *Xba*I, *Pfu* DNA polymerase blunting, and restriction with *Not*I. The $rNa_V1.8$ insert was ligated to the dephosphorylated pFastBacMam1 vector and the construct was checked for recombination or deletions. Multiple restriction digests showed that the plasmid DNA contained the expected band sizes for restriction of the pFastBacMam1-$rNa_V1.8$ construct. Furthermore, sequencing of the entire $rNa_V1.8$ insert and the vector ends showed that the sequence matched the predicted sequence. Thus this strategy was successful in generating the pFastBacMam1-$rNa_V1.8$ construct for expression of the $rNa_V1.8$ channel in mammalian cell lines.

A number of S6 segment amino acid residues are known to play an important role in the functional and pharmacological properties of voltage-gated Na^+ channels. Owing to the difficulties in manipulating and expressing the $Na_V1.8$ channel, the corresponding residues are yet to be investigated. In previous studies, site-directed mutagenesis of voltage-gated sodium channel cDNA was carried out in a small DNA plasmid, and the mutated cDNA is subsequently subcloned into the larger expression vector (Ragsdale et al. 1994; Yarov-Yarovoy et al., 2001; Yarov-Yarovoy et al., 2002). However, in order to reduce the number of manipulations of $Na_V1.8$ channel cDNA, site-directed mutagenesis was carried out directly in the expression vector. Here site-directed mutagenesis was used to generate mutations I380A, N389A, L1411A, V1415A, I1707A, F1711A and Y1718A in the rat $Na_V1.8$ channel and the corresponding I381A, N390A, L1410A, V1414A, I1706A, F1710A and Y1717A mutations in the human $Na_V1.8$ channel. Multiple restriction digests of both the human and rat $Na_V1.8$ channel mutant DNA showed bands of expected size for the 13kb plasmids cut at their respective restriction sites. Sequencing of the entire mutant cDNA confirmed that the mutagenesis was successful and the human and rat $Na_V1.8$ cDNAs did not contain random mutation. Therefore, the use of a high-

fidelity DNA polymerase and low thermal cycle numbers, in combination with recombination-deficient competent *E. coli* cells with high transformation efficiency propagated at reduced temperatures enabled the generation of point mutation in the $Na_V1.8$ channel cDNA. Overall, these results show seven key S6 segment mutations were successfully generated in the human and rat $Na_V1.8$ channel cDNAs, both in the pFastBacMam1 vector.

CHAPTER 4

FUNCTIONAL PROPERTIES OF HUMAN AND RAT $Na_V1.8$ SODIUM CHANNELS

4.1 Introduction

The $Na_V1.8$ channel has distinct functional properties compared to other voltage-gated Na^+ channel subtypes. It shows slower gating kinetics, more depolarised voltage-dependent gating properties, more pronounced slow inactivation, and slower recovery from slow inactivation (Akopian et al., 1996; Blair and Bean, 2003; Elliott and Elliott, 1993; Leffler et al., 2007; Sangameswaran et al., 1996). The human and rat forms of the $Na_V1.8$ channel are highly homologous; showing 83% identity (Fig. 4.1). Owing to difficulties with the expression of the $Na_V1.8$ channel, the comparison of the functional properties of the human and rat channel forms is not extensive and has only been carried out using the *Xenopus laevis* oocytes (Rabert et al., 1998). Moreover, a direct cross-species comparison of the electrophysiological properties of any voltage-gated Na^+ channel subtype is yet to be carried out under the same experimental conditions in the same mammalian background. It can not be assumed that the functional properties and roles of closely related orthologues are conserved across species. Indeed, the expression of the human form of the $Na_V1.8$ channel has led to the speculation that the human and rat $Na_V1.8$ channels might differ in their inactivation properties (Akiba et al., 2003).

In this chapter, $Na_V1.8$ channel currents were recorded from mammalian sensory-neuron derived ND7/23 cells using whole-cell patch clamp. Using this mammalian system, the activation and inactivation properties of human and rat $Na_V1.8$ channels were analysed and compared in detail. Initial experiments were also carried out using *Xenopus laevis* oocytes expression system and two-electrode voltage clamp, although this did not prove to be a suitable expression system.

4.2 Results

4.2.1 Expression of the human $Na_V1.8$ channel in Xenopus laevis oocytes

The oocytes of the South African clawed frog, *Xenopus laevis*, are used extensively for the expression of recombinant ion channel proteins, due to the ease of manipulation and stability of two-electrode voltage clamp recordings. Following the injection of *Xenopus laevis* oocytes with $hNa_V1.8$ cRNA, the human $Na_V1.8$ channel currents were examined using a test pulse to -90mV to +50mV in 10mV increments from a holding potential of -100mV. Only very small Na^+ currents were observed (Fig. 4.2A); the maximum current amplitude (I_{max}) was -530±140nA at 0mV. The peak Na^+ current elicited at each membrane potential was measured in order to

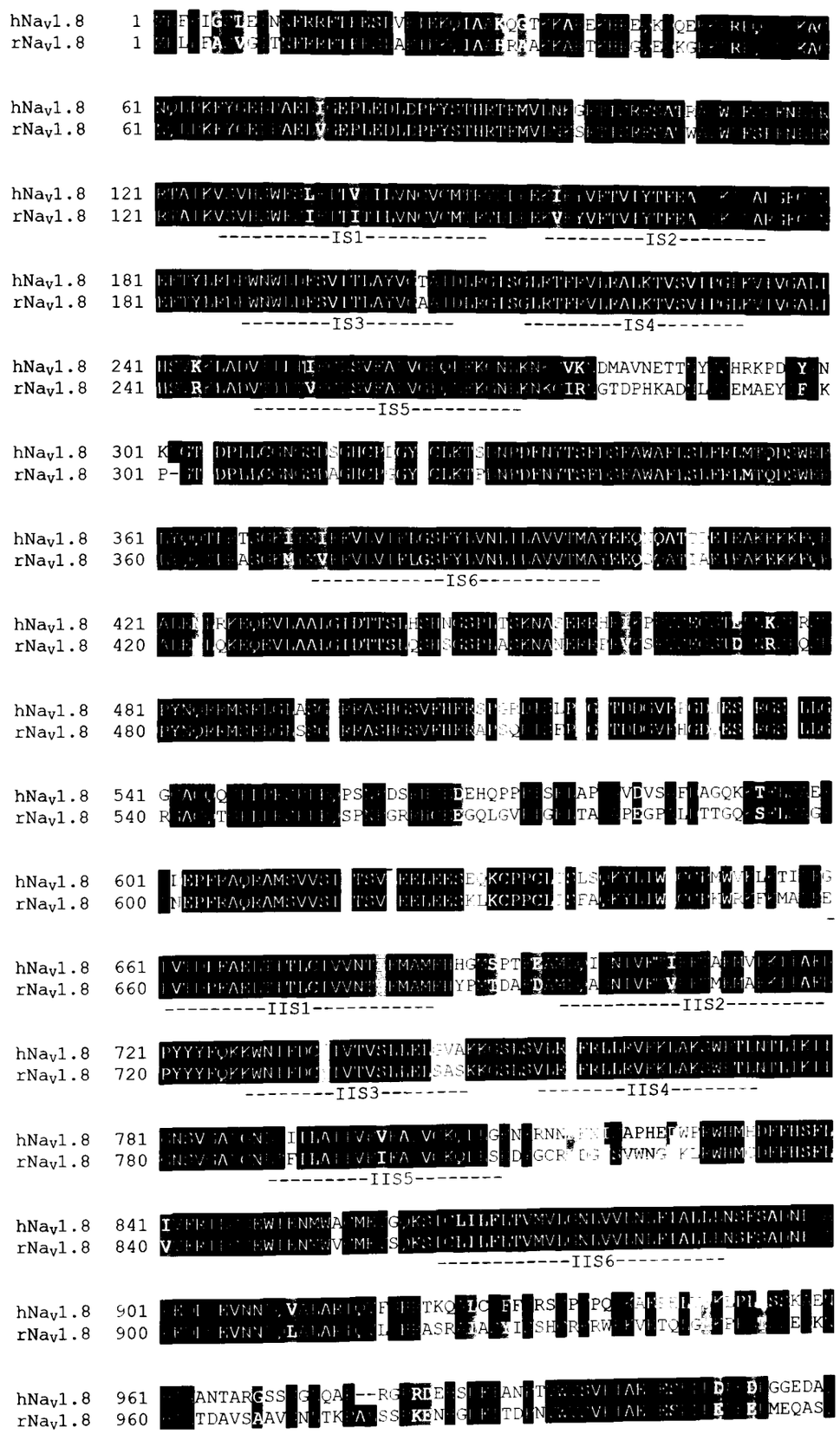
hNav1.8
rNav1.8
IS1
IS2
IS3
IS4
IS5
IS6
IIS1
IIS2
IIS3
IIS4
IIS5
IIS6

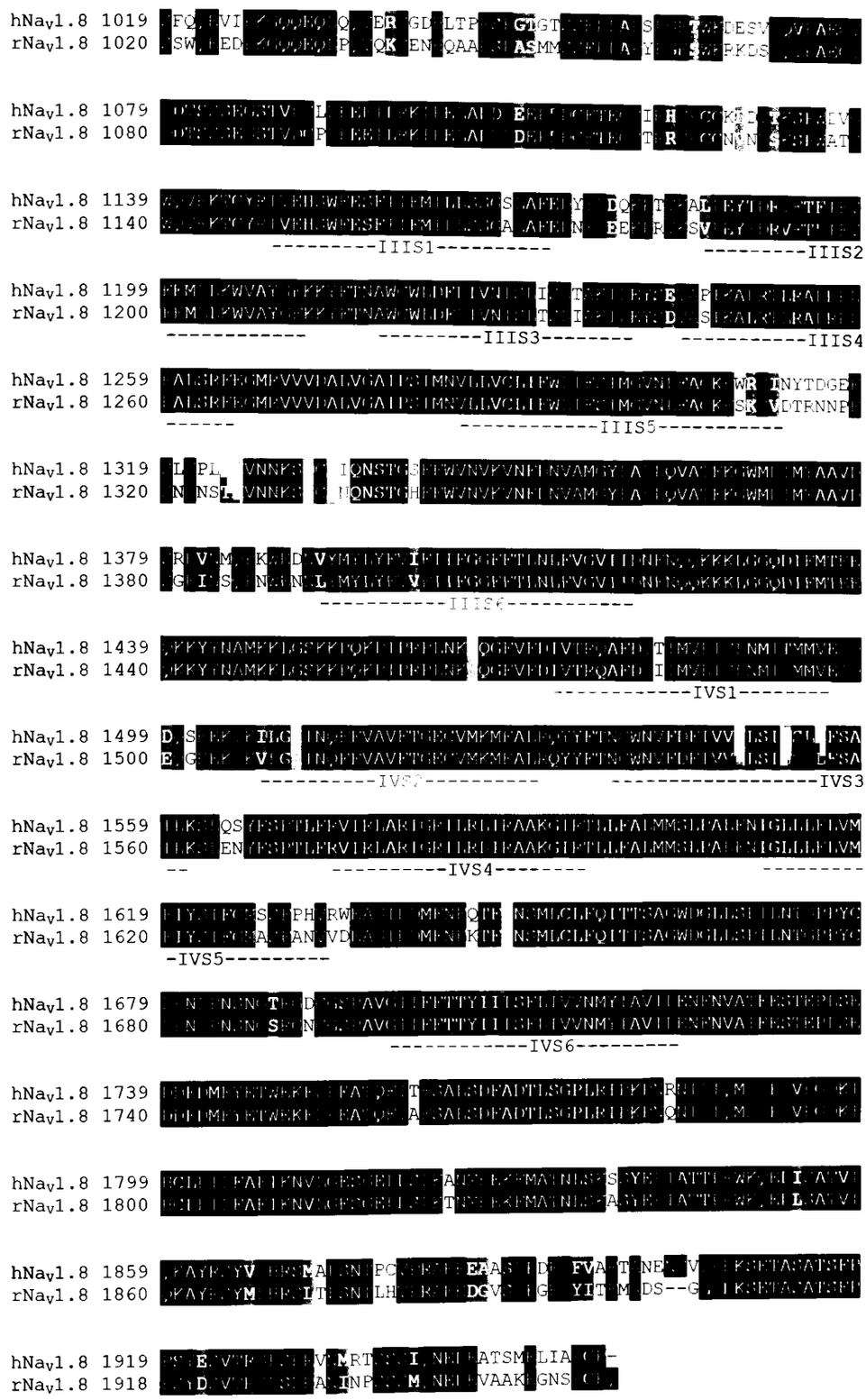

Fig. 4.1. Amino acid sequence alignment of the $hNa_v1.8$ and $rNa_v1.8$ sodium channels. The S1-S6 segments for each domain (I-IV) are labelled. Sequences were aligned using ClustalW and visualised using BoxShade.

construct the *I-V* relationships. Despite the small amplitudes, the currents were significantly larger than for control oocytes injected with water, suggesting that currents in cRNA-injected oocytes are mostly the result of the human $Na_V1.8$ channel (Fig. 4.2B). However, the expression of human $Na_V1.8$ channel varied greatly between oocytes, and only 5 out of 38 oocytes showed I_{max} >200nA. Since currents were small and showed appreciable noise, detailed analysis was difficult. The current-voltage relationship (Fig. 4.2B) shows that the voltage for maximum current was at approximately 0mV, and the reversal potential (E_{rev}) was 43±8mV (n=5). The conductance-voltage relationship for the human $Na_V1.8$ channel expressed in oocytes showed a voltage for half-maximal activation ($V_{1/2}$) of 6±12mV, with a slope factor (k) of 19±3mV (n=5).

The poor expression of this mammalian ion channel in an amphibian (oocyte) cell background may be due to the absence of regulatory, accessory or other factors, which are present in the native mammalian cell background. Thus all work in this chapter and thesis was carried out using mammalian ND7/23 cells.

4.2.2 Expression of the human and rat $Na_V1.8$ channels in mammalian ND7/23 cells

The ND7/23 cell line is derived from the fusion of rat DRG neurons with mouse N18Tg2 neuroblastoma cells (Wood et al., 1990). Figure 4.3 shows the morphology of ND7/23 cells and the selection of a single cell by anti-CD8 beads or GFP fluorescence. Since the ND7/23 cell line is derived from sensory neurons it endogenously expresses TTX-sensitive Na^+ currents (Fig. 4.4A,B). Using whole-cell patch clamp, the maximum current amplitude (I_{max}) of endogenous current was -178±24pA/pF (n=8) for untransfected cells and -190±37pA/pF (n=7) for cells co-transfected with both the pFastBacMam1 vector and the GFP-expressing plasmid pEGFP-N1 (for untransfected and transfected controls) (Fig. 4.5). However, in the presence of TTX (200nM), the endogenous TTX-sensitive Na^+ currents were completely inhibited in both untransfected and transfected controls (Fig. 4.4B, Fig. 4.5). Following transient transfection of ND7/23 cells with TTX-resistant $Na_V1.8$ channels, large currents were observed in the presence of TTX (200nM). Cells transfected with the human $Na_V1.8$ channel showed a maximum current amplitude of -79±7pA/pF (n=80) (Fig. 4.4C, Fig. 4.5), which was not significantly different to the rat $Na_V1.8$ channel current (-74±9pA/pF, n=57) (Fig. 4.4D, Fig. 4.5). The native TTX-resistant Na^+ currents recorded by Elliott and Elliott (1993) are shown in Fig. 4.4F. Overall, these results show that transient transfection of the mammalian cell line, ND7/23, is sufficient for the expression of both human and rat $Na_V1.8$ channels after endogenous Na^+ currents are completely inhibited in the presence of TTX (200nM). Moreover, co-transfection with β-subunits is not necessary since the ND7/23 cell line endogenously expresses β_1 and β_3 subunits (John et al., 2004).

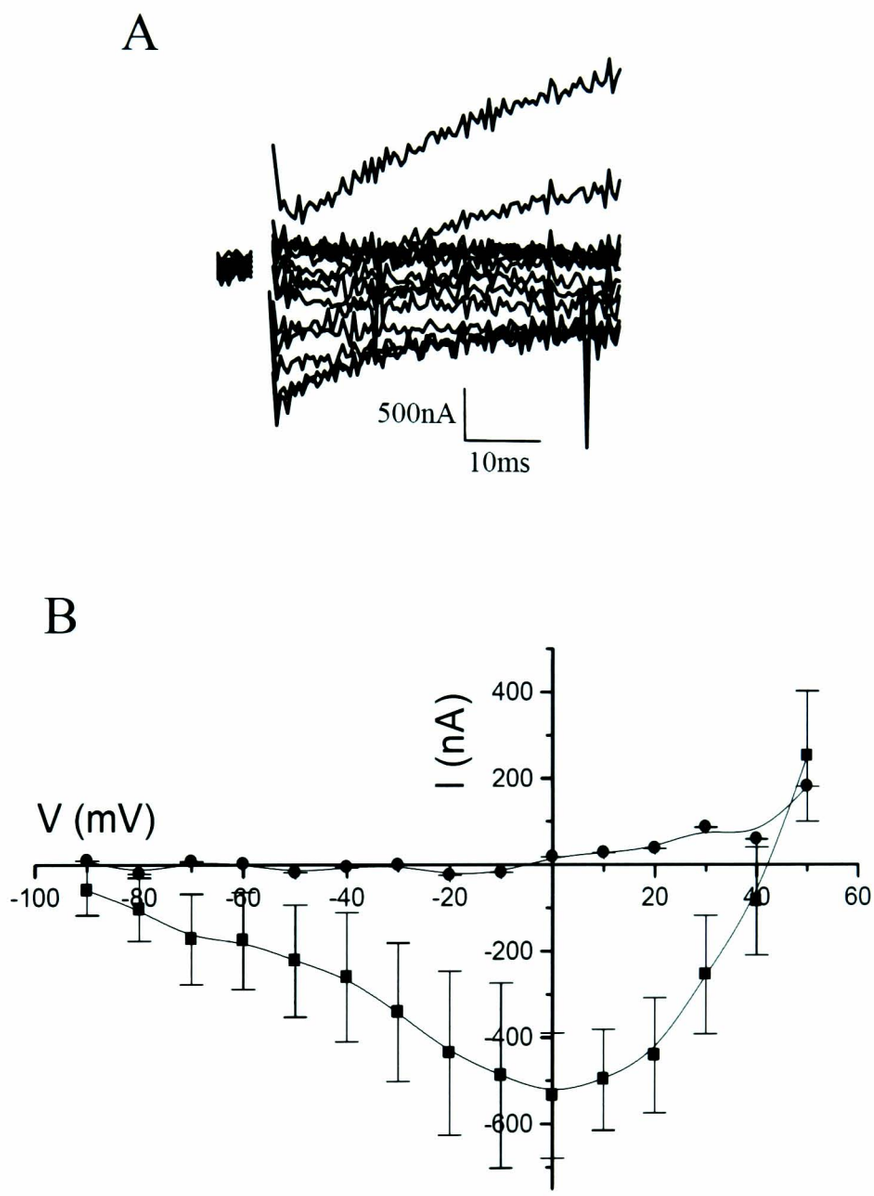

Fig. 4.2. Functional expression of human $Na_V1.8$ channels in *Xenopus* oocytes. A) An example $hNa_V1.8$ channel current trace is shown. Elicited currents were recorded from a holding potential of -100mV using voltage steps to -90mV to 60mV in 10mV increments. **B)** Mean current-voltage relationships of oocytes injected with $hNa_V1.8$ cRNA (■, n=5), and uninjected oocytes (●, n=8). The 5 oocytes that expressed $hNa_V1.8$ channel currents were the only to show >200nA currents out of the 38 oocytes examined.

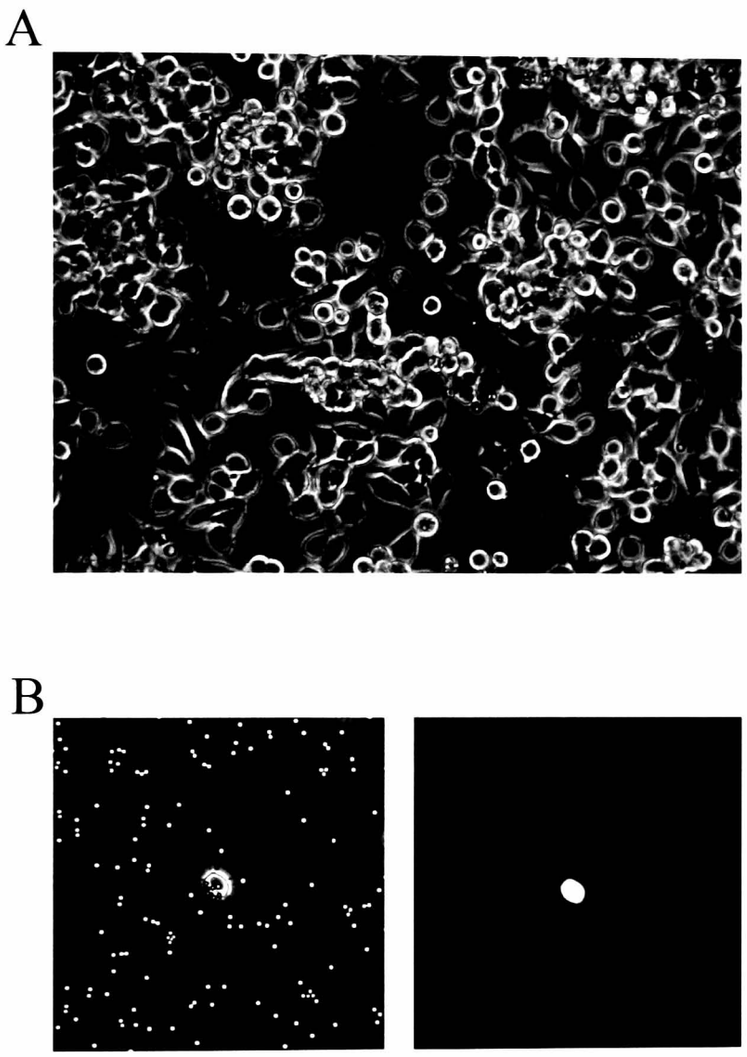

Fig. 4.3. Morphology of ND7/23 cells. A) The figure shows the morphology of ND7/23 cells, which typically have a diameter of 19μm. **B)** A single ND7/23 cell co-transfected with CD8 and GFP encoding plasmids, where associated anti-CD8 beads can be seen on the *left* and the GFP fluorescence can be seen on the *right* for the same cell.

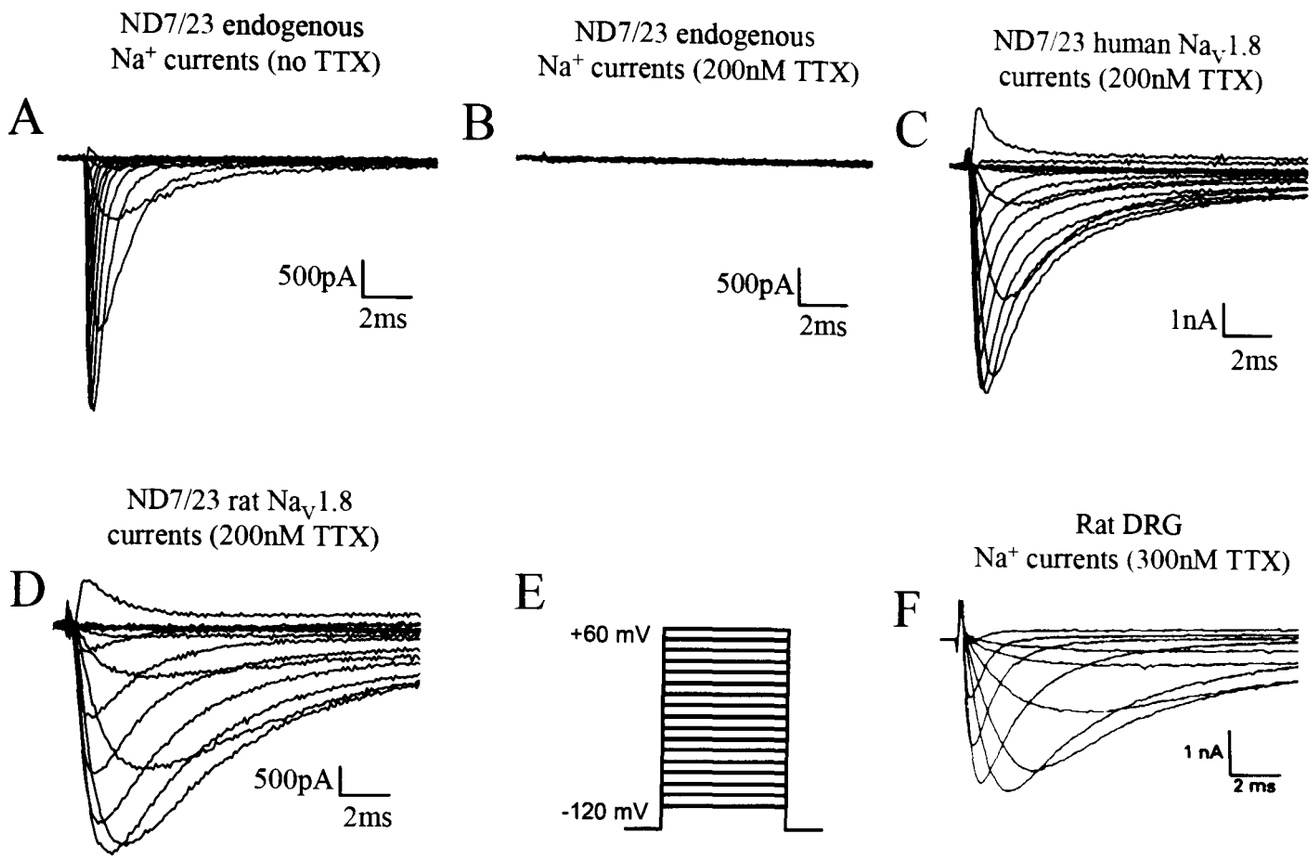

Fig. 4.4. Human and rat Na$_V$1.8 channel current traces recorded from ND7/23 cells. A) An example current trace of endogenous Na^+ currents recorded from ND7/23 cells in the absence of TTX. **B)** In the presence of TTX (200nM), example current traces are shown recorded from ND7/23 cells. **C)** An example current trace recorded from ND7/23 cells transfected with hNa$_V$1.8 channel cDNA in the presence of 200nM TTX. **D)** An example current trace recorded from ND7/23 cells transfected with rNa$_V$1.8 channel cDNA in the presence of 200nM TTX. **E)** The pulse protocol used to elicit current in B-E, where steps to -100mV to +60mV in 10mV increments were used from a holding potential of -120mV. **F)** A current trace from Elliott and Elliott (1993) which shows TTX-resistant Na^+ currents recorded from small cells of the rat dorsal root ganglia. Currents were elicited during -37, -32, -27, -23, -8, 7, 22 and 36mV test pulses from a holding potential of -67mV. This current trace may include the TTX-resistant Na$_V$1.9 channel current.

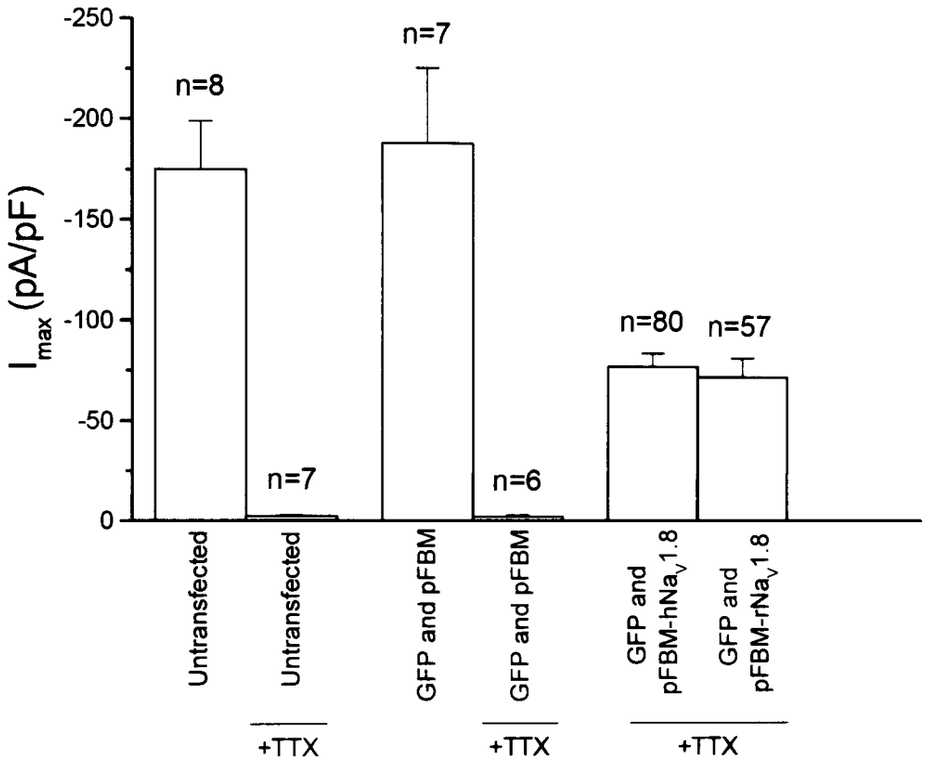

Fig. 4.5. Human and rat $Na_V1.8$ peak current amplitude recorded from ND7/23 cells. The bar diagram shows the peak current amplitude in cells which were untransfected, co-transfected with pFastBacMam1 vector (pFBM) and pEGFP-N1(GFP), co-transfected with pFastBacMam1-h$Na_V1.8$ and pEGFP-N1, or co-transfected with pFastBacMam1-r$Na_V1.8$ and pEGFP-N1. Control experiments were carried out in the absence and presence of TTX (200nM). The peak amplitude was determined from the current-voltage relationships recorded from holding potential of -120mV. The peak amplitude was normalised to the cell capacitance to take into account the size of the cell.

4.2.3 Voltage-dependence of activation for human and rat $Na_V1.8$ channels

The voltage-dependence of activation for TTX-resistant human and rat $Na_V1.8$ channels and endogenous TTX-sensitive Na^+ currents were compared in ND7/23 cells using test pulses to various potentials every 5 seconds, from a holding potential of -120mV or a more physiological potential of -80mV. For the current-voltage (*I-V*) relationships (Fig. 4.6A), the human and rat $Na_V1.8$ currents and TTX-sensitive Na^+ currents showed reversal potentials similar to the theoretical E_{rev} (calculated as +56mV using the Nernst equation for the solutions used).

For the TTX-sensitive Na^+ currents, the *I-V* curve (V_h = -120mV) showed an I_{max} of approximately -12mV. In contrast, the *I-V* curves for human and rat $Na_V1.8$ channels showed an I_{max} of approximately 10mV from both holding potentials of -120mV or -80mV, indicating that the human and rat $Na_V1.8$ channels activate with a similar dependence on the potential but at more depolarised potentials than for TTX-sensitive Na^+ channels. Indeed, when the conductance-voltage (*G-V*) curves were fitted (Fig. 4.6B), the voltage for half-maximal activation ($V_{1/2}$) was significantly depolarised (approx. 28mV more positive, Table 4.1) for the $Na_V1.8$ channel currents compared to the TTX-sensitive Na^+ currents. Furthermore, the $V_{1/2}$ for activation was not significantly different between the human and rat $Na_V1.8$ channels from either holding potential (Fig. 4.6B, Table 4.1). A steeper slope was observed in the *G-V* curve for TTX-resistant Na^+ currents compared to both human and rat $Na_V1.8$ channels (Fig. 4.6B, Table 4.1). Indeed, compared to the TTX-sensitive Na^+ currents, the slope factor (*k*) was approx. 8mV greater for the human $Na_V1.8$ channel and approx. 5mV greater for the rat channel, where there was a small but significant difference in *k* values (approx. 3mV) between the human and rat $Na_V1.8$ channel curves from both holding potentials (Table 4.1). For the maximum conductance, human and rat $Na_V1.8$ channels and TTX-sensitive Na^+ currents showed similar values (Table 4.1). Thus, overall the activation properties were essentially similar for the human and rat $Na_V1.8$ channels (irrespective of the holding potential), and they showed significantly more depolarised activation than for the TTX-sensitive Na^+ currents.

TABLE 4.1

Voltage-dependent activation and inactivation of human and rat $Na_V1.8$ sodium channels

$Na_V1.8$ channel	Holding potential (mV)	Activation				Inactivation				
		$V_{½}$ (mV)	k (mV)	G_{max} (nS)	n	$V_{½}$ (mV)	k (mV)	B (nA)	A (nA)	n
Human	–120	–2.7 ± 0.8	14.7 ± 0.3	61.9 ± 4.6	79	–79.9 ± 1.0	10.5 ± 0.4	1.8 ± 0.2	0.12 ± 0.01	84
Human	–80	–4.0 ± 1.0	12.4 ± 0.3	47.9 ± 4.6	43	–76.3 ± 1.5	8.7 ± 0.4	3.1 ± 0.4	0.15 ± 0.03	39
Rat	–120	–2.4 ± 0.8	11.7 ± 0.3	57.0 ± 5.8	57	–64.1 ± 1.2	8.0 ± 0.4	2.0 ± 0.3	0.08 ± 0.01	51
Rat	–80	–1.6 ± 0.9	10.3 ± 0.3	61.2 ± 6.0	41	–57.9 ± 1.0	7.6 ± 0.2	2.3 ± 0.2	0.03 ± 0.01	38
TTX-sensitive Na^+	–120	–30.4 ± 0.8	6.7 ± 0.1	51.2 ± 6.6	8	–76.2 ± 1.2	5.3 ± 0.2	2.9 ± 0.4	0.03 ± 0.01	8
Human +hβ1	-80		ND			–79.0 ± 4.5	9.0 ± 1.2	1.4 ± 0.5	0.08 ± 0.02	5
Human +hβ3	-80		ND			–75.3 ± 5.7	11.1 ± 1.9	2.0 ± 0.2	0.07 ± 0.05	4

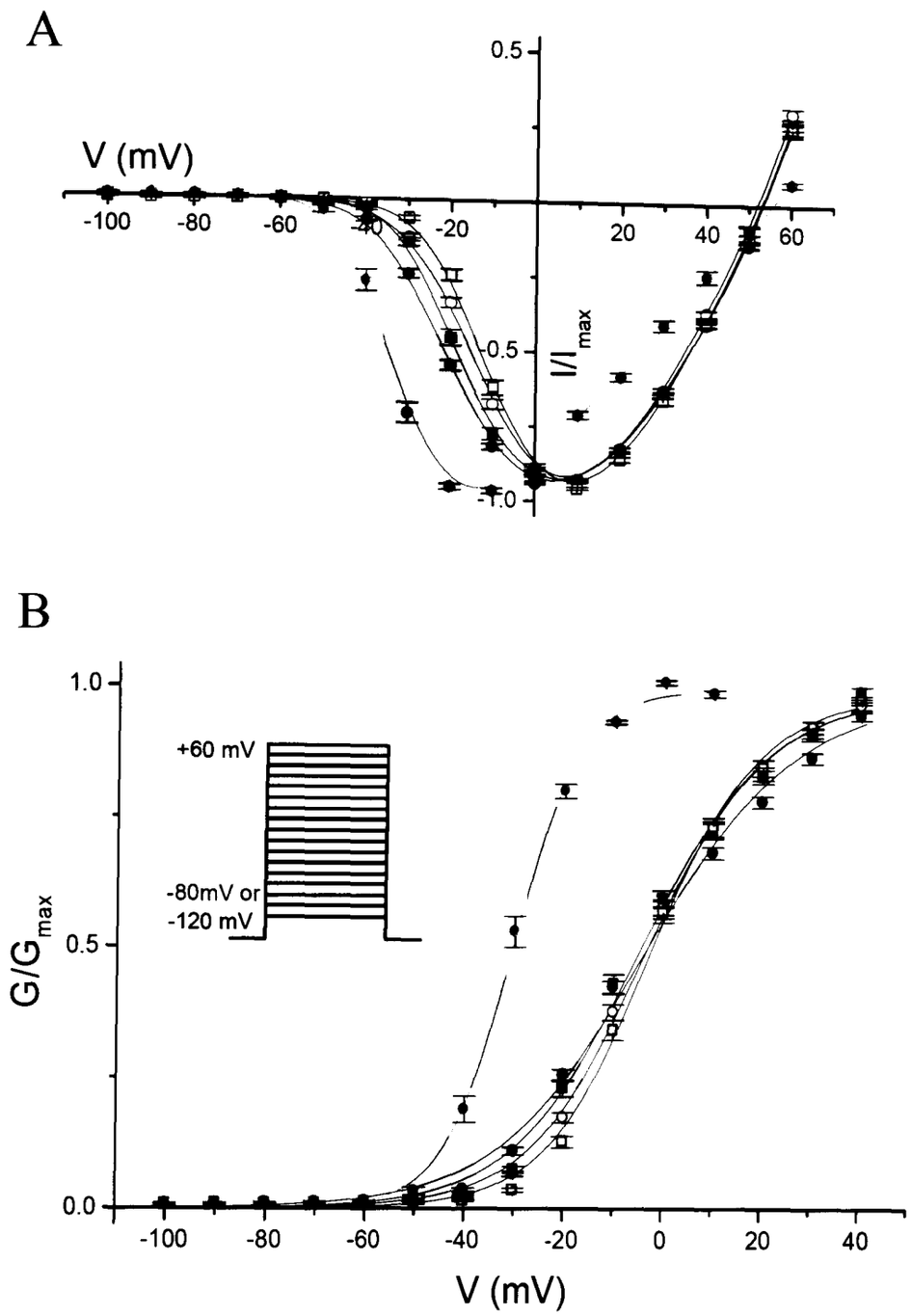

Fig. 4.6. Voltage-dependence of activation for human and rat $Na_V1.8$ channels. A) Current-voltage (*I-V*) relationships are shown for the peak current for human (●) and rat (○) $Na_V1.8$ channels and TTX-sensitive Na^+ channels (●) from a holding potential of -120mV, and also for human (■) and rat (□) $Na_V1.8$ channels from a holding potential of -80mV. Currents were normalised to the maximum current (I_{max}). **B)** Conductance-voltage curves are shown for human (●) and rat (○) $Na_V1.8$ channels and TTX-sensitive Na^- channels (●) from a holding potential of -120mV, and also for human (■) and rat (□) $Na_V1.8$ channels from a holding potential of -80mV. The curves were fit with the Boltzmann equation and normalised to the maximum conductance (G_{max}). The pulse protocol is shown in the inset of B. The n numbers are given in Table 4.1.

4.2.4 Voltage-dependence of inactivation for human and rat $Na_V1.8$ channels

The voltage-dependence of steady-state inactivation for human and rat $Na_V1.8$ channel currents was compared using a test pulse to 0mV preceded by 4 second prepulses from a holding potential of -120mV or -80mV (Fig. 4.7). The endogenous TTX-sensitive Na^+ currents were also studied from a holding potential of -120mV. The steady-state inactivation curves for the human $Na_V1.8$ channel were more negative than for the rat $Na_V1.8$ channel for both holding potentials (Fig. 4.7). Indeed, from a holding potential of -120mV, the $V_{1/2}$ for inactivation was 15.8mV more hyperpolarised for the human than for the rat $Na_V1.8$ channel (Table 4.1). In fact the inactivation curve for the human $Na_V1.8$ channel showed similar $V_{1/2}$ values to the TTX-sensitive Na^+ current (Fig. 4.7, Table 4.1). It is also noteworthy that from a holding potential of -80mV, the human and rat $Na_V1.8$ channels both showed a small depolarising shift in the steady-state inactivation curve. Compared to the TTX-sensitive Na^+ currents, the slope factor (k) was approx. 8mV greater for the human $Na_V1.8$ channel and approx. 5mV greater for the rat $Na_V1.8$ channel, where there was a very small difference in k values (approx. 3mV) between the human and rat $Na_V1.8$ channel curves from both holding potentials. These results show that the human $Na_V1.8$ channel inactivates at more hyperpolarised potentials than the rat $Na_V1.8$ channel.

The ND7/23 cell line has been shown to express β_1 and β_3 subunits (John et al., 2004), which are likely to be mouse or rat orthologues due to the origin of the cell line. Despite human, rat and mouse β subunits being near-identical in protein sequence, species-specific modulation of the $Na_V1.8$ channel might nevertheless contribute to the differential voltage-dependence of inactivation observed between human and rat $Na_V1.8$ channels. In experiments co-expressing human β_1 or β_3, the voltage-dependence of inactivation for human $Na_V1.8$ channel was unaltered, and indeed the Boltzmann curve parameters were not significantly different (Table 4.1). Therefore, the presence of endogenous modulatory β subunits does not seem to explain the more hyperpolarised inactivation of the human $Na_V1.8$ channel compared to the rat channel.

Overall the voltage-dependence of steady-state inactivation is different between human and rat $Na_V1.8$ channels. In order to determine whether other inactivation properties differed between human and rat $Na_V1.8$ channels, the time course for development of inactivation, and for recovery from inactivation, and use-dependent current inhibition will be compared (following sections).

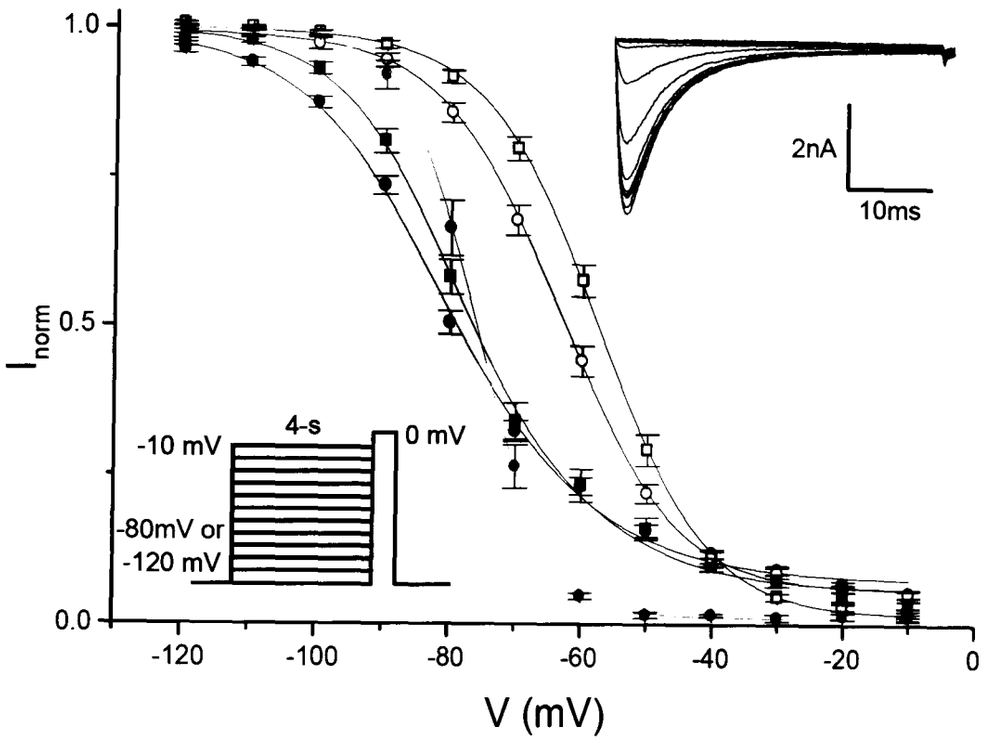

Fig. 4.7. Voltage-dependence of steady-state inactivation for human and rat $Na_V1.8$ channels. Curves are shown for steady-state voltage-dependence of inactivation for human (●) and rat (○) $Na_V1.8$ channels and TTX-sensitive Na^+ channels (●) from a holding potential of -120mV, and also for human (■) and rat (□) $Na_V1.8$ channels from a holding potential of -80mV. Currents were normalised to the maximum current (parameter *B*, see *Chapter 2*). The pulse protocol and example currents elicited during the 0mV test pulse are shown inset. The n numbers are given in Table 4.1.

4.2.5 Time course for development of inactivation for human and rat $Na_V1.8$ channels

Inactivation from open states is responsible for the decay phase observed for voltage-gated Na^+ channel macroscopic current (Yarov-Yarovoy et al., 2001). The example current traces shown in Figure 4.4 indicate the kinetics for inactivation are different for the human and rat $Na_V1.8$ channels. The mean time constants of inactivation fit to the time courses (Fig. 4.8) show that the rat $Na_V1.8$ channel showed significantly slower inactivation for all potentials examined than the human $Na_V1.8$ channel from a holding potential of -120mV. From a more physiological holding potential of -80mV, rat $Na_V1.8$ was still slower than the human channel. It is also noteworthy that the rat channel was significantly slower from a holding potential of -80mV compared to -120mV, while the human channel showed near-identical time constants between the two holding potentials. Compared to the human and rat $Na_V1.8$ channel currents from a holding potential of -120mV, the TTX-sensitive Na^+ currents were significantly faster for all potentials examined (Fig. 4.8). The time course for inactivation was examined over relatively short 15ms depolarising pulses, and although they fit well with two exponentials, any component with much slower time course was too small in magnitude to be measured. Therefore, another protocol was used to study the time course for development of inactivation. In this protocol, a control pulse to 0mV of varying duration was preceded by a 4ms recovery period and a test pulse to 0mV (protocol as in the inset of Fig. 4.9A). The test current amplitude was measured and normalised to the control current amplitude. The current was plotted as a function of the control pulse duration and fitted with two time constants, τ_{fast} and τ_{slow}. The time course shows that both time constants were significantly smaller for the human $Na_V1.8$ channel than for the rat channel (Fig 4.9B,C, Table 4.2). Therefore, both fast and slow components of inactivation appear to develop faster for human $Na_V1.8$ than for rat $Na_V1.8$ channels (Fig. 4.9). Furthermore, the magnitude of the fast component was significantly larger for the human $Na_V1.8$ channel than the rat channel (and accordingly vice versa for the slow component). This indicates that the fast component of inactivation is more pronounced in the human $Na_V1.8$ channel compared to the rat $Na_V1.8$ channel. The extent of inactivation at 4 seconds also appeared to be more pronounced for the human $Na_V1.8$ channel than the rat channel; the asymptote was significantly smaller for the human channel 0.17±0.02 (n=5) than the rat channel 0.28±0.04 (n=5) (Fig. 4.9). It is also noteworthy that since inactivation appears complete at 4 seconds, this time course confirms that inactivation is indeed steady-state following a 4 second pulse.

Therefore, these results suggest that the human and rat $Na_V1.8$ channels inactivate with at least two components. Both components of inactivation appear faster for the human $Na_V1.8$ channel compared to the rat channel. Furthermore, the development of inactivation is faster for the human and rat $Na_V1.8$ channel currents than for the TTX-sensitive Na^+ currents.

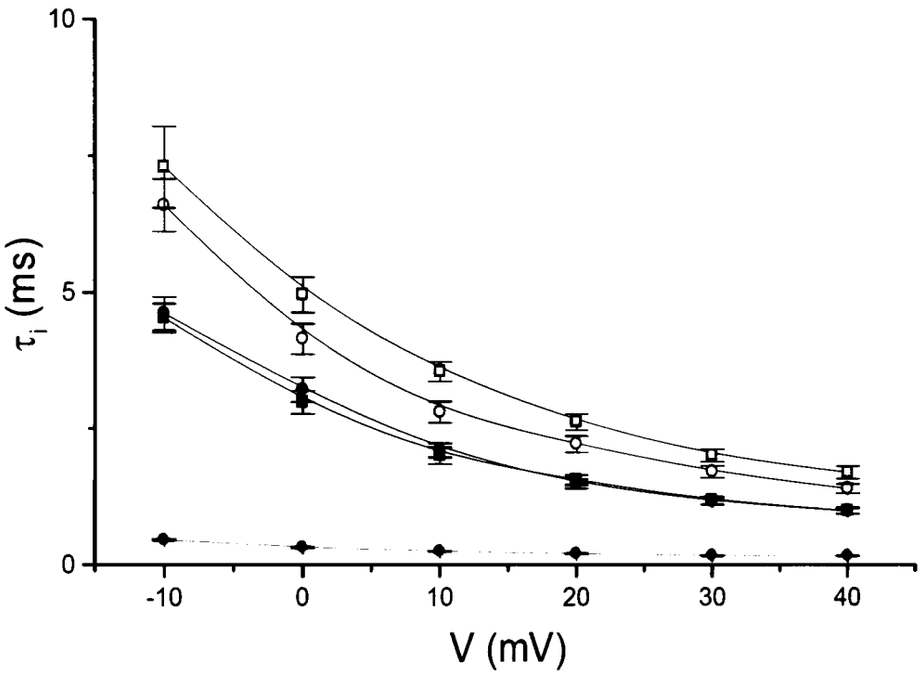

Fig. 4.8. Voltage-dependence of the inactivation time course for human and rat $Na_V1.8$ channels. The time constant of inactivation, τ_i, is shown at each test potential, V, for human (●) and rat (○) $Na_V1.8$ channels and TTX-sensitive Na^+ channels (●) from a holding potential of -120mV, and also for human (■) and rat (□) $Na_V1.8$ channels from a holding potential of -80mV The n numbers are given in Table 4.2.

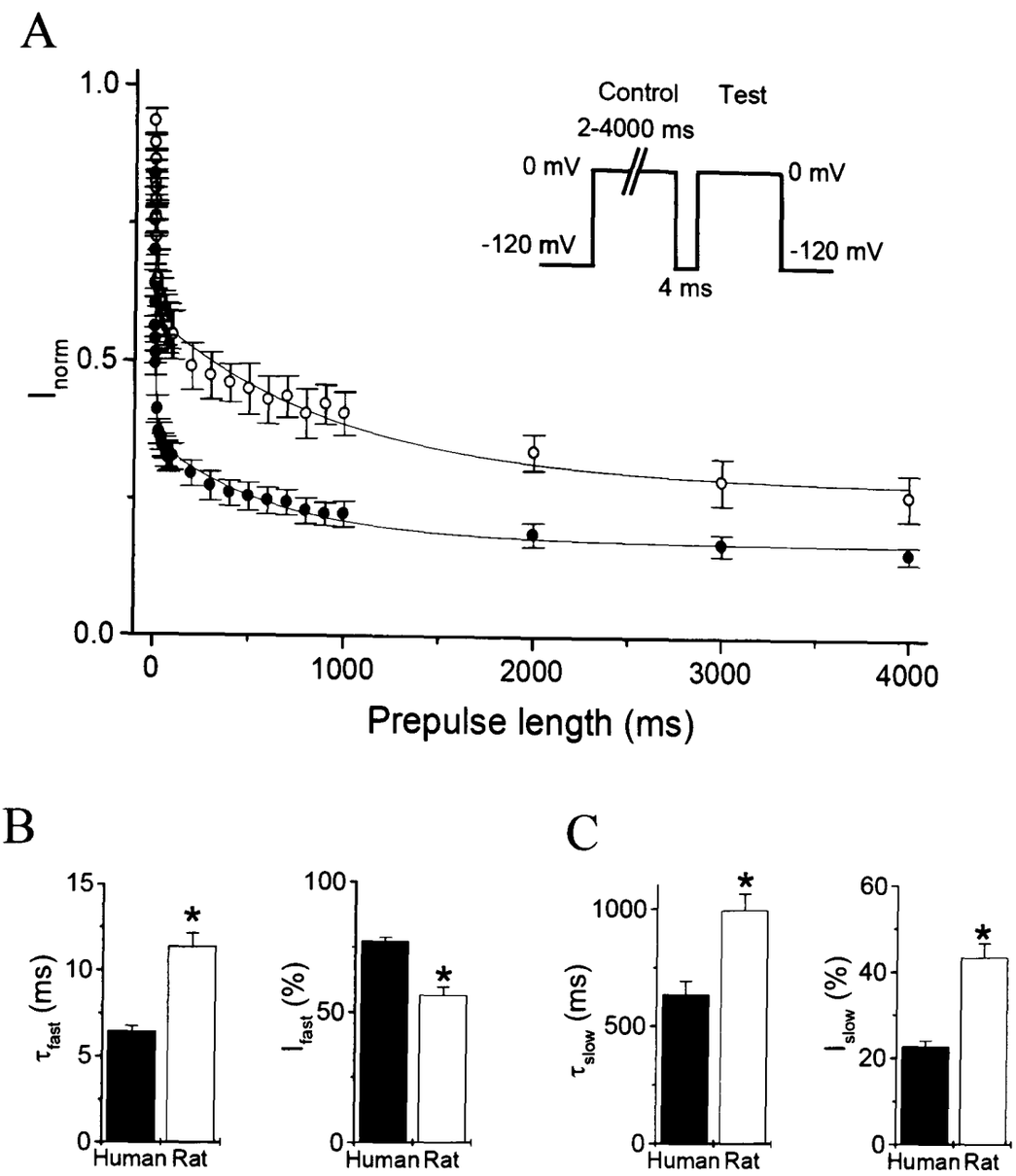

Fig. 4.9. Development of inactivation for human and rat $Na_V1.8$ channels. A) The figure shows the time course for the development of inactivation for human (●) and rat (○) $Na_V1.8$ channels and from a holding potential of -120mV. The pulse protocol is shown inset. The current amplitude during the test pulse was expressed as a fraction of the current amplitude during the control pulse, and plotted against the duration of the prepulse. The curves were fit with a double exponential equation. **B)** The bar diagrams of the fitted parameters are shown for the fast component, showing time constant τ_{fast} and its amplitude I_{fast} for human (*filled* bars) and rat (*unfilled* bars) $Na_V1.8$ channels. **C)** The bar diagrams of the fitted parameters are shown for the slow component, showing time constant τ_{slow} and its amplitude I_{slow} for human (*filled* bars) and rat (*unfilled* bars) $Na_V1.8$ channels. The n numbers are given in Table 4.2.

TABLE 4.2

Time course of inactivation for human and rat $Na_V1.8$ channels

$Na_V1.8$ channel	Holding potential (mV)	Entry into inactivation							Recovery from inactivation				
		τ_i (ms)	n	τ_{fast} (ms)	I_{fast} (%)	τ_{slow} (ms)	I_{slow} (%)	n	τ_{fast} (ms)	I_{fast} (%)	τ_{slow} (ms)	I_{slow} (%)	n
Human	−120	3.2 ± 0.2	56	6.5 ± 0.3	77 ± 1	635 ± 57	23 ± 1	5	10.2 ± 0.4	67 ± 1	126 ± 15	33 ± 1	71
Human	−80	3.0 ± 0.2	36			ND					ND		
Rat	−120	4.2 ± 0.3	50	11.4 ± 0.8	57 ± 3	995 ± 71	43 ± 3	5	5.9 ± 0.5	67 ± 1	354 ± 58	33 ± 1	55
Rat	−80	5.0 ± 0.3	30			ND					ND		
TTX-sensitive Na^+	−120	0.32 ± 0.01	8			ND			4.3 ± 0.3	80 ± 4	65 ± 9	20 ± 2.2	6

The τi shown is measured from test current elictited at 0mV

4.2.6 Time course of recovery from inactivation for human and rat $Na_V1.8$ channels

In order to study the recovery from inactivation, a two-pulse protocol was used similarly to the latter part of *Section 4.2.5*, except the duration of the recovery periods between the control pulse and test pulse was varied (instead of the duration of the control pulse, Fig. 4.10A inset). The current was plotted as a function of the duration of the recovery period and fitted with two time constants, τ_{fast} and τ_{slow}. Recovery from inactivation was compared between human and rat $Na_V1.8$ channels, and also compared with the TTX-sensitive Na^+ current, all from a holding potential of -120mV. The time course of recovery showed a τ_{fast} in the order of tens of milliseconds and τ_{slow} in the order of hundreds of milliseconds (Fig 4.10B,C, Table 4.2). At short recovery periods (corresponding to the fast component of inactivation), recovery was slower for the human channel than for the rat $Na_V1.8$ channel (Fig. 4.10A), and indeed the initial time constant (τ_{fast}) was 1.6-fold slower for the human channel (Fig. 4.10B, Table 4.2). Conversely, at longer recovery periods (corresponding to the slow component of inactivation), recovery was 2.8-fold faster for the human channel than the rat $Na_V1.8$ channel (Fig. 4.10A,C, Table 4.2). For the TTX-sensitive Na^+ currents, recovery from inactivation was faster for both initial and later components compared to the human and rat $Na_V1.8$ channels. Furthermore, while the human $Na_V1.8$ channel showed identical magnitudes of the fast (67%) and slow (33%) components to the rat $Na_V1.8$, for the TTX-sensitive Na^+ current, there was a significantly ($P<0.005$) greater magnitude of the fast component, and accordingly, a smaller magnitude slow component (Table 4.2, Fig. 4.10). Therefore this suggests that compared to the TTX-sensitive Na^+ currents, the human and rat $Na_V1.8$ channels show a larger slow component of inactivation. Thus, overall these results show that $Na_V1.8$ channels show slower recovery from inactivation, with more favoured slow component of inactivation compared to TTX-sensitive Na^+ currents. The human $Na_V1.8$ channel recovered from the initial component more slowly than the rat channel, and conversely, human $Na_V1.8$ recovered faster from the later component of inactivation than the rat channel.

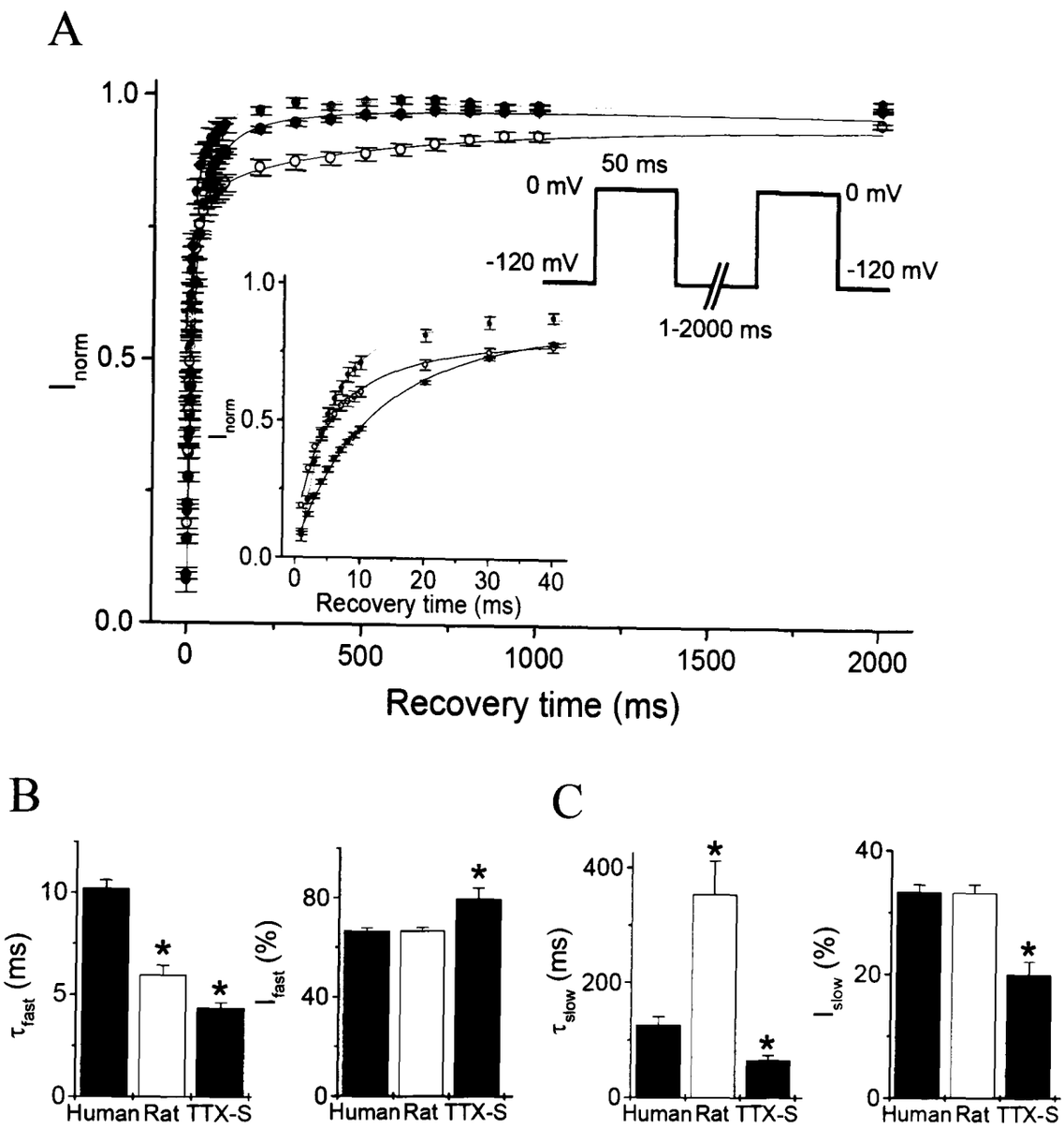

Fig. 4.10. Recovery from inactivation for human and rat $Na_V1.8$ channels. A) The time course for the recovery from inactivation is shown for human (●) and rat (○) $Na_V1.8$ channels and TTX-sensitive Na^+ channels (●) from a holding potential of -120mV. The pulse protocol is shown inset. The current amplitude during the test pulse was expressed as a fraction of the current amplitude during the control pulse, and plotted against the duration of the recovery period. The curve was fit with a double exponential equation. **B)** The bar diagrams of the fitted parameters are shown for the fast component, showing time constant τ_{fast} and its amplitude I_{fast} for human (*filled* bars) and rat (*unfilled* bars) $Na_V1.8$ channels, and TTX-sensitive Na^+ channels (*grey* bars) **C)** The bar diagrams of the fitted parameters are shown for the slow component, showing time constant τ_{slow} and its amplitude I_{slow} for human (*filled* bars) and rat (*unfilled* bars) $Na_V1.8$ channels, and TTX-sensitive Na^+ channels (*grey* bars). * indicates a statistically significant difference from human $Na_V1.8$ channels $p<0.05$. The n numbers are given in Table 4.2.

4.2.7 Use-dependent current inhibition of human and rat $Na_V1.8$ channels

Frequent stimulation of voltage-gated Na^+ channels in the absence of any drug results in the accumulation of inactivated channels until the rate development of inactivation reaches equilibrium with the rate of recovery from inactivation. This effect is known as use-dependent current inhibition, and is important for the study of the effects of specific stimulation frequencies on Na_V channels, which may be related to action potential firing frequencies.

The effect of frequent stimulation on human and rat $Na_V1.8$ channels was examined by applying a 10Hz train of 60 depolarising pulses to 0mV (10ms in duration) from a holding potential of -120mV, or a more physiological holding potential of -80mV (Fig. 4.11). Example current traces recorded during the first and 60th pulses are shown for human (Fig. 4.11A) and rat (Fig. 4.11B) $Na_V1.8$ channels. For mean values taken at 10Hz stimulation, the current amplitude for human $Na_V1.8$ was reduced by 15±1% (n=121) at steady-state compared to the first pulse from a holding potential of -120mV, but reduced by 28±2% (n=26) from a holding potential of -80mV (Fig. 4.11C, Table 4.3). The more extensive use-dependent current inhibition at -80mV is the consequence of a greater probability of inactivated channels at a more depolarised holding potential. Indeed, this was also observed for the rat $Na_V1.8$ channel, where at 10Hz stimulation 27±2% (n=86) inhibition was observed from a holding potential of -120mV, but 39±2% (n=32) from a holding potential of -80mV (Fig. 4.11C, Table 4.3). Interestingly, these results show that from holding potentials of both -120mV and -80mV, use-dependent current inhibition was significantly less pronounced for the human $Na_V1.8$ channel, compared to the rat $Na_V1.8$ channel.

TABLE 4.3

Use-dependent current inhbition of human and rat $Na_V1.8$ channels

$Na_V1.8$ channel	Holding potential (mV)	Use-dependent inhibition (I_{norm})					
		5Hz	n	10Hz	n	20Hz	n
Human	–120	0.89 ± 0.01	52	0.85 ± 0.01	121	0.74 ± 0.01	51
Human	–80	0.79 ± 0.02	33	0.72 ± 0.02	26	0.55 ± 0.03	26
Rat	–120	0.74 ± 0.02	40	0.73 ± 0.02	86	0.60 ± 0.02	39
Rat	–80	0.67 ± 0.02	32	0.61 ± 0.02	32	0.50 ± 0.02	32
TTX-sensitive Na^+	–120	0.98 ± 0.01	8	0.95 ± 0.01	7	0.85 ± 0.01	7

The TTX-sensitive Na^+ current also showed use-dependent current inhibition at 10Hz (V_h= -120mV), but this was significantly less pronounced than for both human and rat $Na_V1.8$ channels (Fig. 4.11C, Table 4.3). This suggests that relative to the rate of entry into inactivation, the rate of recovery from inactivation is fastest for TTX-sensitive Na^+ current and slowest for the rat $Na_V1.8$ channel, with human $Na_V1.8$ channel intermediate. The extent of use-dependent inhibition correlates well with the time course of recovery from inactivation. Indeed, in Figure

4.12 depolarising trains at 20Hz show the greatest extent of inhibition, and at 5Hz show the least, where an equal dependence of the frequency of stimulation was observed for the human and rat $Na_V1.8$ channel currents and the TTX-sensitive Na^+ currents (Fig. 4.12, Table 4.3). Furthermore, the 5Hz, 10Hz and 20Hz train all probe the slow component of the recovery from inactivation (with recovery periods of 190ms, 90ms and 40ms, respectively). In the previous section, the recovery from the slow component of inactivation was found to be faster for the TTX-sensitive Na^+ current and slowest for the rat $Na_V1.8$ channel, with human $Na_V1.8$ channel intermediate.

Therefore, the extent of use-dependent current inhibition was more pronounced for rat $Na_V1.8$ channels than for human $Na_V1.8$ channels. The TTX-sensitive Na^+ currents showed less pronounced use-dependent current inhibition than both human and rat $Na_V1.8$ channels. These findings correlate well with the extent of recovery from the slow component of inactivation.

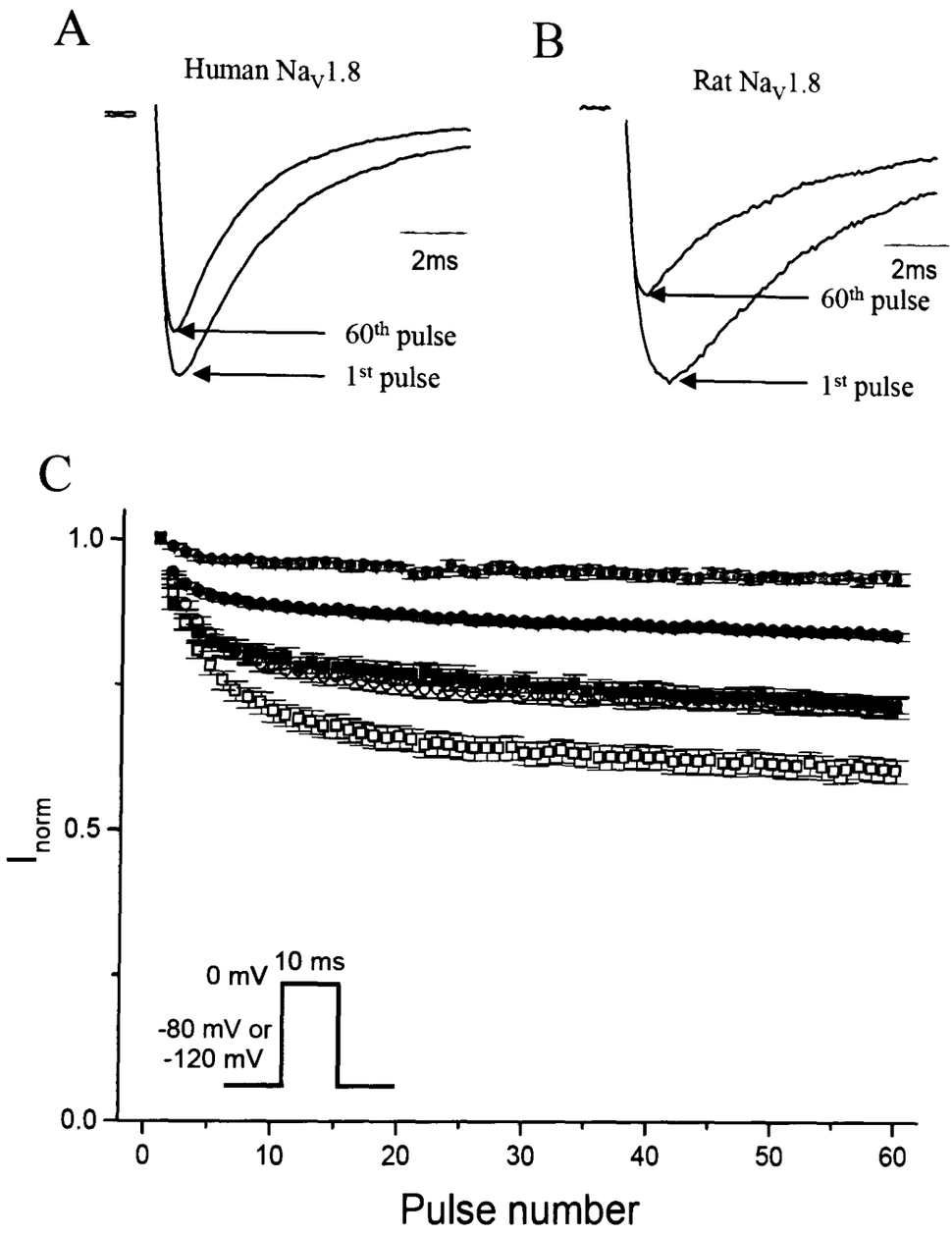

Fig. 4.11. Use-dependent current inhibition of human and rat $Na_V1.8$ channels. A) Example human $Na_V1.8$ channel currents are shown elicited by the first and 60^{th} depolarising test pulses (to 0mV) of a 10Hz train. **B)** Example rat $Na_V1.8$ channel currents are shown elicited by the first and last depolarising test pulses (to 0mV) of a 10Hz train. **C)** The current amplitude elicited during a 10Hz train of 60 test pulses to 0mV (10ms in duration) was expressed as a fraction of the amplitude of the first pulse. The use-dependent current inhibition curves are shown for human (●) and rat (○) $Na_V1.8$ channels and TTX-sensitive Na^+ channels (●) from a holding potential of -120mV, and also for human (■) and rat (□) $Na_V1.8$ channels from a holding potential of -80mV. The pulse protocol is shown inset. The n numbers are given in Table 4.3.

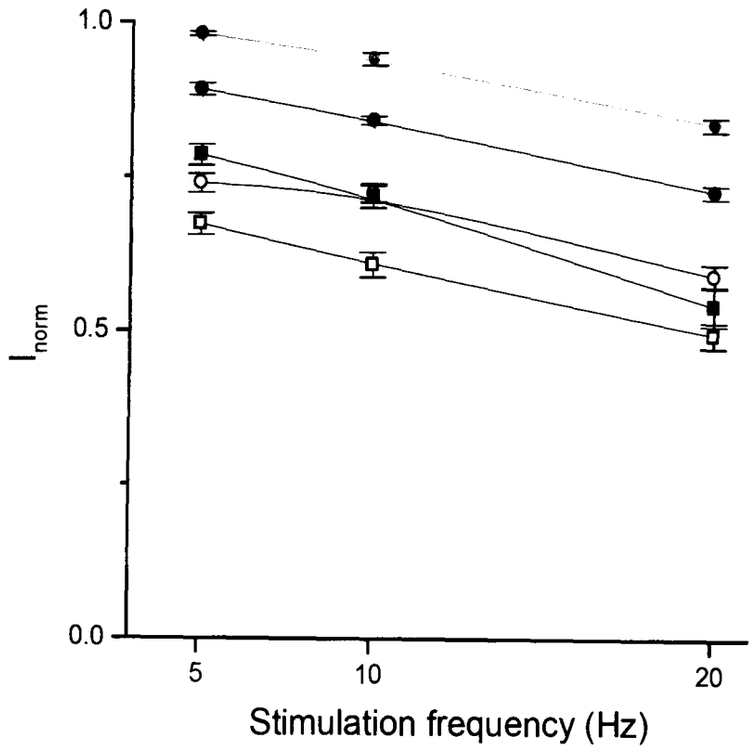

Fig. 4.12. Use-dependent current inhibition of human and rat $Na_V1.8$ channels at different stimulation frequencies. The figure shows the current amplitude elicited at the end of a 5Hz, 10Hz or 20Hz train of 60 test pulses to 0mV (10ms in duration), which was expressed as a fraction of the amplitude of the first pulse. The extent of use-dependent inhibition is shown for human (●) and rat (○) $Na_V1.8$ channels and TTX-sensitive Na^+ channels (●) from a holding potential of -120mV, and also for human (■) and rat (□) $Na_V1.8$ channels from a holding potential of -80mV. The pulse protocol is shown inset. The n numbers are given in Table 4.3.

4.3 Discussion

4.3.1 Expression of $Na_V1.8$ channels

In this study, the functional properties of $Na_V1.8$ were examined. These experiments were carried out using the *Xenopus laevis* oocyte expression system and transient expression of the mammalian sensory-neuron derived ND7/23 cell line. Although the *Xenopus laevis* oocyte expression system has been previously used for the expression of both human and rat $Na_V1.8$ channels (Akopian et al., 1996; Rabert et al., 1998; Sangameswaran et al., 1996), here the human $Na_V1.8$ channel currents were observed in only 13% of examined oocytes. Despite β-globin sequences flanking either side of the human $Na_V1.8$ channel sequence, channel currents were of small amplitude. The maximum current was similar here (approx. 500pA at 0mV) to the previously reported values for human $Na_V1.8$ channels expressed in oocytes (approx. 700pA at 10mV, Rabert et al., 1998). Furthermore, the latter authors reported an E_{rev} of 45mV, which is similar to the value here (43mV). The voltage for half-maximal activation was shown here to be 6mV, which is also consistent with the value of 12mV reported by Rabert et al., (1998). Although it was possible to record human $Na_V1.8$ channels expressed in oocytes, it was difficult to carry out accurate analysis of such small amplitude currents. Therefore the oocyte expression system was shown here to unsuitable for the expression of $Na_V1.8$ channels for these experiments.

The mammalian ND7/23 cell line was shown to be sufficient for the transient expression of human and rat $Na_V1.8$ channels. The $Na_V1.8$ channel currents were recorded in the presence of TTX (200nM) in order to completely inhibit the endogenous TTX-sensitive Na^+ current.

4.3.2 Functional properties of human and rat $Na_V1.8$ channels

A detailed comparison of the human and rat $Na_V1.8$ channels was carried out in ND7/23 cells under the same experimental conditions. In this thesis, the voltage-dependence of activation was found to be similar for the human and rat forms of the $Na_V1.8$ channel, while the TTX-sensitive Na^+ currents were significantly more hyperpolarised. Indeed, in rat DRG cells the TTX-sensitive Na^+ currents are widely reported to be more hyperpolarised than the TTX-resistant currents (Catterall et al., 2005; Elliott and Elliott, 1993), to a similar extent as shown in this chapter.

The human $Na_V1.8$ channel was shown here to inactivate at more hyperpolarised potentials ($V_{1/2}$ approx. -80mV) than the rat $Na_V1.8$ channel ($V_{1/2}$ approx. -64mV) from a holding potential

of -120mV. Indeed, the human $Na_V1.8$ channel was shown to have a similar $V_{1/2}$ values as TTX-sensitive Na^+ currents. This contrasts with the relatively more depolarised voltage-dependence of inactivation for $Na_V1.8$ that has been widely reported in studies of the rat $Na_V1.8$ channel (Akopian et al., 1996; Sangameswaran et al., 1996). From a more physiological holding potential of -80mV, a similar trend was observed for the human and rat $Na_V1.8$ channels. The $V_{1/2}$ for inactivation observed here (-58mV) for rat $Na_V1.8$ channels (V_h = -80mV) was similar to the value reported for the same channel expressed in the same cell line (-54mV) and also to the value reported for TTX-resistant Na^+ currents recorded from rat DRG (-54mV) (John et al., 2004).

Overall, these results suggest that at normal resting potentials for nociceptive neurons, where these channels are predominantly expressed, a larger proportion of $Na_V1.8$ channels will be inactivated in humans compared to rats.

For both human and rat $Na_V1.8$ channels, the $V_{1/2}$ values for inactivation are generally more hyperpolarised here than compared to previously obtained values (Table 4.4). However, as noted above the $V_{1/2}$ value for rat $Na_V1.8$ (-58mV) from a holding potential of -80mV is consistent with John et al. (2004). The more hyperpolarised $V_{1/2}$ value (-64mV) at -120mV holding potential, indicates the $V_{1/2}$ values obtained at the less hyperpolarised holding potential may be distorted, as they already include partly inactivated channels. The strength of this present study is due to the fact that human and rat $Na_V1.8$ channels have been compared under the same experimental conditions, removing the effects of pulse protocols and other experimental conditions. Under these identical conditions, it is clear that the human $Na_V1.8$ channel shows a more hyperpolarised voltage-dependence of inactivation than the rat $Na_V1.8$ channel.

TABLE 4.4

Voltage-dependence of inactivation for human and rat $Na_V1.8$ channels in the literature

$Na_V1.8$ channel	Holding potential (mV)	Expression system	$V_{1/2}$ for inactivation (mV)	Reference
Human	**-120**	**ND7/23**	**-80**	**This thesis**
Human	**-80**	**ND7/23**	**-76**	**This thesis**
Human	-100	Oocytes	-54	Rabert et al., 1998
Human	-100	CHO	-63	Akiba et al., 2003
Human	-100	HEK293	-50	Jarvis et al., 2007
Rat	**-120**	**ND7/23**	**-64**	**This thesis**
Rat	**-80**	**ND7/23**	**-58**	**This thesis**
Rat	-100	Oocytes	-48	Rabert et al., 1998
Rat	-60	Oocytes	-30	Akopian et al., 1996
Rat	-100	Oocytes	-53	Vijayaragaven et al., 2004
Rat	-90	ND7/23	-54	John et al., 2004
Rat	-140	ND7/23	-47	Leffler et al., 2007
Rat	-120	ND7/23	-41	Choi et al., 2004
Rat	-140	tsA201	-75, -34	Zhao et al., 2007

NB: While Fitzgerald et al. (1999) and Sangameswaran et al. (1996) also examined the functional properties of $Na_V1.8$ channels, the voltage-dependence of inactivation was not studied.

Although some previous studies have investigated properties of human and rat $Na_V1.8$ channels (Table 4.4), only Rabert et al., (1998) have carried out a direct comparison between human and rat channels in the same laboratory under the same experimental conditions, as described in this chapter. The comparison by the latter authors was done using oocyte expression system rather than the mammalian expression system used here. They were not able to discriminate clearly between the properties of human and rat channels, due to low numbers of recordings. However, the trend of the latter authors results for voltage-dependence of steady-state inactivation were similar to those described in this chapter. Furthermore, Akiba et al. (2003) also noted that inactivation was more hyperpolarised for human $Na_V1.8$ channels expressed in CHO cells compared to values observed by Akopian et al. (1996) for the rat $Na_V1.8$ channel (Table 4.4).

The hybrid cell line, ND7/23, is derived from rat and mouse cells and thus species-specific modulatory proteins may potentially contribute to differences in properties between the rat and human $Na_V1.8$ channels. However, species-specific modulation by endogenously expressed β subunits did not appear to explain the more depolarised voltage-dependence of inactivation observed for the human $Na_V1.8$ channel, since co-transfection with human β subunits did not significantly affect the inactivation curve parameters. However, it is not possible to rule out the possibility that the endogenously expressed β subunits are already at maximal levels, so that heterologous expression would have negligible effect. As noted above, previous studies have suggested that human $Na_V1.8$ channels inactivate at more hyperpolarised potentials compared to rat $Na_V1.8$ channels (Akiba et al., 2003; Rabert et al., 1998). Thus, it seems unlikely that the use of ND7/23 cells contributed to the observed differences between human and rat $Na_V1.8$ channels. Furthermore, the results here are perhaps more relevant to physiological cases since a mammalian cell line was used. Thus, overall the results indicate that the ND7/23 cells did not contribute to the differences observed between human and rat $Na_V1.8$ channels.

In order to determine whether other inactivation properties differed between human and rat $Na_V1.8$ channels, the time course for development of inactivation, and recovery from inactivation, and use-dependent current inhibition were studied. For the time course of inactivation during a single pulse, human $Na_V1.8$ channel kinetics decayed faster than for rat $Na_V1.8$ channels, but slower than TTX-sensitive Na^+ currents for all potentials examined. This was also supported by use of a two-pulse protocol. For the latter protocol the control pulse duration was varied, and the extent of inactivation at each control pulse period was plotted. There were two components to the time course, where the human $Na_V1.8$ channel showed faster development of both components of inactivation compared to the rat $Na_V1.8$ channel. Furthermore, the amplitude of the slow component was smaller for the human $Na_V1.8$ channel, than for the rat channel. For the recovery from inactivation, there were also two components to the time course, where human $Na_V1.8$ showed slower recovery from the fast component, and

faster recovery from the slow component compared to the rat $Na_V1.8$ channel. Furthermore, consistent with the literature, TTX-resistant $Na_V1.8$ channels showed slower recovery from inactivation with more favoured slow inactivation than TTX-sensitive Na^+ current (Blair and Bean, 2003; Leffler et al., 2007).

In summary, for the fast component, inactivation of the human $Na_V1.8$ channel develops faster but recovers slower than the rat $Na_V1.8$ channel. For the slow component, the development of inactivation was faster for the human $Na_V1.8$ channel, but the recovery was also faster. The fast component of inactivation and slow component of inactivation appear to represent two kinetically distinct inactivation states; it seems likely that these states are perhaps the fast inactivation state and a slow inactivation state. Moreover, a greater proportion of rat $Na_V1.8$ channels enter the slow inactivation states than human $Na_V1.8$ channels. Thus the fast and slow components of $Na_V1.8$ inactivation appear to have a different mechanism.

The slower recovery of the slow component of inactivation for the human $Na_V1.8$ channel also explains its greater use-dependent current inhibition at 10Hz. As at this frequency, a recovery period would be present between depolarisations that would probe the slow component of the time course of recovery from inactivation. This is relevant physiologically because high frequency firing occurs in nociceptive C-fibres following neuropathy (approx. 10Hz), thus the human $Na_V1.8$ channel is capable of supporting high frequencies and more sustained action potential firing in these fibres (Akopian et al., 1996; Elliott and Elliott, 1993; Jeftinija, 1994; Kajander and Bennett, 1992; Sangameswaran et al., 1996; Schild and Kunze, 1997). Therefore because of the differences in the functional properties between human and rat $Na_V1.8$ channels, the use of rats to investigate nociceptive nerve transmission and excitability may not exactly reflect the situation in humans.

The human $Na_V1.8$ channel shares 83% identity with the rat channel; 2% of differences occur in the transmembrane segments and 15% in the loop regions. However it is difficult to predict which regions might be particularly important for the differential functional properties of the two channels. The following list gives five examples that perhaps could be important for the different functional properties between the human and rat $Na_V1.8$ channels:

1) Five serines of the I-II linker have been shown to be sites of cAMP-dependent kinase A (PKA) modification in rat $Na_V1.8$ channels (Fitzgerald et al., 1999). The human $Na_V1.8$ channel shares identity with only three of these sites. While the inactivation properties of the rat $Na_V1.8$ channel were not affected by PKA in oocytes (Vijayaragavan et al., 2004a), the effects of PKA on the human $Na_V1.8$ channel I-II linker are yet to be investigated.

2) A single amino acid difference between the human (F1465) and rat (Y1466) $Na_V1.8$ channels is present in the DIII-IV linker which comprises the fast inactivation gate. Although the role of this residue in inactivation has not been investigated in the $Na_V1.8$ channel, the additional hydroxyl group might perhaps reduce interactions leading to the slower inactivation kinetics for the rat $Na_V1.8$ channel compared to the human channel.

3) The N-terminus of the rat $Na_V1.4$ channel has also been demonstrated to interact with the C-terminus through a 22 amino acid residue region overlapping the calmodulin IQ motif (Choi et al., 2006; Zhang et al., 2000), which differs by two residues between human and rat $Na_V1.8$ channels. While the role of the interaction between the N- and C-termini is unknown, the interaction between the C-terminus and calmodulin was shown to be involved in the extent of use-dependent current inhibition (Choi et al., 2006). Perhaps the differences in the amino acid sequence lead to reduced interactions between the N-terminus and the C-terminus, the C-terminus and calmodulin, or both.

4) The rapid recovery from fast inactivation of the rat $Na_V1.8$ channel has been attributed to a tetrapeptide (serine-leucine-glutamic acid-asparagine) in the IVS3/S4 linker (Dib-Hajj et al., 1997). However, the corresponding tetrapeptide differs in the human $Na_V1.8$ channel (glutamine-serine-glutamic acid-asparagine). Perhaps this difference contributes to the different recovery inactivation between human and rat $Na_V1.8$ channels.

5) In addition to the intracellular linkers, the transmembrane segments and P-loops have also been shown to be involved in inactivation (Ulbricht, 2005). It is possible that these regions may also be involved in the different inactivation properties observed between the human and rat $Na_V1.8$ channels.

In conclusion, transient transfection of mammalian ND7/23 cells is sufficient for recording human and rat $Na_V1.8$ channel currents. While the voltage-dependence of activation was similar between human and rat $Na_V1.8$ channels, the human $Na_V1.8$ channel showed different inactivation properties; the voltage-dependence of inactivation was more hyperpolarised, development of inactivation was faster, and recovery from the first component of inactivation was slower, and vice versa, recovery from the second component of inactivation was faster. Therefore these results suggest that under physiological conditions, there would be a greater proportion of $Na_V1.8$ channels inactivated in humans compared to rats (except at very depolarised potentials), and higher action potential firing frequencies may be achieved for humans.

CHAPTER 5

PHARMACOLOGICAL PROPERTIES OF HUMAN AND RAT $Na_V1.8$ SODIUM CHANNELS

5.1 Introduction

The $Na_V1.8$ channel is known to play an important role in pain signalling. Agents which block $Na_V1.8$ channels have been shown to be anti-hyperalgesic and anti-allodynic in inflammatory and neuropathic pain animal models. Many drugs (such as local anaesthetics), act on voltage-gated Na^+ channels mainly by their preferential action on the inactivated state of the channel (Hille, 1977). The selectivity for inactivated channels results in a voltage- and use-dependent action leading to greatly augmented drug block during repetitive firing or sustained depolarisation, as may occur, during pain signalling (Blair and Bean, 2002; Renganathan et al., 2001).

In the previous chapter it was shown that the electrophysiological properties differ between human and rat $Na_V1.8$ channels. In this chapter, electrophysiological measurements using whole-cell patch clamp were used to analyse and compare the pharmacological actions of a range of drugs on human and rat $Na_V1.8$ channels expressed in ND7/23 cells. The tonic and use-dependent actions of the local anaesthetic tetracaine, the α-aminoamide derivative ralfinamide (which shows analgesic properties, Stummann et al. 2005), the lamotrigine derivative 227c89 (which also shows analgesic properties, Liu et al. 2003), the potent anticonvulsant V102862 (which has the potential utility as an analgesic, Ilyin et al. 2005), and the potent and highly selective $Na_V1.8$ channel inhibitor A-803467 (which also has analgesic properties, Jarvis et al. 2007). These five known sodium channel blockers (Fig. 5.1) were chosen to further understand their action on the $Na_V1.8$ channel, which is known to be involved in pain signalling.

5.2 Results

5.2.1 The effect of drug application on $Na_V1.8$ channel currents over time

In order to study the effects of drugs on resting and inactivated channels, it is first necessary to determine the most appropriate method for drug application. The length of time required for the effects of drug application on $Na_V1.8$ channel currents to reach steady-state was addressed for each drug in preliminary experiments using a test pulse to 0mV every 20 seconds. Currents for all five drugs reached steady-state before 4 minutes. For instance, application of tetracaine (1μM) to human $Na_V1.8$ channels (V_h= -80mV, therefore approx. 50% inactivated) showed that steady-state drug block of $Na_V1.8$ channel currents was reached at approximately 2 minutes (Fig 5.2). The time required for drug block is the result of the solution changer system delay, the

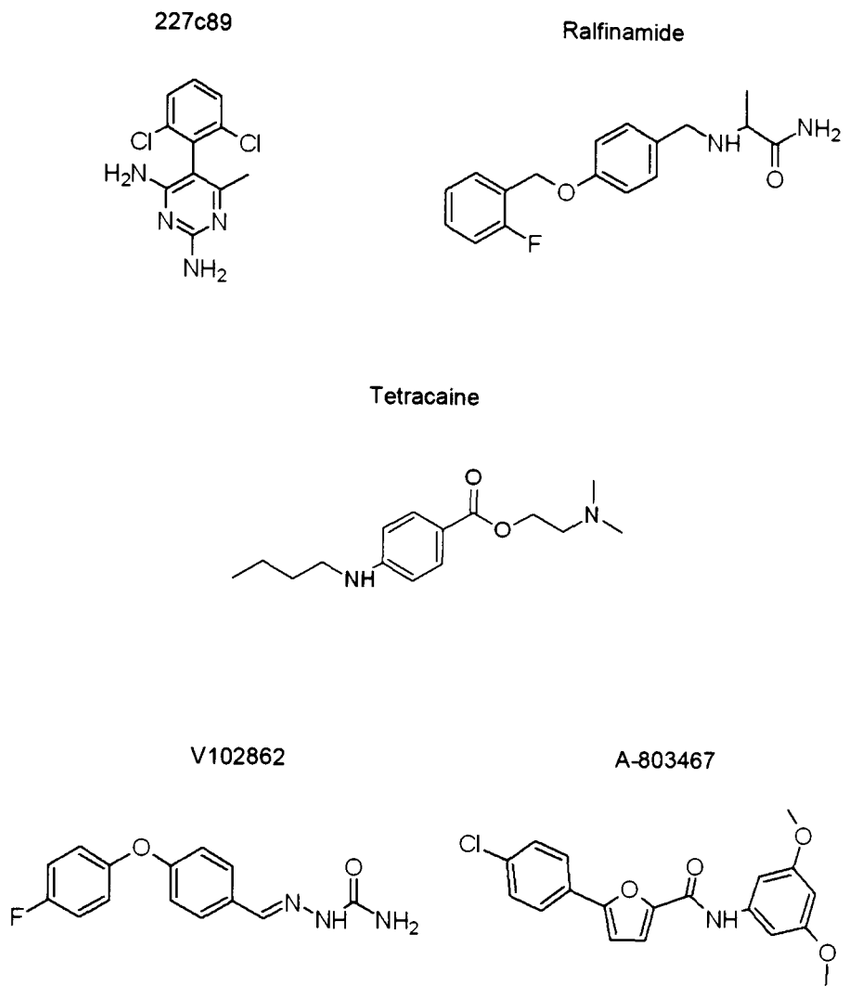

Fig. 5.1. Chemical structures of test compounds. The structures for 227c89, ralfinamide, tetracaine, V102862 and A-803467 are shown. These structures were created using ChemSketch 11.0 (ACD).

time for the diffusion of drug across the cell membrane, and the time for onset of drug onto channels. Application of a drug-free solution to remove drug also showed a delay apparently for the same reasons.

Many mammalian cell lines show a hyperpolarised shift in the inactivation curve over time, although the reason for this is presently unknown (Catterall, 2002). Indeed, both human and rat $Na_V1.8$ channels showed a shift in the inactivation curve to more hyperpolarised potentials after 15 minutes between inactivation protocols (Fig. 5.3). This suggests that the effects of drug application on the inactivation curve, and the shift in the inactivation curve over time would be difficult to separate. Therefore, in order to reduce the shift in the inactivation curve over time, generally only one drug concentration was applied to each cell. The dissociation constants were determined from the effects of a single drug concentration on the $Na_V1.8$ channel currents, as carried out in previous studies for other voltage-gated Na^+ channels (Ilyin et al., 2005; Li et al., 1999; Liu et al., 2003; Yarov-Yarovoy et al., 2001; Yarov-Yarovoy et al., 2002). The procedure for the determination of dissociation constants is described for resting channels in the next section and inactivated channels in the section after, and the theory was described in *Chapter 2*. The resting and inactivated state dissociation constants were determined using pulse protocols at the same time point between cells, always immediately before drug application, and immediately after drug application. This reduced the time period between untreated and treated $Na_V1.8$ channel currents. To reduce any differences between cells untreated and treated experiments were carried out in the same cell and the data was paired.

5.2.2 Resting state affinity of drugs for human and rat $Na_V1.8$ channels

The state-dependent properties of voltage-gated sodium channel blocking drugs are important for their mechanism of action. The known drugs preferentially act on inactivated channels rather than resting channels. Therefore the extent of block is greatly increased during periods of repetitive firing (use-dependent block) or sustained depolarisation (tonic block), when inactivated channels are more prevalent. The extent that the inactivated state affinity is greater than the resting state affinity indicates how selective the drug is for neurons that are more depolarised than others. Here the resting state affinity (more precisely, the resting state dissociation constant, K_r, see *Section 2.6.7*) for $Na_V1.8$ channels was studied from a holding potential of -120mV, at which virtually all channels are in the resting state (*Chapter 4*). The peak current amplitude during a test pulse (10ms in duration to 0mV, Fig. 5.4A) was measured in the presence and absence of a test compound and the ratio of these currents, I_{Dr}, was determined as described in *Chapter 2*. The resting dissociation constants were calculated from the values of I_{Dr} and drug concentration. The drug concentration used, D, was chosen to produce appreciable resting state inhibition, with 10% to 60% resting state block. For example, the

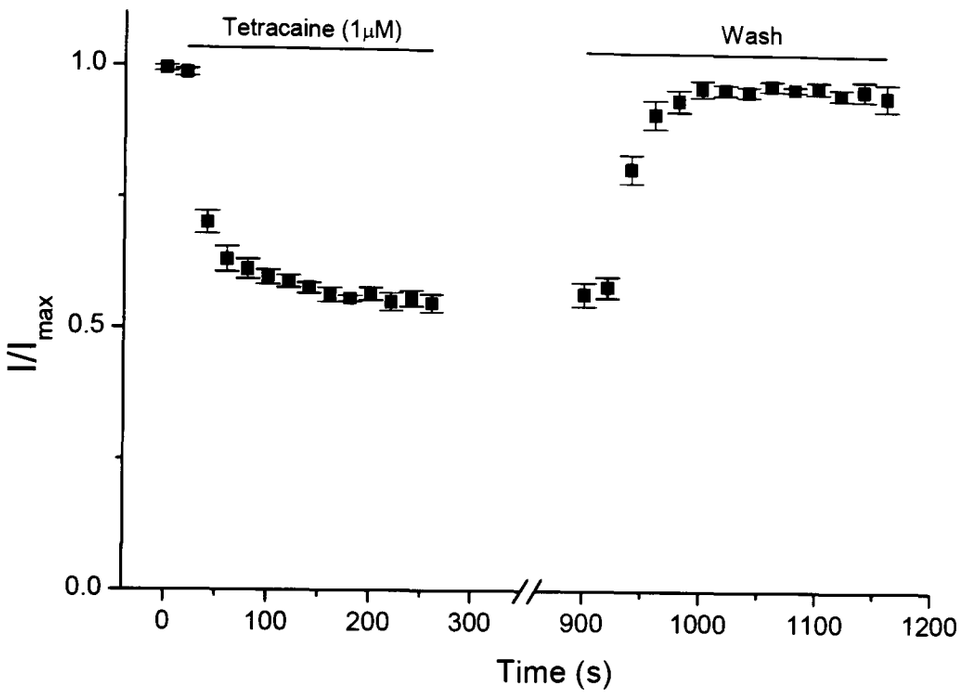

Fig. 5.2. The time course of the effect of drug on hNa$_v$1.8 channels. The graph shows the effect of the application of tetracaine (1μM) on human Na$_v$1.8 channels from a holding potential of -80mV (where channels are half-inactivated). The peak current amplitude was measured at a 0mV test pulse every 20 seconds (n=4). The effect of tetracaine was removed following perfusion of the paired cells with a drug-free solution.

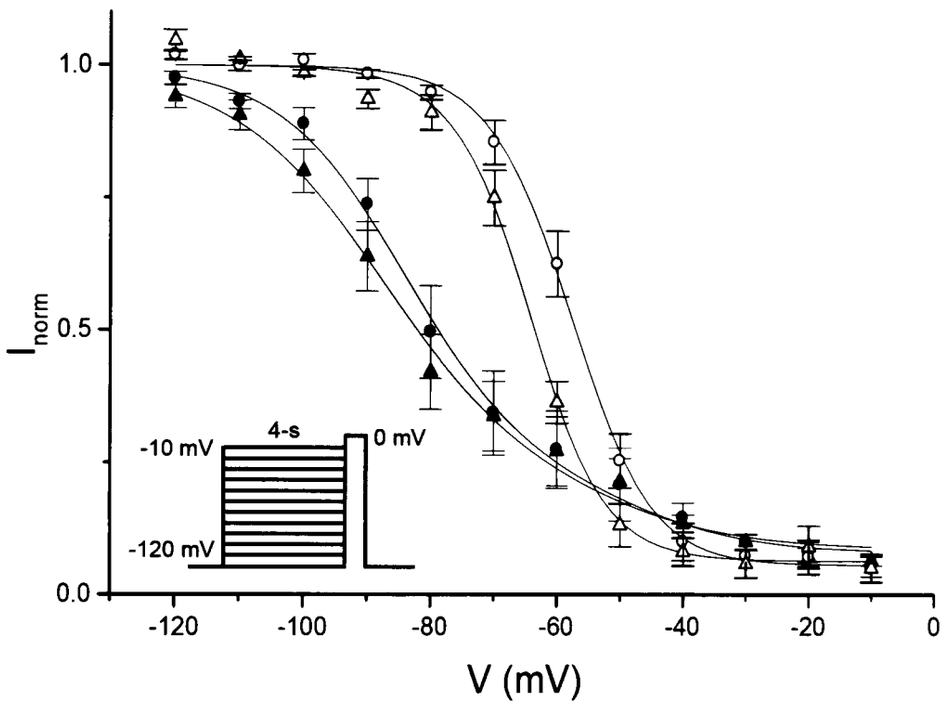

Fig. 5.3. Shift in the voltage-dependence of inactivation over time for human and rat $Na_V1.8$ channels. Curves for steady-state voltage-dependence of inactivation are shown for human (●, n=8) and rat (○, n=4) $Na_V1.8$ channels after 12 minutes, and for human (▲) and rat (△) $Na_V1.8$ channels after 27 minutes, of entering the whole-cell configuration in paired cells. The currents shown were elicited from a holding potential of -120mV and expressed as a fraction of the maximum current (parameter *B*, see *Chapter 2*).

current traces in Figure 5.4B show the test current is dramatically reduced after the application of tetracaine (10μM). The values for %resting block and I_{Dr} at the respective drug concentrations are given in Table 5.1 together with the calculated resting state dissociation constants for human and rat $Na_V1.8$ channels. The resting state dissociation constants are also shown graphically in Fig. 5.4C.

Compound A-803467 had the highest resting state affinity (i.e. lowest dissociation constant, K_r approx. 150nM), while compound 227c89 and ralfinamide showed the lowest resting state affinities of the drugs studied with similar affinities (K_r approx. 100μM). Tetracaine and compound V102862 had intermediate affinities (K_r approx. 20μM and 1μM, respectively) (Fig. 5.4C, Table 5.1). While the resting state affinity for 227c89, ralfinamide and A-803467 was similar between human and rat $Na_V1.8$ channels, the resting state affinity for tetracaine and V102862 was greater for human $Na_V1.8$ channels than for rat $Na_V1.8$ channels (2.7-fold and 2.9-fold, respectively).

TABLE 5.1

Dissociation constants for block of resting $Na_V1.8$ channels

$Na_V1.8$ channel	Drug	Concentration (μM)	% Resting block	I_{Dr}	K_r (μM)	n
Human	227c89	10	13 ± 2	0.87 ± 0.02	81.3 ± 19.4	5
Rat	227c89	10	9 ± 3	0.91 ± 0.03	118 ± 34	3
Human	Ralfinamide	50	31 ± 8	0.69 ± 0.08	129 ± 36	3
Rat	Ralfinamide	50	30 ± 3	0.70 ± 0.03	126 ± 21	5
Human	Tetracaine	10	56 ± 7	0.44 ± 0.07	10.3 ± 3.9	6
Rat	Tetracaine	10	27 ± 3	0.73 ± 0.03	27.3 ± 4.0	3
Human	V102862	1	58 ± 2	0.42 ± 0.02	0.73 ± 0.06	6
Rat	V102862	1	33 ± 2	0.67 ± 0.02	2.1 ± 0.2	5
Human	A-803467	0.1	49 ± 9	0.51 ± 0.09	0.13 ± 0.03	5
Rat	A-803467	0.1	36 ± 2	0.64 ± 0.02	0.18 ± 0.02	5

5.2.3 Inactivated state affinity of drugs for human and rat $Na_V1.8$ channels.

In order to calculate the inactivated state affinity (the inactivated state dissociation constant, K_i) for each drug, a two-pulse protocol (Fig. 5.5A) was used before and after the application of drug. Here a 4 second depolarisation was used give 60 to 80% inactivation before the test pulse (see *Section 2.6.8*). In the absence of drug, the test current amplitude expressed as a fraction of control current amplitude was used to determine the amount of non-inactivated channels *h* (Table 5.2). The test current amplitude in the presence of drug, expressed as a fraction of the current amplitude before drug application, is the parameter I_{Di} (see *Section 2.6.8*). Since the $Na_V1.8$ channels showed altered voltage-dependent gating over time, control experiments

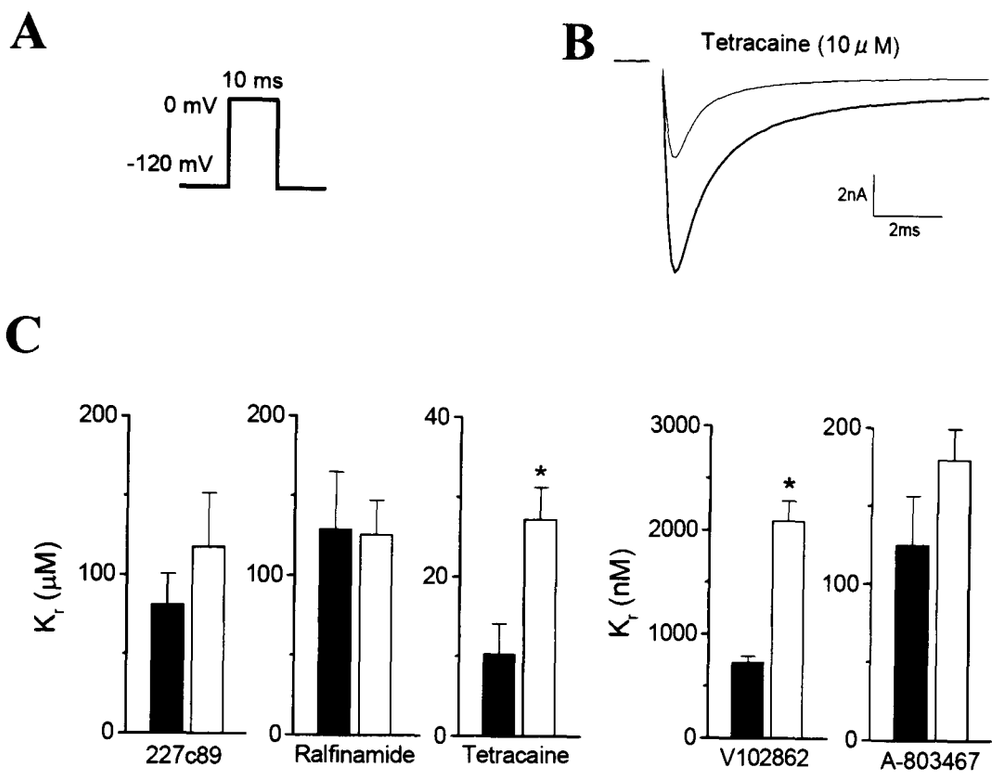

Fig. 5.4. Dissociation constants for each drug for resting $Na_V1.8$ channels. A) The pulse protocol shown was used in the absence and presence of drug to determine resting state dissociation constants (K_r). **B)** Example current traces are shown elicited by the pulse protocol in A, where current in bold was elicited in the absence of drug and the fine trace was elicited in the presence of drug. **C)** Bar diagrams are shown representing the K_r values for test compounds 227c89, ralfinamide, tetracaine, V102862 and A-803467, for human (*filled* bars) and rat (*unfilled* bars) $Na_V1.8$ channels. The concentrations (chosen to give 10-60% resting state block) and n numbers are shown in Table 5.1.

showed that after a 4 minute incubation period, the test pulse current amplitude increased by 11% (n=6) for the human $Na_V1.8$ channel and 5% (n=6) for the rat $Na_V1.8$ channel. Therefore the I_{Di} parameter was corrected by these values for the determination of the inactivated state dissociation constants. The inactivated state dissociation constants were calculated from h and I_{Di}, and the drug concentrations (Table 5.2). The calculated inactivated state dissociation constants are also shown graphically in Fig. 5.5C.

TABLE 5.2

Dissociation constants for block of inactivated $Na_V1.8$ channels

$Na_V1.8$ channel	Drug	Concentration (μM)	I_{Di}	h	K_i (μM)	n
Human	227c89	10	0.61 ± 0.05	0.32 ± 0.03	12.1 ± 2.4	5
Rat	227c89			ND		
Human	Ralfinamide	10	0.60 ± 0.08	0.31 ± 0.04	15.4 ± 5.0	5
Rat	Ralfinamide	10	0.56 ± 0.04	0.24 ± 0.01	10.2 ± 1.8	4
Human	Tetracaine	1	0.62 ± 0.05	0.28 ± 0.05	1.12 ± 0.31	7
Rat	Tetracaine	1	0.59 ± 0.09	0.31 ± 0.05	1.61 ± 0.35	8
Human	V102862	1	0.16 ± 0.03	0.28 ± 0.03	0.15 ± 0.03	6
Rat	V102862	1	0.15 ± 0.02	0.36 ± 0.04	0.11 ± 0.01	5
Human	A-803467	0.01	0.63 ± 0.06	0.34 ± 0.03	0.015 ± 0.004	7
Rat	A-803467	0.01	0.83 ± 0.06	0.35 ± 0.04	0.043 ± 0.015	3

Compounds 227c89 and ralfinamide showed the lowest inactivated state affinities of the drugs studied with similar dissociation constants (K_i approx. 12μM), and compound A-803467 had the highest resting state affinity (K_i approx. 30nM). Tetracaine and compound V102862 had intermediate dissociation constants (K_i approx. 1μM and 120nM, respectively) (Fig. 5.5C, Table 5.2). The order of affinity of drugs for the inactivated state was the same as for the resting state. While the inactivated state affinities were not significant different between human and rat $Na_V1.8$ channels for most compounds studied here, compound A-803467 showed a 2.9-fold greater affinity for the human channel. Importantly, these dissociation constants were all significantly greater for the resting state than for the inactivated state (i.e. greater affinity for the inactivated state). Indeed, the example current traces in Figure 5.5B, show that while tetracaine (1μM) has little effect on the resting channels, a marked effect was observed for inactivated channels. The ratio of the inactivated state affinity to the resting state affinity is a measure of the preferential inactivated state block. Compared to the resting state affinity, the human $Na_V1.8$ channel showed an inactivated state affinity that was 7-fold greater for 227c89, 8-fold greater for ralfinamide, 9-fold greater for tetracaine, 5-fold greater for V102862 and 8-fold greater for A-803467. However, for the rat $Na_V1.8$ channel this ratio was lower for A-803467 (4-fold), greater for 227c89 (9-fold) and ralfinamide (12-fold) and greater still for tetracaine (17-fold) and compound V102862 (19-fold) (Tables 5.1 and 5.2). Therefore, these results suggest that all

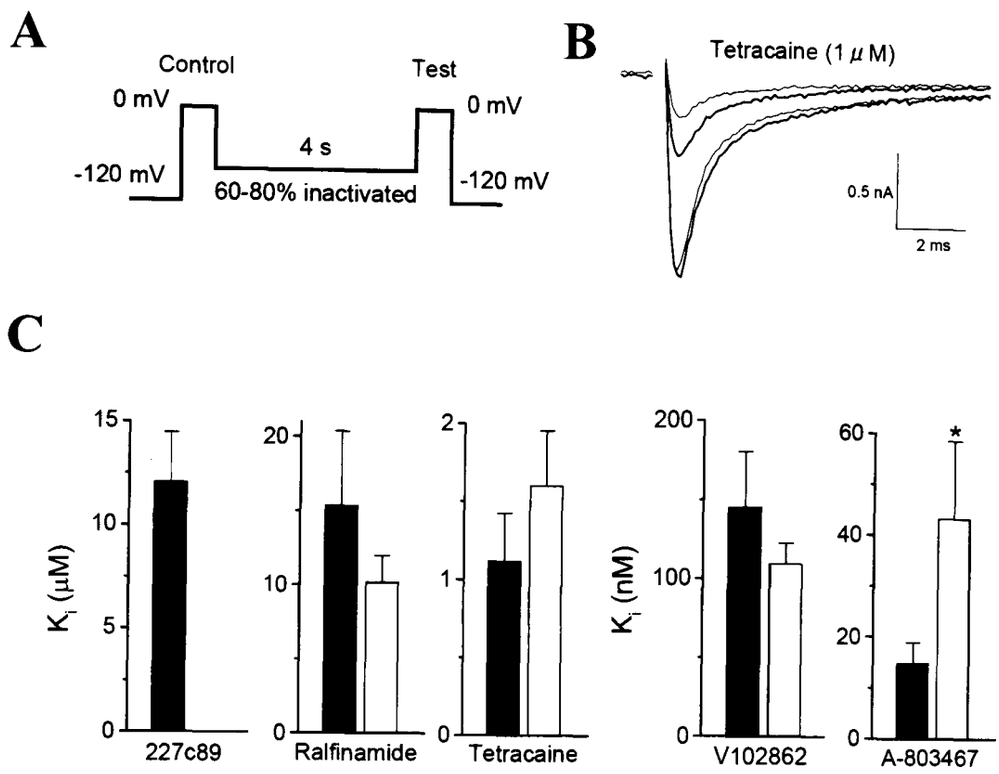

Fig. 5.5. Dissociation constants for each drug for the inactivated $Na_V1.8$ channels. A) The pulse protocol shown was used in the absence and presence of a drug to determine inactivated state dissociation constants (K_i), where the 4 second pulse indicated was taken at membrane potentials of -50 to -80 mV, such that 60% to 80% inactivation occurred. **B)** Example current traces are shown using the pulse protocol in A, where currents in bold are in absence of drug and the fine traces are in the presence of drug; the currents larger in magnitude correspond to the control pulses and currents smaller in magnitude correspond to the test pulse. **C)** Bar diagrams are shown representing the K_i values for test compounds 227c89, ralfinamide, tetracaine, V102862 and A-803467, for human (*filled* bars) and rat (*unfilled* bars) $Na_V1.8$ channels. The concentrations used and n numbers are shown in Table 5.2.

the drugs examined here preferentially bind to the inactivated state. The resting state affinity for tetracaine and V102867, and the inactivated state affinity for A-803467 were greater for human $Na_V1.8$ channels than for rat $Na_V1.8$ channels. The human and rat forms of the $Na_V1.8$ channel also differed in terms of the preference of the five drugs for the inactivated state over the resting state.

5.2.4 Use-dependent drug block of human and rat $Na_V1.8$ channels

Use-dependent block underlies an important pharmacological property of voltage-gated Na^+ channel blocking drugs, where neuronal excitability determines the level of drug block. As it was noted above (*Section 4.2.7*), frequent stimulation of channels results in channel opening and subsequent inactivation, such that, in the absence of drug, use-dependent current inhibition depends on the rate of development of inactivation during each depolarising pulse as well as the recovery from inactivation during the period between pulses. In the presence of a drug that preferentially binds to open/inactivated channels, this use-dependent effect is more pronounced. Therefore, in addition to the kinetics of drug binding and dissociation, the presence of drug alters the rates for development of inactivation and recovery from inactivation. Indeed, the states induced by frequent stimulation are usually stabilised by the drug and the recovery from inactivation is slowed, resulting in more pronounced inhibition (termed "use-dependent block" for treated cells, to distinguish from "use-dependent current inhibition" for untreated cells).

In order to investigate the use-dependent block of human and rat $Na_V1.8$ channels in the presence of drugs, a 5Hz or 10Hz train of 60 depolarising pulses (10ms duration, to 0mV from a holding potential -120mV) was used in the absence of drug and during the continual application of drug (drugs were applied before and during the train). Currents elicited in the absence and presence of drug in paired cells were first expressed as a function of the peak current amplitude recorded during the first pulse of the train (Fig. 5.6). The peak current amplitude recorded in the presence of drug were then expressed as a function of the peak current amplitude recorded in the absence of drug (Fig. 5.6). Thus the use-dependent block shown in Figures 5.7 to 5.9 (and Table 5.3) take into account the use-dependent current inhibition in the absence of drug, and show the effect of the drug only. The mean currents recorded during trains at 10Hz are shown in Fig. 5.7 for compound 227c89 and ralfinamide, Fig. 5.8 for tetracaine and V102862, and Fig. 5.9 for A-803467. The current amplitude of inhibition at steady-state (i.e. the 60^{th} pulse) following 5Hz and 10Hz trains is shown as a fraction of the current amplitude of the first pulse in the train (Fig. 5.10). Overall, a range of use-dependent properties were observed for the different drugs studied here. Compound 227c89 (Fig. 5.7A; 10μM), showed moderate onset of use-dependent block and significant ($P<0.005$) inhibition was observed at the end of the 10Hz train for both

1.

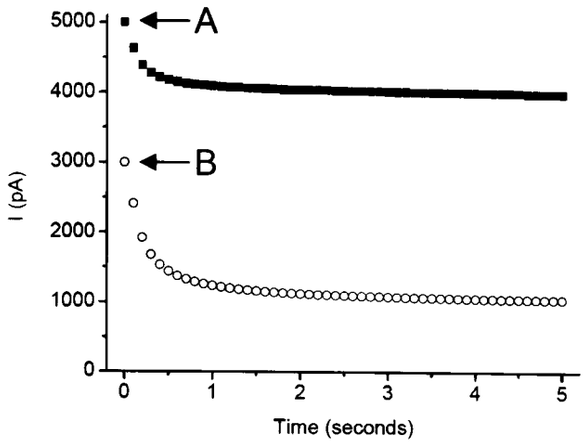

Peak current amplitudes were recorded in the absence (■) and presence (○) of drug during a train of depolarising pulses. The arrows indicates the first pulse of each train. The experiments were carried out in paired cells.

2.

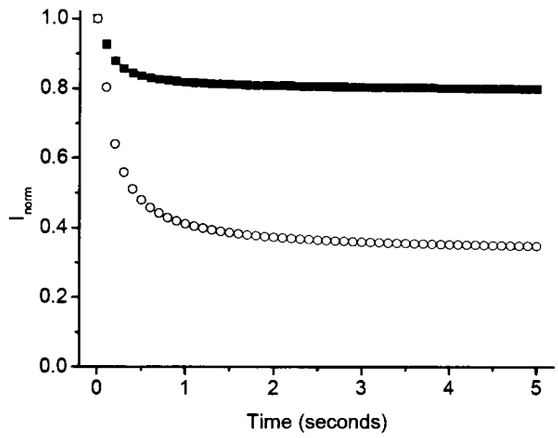

The currents at each time point were expressed as a fraction of the current elicited by the first pulse of the train. For instance, currents recorded in the absence of drug (■) were normalised to current marked "A" in above figure, and currents recorded in the presence of drug (○) were normalised to current marked "B" in above figure.

3.

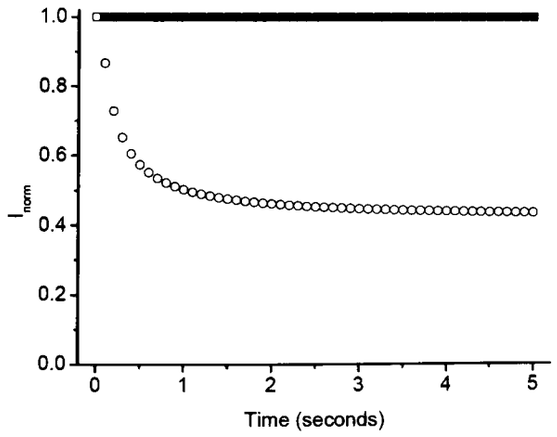

The currents at each time point were then expressed as a fraction of the current at the same time point recorded in the absence of drug in the same cell. This second normalisation of currents ensures that the currents recorded in the presence of drug (○) only show the effect of the drug, since the current inhibition recorded in the absence of drug (■) was shown to be compensated.

Fig. 5.6. Overview of the method used to normalise the currents recorded during repetitive stimulation in the absence and presence of drug. For purposes of clarity, these data points are not real recordings from cells.

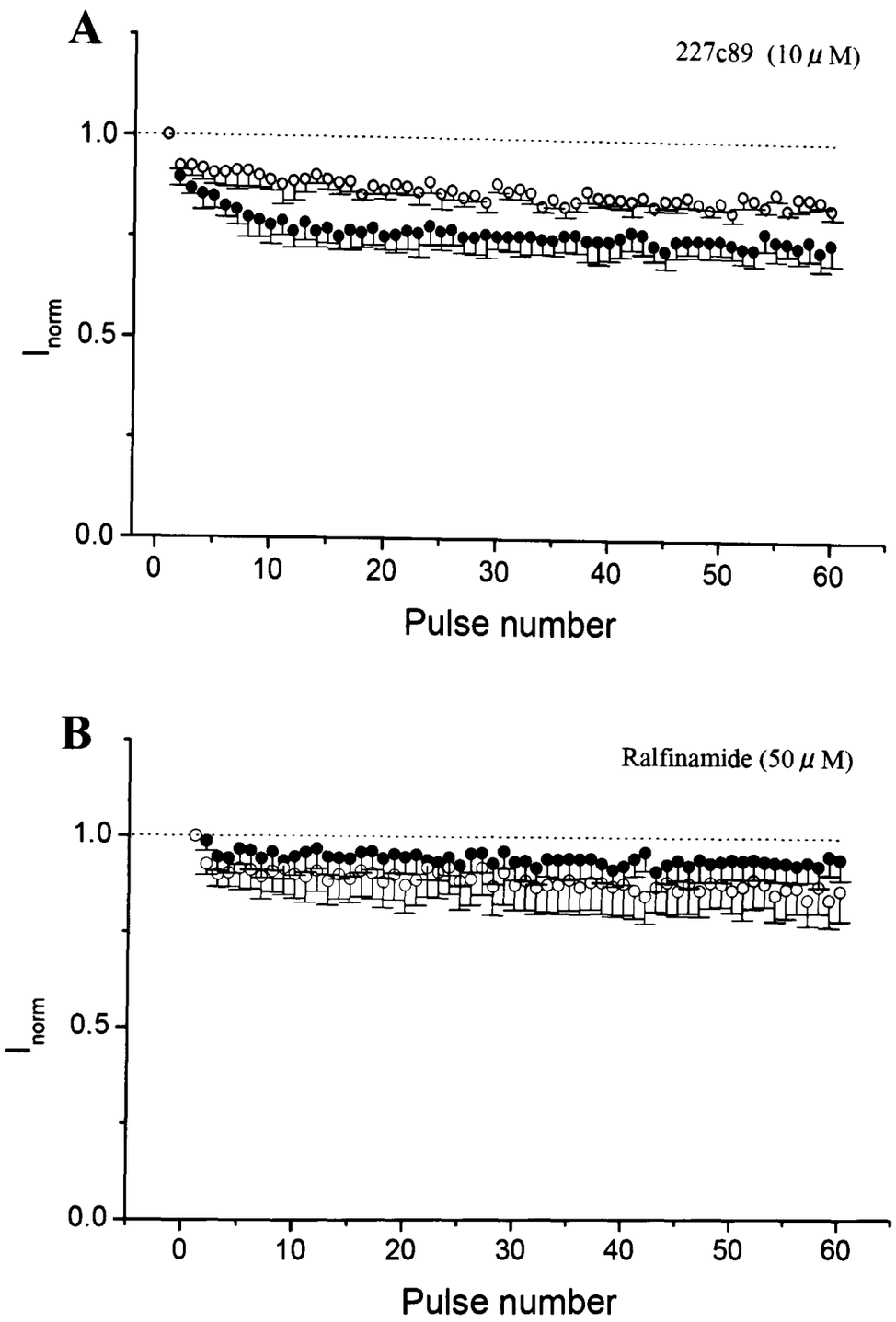

Fig. 5.7. Use-dependent effects of 227c89 and ralfinamide. A) The normalised current is shown plotted against pulse number during stimulation at 10Hz (pulses to 0mV of 10ms duration from a holding potential of -120mV) in the continual presence of 227c89 (10μM). Curves are for human (●) and rat (○) $Na_V1.8$ channels. **B)** Normalised current is shown plotted against pulse number during stimulation at 10Hz (pulses to 0mV of 10ms duration) in the continual presence of ralfinamide (50μM). Curves are for human (●) and rat (○) $Na_V1.8$ channels. Currents were normalised as shown in Figure 5.6. The n numbers are shown in Table 5.3.

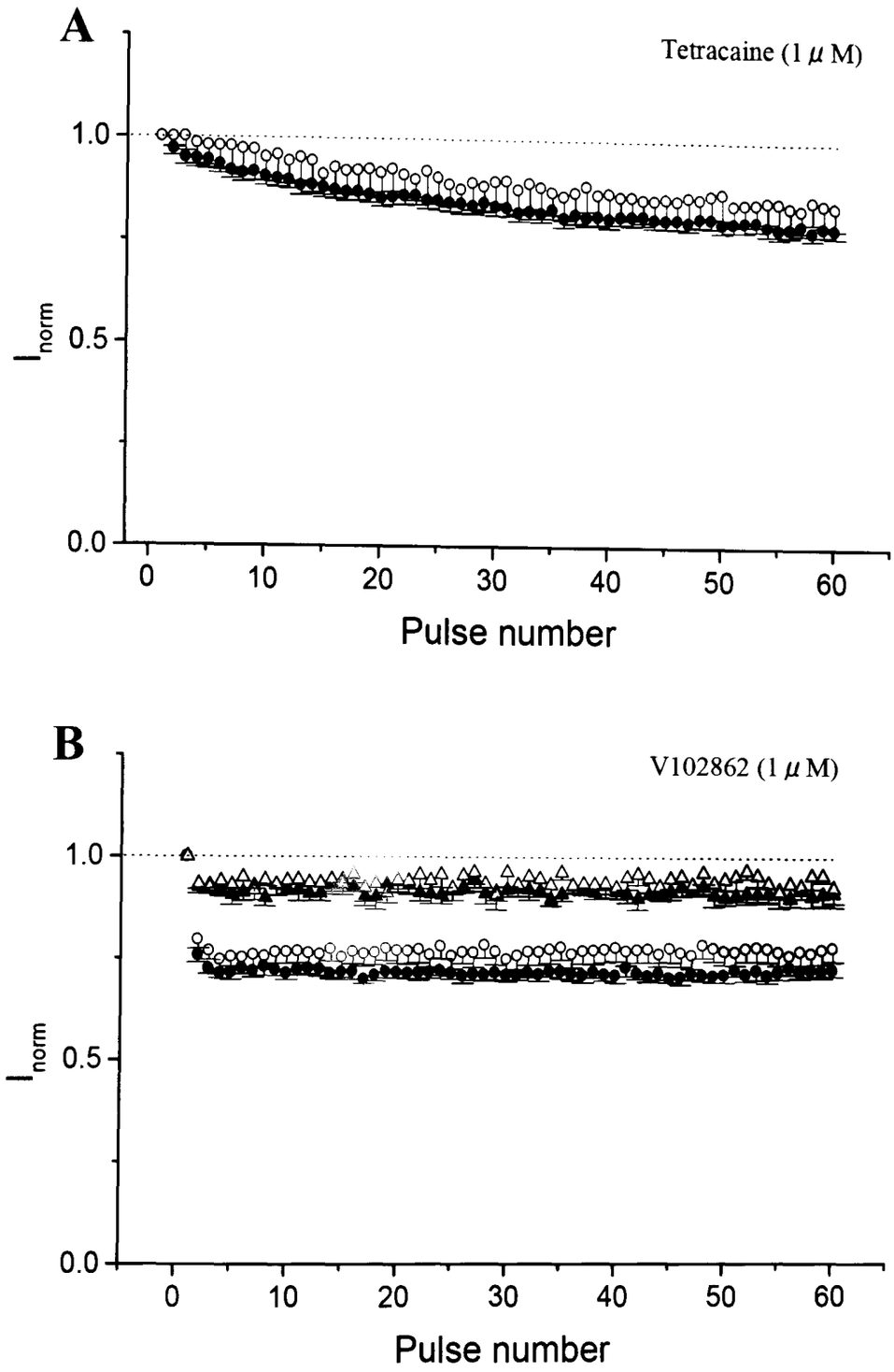

Fig. 5.8. Use-dependent effects of tetracaine and V102862. A) Normalised current is shown plotted against pulse number during stimulation at 10Hz (pulses to 0mV of 10ms duration from a holding potential of -120mV) in the continual presence of tetracaine (1μM). Curves are for human (●) and rat (○) $Na_V1.8$ channels. **B)** Normalised current is shown plotted against pulse number during stimulation (pulses to 0mV of 10ms duration) in the continual presence of ralfinamide (50μM) for human (●) and rat (○) $Na_V1.8$ channels at 10Hz, and for human (▲) and rat (△) $Na_V1.8$ channels at 5Hz. Currents were normalised as shown in Figure 5.6. The n numbers are shown in Table 5.3.

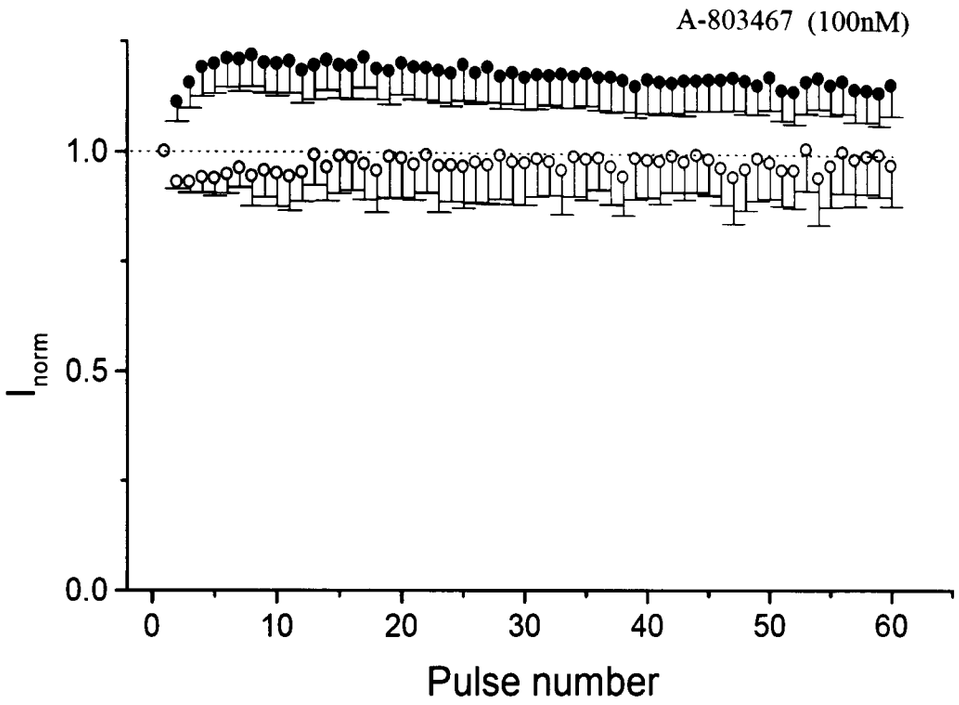

Fig. 5.9. Use-dependent effects of A-803467. Normalised current is shown plotted against pulse number during stimulation at 10Hz (pulses to 0mV of 10ms duration from a holding potential of -120mV) in the continual presence of A-803467 (100nM). Curves are for human (●) and rat (○) $Na_V1.8$ channels. Currents were normalised as shown in Figure 5.6. The n numbers are shown in Table 5.3.

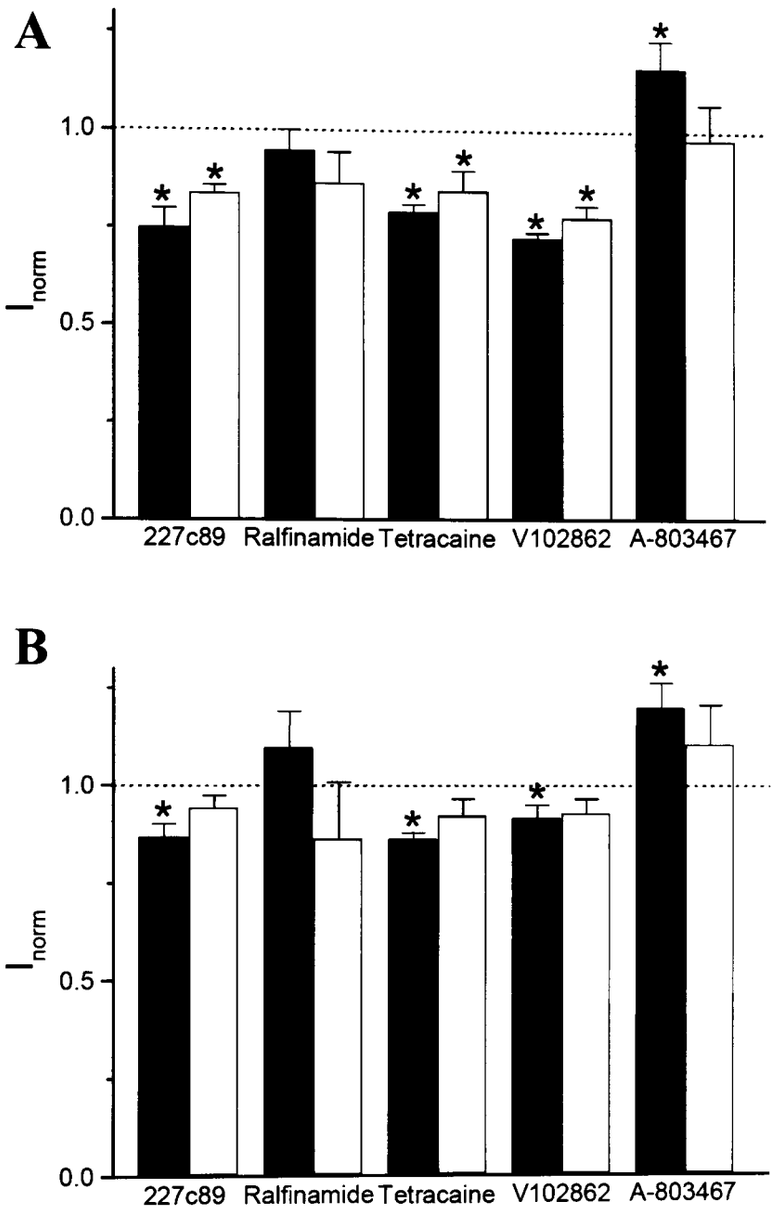

Fig. 5.10. Use-dependent properties of each compound. A) Currents are shown for the 60th pulse of a 10Hz train for 227c89, ralfinamide, tetracaine, V102862 and A-803467 for human (*filled* bars) and rat (*unfilled* bars) $Na_V1.8$ channels. **B)** Currents are shown for the 60th pulse of a 5Hz train for each drug for human (*filled* bars) and rat (*unfilled* bars) $Na_V1.8$ channels. * $p<0.05$, compared to the first pulse. Currents were normalised as shown in Figure 5.6. The n numbers are shown in Table 5.3.

human and rat $Na_V1.8$ channels. The main feature at 5Hz generally was a decrease in the effect of the compound (Table 5.3). For ralfinamide (50μM), little use-dependent block was observed at both stimulation frequencies at a holding potential of -120mV. Tetracaine (1μM) showed the slowest onset of use-dependent block, and significant ($P<0.05$) use-dependent block was observed from 10Hz stimulation frequencies for both human and rat forms of the $Na_V1.8$ channel (Figs. 5.8A and 5.10A, Table 5.3). The effect of tetracaine was reduced at 5Hz for both human and rat $Na_V1.8$ channels (Fig. 5.10B, Table 5.3). Compound V102862 showed significant ($P<0.005$) block at 10Hz with the fastest onset of the drugs studied. Interestingly, a 5Hz stimulation frequency showed a significantly reduced extent of V102862 block at the end of the train (Figs. 5.8B and 5.10, Table 5.3). For compound A-803467, use-dependent block was not observed for rat $Na_V1.8$ from both 5Hz and 10Hz stimulation frequencies (Fig. 5.9). For human $Na_V1.8$ the presence of compound A-803467 increased the current rather than showing use-dependent block (effectively increasing the current) by approximately 17% at 10Hz (Figs. 5.9 and 5.10, Table 5.3).

Overall, compound 227c89, tetracaine and compound V102862 showed the greatest extent of inhibition at the end of a 10Hz train. A similar trend was also observed for use-dependent current inhibition at 5Hz, but to a lesser extent (most notably for compound V102862).

TABLE 5.3

Effects of drugs on use-dependent block

$Na_V1.8$ channel	Drug	Concentration (μM)	Use-dependent block			
			5Hz	n	10Hz	n
Human	227c89	10	0.87 ± 0.03	4	0.75 ± 0.05	4
Rat	227c89	10	0.94 ± 0.03	5	0.84 ± 0.02	5
Human	Ralfinamide	50	1.10 ± 0.09	3	0.95 ± 0.05	7
Rat	Ralfinamide	50	0.86 ± 0.15	3	0.87 ± 0.08	8
Human	Tetracaine	1	0.86 ± 0.02	10	0.79 ± 0.02	20
Rat	Tetracaine	1	0.92 ± 0.04	6	0.85 ± 0.05	10
Human	V102862	1	0.92 ± 0.03	5	0.73 ± 0.01	11
Rat	V102862	1	0.93 ± 0.04	5	0.78 ± 0.03	12
Human	A-803467	0.1	1.20 ± 0.06	6	1.17 ± 0.07	11
Rat	A-803467	0.1	1.11 ± 0.10	4	0.98 ± 0.09	4

5.2.5 Effects of drug block on the recovery from inactivation

In order to further understand the use-dependent properties of compounds 227c89, ralfinamide, tetracaine, V102862 and A-803467, their effects on recovery from inactivation was studied. In these experiments, the same protocol as in Fig. 4.10 (also shown in Fig. 5.11A) was

used before and after the application of test compound, in order to study the effect of the drug on the time course of recovery from inactivation.

As discussed above in *Chapter 4*, the time course of recovery from inactivation for both human and rat $Na_V1.8$ channels showed an initial fast component (time constant approx. 10ms) followed by a slower component (time constant approx. 150ms). Compound 227c89 (10μM) did not affect recovery from inactivation (Fig. 5.11A); the values for the fast and slow components of recovery were similar to those of the untreated cells (Figs. 5.14 and 5.15, and Table 5.4). In contrast, ralfinamide (50μM) and tetracaine (10μM, Figs. 5.11B and 5.12A) slowed both the fast and slow time constants (Figs. 5.14 and 5.15 and Table 5.4), suggesting that these drugs stabilise both components of inactivation. Furthermore, ralfinamide and tetracaine decreased the fast component amplitude while they increased the amplitude of the slow component (Figs. 5.14 and 5.15 and Table 5.4).

Compound V102862 (1μM, Fig. 5.12B), showed an additional slow component of recovery with increased current for human $Na_V1.8$, but not for rat $Na_V1.8$. Therefore, for the human $Na_V1.8$ channel the curve was fitted with three exponential time constants (see *Section 2.6.5*). This increase in current is most likely due to a removal of drug block by stimulation, since the experiments were carried out in the continual presence of drug and the data includes resting channel block (58±2%; Table 5.1). The first exponential component was of small amplitude and the second component of recovery was slower and of greater amplitude in the presence of drug (Fig. 5.12B and Figs. 5.14,5.15). The third component (due to the increased current) had amplitude I_3 (see *Section 2.6.5*) of 29.9±7.3% (taking the fully recovered total current as 100%) and a slow decay time constant of 1.1±0.2 seconds (Table 5.4). The increase in current amplitude above the control value may be a result of the removal of resting block from the channel, and the time course represents a slow reinstatement of resting block.

Similarly to compound V102862, compound A-803467 (100nM, Fig. 5.13) also showed a marked increase in current above the control value for the time course of recovery from inactivation. Indeed, the time course of recovery also required a three-exponential fit following the application of compound A-803467. For the first component, there was a small increase in the amplitude, while the time constant was unaltered by the drug (Fig. 5.14). The second component showed little change in either amplitude or the time constant (Fig. 5.15). The third component showed an amplitude I_3 of 22.1±3.2% and time constant of 1.7±0.2 seconds. For A-803467 (100nM), 49±9% of resting channels were blocked (Table 5.1), again indicating that the increased current may be due to an appreciable removal of the resting component, and its consequent time course is due to resting block returning.

The removal of drug block observed following frequent stimulation and recovery from inactivation is an unexpected result and has not previously been observed for voltage-gated Na^+ channel blocking drugs. The term "*disinhibition*" will be used to describe this effect.

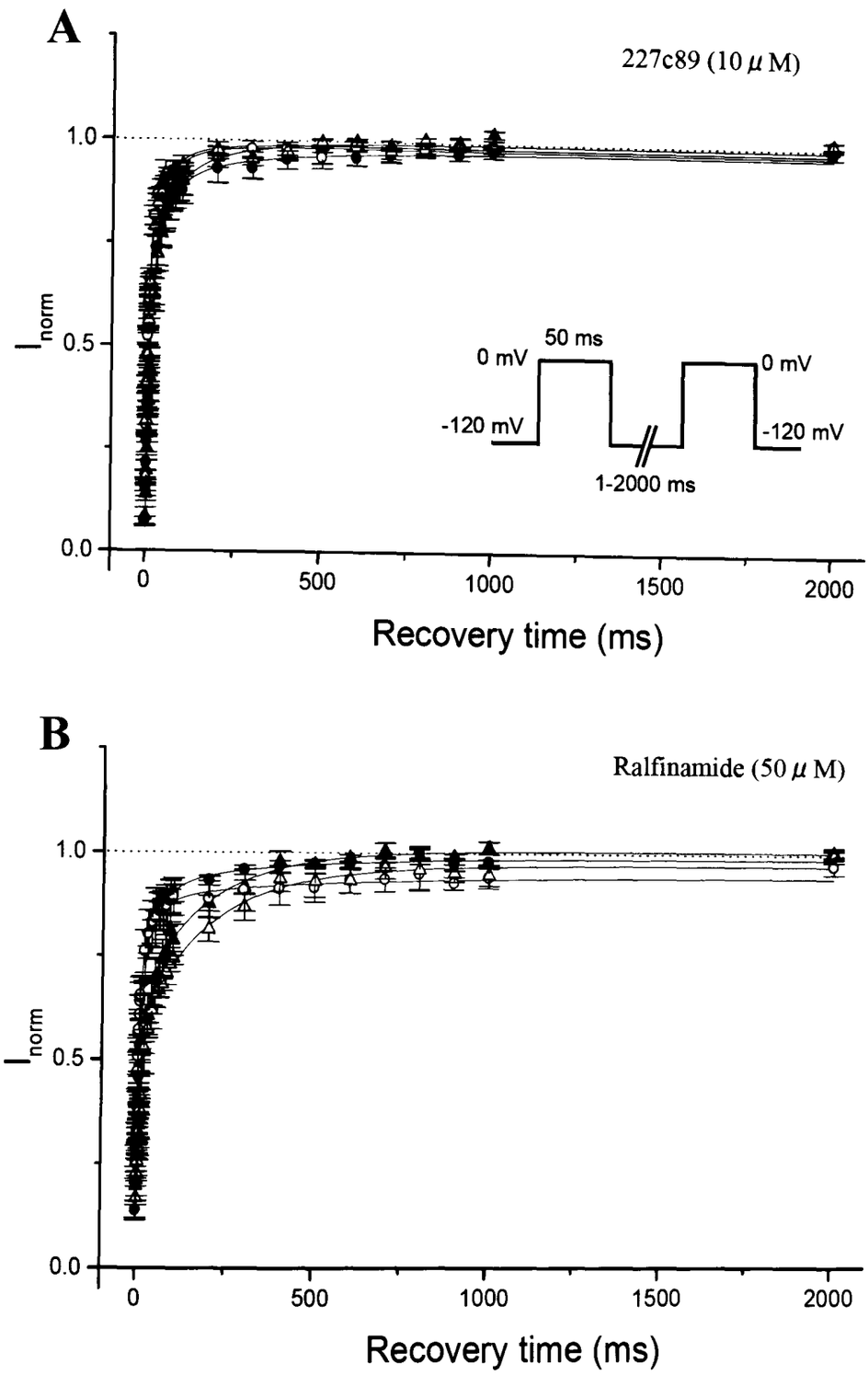

Fig. 5.11. The effects of 227c89 and ralfinamide on the time course of recovery from inactivation. A) Time courses are shown for human (●) and rat (○) $Na_V1.8$ channels in the absence of drug, and for human (▲) and rat (△) $Na_V1.8$ channels after the application of 227c89 (10μM) in paired cells. **B)** Time courses are shown for human (●) and rat (○) $Na_V1.8$ channels in the absence of drug, and for human (▲) and rat (△) $Na_V1.8$ channels after the application of ralfinamide (50μM) in paired cells. The current amplitude during the test pulse was expressed as a fraction of the current amplitude during the control pulse, and plotted against the duration of the recovery period. The pulse protocol is shown in the inset of A. The curves were fit with a double exponential equation. The n numbers are shown in Table 5.3.

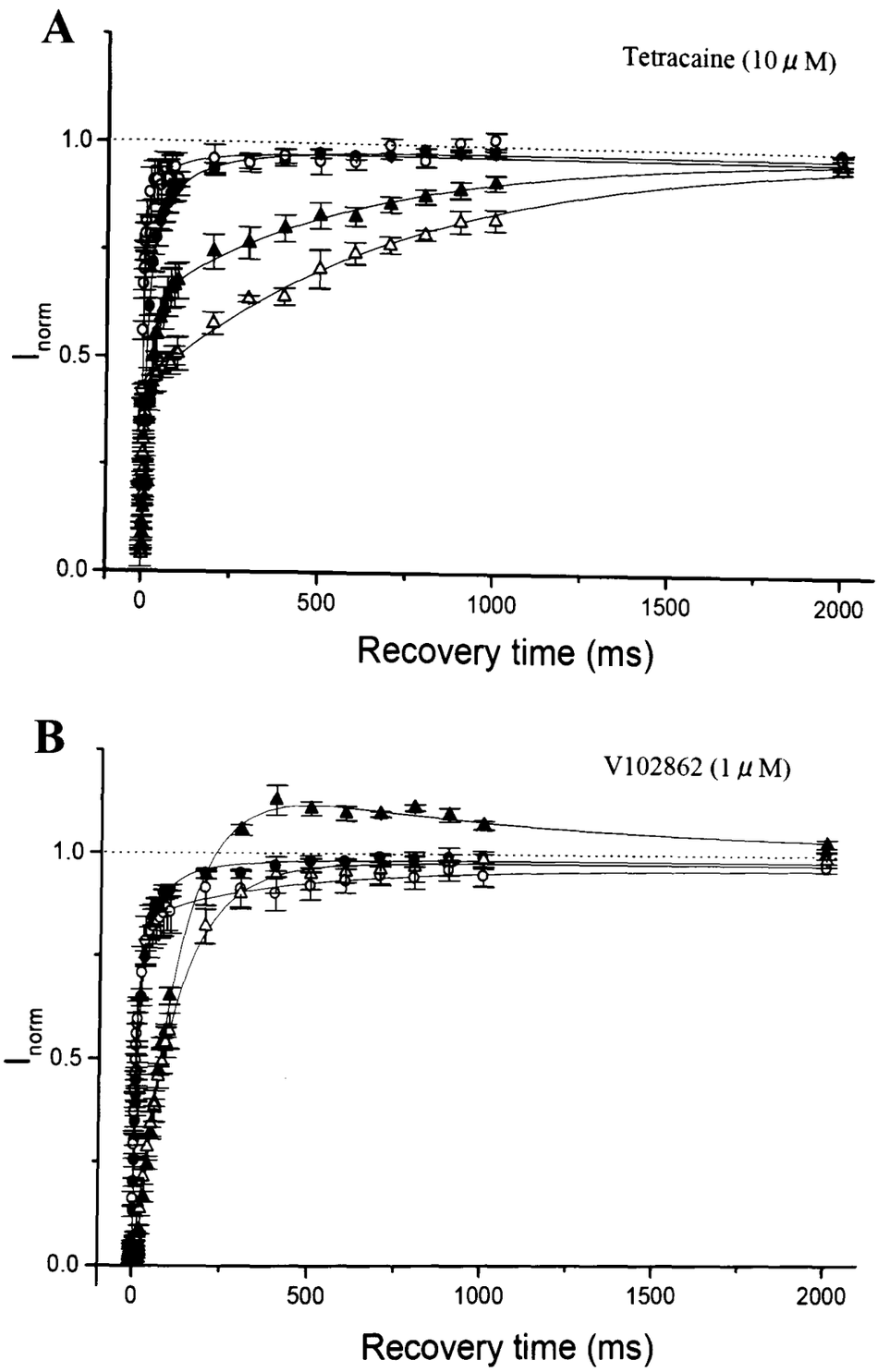

Fig. 5.12. The effects of tetracaine and V102862 on the time course of recovery from inactivation. A) Time courses are shown for human (●) and rat (○) $Na_V1.8$ channels in the absence of drug, and for human (▲) and rat (△) $Na_V1.8$ channels after the application of tetracaine (10μM) in paired cells. **B)** Time courses are shown for human (●) and rat (○) $Na_V1.8$ channels in the absence of drug, and for human (▲) and rat (△) $Na_V1.8$ channels after the application of V102862 (1μM) in paired cells. The current amplitude during the test pulse was normalised as a fraction of the current amplitude during the control pulse, and plotted against the duration of the recovery period. The curves were fit with a two exponential components, except for the $hNa_V1.8$ channel in the presence of V102862, which was fit with three. The n numbers are shown in Table 5.3.

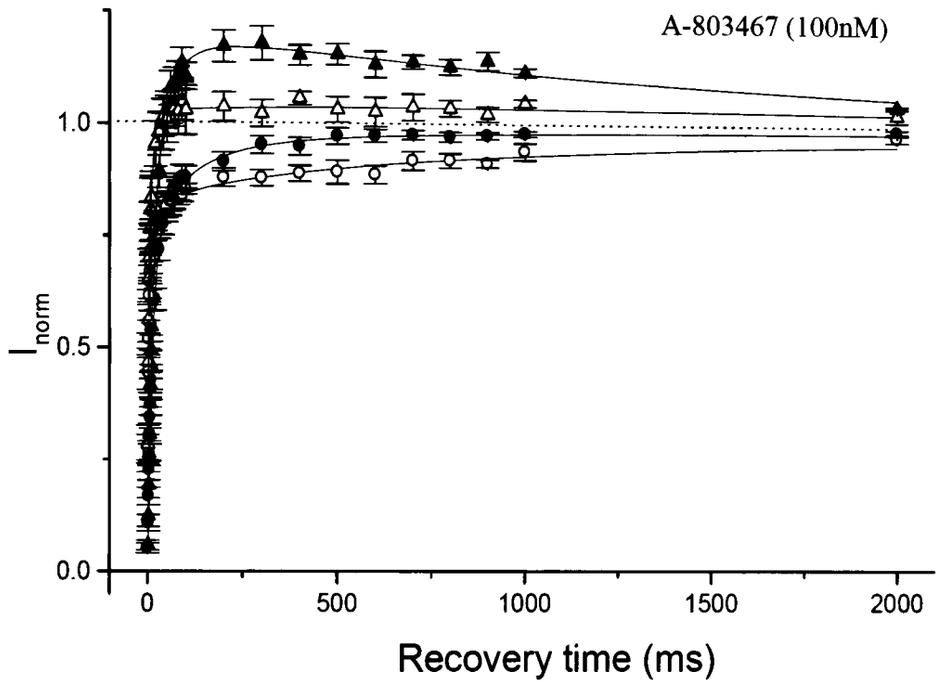

Fig. 5.13. The effect of A-803467 on the time course of recovery from inactivation. Time courses are shown for human (●) and rat (○) $Na_V1.8$ channels in the absence of drug, and for human (▲) and rat (△) $Na_V1.8$ channels after the application of A-803467 (100nM) in paired cells. The current amplitude during the test pulse was normalised as a fraction of the current amplitude during the control pulse, and plotted against the duration of the recovery period. The curves were fit with a two exponential components, except for the $hNa_V1.8$ channel in the presence of A-803467, which was fit with three. The n numbers are shown in Table 5.3.

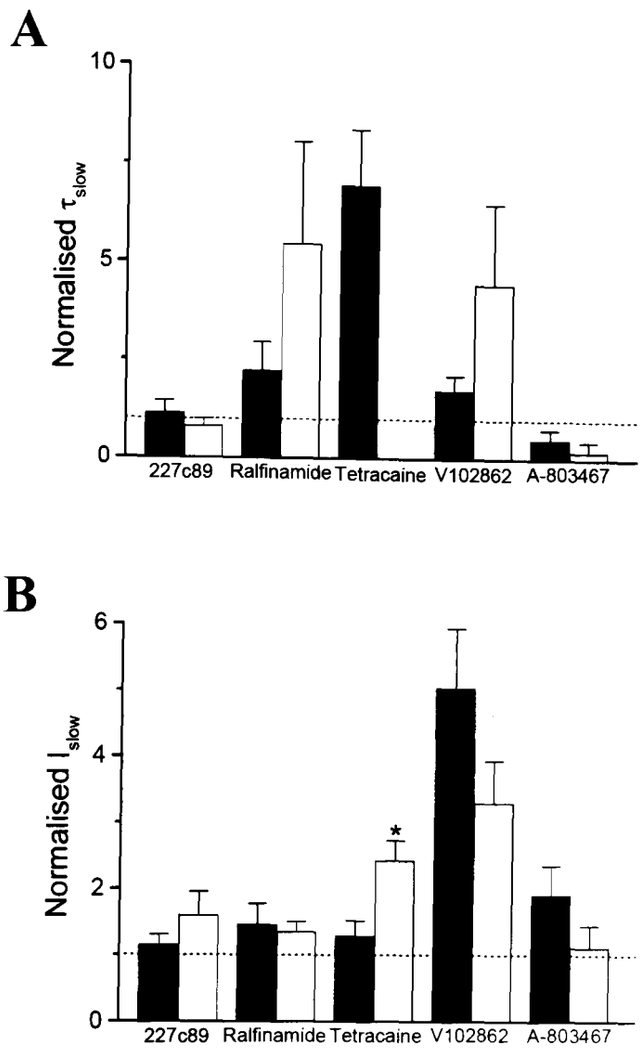

Fig. 5.15. The effects of each drug on the parameters of the slow component of recovery. A) The bar diagram shows the fitted parameters for the slow component time constant, τ_{slow}, for human (*filled* bars) and rat (*unfilled* bars) $Na_V1.8$ channels. The parameters shown for each drug were normalised to the paired values before drug application. **B)** The bar diagram shows the fitted parameters for the slow component amplitude, I_{slow}, for human (*filled* bars) and rat (*unfilled* bars) $Na_V1.8$ channels. The parameters shown for each drug were normalised to the paired values before drug application. τ_{slow} is not shown for tetracaine (rat $Na_V1.8$ channel) in A due to large experimental errors. * $p<0.05$. The n numbers are shown in Table 5.3.

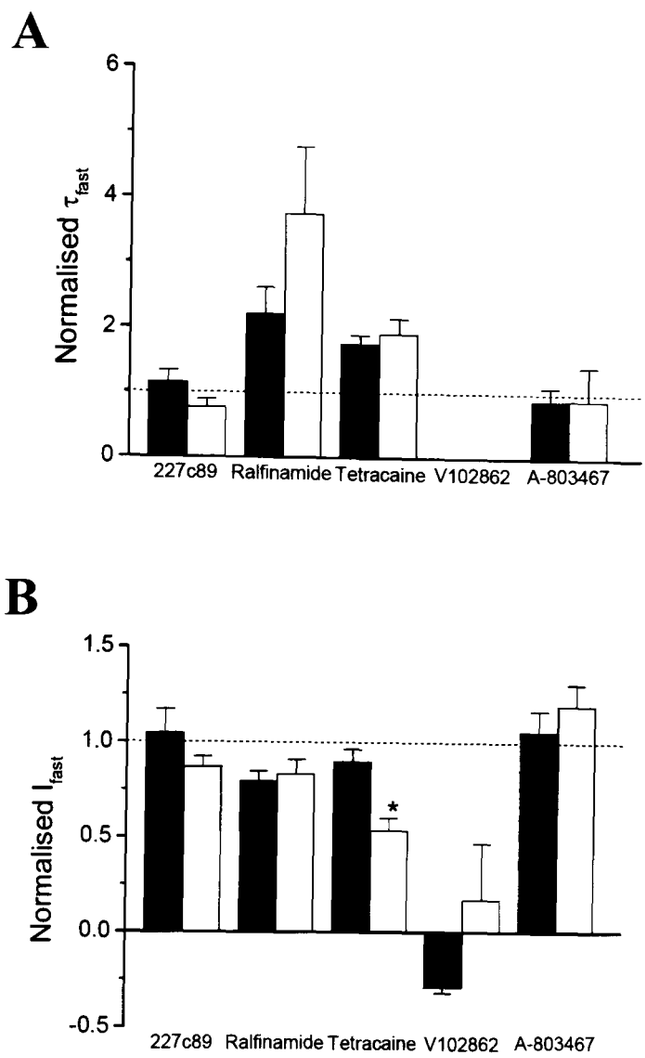

Fig. 5.14. The effects of each drug on the parameters of the fast component of recovery. A) The bar diagram shows the fitted parameters for the fast component time constant, τ_{fast}, for human (*filled* bars) and rat (*unfilled* bars) $Na_V1.8$ channels. The parameters shown for each drug were normalised to the paired values before drug application. **B)** The bar diagram shows the fitted parameters for the fast component amplitude, I_{fast}, for human (*filled* bars) and rat (*unfilled* bars) $Na_V1.8$ channels. The parameters shown for each drug were normalised to the paired values before drug application. * $p<0.05$. The n numbers are shown in Table 5.3.

TABLE 5.4

Effects of drugs on recovery from inactivation

$Na_V1.8$ channel	Drug	Concentration (μM)	Recovery from inactivation						
			τ_{fast} norm	I_{fast} norm	τ_{slow} norm	I_{slow} norm	τ_3 (ms)	I_3 (%)	n
Human	227c89	10	1.12 ± 0.25	1.00 ± 0.13	0.87 ± 0.48	1.06 ± 0.23	-	-	5
Rat	227c89	10	0.76 ± 0.24	0.87 ± 0.07	0.82 ± 0.46	1.50 ± 0.49	-	-	3
Human	Ralfinamide	50	2.14 ± 0.42	0.79 ± 0.05	0.99 ± 0.46	1.32 ± 0.28	-	-	5
Rat	Ralfinamide	50	2.90 ± 0.86	0.82 ± 0.13	1.34 ± 1.06	1.29 ± 0.20	-	-	4
Human	Tetracaine	10	1.74 ± 0.20	0.90 ± 0.07	5.46 ± 1.80	1.24 ± 0.20	-	-	6
Rat	Tetracaine	10	1.89 ± 0.29	0.53 ± 0.06	15.9 ± 9.3	2.40 ± 0.27	-	-	3
Human	V102862	1	-	-0.29 ± 0.04	1.21 ± 0.46	4.64 ± 0.66	1073 ± 232	29.9 ± 7.3	5
Rat	V102862	1	-	0.11 ± 0.24	3.63 ± 3.60	2.91 ± 0.52	-	-	6
Human	A-803467	0.1	0.90 ± 0.20	1.06 ± 0.11	0.50 ± 0.27	1.92 ± 0.41	1668 ± 183	22.1 ± 3.2	5
Rat	A-803467	0.1	0.91 ± 0.51	1.20 ± 0.11	0.25 ± 0.26	1.12 ± 0.34	-	-	4

5.3 Discussion

5.3.1 Tonic block of resting and inactivated $Na_V1.8$ channels

In this chapter the properties of compounds 227c89, A-803467, ralfinamide, tetracaine and V102862 were compared between human and rat $Na_V1.8$ channels. Experiments were carried out such that protocols were as short as possible, to reduce effects of whole-cell patch clamp holding time on the functional properties of the $Na_V1.8$ channels. For the resting state, the compounds tested showed drug affinities in the order ralfinamide < 227c89 < tetracaine < V102862 < A-803467 for both human and rat $Na_V1.8$ channels, although tetracaine and V102862 showed an approximately 2-fold greater affinity for resting human $Na_V1.8$ channel compared to the rat $Na_V1.8$ channel. The binding affinity for inactivated channels was higher than for resting channels for all drugs studied, suggesting they all preferentially act on inactivated channels. Affinities for the inactivated state showed the same drug order as for resting channels for both human and rat $Na_V1.8$ channels. Compound A-803467 showed an approximately 3-fold greater affinity for the inactivated human $Na_V1.8$ channel than for the inactivated rat $Na_V1.8$ channel. The affinity for the inactivated human $Na_V1.8$ channel was 5- to 9-fold greater than for the resting channel, whereas the affinity for the inactivated rat $Na_V1.8$ channels was 4- to 18-fold greater than for the resting channel. These results suggest differences in the state-dependent properties of these drugs acting on the human and rat $Na_V1.8$ channels, where a wider range of drug selectivity for the inactivated state over the resting state was shown for rat $Na_V1.8$ compared to human $Na_V1.8$. For instance, a much greater differential between block of resting and inactivated channels was shown for rat $Na_V1.8$ for tetracaine (17-fold) and V102862 (19-fold) compared to the human channel for tetracaine (9-fold) and V102862 (5-fold). Conversely, compound A-803467 showed a smaller differential between block of resting and inactivated channels for the rat $Na_V1.8$ channel (4-fold) compared to the human $Na_V1.8$ channel (8-fold). Following the stable expression of rat $Na_V1.8$ in ND7/23 cells, John et al. (2004) determined the concentration for half-maximal inhibition (IC_{50}) of tetracaine for resting states (holding potential -90mV) as 13μM, which is comparable to the value determined in this chapter (27μM) for the resting rat $Na_V1.8$ channel.

Dekker et al. (2005) showed that tetracaine is 16-fold more potent for human $Na_V1.8$ channels than for rat $Na_V1.8$ channels stably expressed in SH-SY5Y cells. At first sight this would appear to contradict the results of this chapter (a 2-fold difference in the affinity for resting human and rat $Na_V1.8$ channels, and near-identical affinities for the inactivated $Na_V1.8$ channels). However, in the membrane potential fluorescence assay used by Dekker et al., the

cells are not voltage clamped and are at resting membrane potentials of the neuroblastoma SH-SY5Y cells. Since human $Na_V1.8$ displays a significantly more depolarised inactivation curve compared to rat $Na_V1.8$ channels (*Chapter 4*), at resting membrane potentials human $Na_V1.8$ will be substantially more inactivated and able to bind tetracaine with higher affinity compared to rat $Na_V1.8$. This would explain the apparent higher selectivity for human $Na_V1.8$ observed by Dekker et al., since many channels would be inactivated at these resting membrane potentials. Moreover, the latter authors also reported an IC_{50} value of 10μM for ralfinamide. This value is also consistent with the substantial inactivation of human $Na_V1.8$ compared to rat $Na_V1.8$ since it was similar to the human $Na_V1.8$ inactivated state dissociation constant (15μM), but not the resting dissociation constant (125μM). Similarly, the IC_{50} value for ralfinamide binding to the rat $Na_V1.8$ channel determined by Dekker et al. (55μM) is intermediate between resting (127μM) and inactivated (10μM) dissociation constants, consistent with less inactivation of the rat channel at the membrane potentials used. Therefore these results indicate that the measurements made by Dekker et al. using a membrane potential fluorescence assay largely represent binding to the substantially inactivated human $Na_V1.8$ channel as compared with the rat $Na_V1.8$ channel. Furthermore, in agreement with the value for ralfinamide binding to inactivated rat $Na_V1.8$ channels determined in this chapter (10μM), Stummann et al. (2005) reported an IC_{50} value of 10μM for ralfinamide binding to inactivated rat TTX-resistant channels. These findings are consistent with the findings here and exemplify the necessity to control the membrane potential for the investigation of voltage-dependent blocking drugs.

It is also interesting to compare the inactivated state binding affinity data for $Na_V1.8$ channels with data in the literature for other Na_V channel subtypes. Compared to the inactivated state binding affinity of tetracaine for the $rNa_V1.3$ channel (K_i 6.3 μM; Li et al., 1999), the human $Na_V1.8$ channel showed a 6-fold greater affinity and the rat $Na_V1.8$ channel showed 4-fold greater affinity. Subtype-selectivity was also observed for compound V102862, where both human and rat $Na_V1.8$ channels showed a 4-fold greater inactivated state affinity than for $rNa_V1.2$ channels (K_i 0.4μM; Ilyin et al., 2005). Furthermore, the affinity of compound A-803467 for human $Na_V1.8$ was similar to the IC_{50} reported by Jarvis et al. (2007) for the same channel. The latter authors showed an approximate 100-fold greater affinity for human $Na_V1.8$ than for $hNa_V1.2$, $hNa_V1.3$, $hNa_V1.5$ and $hNa_V1.7$. Consistent with the results described here, Jarvis et al. also reported a greater inactivated state affinity of A-803467 for human $Na_V1.8$ channels, as compared with rat TTX-resistant Na^+ currents. The results here for ralfinamide are also consistent with those of Stummann et al. (2005), and suggest a 2-fold greater affinity for $Na_V1.8$ channels as compared with TTX-sensitive Na^+ channels. In contrast, compound 227c89 showed an inactivated state binding affinity for rat $Na_V1.2$ channels (K_i 17.3 μM; Liu et al., 2003), similar to the value shown for human and rat $Na_V1.8$ channels.

The binding affinity of a compound depends on the relative strengths of interaction with accessible amino acid residues in the binding site. The drugs studied here are expected to interact with previously identified amino acid residues of the pore-lining S6 segments (Catterall, 2002; Nau and Wang, 2004). However, the greater affinity of tetracaine, V102862, A-803467 and ralfinamide for $Na_V1.8$ over other channel subtypes indicates differences in relative strengths of binding to these residues. Despite the near identity of these residues in the S6 segments, interactions must somehow differ between Na_V subtypes, and indeed between human and rat $Na_V1.8$ channels. It is also possible that because the properties of the first and second components of recovery from inactivation are also different between human and rat $Na_V1.8$ channels (first component slower for human and vice versa, second component faster for human, see *Chapter 4*) the relative drug binding affinity to the kinetically distinct inactivation states may be different. It has been reported that there can be differences in drug affinity (and hence drug action) between slow and fast inactivated channels (Cardenas et al., 2006). For example, lacosamide appears to interact with slow (rather than fast) inactivation states of TTX-sensitive Na_V currents (Errington et al., 2008). Furthermore, the more pronounced frequency-dependent block for $Na_V1.8$ channels by lidocaine compared to TTX-sensitive channels was explained by the greater tendency for $Na_V1.8$ to enter slow inactivation states (Leffler et al., 2007).

In summary, the block of inactivated channels was greater than for resting channels for all drugs studied, and differences in the drug binding affinities were observed between human and rat $Na_V1.8$ channels, and also between $Na_V1.8$ and other subtypes in the literature.

5.3.2 The effect of drugs on $Na_V1.8$ channel recovery from inactivation

In the continual presence of compounds 227c89, tetracaine and ralfinamide, the recovery from inactivation was fitted with two exponential components. While 227c89 did not appear to affect the recovery from inactivation, both tetracaine and ralfinamide slowed the fast and slow components of inactivation and increased the amplitude of the latter. These results suggest that tetracaine and ralfinamide stabilise the inactivation states of human and rat $Na_V1.8$ channels.

Following the application of compound V102862 or A-803467 a striking and unexpected effect was observed for the human $Na_V1.8$ channel during recovery from inactivation. Recovery involved not simply the removal of inactivation, but also a period where resting drug block was apparently removed, and the current amplitude of the test pulse became greater than control, termed "disinhibition". The time course of recovery from inactivation was fitted with an additional slow component representing this disinhibitory component. The compounds that showed this effect for the human $Na_V1.8$ channel (V102862 and A-803467) were also the most potent $Na_V1.8$ channel blockers studied. For rat $Na_V1.8$ channels, the effect was not observed in

the presence of V102862, and only to a small extent in the presence of A-803467. Furthermore, this phenomenon has never been reported for any Na_V blocking drugs acting on any Na_V channel subtype, for example it was not observed for rat $Na_V1.2$ channels in the presence of compound V102862 (Ilyin et al., 2005).

Since disinhibition by compounds A-803467 and V102862 was not observed for rat $Na_V1.8$, but was observed for human $Na_V1.8$ channels, this suggests that the binding of these compounds is different between the two channels under these conditions. The reason for the difference is unclear, but both compounds A-803467 and V102862 have differential drug binding affinities between the two channels for the inactivated and resting states respectively.

5.3.3 The effect of drugs on repetitive stimulation

Lamotrigine derivative 227c89 was found here to show marked use-dependent block at 10Hz. The extent of 227c89 (10μM) block at the end of a 10Hz train observed here (approx. 20%) is similar to the extent described for the much greater concentration of 227c89 (300μM) acting on the rat $Na_V1.2$ channel during a 10Hz train (approx. 20%). Although it is difficult to compare results where different experimental conditions have been used, these obsevations suggest that use-dependent block by 227c89 is more pronounced for $Na_V1.8$ channels than for $Na_V1.2$ channels. It would be interesting to test whether use-dependent block by 227c89 is indeed greater for $Na_V1.8$ channels than for $Na_V1.2$ channels, and whether this underlies the basis for the analgesic properties of compound 227c89.

In the presence of ralfinamide the human and rat $Na_V1.8$ channels showed very little use-dependent block during 5Hz or 10Hz stimulation. This finding is in contrast with the marked use-dependent inhibition reported for the same concentration of ralfinamide at 5Hz stimulation in rat TTX-resistant Na^+ currents (Stummann et al., 2005). However, the latter authors used 40ms test pulses (rather than the 10ms test pulses used here), which may allow more drug to bind during the depolarisation.

Tetracaine showed marked use-dependent block for both human and rat $Na_V1.8$ channels at 10Hz with relatively slow onset. Compared to the results here, the extent of use-dependent block of the rat $Na_V1.8$ channel by tetracaine was more pronounced in a previous study (John et al., 2004). This may be explained by the use of a higher (3-fold) concentration of tetracaine.

Compound A-803467 is a potent and highly selective blocker of $Na_V1.8$ channels and has been shown to reduce pain in certain rat models of hyperalgesia and allodynia (Jarvis et al., 2007). Use-dependent inhibition was not observed here for compound A-803467 at 10Hz for rat $Na_V1.8$ channels (as also found for rat TTX-resistant Na^+ currents, Jarvis et al., 2007), this suggests that the physiological action of A-803467 is by tonic rather than use-dependent block; $Na_V1.8$ channels in sensory neurons would not be inhibited based on their excitability (use-

dependent block) but rather in sensory neurons that are more depolarised (tonic block). However, for the human $Na_V1.8$ channel in the presence of A-803467, the observed disinhibition during the recovery from inactivation would be expected to also increase the current following frequent stimulation. Indeed, at 10Hz stimulation a "reverse use-dependence" was observed as an increase in current above the control values. This is consistent with a supplementary data of a previous report, which suggests a small increase in current (Jarvis et al. 2007). This suggests that when physiological frequencies are of this order (Kajander and Bennett, 1992), compound A-803467 would show disinhibition, and thus may be less effective than anticipated for humans.

For compound V102862, although recovery from inactivation showed a disinhibition of current for human $Na_V1.8$, no increase in current over the control value was observed during 5Hz or 10Hz stimulation frequencies. The absence of "reverse use-dependence" may be explained by the observation that disinhibition in the presence of V102862 is prevalent at longer periods of recovery than in the presence of A-803467. For instance, a 10Hz train of 10ms depolarising pulses includes a 90ms recovery period between pulses, at which the component of disinhibition is too small, indeed only inhibition was observed at 10Hz (Fig. 5.8). However, a 5Hz stimulation frequency (including a 190ms recovery period between pulses); there was an apparent component of disinhibition that partially compensated the background inhibition leading to almost no inhibition. Thus the magnitude of the disinhibitory component determines the extent of the use-dependent block for compound V102862, and explains the pronounced use-dependent block observed at 10Hz and apparent absence of use-dependent block observed at 5Hz. Therefore when action potential firing frequencies are in the higher range during pain conditions (Kajander and Bennett, 1992), this property is likely to be important for the frequency-dependent inhibition of excitable sensory neurons. One highly interesting prediction may be that at lower stimulation frequencies (perhaps 2Hz), current disinhibition would be observed for V102862, as for the longer periods of recovery. Indeed, disinhibition of resting block at low firing frequencies, but pronounced use-dependent block at higher frequency firing nerve fibres would be highly desirable for an effective drug for use in the treatment of pain arising from hyperexcitability.

5.3.4 Mechanisms for the current disinhibition effect

In cases where disinhibition occurs, the initial control value in the experiments carried out here includes a component of resting channel drug block. The observed increase in current at certain periods of recovery from inactivation is likely due to the removal of drug block from resting channels. Indeed, the current amplitude of disinhibited current did not exceed the current amplitude of channels before resting block. Although the mechanism for this phenomenon is not

clear, it seems likely that in the presence of certain drugs, recovery involves dissociation of drug from the resting state and/or shift in equilibrium toward the unblocked resting state. While at first glance this might seem to contradict the finding that both V102862 and A-803467 have higher affinities for the inactivated state than the resting state, the disinhibitory state may occur just after recovery from the inactivated states, and seemingly not while the channels are in the same higher affinity state. This model would suggest the additional slow component during recovery represents the reinstatement of resting block after the initial depolarisation in the presence of drug. An alternative mechanism for this effect might be that the presence of drug causes the induction of new states, with a greater single channel conductance or open probability, explaining the increase in current amplitude. Thus, there appears to be at least two possible mechanisms to explain the increase in current amplitude during recovery from inactivation in the presence of certain drugs: the dissociation of drug from resting channels, or perhaps less likely, the modification of single channel conductance. The study of single $Na_V1.8$ channels would provide more understanding of the mechanism leading to disinhibition.

In summary, all drugs studied here showed a greater affinity for the inactivated state than for the resting state, suggesting preferential tonic block of inactivated channels. Compounds A-803467 and V102862 were the most potent, and the inactivated state affinity of A-803476 was greater for human $Na_V1.8$ than for rat $Na_V1.8$ channels. Furthermore, tetracaine, V102862, ralfinamide and A-803467 block of inactivated $Na_V1.8$ channel appears more potent than for TTX-sensitive subtypes in the literature. Unexpectedly, the time course of recovery from inactivation showed an increase in current in the presence of V102862 and A-803467, perhaps due to disinhibition of resting block. For A-803467, this led to an increase in current during high frequency repetitive stimulation. For V102862, while low frequency stimulation showed no inhibition, high frequency stimulation showed marked inhibition. This supports the suggestion that V102862, rather than A-803467, may be useful as an analgesic where physiological firing frequencies are higher. Indeed, despite 83% identity and highly homologous S6 segments (Fig. 4.1), the human and rat $Na_V1.8$ channels show differences in the tonic block of resting and inactivated channel states, and use-dependent block with a range of anti-nociceptive agents. The structural determinants for drug block will be studied in the next two chapters.

CHAPTER 6

FUNCTIONAL PROPERTIES OF S6 SEGMENTS MUTATIONS OF $Na_V1.8$ SODIUM CHANNELS

6.1 Introduction

The generation and propagation of action potentials in excitable cells is largely influenced by the voltage-dependent gating mechanisms of voltage-gated Na^+ channels. The pore-lining S6 segments are thought to be involved in conformational changes leading to channel opening and inactivation (Jiang et al., 2002; Nau and Wang, 2004; Perozo et al., 1999; Yellen, 1998). Compared to other voltage-gated Na^+ channel subtypes, the $Na_V1.8$ channel has distinct activation and inactivation properties, contributing to its role in action potential electrogenesis in sensory neurons.

While the role of the S6 transmembrane segments in the functional properties and drug action is well established for other voltage-gated Na^+ channel subtypes, and the key residues in the S6 segments for drug action have been identified (see *Chapter 1*), the corresponding residues for the $Na_V1.8$ channel subtype have not been addressed (Fig. 6.1 and 6.2). In this chapter, the activation and inactivation properties of mutant human and rat $Na_V1.8$ channels containing alanine substitutions at the corresponding key positions in the S6 segments were investigated. As in previous chapters, $Na_V1.8$ channels were expressed in ND7/23 cells and the functional properties were examined using whole-cell patch clamp.

6.2 Results

6.2.1 Effects on the voltage-dependence of activation by $Na_V1.8$ channel mutations in the S6 segments

Using site-directed mutagenesis, seven key S6 segment amino acid residues of the human and rat $Na_V1.8$ channels were mutated to alanine (*Chapter 3*) and expressed in ND7/23 cells. Whole-cell currents were recorded in the presence of TTX (200nM), and currents were elicited using test pulses from a holding potential of -120mV for human $Na_V1.8$, and a holding potential of -80mV for rat $Na_V1.8$. To examine the effects of alanine mutations on the functional properties of rat $Na_V1.8$ mutations, a holding potential of -80mV was used to study physiologically relevant closed and inactivation states. However, due to the relatively hyperpolarised inactivation of human $Na_V1.8$ channels, the human $Na_V1.8$ mutations were recorded from a holding potential of -120mV. The macroscopic currents for human $Na_V1.8$ channel mutations I381A, N390A, L1410A, V1414A, I1706A, F1710A and Y1717A, and for rat $Na_V1.8$ channel mutations I380A, N389A, L1411A, V1415A, I1707A, F1711A and Y1718A are shown in Figures 6.3 and 6.4.

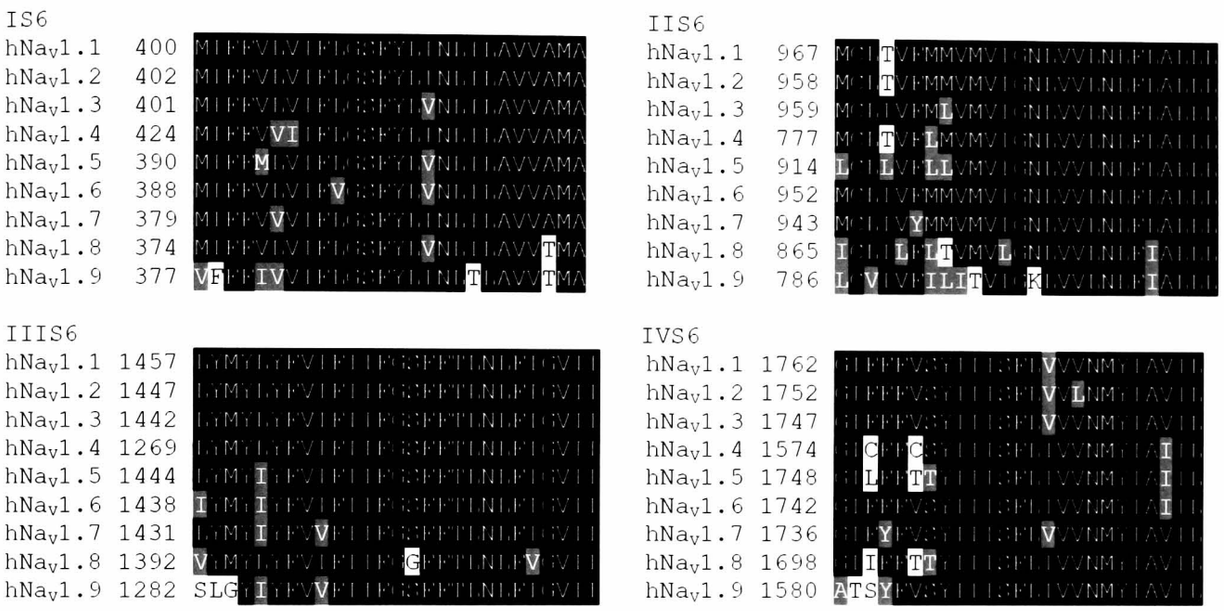

Fig. 6.1. Amino acid sequence similarity between human Na_V channel S6 segments from domains I-IV. Sequences were aligned using ClustalW and visualised using BoxShade.

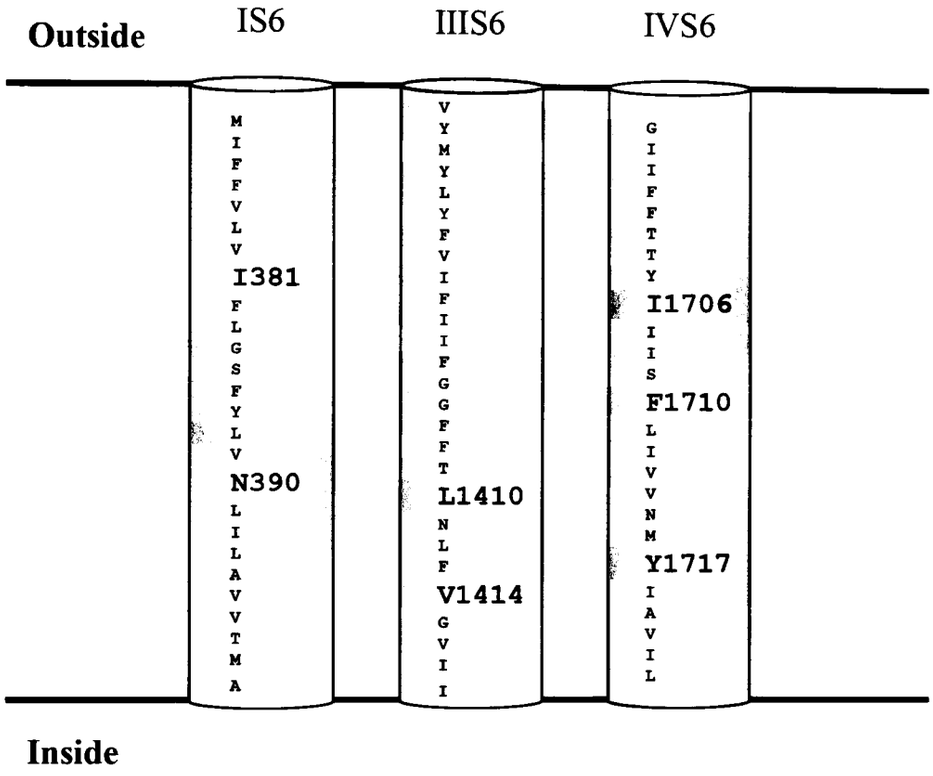

Fig. 6.2. Positions of mutated residues of S6 segments in domains I, III and IV. The S6 segment residues of domain I, III and IV are shown, with the mutated residues in *red.*

For both human and rat $Na_V1.8$ channel mutations, the *I-V* curves showed similar reversal potentials to wild type channels, showing that the ion selectivity was not altered by the substitution of amino acid to alanine (Fig. 6.5). However, the voltage for the maximum current (I_{max}) appeared to be different for a number of mutations of the human and rat $Na_V1.8$ channels. Accordingly, the *G-V* curves show both hyperpolarising and depolarising shifts for mutant human $Na_V1.8$ channels compared to the wild type human $Na_V1.8$ channel, while mutant rat $Na_V1.8$ channels showed only depolarising shifts compared to the wild type channel (Fig. 6.6). These effects were studied in detail by comparing the Boltzmann parameters for activation. For the human $Na_V1.8$ channel, a 9mV shift to more depolarised potentials was observed for mutations N390A and V1414A, while mutations I381A and F1710A showed hyperpolarised shifts by 5mV and 7mV respectively (Fig. 6.7A, Table 6.1). In contrast, the $V_{1/2}$ for activation was unaffected by human $Na_V1.8$ mutations L1410A, I1706A and Y1717A. For the rat $Na_V1.8$ channel, mutations I1707A and Y1718A showed depolarised shifts in the activation curve (8mV and 7mV respectively), and even greater depolarising shifts were observed for mutations N389A, L1411A and V1415A (20mV, 21mV and 15mV respectively, Fig 6.7B, Table 6.1). However, the $V_{1/2}$ for activation was unaffected by mutations I380A and F1711A. The slope of the activation was slightly steeper for human $Na_V1.8$ channel mutations N390A and F1710A, as shown by a small (but significant) decrease in the *k* values (2 and 1mV, respectively) (Figs. 6.6A and 6.7A, Table 6.1). The rat $Na_V1.8$ mutations L1411A and I1707A also slightly affected the slope, showing a small increase (2 and 3mV respectively) in the *k* value (Figs. 6.6B and 6.7B, Table 6.1). The maximum conductance (G_{max}) was significantly decreased by human $Na_V1.8$ channel mutations I381A, L1410A, I1706A, F1710A and Y1717A, and increased by mutation N390A, (Fig. 6.7A, Table 6.1). For rat $Na_V1.8$, only mutation F1711A altered the G_{max}, showing a significant decrease in its value (Fig. 6.7B, Table 6.1). It is not possible to explain these changes in the G_{max} without recording from single channels.

TABLE 6.1

Voltage-dependent activation and inactivation of human and rat $Na_V1.8$ sodium channel S6 mutations

$Na_V1.8$ channel	Activation				Inactivation				
	$V_{½}$ (mV)	k (mV)	G_{max} (nS)	n	$V_{½}$ (mV)	k (mV)	B (nA)	A (nA)	n
$hNa_V1.8$ WT	−2.7 ± 0.8	14.7 ± 0.3	61.9 ± 4.6	79	−79.9 ± 1.0	10.5 ± 0.4	1.8 ± 0.2	0.12 ± 0.01	84
$hNa_V1.8$ I381A	−8.0 ± 1.1	14.2 ± 0.4	34.6 ± 2.5	50	−94.0 ± 1.1	9.6 ± 0.5	1.3 ± 0.2	0.07 ± 0.01	13
$hNa_V1.8$ N390A	5.8 ± 0.9	12.7 ± 0.2	89.4 ± 10.2	52	−87.2 ± 1.0	9.7 ± 0.3	2.0 ± 0.5	0.10 ± 0.01	14
$hNa_V1.8$ L1410A	−0.2 ± 1.7	14.5 ± 0.6	27.2 ± 2.1	31	−95.7 ± 2.2	6.4 ± 0.4	0.9 ± 0.2	0.08 ± 0.02	6
$hNa_V1.8$ V1414A	6.0 ± 1.0	14.8 ± 0.3	57.6 ± 4.9	58	−86.4 ± 1.3	9.7 ± 0.7	1.5 ± 0.2	0.09 ± 0.01	25
$hNa_V1.8$ I1706A	−1.4 ± 1.4	15.2 ± 0.4	27.3 ± 2.4	38	−89.5 ± 2.8	9.9 ± 0.9	0.9 ± 0.2	0.09 ± 0.02	12
$hNa_V1.8$ F1710A	−9.3 ± 0.9	13.7 ± 0.3	43.1 ± 3.8	45	−77.9 ± 1.7	10.1 ± 0.8	1.5 ± 0.3	0.17 ± 0.04	18
$hNa_V1.8$ Y1717A	−0.5 ± 1.3	15.5 ± 0.4	36.4 ± 2.8	54	−104 ± 3	15.6 ± 1.2	1.2 ± 0.2	0.20 ± 0.05	14
$rNa_V1.8$ WT	−1.6 ± 0.9	10.3 ± 0.3	61.2 ± 6.0	41	−57.9 ± 1.0	7.6 ± 0.2	2.3 ± 0.2	0.03 ± 0.01	38
$rNa_V1.8$ I380A	1.4 ± 1.6	9.9 ± 1.0	62.2 ± 14.1	8	−67.5 ± 2.8	8.1 ± 0.2	2.9 ± 0.3	0.12 ± 0.05	5
$rNa_V1.8$ N389A	18.4 ± 1.3	10.0 ± 0.6	66.5 ± 10.5	10	−58.2 ± 3.3	8.5 ± 0.6	0.7 ± 0.2	-	4
$rNa_V1.8$ L1411A	18.9 ± 2.2	12.7 ± 1.1	39.1 ± 14.8	5	−67.6 ± 0.9	7.2 ± 0.4	0.6 ± 0.2	0.03 ± 0.01	4
$rNa_V1.8$ V1415A	13.5 ± 1.9	11.6 ± 0.8	57.7 ± 12.3	9	−57.5 ± 2.3	6.9 ± 0.4	0.9 ± 0.2	0.03 ± 0.02	7
$rNa_V1.8$ I1707A	6.6 ± 2.5	12.5 ± 0.5	44.7 ± 10.3	6	−65.2 ± 1.6	6.6 ± 0.9	1.1 ± 0.3	0.06 ± 0.02	4
$rNa_V1.8$ F1711A	0.6 ± 1.9	11.5 ± 0.6	28.9 ± 6.5	15	−53.7 ± 3.1	8.3 ± 0.3	1.1 ± 0.4	-	6
$rNa_V1.8$ Y1718A	5.3 ± 1.5	10.8 ± 0.6	49.3 ± 10.4	12	−70.3 ± 2.6	10.8 ± 0.9	2.4 ± 0.6	-	8

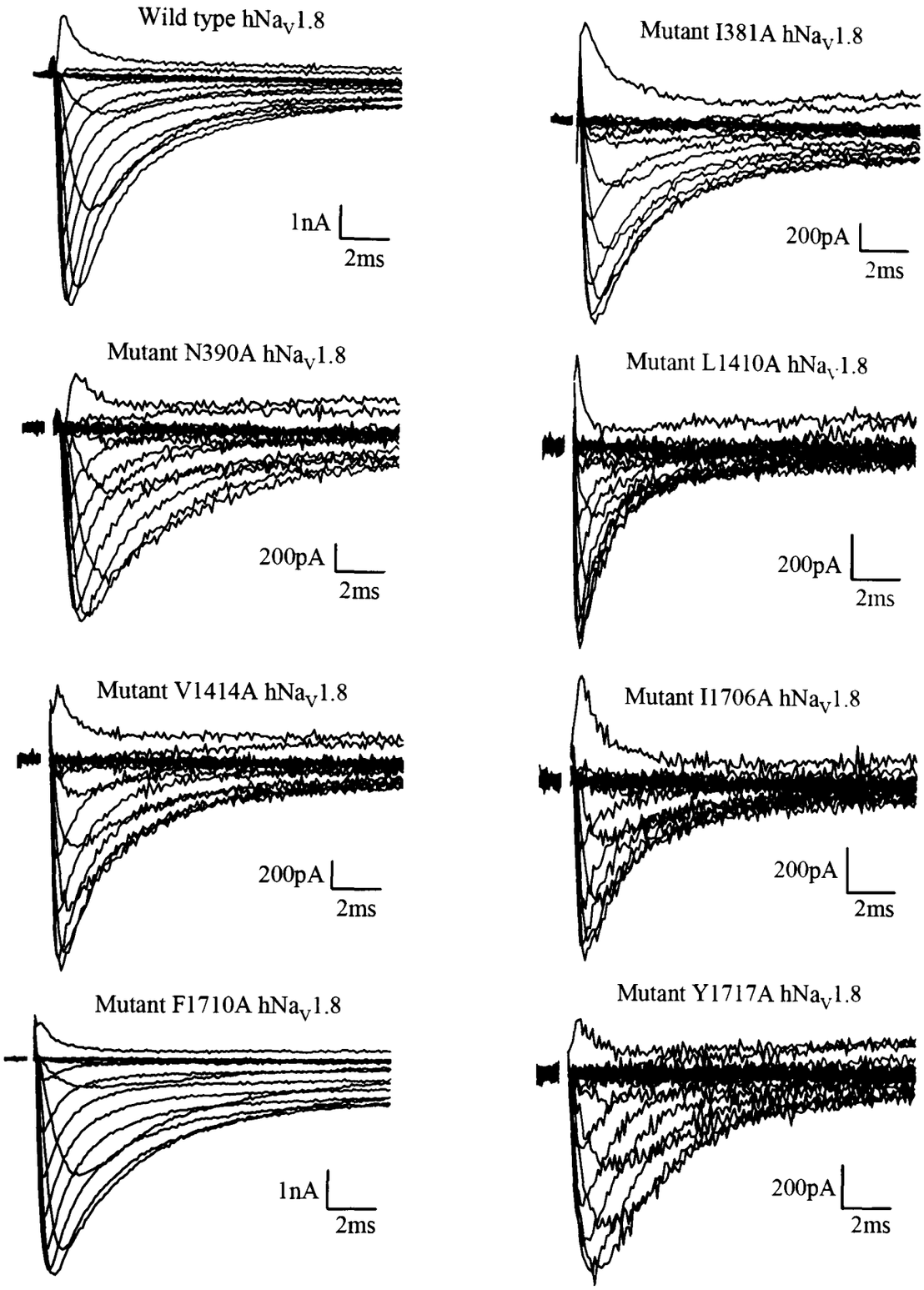

Fig. 6.3. Mutant human Na$_V$1.8 channel current traces recorded from ND7/23 cells. Example current trace are shown for ND7/23 cells transfected with wild type or mutant hNa$_V$1.8 channel cDNA in the presence of 200nM TTX. Currents were elicited for voltage steps to -100mV to +60mV (in 10mV increments) from a holding potential of -120mV.

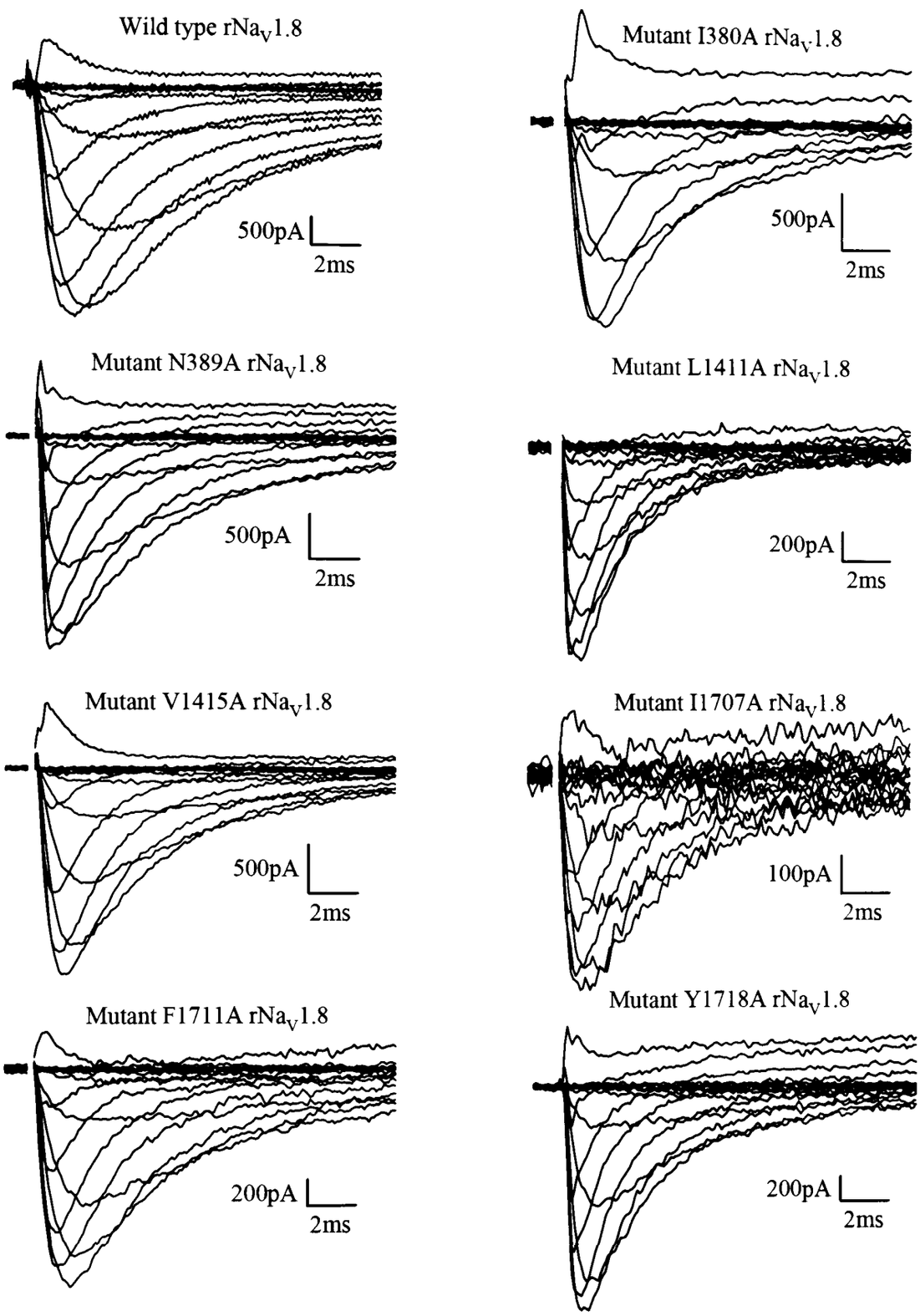

Fig. 6.4. Mutant rat Na$_V$1.8 channel current traces recorded from ND7/23 cells. Example current trace are shown for ND7/23 cells transfected with wild type or mutant rNa$_V$1.8 channel cDNA in the presence of 200nM TTX. Currents were elicited for voltage steps to -100mV to +60mV (in 10mV increments) from a holding potential of -80mV.

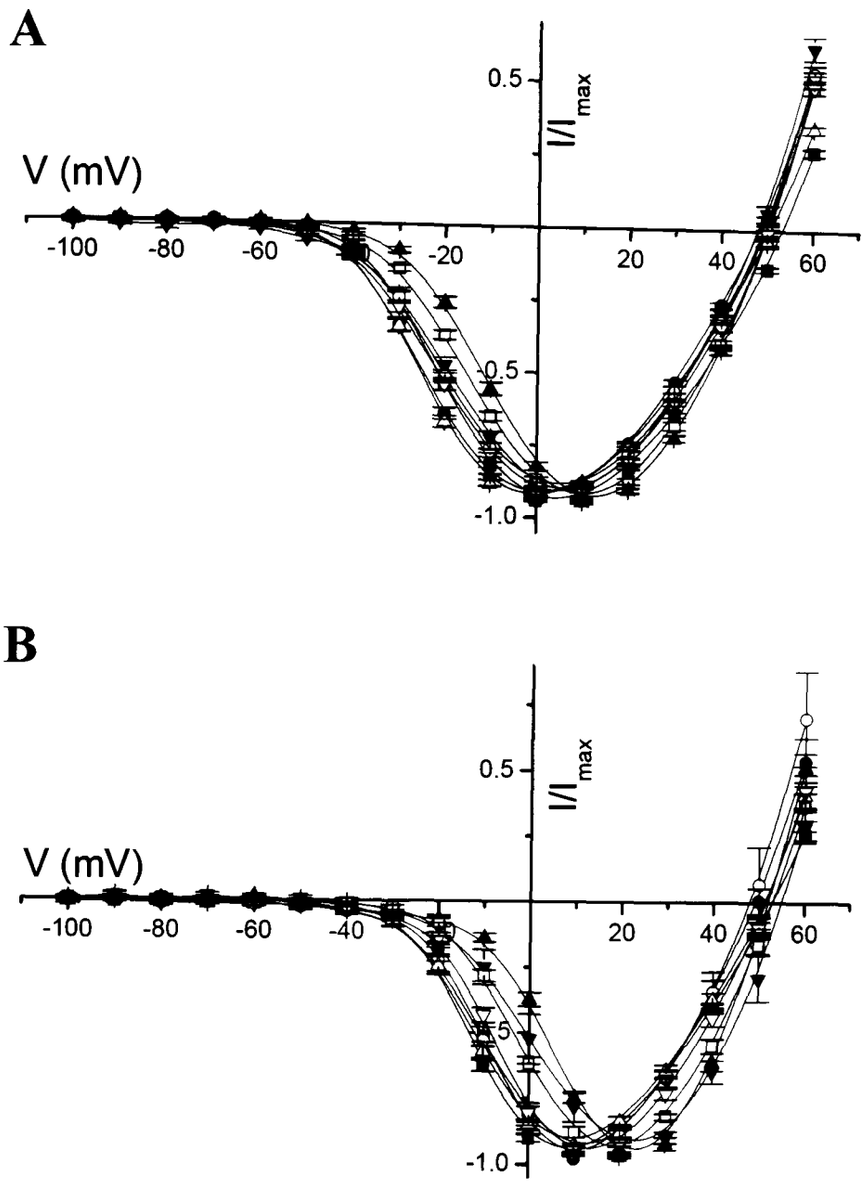

Fig. 6.5. Current-voltage relationships for human and rat $Na_V1.8$ channel mutations. A) Current-voltage relationships are shown for the peak current for human $Na_V1.8$ channels normalised to the maximum current, I_{max}. The I_{max} was obtained separately from the current-voltage relationship recorded from each cell. Relationships are shown for wild type (■), and mutations I381A (●), N390A (▲), L1410A (▼), V1414A (□), I1706A (○), F1710A (△) and Y1717A (▽). **B)** For rat $Na_V1.8$ channels, relationships are shown for wild type (■), and mutations I380A (●), N389A (▲), L1411A (▼), V1415A (□), I1707A (○), F1711A (△) and Y1718A (▽). The n numbers are given in Table 6.1.

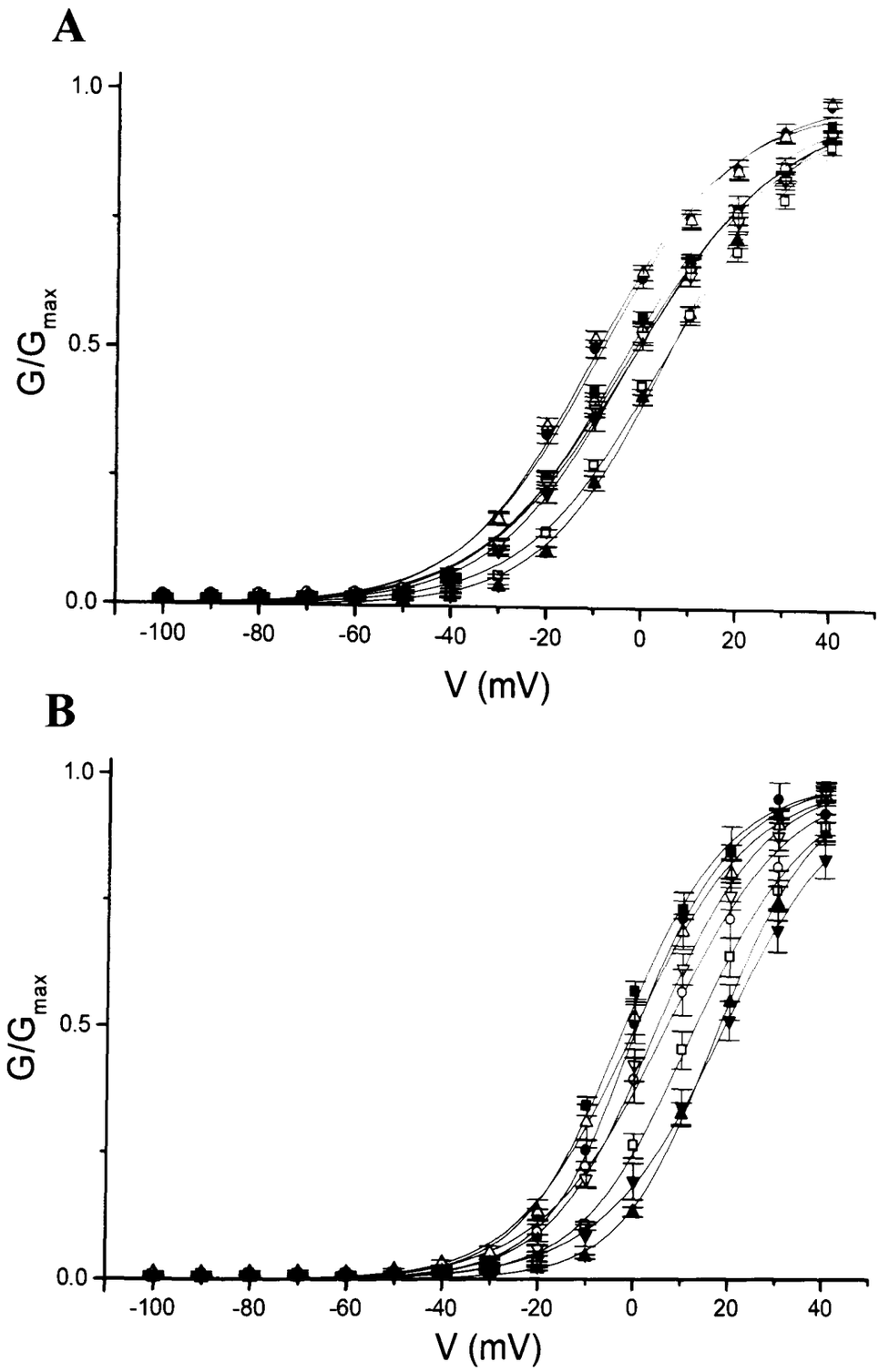

Fig. 6.6. Conductance-voltage relationships for human and rat $Na_V1.8$ channel mutations. A) The conductance-voltage curves are shown for human $Na_V1.8$ channels; wild type (■), and mutations I381A (●), N390A (▲), L1410A (▼), V1414A (□), I1706A (○), F1710A (△) and Y1717A (▽). **B)** Conductance-voltage curves are shown for rat $Na_V1.8$ channels; wild type (■), and mutations I380A (●), N389A (▲), L1411A (▼), V1415A (□), I1707A (○), F1711A (△) and Y1718A (▽). The n numbers are given in Table 6.1.

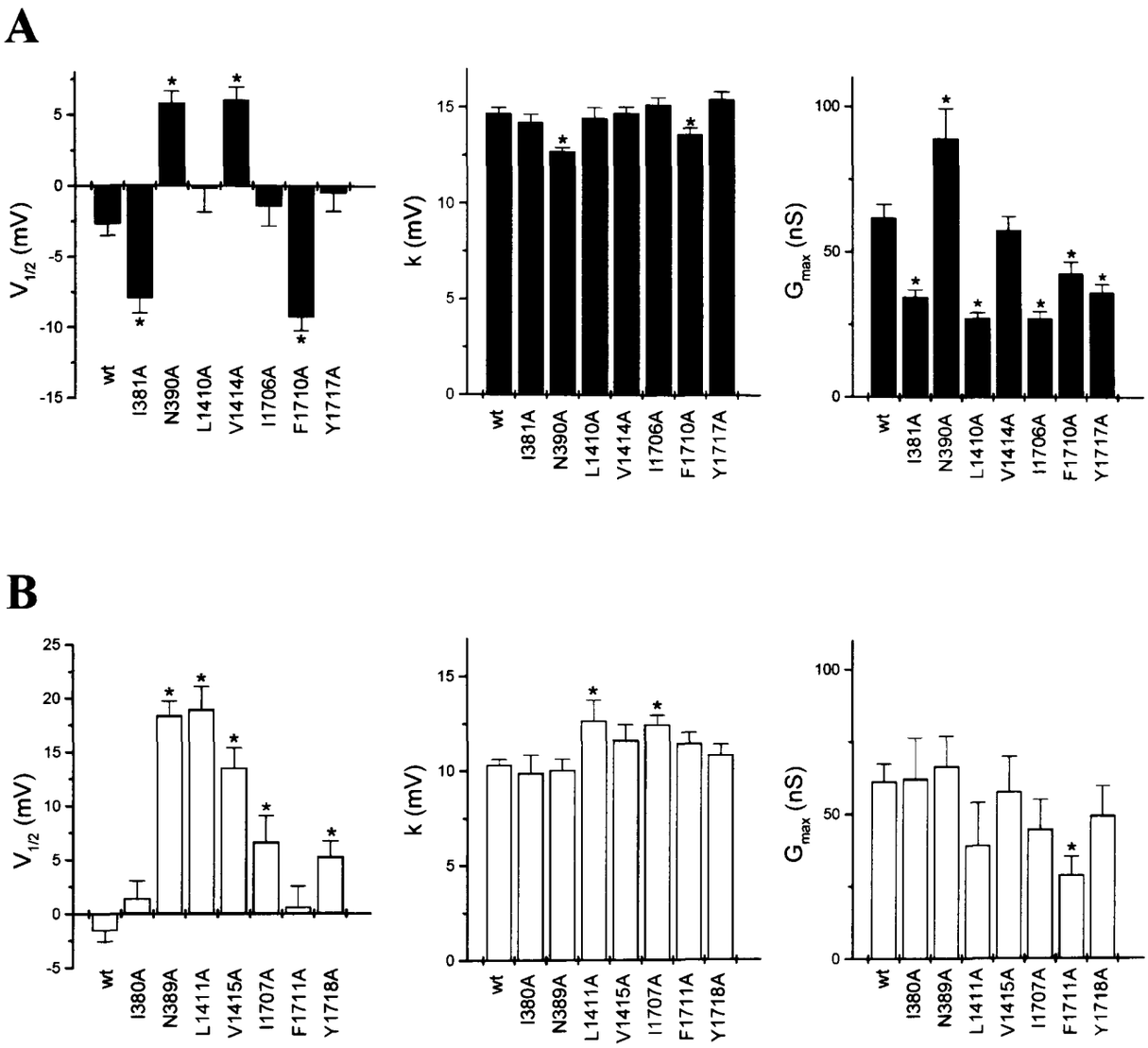

Fig. 6.7. The effects of mutations on the Boltzmann parameters for activation. Bar diagrams show the voltage for half-maximal activation ($V_{1/2}$), the slope factor (k) and maximum conductance (G_{max}) for mutations of human (**A**) and rat (**B**) $Na_V1.8$ channels. * indicates a statistically significant difference from wild type channels $p<0.05$. The n numbers are given in Table 6.1.

6.2.2 Effects on the voltage-dependence of inactivation by $Na_V1.8$ channel mutations in the S6 segments

The inactivation properties of the alanine mutations were firstly studied by examining the voltage-dependence of inactivation. The current amplitude was measured during a test pulse using the protocol shown in the inset of Fig. 6.8, from a holding potential of -120mV for human $Na_V1.8$, and -80mV for rat $Na_V1.8$. The steady-state inactivation curves show that a number of human and rat $Na_V1.8$ mutations gave strong hyperpolarising shifts (Fig. 6.8). Human $Na_V1.8$ mutations N390A, V1414A and I1706A showed significant hyperpolarising shifts (7 to 10mV), and even greater hyperpolarising shifts were observed for human $Na_V1.8$ mutations I381A, L1410A and Y1717A (14 to 24mV) (Figs. 6.8A and 6.9A, Table 6.1). For the rat $Na_V1.8$ channel, mutations I380A, L1411A, I1707A and Y1718A showed hyperpolarising shifts in the range of 7 to 12mV (Figs. 6.8B and 6.9B, Table 6.1).

Most of the mutants did not affect the slope parameter, *k* (Fig. 6.9, Table 6.1). However, human $Na_V1.8$ mutation L1410A gave a steeper slope (4mV decrease in the *k* value), and mutation Y1717A showed a less steep slope (5mV increase in the *k* value) (Figs. 6.8A and 6.9A, Table 6.1). Rat $Na_V1.8$ mutation Y1718A also showed a less steep slope (3mV increase in the *k* value) (Figs. 6.8B and 6.9B, Table 6.1).

For human $Na_V1.8$, mutations I1706A, F1710A and Y1717A (all located in the IVS6 segment) showed less inactivation at positive potentials compared with the wild type channel (inactivation curve parameter, *A*, see *Section 2.6.3*). In the human $Na_V1.8$ channel the fraction of non-inactivated current remaining during strong depolarisation (parameter *A/B*, see *Chapter 2*) was 1.7-fold greater for mutation I1706A and F1710A and 2.3-fold greater for Y1717A compared to the wild type channel (Fig. 6.9). The remaining human $Na_V1.8$ channel mutations (I381A, N390A, L1410A and V1414A) did not affect the fraction of non-inactivated current. For the rat $Na_V1.8$ channel, although there were some increases in the fraction of non-inactivated current, they were not statistically significant.

Taken together, these results suggest that in addition to their role in voltage-dependent activation, residues of the S6 segments also appear to be important for the voltage-dependent inactivation of $Na_V1.8$.

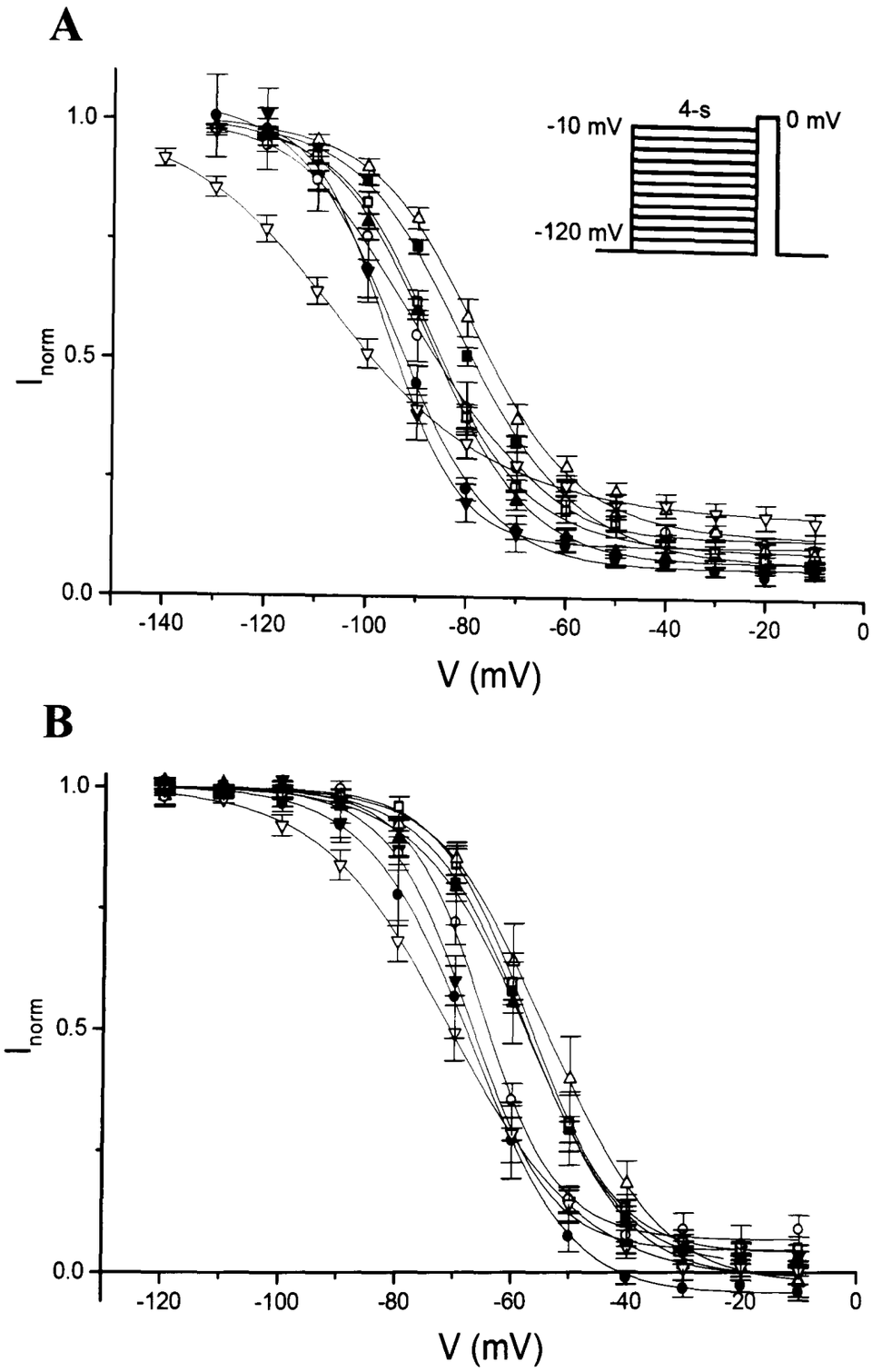

Fig. 6.8. Voltage-dependence of inactivation for human and rat $Na_V1.8$ channel mutations. **A)** Curves are shown for the peak current for human $Na_V1.8$ channels; wild type (■), and mutations I381A (●), N390A (▲), L1410A (▼), V1414A (□), I1706A (○), F1710A (△) and Y1717A (▽). The pulse protocol is shown inset. For a number mutations, voltage steps to more hyperpolarising potentials were required. **B)** Curves are shown for the peak current for rat $Na_V1.8$ channels; wild type (■), and mutations I380A (●), N389A (▲), L1411A (▼), V1415A (□), I1707A (○), F1711A (△) and Y1718A (▽). Currents were normalised to the maximum current (parameter *B*, see *Chapter 2*). The n numbers are given in Table 6.1.

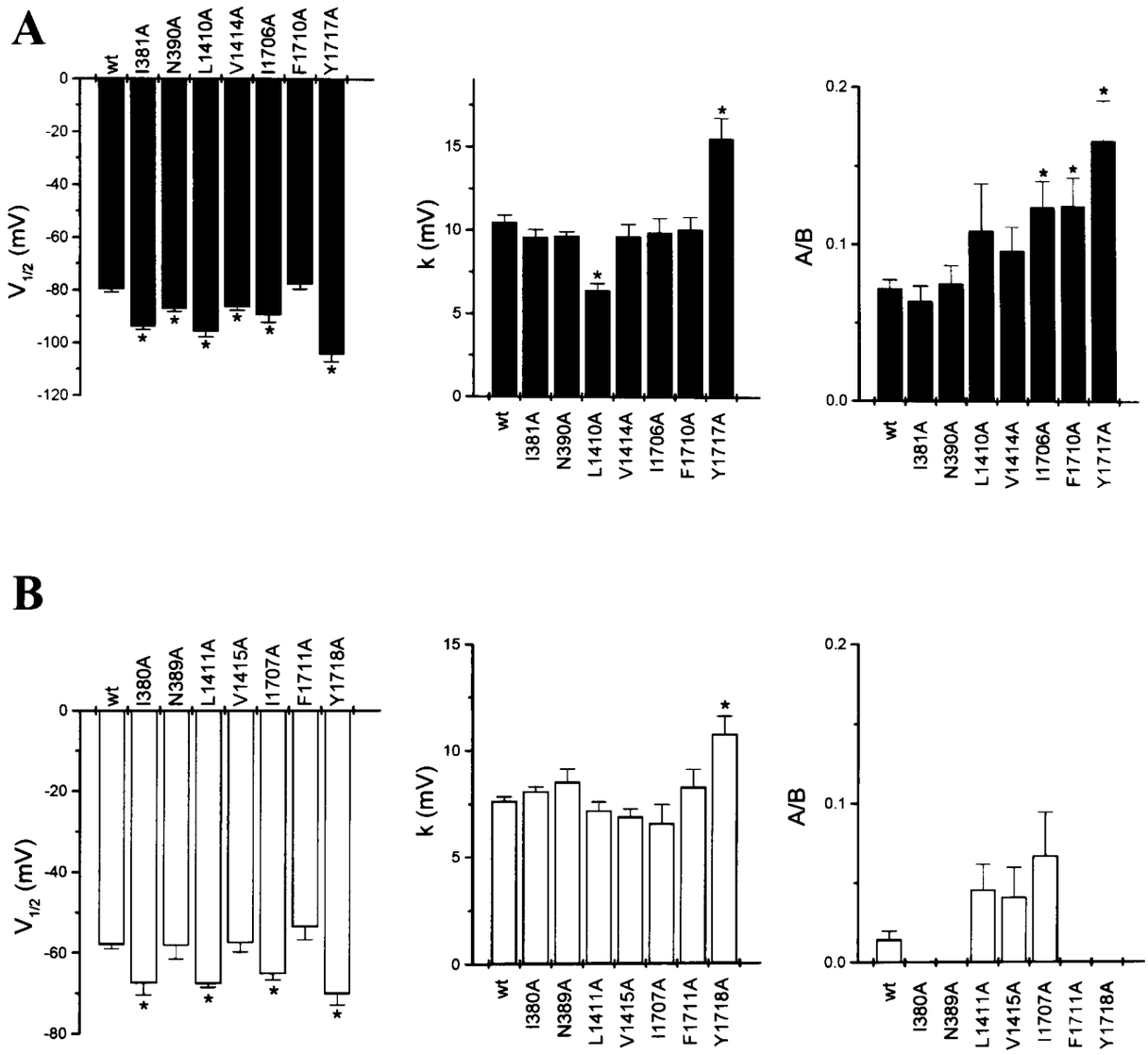

Fig. 6.9. The effects of mutations on the Boltzmann parameters for inactivation. Bar diagrams show the voltage for half-maximal activation ($V_{1/2}$), the slope factor (k) and the amplitude of the non-inactivated component normalised to the maximum current (A/B) of human (**A**) and rat (**B**) $Na_V1.8$ channels. The A/B ratio for mutations I380A, N389A, F1711A and Y1718A was too small to be measured accurately. * indicates a statistically significant difference from wild type channels $p<0.05$. The n numbers are given in Table 6.1.

6.2.3 Effects on the entry into open-inactivated states by $Na_V1.8$ channel mutations in the S6 segments

The example current traces shown in Figures 6.3 and 6.4 suggest that the rate of inactivation is faster for most $Na_V1.8$ mutations compared to the wild type channels. Therefore the current decay phase was fitted with an exponential equation in order to determine the time constant for inactivation (τ_i). The current elicited at 0mV decayed with a significantly smaller τ_i indicating faster inactivation for most human and rat $Na_V1.8$ mutations studied compared to the wild type channels (Figs. 6.10 and 6.11, Table 6.2). For human $Na_V1.8$, mutations I381A, L1410A, V1414A, I1706A F1710A and Y1717A showed τ_i values that indicate faster inactivation compared to the wild type channel (2.0-, 2.6-, 2.2-, 2.0-, 1.6- and 1.4-fold faster inactivation respectively). Furthermore, while human $Na_V1.8$ mutation N390A did not show a significant difference in the τ_i value at 0mV, at 10mV it showed faster inactivation. For rat $Na_V1.8$, mutations N390A, I1707A and Y1718A showed τ_i values, which indicate 1.3- and 1.9-fold faster inactivation respectively. The N390A mutation in rat $Na_V1.8$ showed a 1.8-fold larger τ_i value at 0mV. These results suggest that human $Na_V1.8$ S6 segment mutations I381A, L1410A, V1414A, I1706A, F1710A and Y1717A and rat $Na_V1.8$ mutations I1707A and Y1717A studied here enter inactivated states from open states faster than the wild type $Na_V1.8$ channels, while rat $Na_V1.8$ mutation N389A appeared to slow this transition.

6.2.4 Effects on the recovery from inactivation by human $Na_V1.8$ channel mutations in the S6 segments

The time course of recovery from inactivation for the mutant human $Na_V1.8$ channel were determined as described for the wild type channel in *Chapter 4*. The recovery from inactivation time courses were fitted with two exponential components and the mean curves for wild type human $Na_V1.8$ and the L1410A mutant are shown in Figure 6.12. The parameters of the fits are shown for all human $Na_V1.8$ mutations in Figure 6.13. For wild type, the initial component showed a time constant (τ_{fast}) of 10ms and a later component (τ_{slow}) of 130ms (Figs. 6.12 and 6.13). For the initial component, τ_{fast} was unaltered for human $Na_V1.8$ mutations N390A, V1414A and F1710A (Fig. 6.13A, Table 6.2). However, τ_{fast} was significantly larger for mutations I381A, L1410A, I1706A and Y1717A (Fig. 6.13A). For the slow component, all mutations showed a similar time constant, τ_{slow}, with the exception of a larger value for mutation I1706A (Fig. 6.13B, Table 6.2).

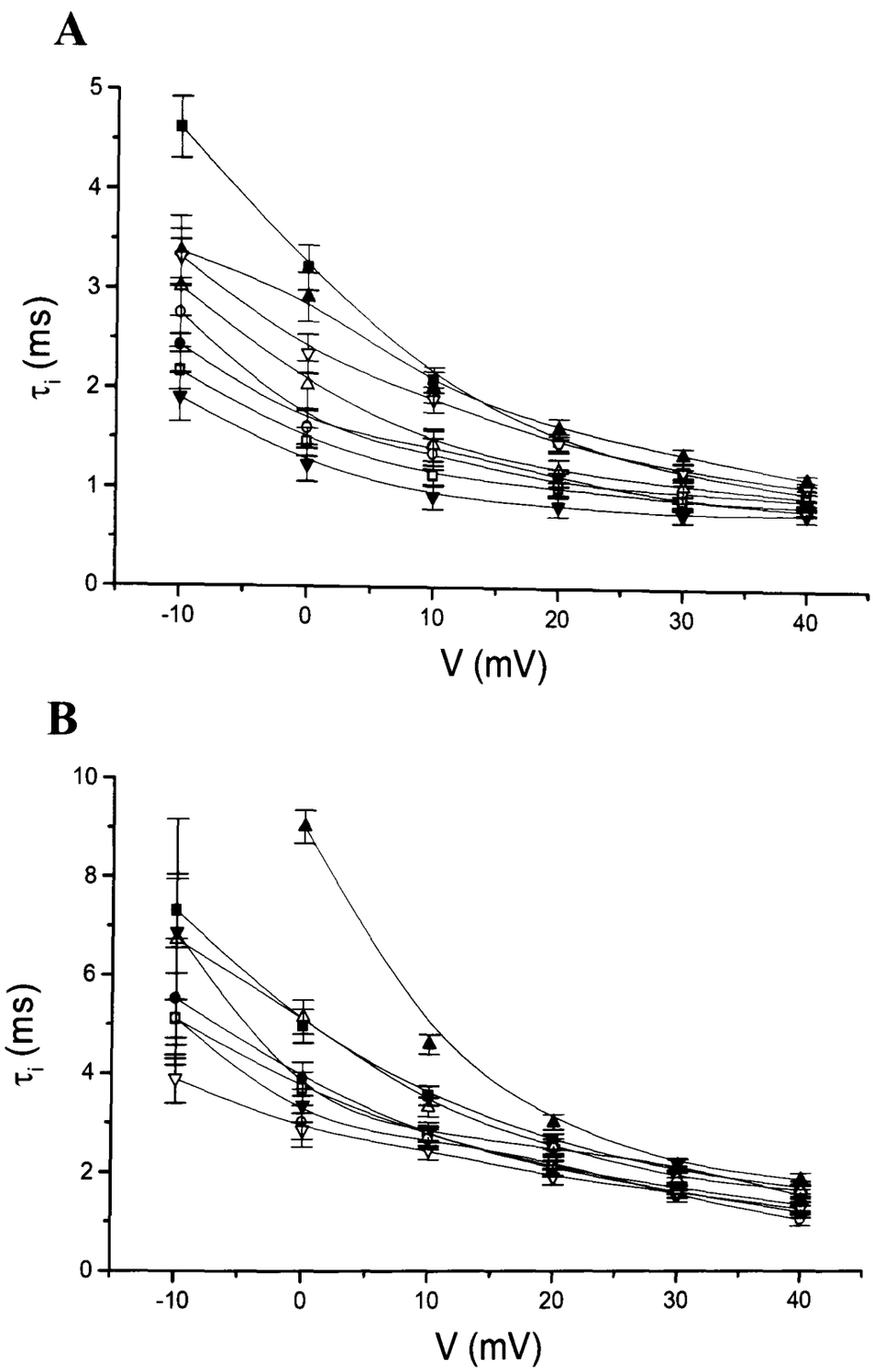

Fig. 6.10. Voltage-dependence of the inactivation time course for human and rat $Na_V1.8$ mutations. The time constant of inactivation, τ_i, is shown at each test potential, V. **A)** Curves are shown for human $Na_V1.8$ channels; wild type (■), and mutations I381A (●), N390A (▲), L1410A (▼), V1414A (□), I1706A (○), F1710A (△) and Y1717A (▽). **B)** Curves are shown for rat $Na_V1.8$ channels; wild type (■), and mutations I380A (●), N389A (▲), L1411A (▼), V1415A (□), I1707A (○), F1711A (△) and Y1718A (▽). The n numbers are given in Table 6.2.

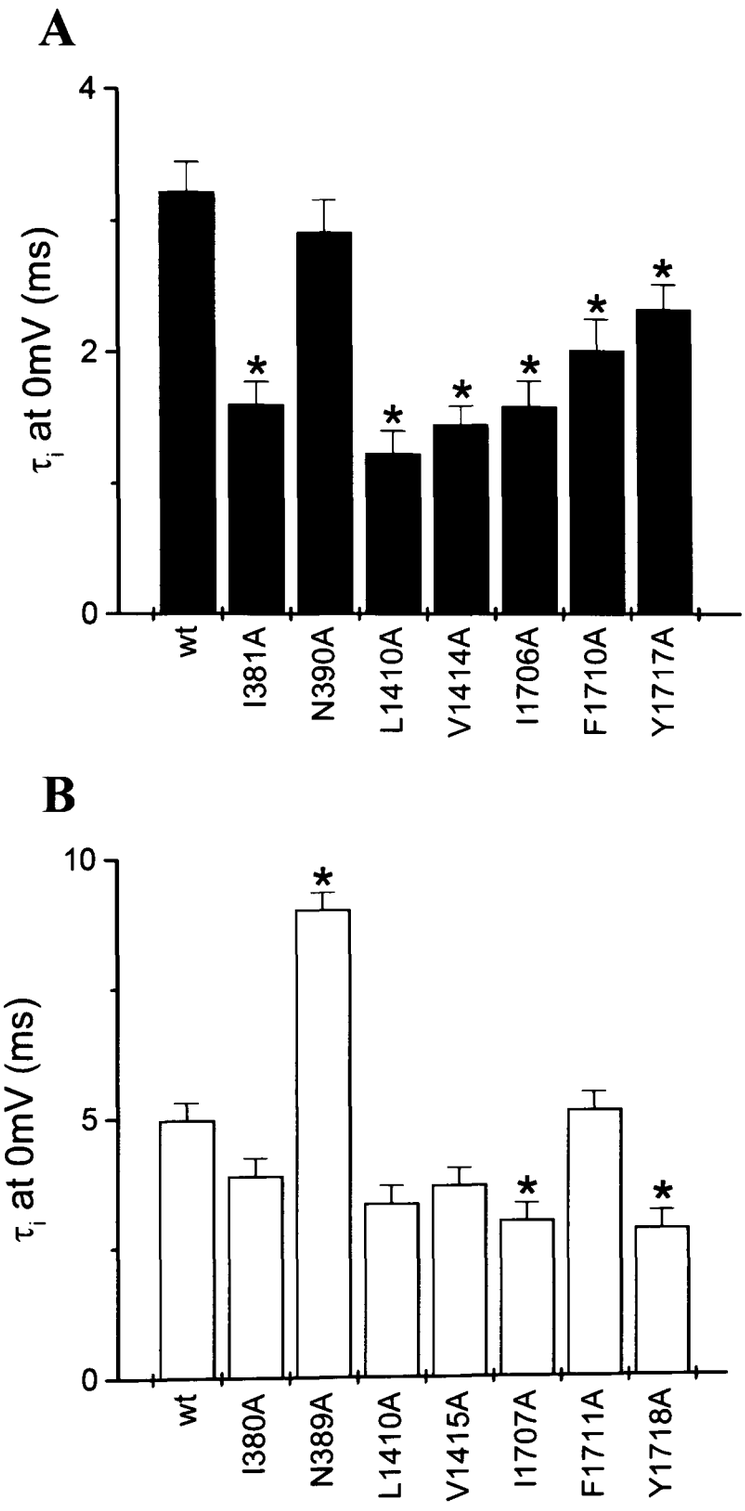

Fig. 6.11. The effects of mutations on the inactivation time constant. Bar diagrams show the time constant for inactivation of currents elicited with a step to 0mV for mutations of human (**A**) and rat (**B**) $Na_V1.8$ channels. * indicates a statistically significant difference from wild type channels $p<0.05$. The n numbers are given in Table 6.2, and the values shown here are from the same data as in Fig. 6.10.

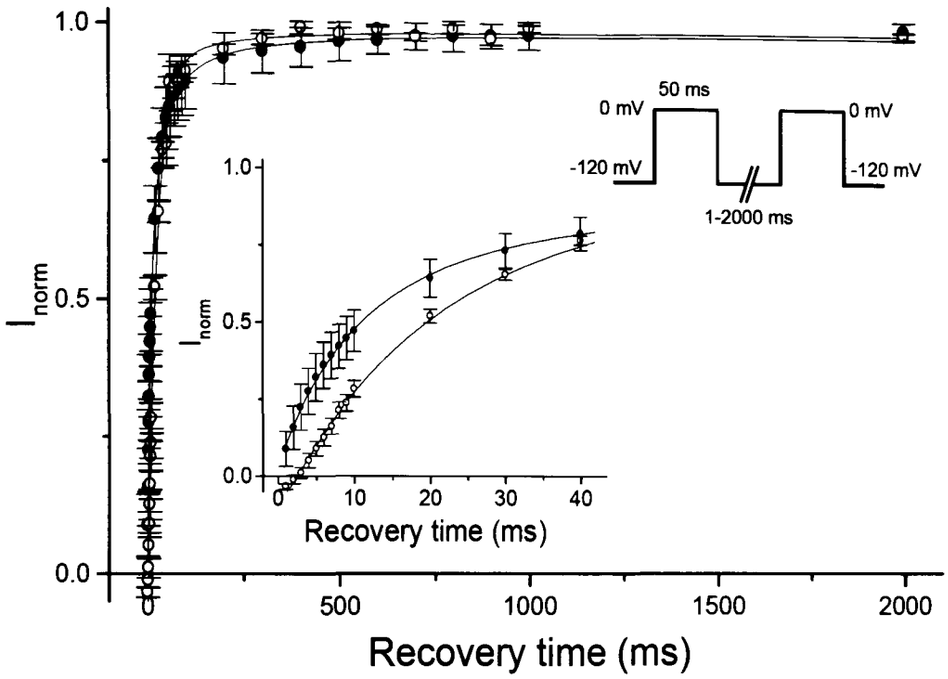

Fig. 6.12. Recovery from inactivation for wild type and L1410A human $Na_V1.8$ channels. Time course for the recovery from inactivation for wild type (●) and L1410A (○) human $Na_V1.8$ channels is shown. The pulse protocol is shown inset. The curve was fit with a double exponential equation. The n numbers are given in Table 6.2.

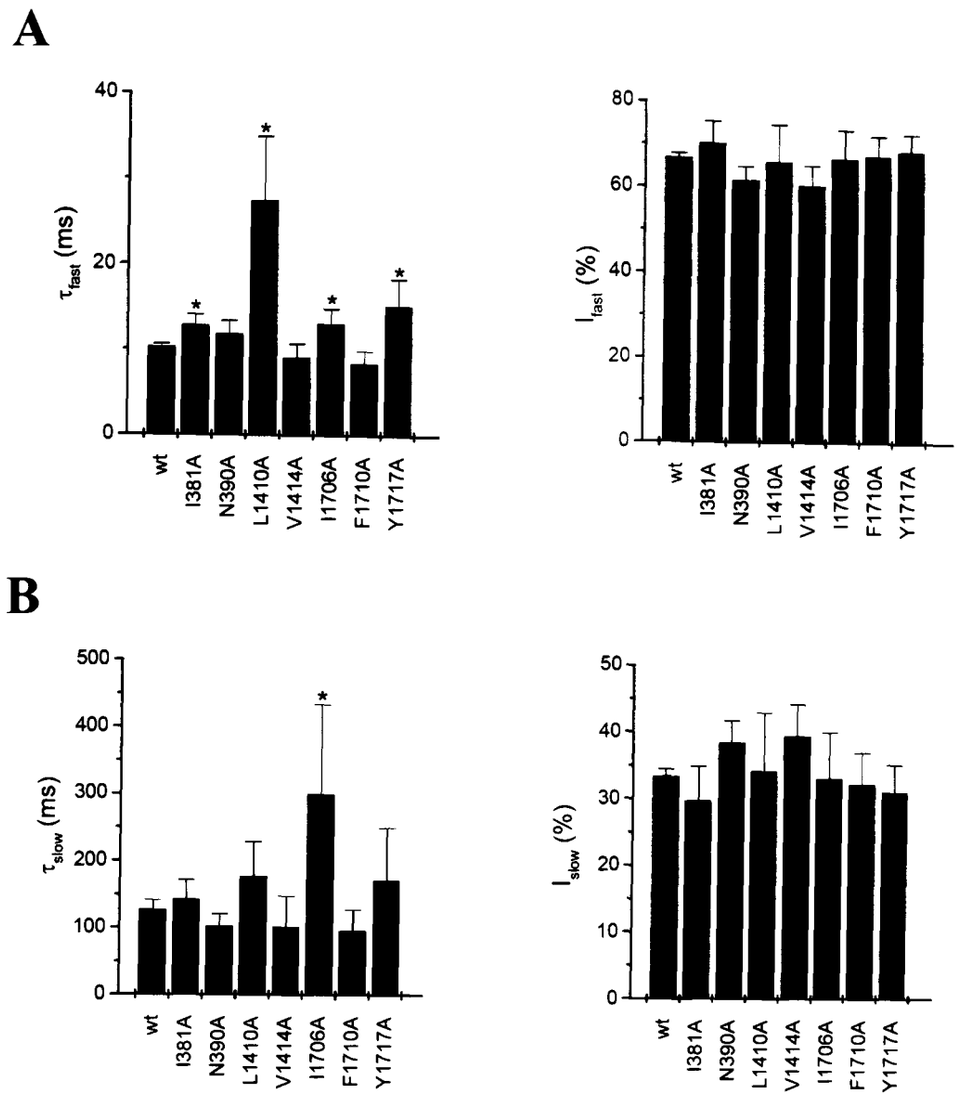

Fig. 6.13. The effects of mutations on the recovery from inactivation. A) Bar diagrams are shown for the fitted parameters for the fast component, showing time constant, τ_{fast}, and its amplitude, I_{fast}, for wild type and mutant $Na_V1.8$ channels. **B)** Bar diagrams are shown for the fitted parameters for the slow component, showing time constant, τ_{slow}, and its amplitude, I_{slow}, for wild type and mutant $Na_V1.8$ channels. * indicates a statistically significant difference from wild type channels $p<0.05$. The n numbers are given in Table 6.2.

6.2.5 Effects on the use-dependent current inhibition by $Na_V1.8$ channel mutations in the S6 segments

Experiments were carried out with repetitive stimulation at 10Hz to investigate use-dependent current inhibition of the mutant human $Na_V1.8$ channel currents. While mutations N390A and L1410A showed slightly more pronounced (4–5%) current inhibition than for wild type channel, less current inhibition was observed for mutations V1414A and F1710A (also 4–5%, Fig. 6.14, Table 6.2). The other mutants did not significantly alter the extent of use-dependent current inhibition at the 60th pulse (Fig. 6.14, Table 6.2). Since these are only small effects on the use-dependent current inhibition it is difficult to attribute the changes in the rate of development of inactivation and the rate of recovery from inactivation to these effects.

TABLE 6.2

Time course of inactivation for human and rat $Na_V1.8$ channel S6 mutations

$Na_V1.8$ channel	Entry into inactivation		Recovery from inactivation					UD inhibition	
	τ_i (ms)	n	τ_{fast} (ms)	I_{fast} (%)	τ_{slow} (ms)	I_{slow} (%)	n	I_{norm}	n
$hNa_V1.8$ WT	3.2 ± 0.2	56	10.2 ± 0.4	67 ± 1	126 ± 15	33 ± 1	71	0.85 ± 0.01	121
$hNa_V1.8$ I381A	1.6 ± 0.2	35	12.8 ± 1.3	70 ± 5	142 ±29	30 ± 5	13	0.85 ± 0.01	43
$hNa_V1.8$ N390A	2.9 ± 0.2	34	11.8 ± 1.6	62 ± 3	102 ± 18	38 ± 3	13	0.79 ± 0.01	50
$hNa_V1.8$ L1410A	1.2 ± 0.2	32	27.5 ± 7.5	66 ± 9	177 ± 52	34 ± 9	12	0.81 ± 0.01	28
$hNa_V1.8$ V1414A	1.5 ± 0.1	36	9.1 ± 1.6	61 ± 5	101 ± 47	39 ± 5	11	0.89 ± 0.01	38
$hNa_V1.8$ I1706A	1.6 ± 0.2	32	13.1 ± 7.8	67 ± 7	299 ± 135	33 ± 7	7	0.84 ± 0.01	37
$hNa_V1.8$ F1710A	2.0 ± 0.2	37	8.4 ± 1.5	68 ± 5	95 ± 32	32 ± 5	12	0.90 ± 0.01	56
$hNa_V1.8$ Y1717A	2.4 ± 0.2	38	15.2 ± 3.2	69 ± 4	171 ±79	31 ± 4	7	0.82 ± 0.02	43
$rNa_V1.8$ WT	5.0 ± 0.3	30	5.9 ± 0.5	66 ± 1	354 ± 58	33 ± 1	55	0.73 ± 0.02	86
$rNa_V1.8$ I380A	3.9 ± 0.3	6			ND			ND	
$rNa_V1.8$ N389A	9.0 ± 0.3	9			ND			ND	
$rNa_V1.8$ L1411A	3.3 ± 0.3	4			ND			ND	
$rNa_V1.8$ V1415A	3.7 ± 0.3	9			ND			ND	
$rNa_V1.8$ I1707A	3.0 ± 0.3	5			ND			ND	
$rNa_V1.8$ F1711A	5.2 ± 0.3	11			ND			ND	
$rNa_V1.8$ Y1718A	2.6 ± 0.3	10			ND			ND	

In summary, the IS6, IIIS6 and IVS6 segment residues studied here appear to be important for the voltage-dependence of activation, and also inactivation properties; the voltage-dependence of inactivation, time course for entry into inactivation and recovery from inactivation, and indeed, the use-dependent current inhibition of $Na_V1.8$ channels were all affected by alanine mutation. Furthermore the effect of amino acid residues in activation and inactivation of the $Na_V1.8$ channel were often different between the human and rat orthologues.

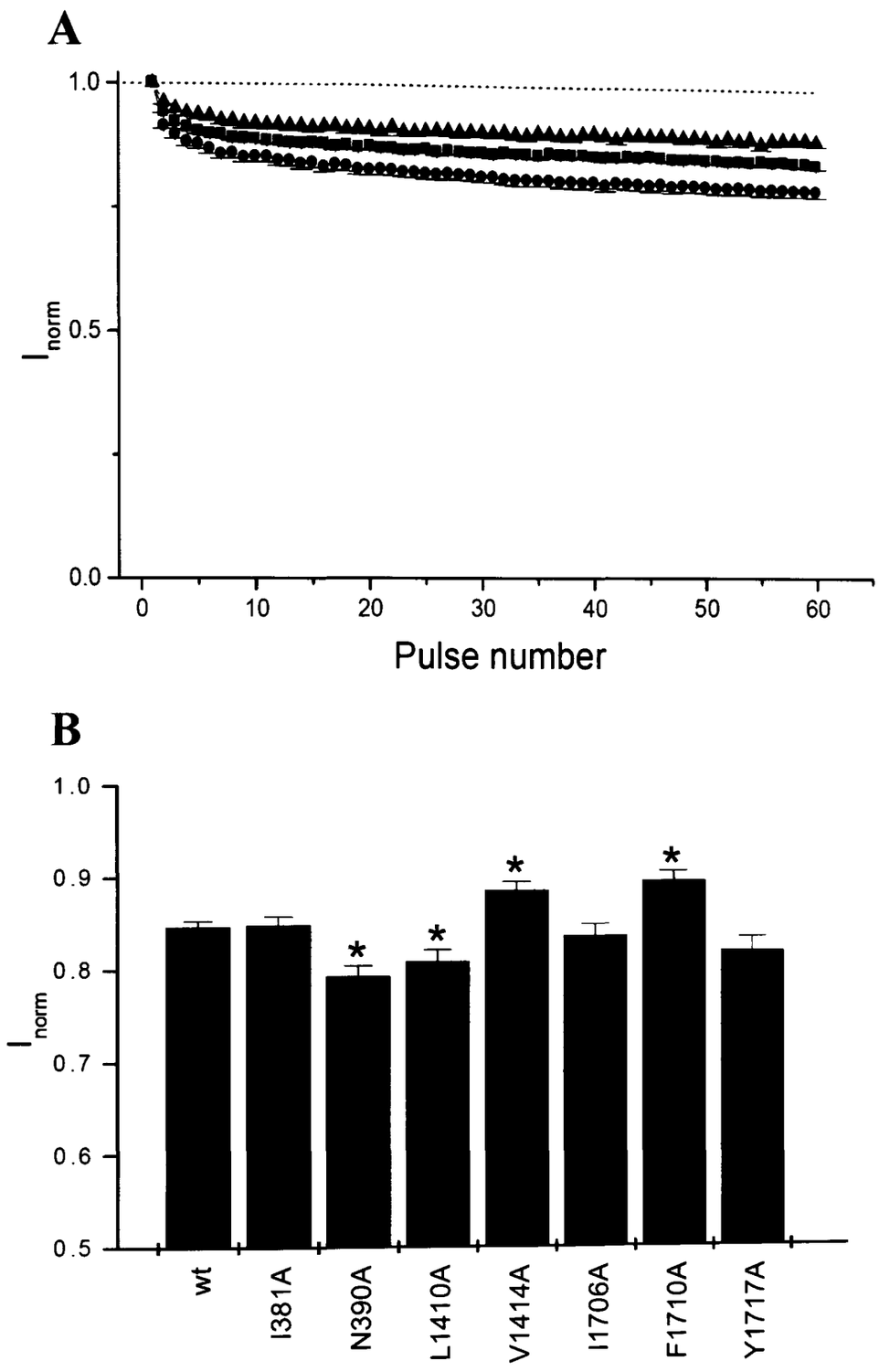

Fig. 6.14. Use-dependent current inhibition of mutant human $Na_V1.8$ channels. A) Current amplitudes are shown elicited during a 10Hz train of 60 test pulses to 0mV (10ms in duration) for wild type (■), N390A (●) and F1710A (▲) $hNa_V1.8$ channels. Only currents from two mutations are shown for clarity. Currents were normalised to the amplitude of the first pulse. **B)** The bar diagram shows the current at the 60th pulse expressed as a fraction of the current at the 1st pulse of a 10Hz train. * $p<0.05$, compared to the first pulse. The n numbers are given in Table 6.2.

6.3 Discussion

In addition to their role in the local anaesthetic binding site, the pore-lining S6 segments of the $Na_V1.8$ channel are also proposed to play an important role in the activation and inactivation gating processes of many voltage-gated Na^+ channels. Here the role of seven key S6 segment amino acid residues in activation and inactivation properties were studied in human and rat $Na_V1.8$ channels.

6.3.1 Effects on the voltage-dependence of activation by $Na_V1.8$ channel mutations in the S6 segments

For the activation curve, human $Na_V1.8$ mutations I381A and F1710A gave strong hyperpolarising shifts. The corresponding mutations of the rat $Na_V1.8$ channel (I380A and F1711A) were the only not to show a shift in the activation curve. Hyperpolarising shifts in the activation curve suggest that the native residues are involved in interactions that reduced open states or stabilise closed states, since the probability of channel activation is decreased at any one membrane potential. Thus the native residues at these positions are important for destabilising open states or stabilising closed states for human $Na_V1.8$, but not for rat $Na_V1.8$. In contrast, the rat $Na_V1.8$ channel mutations N389A, L1411A, V1415A, I1707A and Y1718A shifted the activation curve to significantly more depolarised potentials. For human $Na_V1.8$, only the N390A and V1414A mutations showed depolarised shifts. Therefore, the native asparagine and valine residues at these positions are important for stabilising open states or destabilising closed states for human and rat $Na_V1.8$. Consistent with this finding, a molecular model of the open human $Na_V1.8$ channel (based on homology with the rat $K_V1.2$ channel structure by Long et al., 2005) carried out by Frank Blaney (GlaxoSmithKline, Harlow) suggests that residues N390 and V1414 form interactions with adjacent helices. The N390 residue in domain I appears to hydrogen bond with T250 in S5 of domain I and N1724 in S6 of domain IV (Fig 6.15A). The V1414 residue in domain III appears to make hydrophobic interactions with L889 and F893 on S6 of domain II (Fig. 6.15B). These residues appear to be located in the cytoplasmic side of the transmembrane bundle in the open state (Fig. 1.9B), so that these residues may indeed stabilise open states. Furthermore, the corresponding mutations at these positions (390 and 1414 in human $Na_V1.8$) showed similar positive shifts in $rNa_V1.2$ and $rNa_V1.4$ (Nau et al., 1999; Wang and Wang, 1997; Yarov-Yarovoy et al., 2002). The valine residue is an isoleucine residue in all other known Na_V subtypes, which shows similar hydrophobicity.

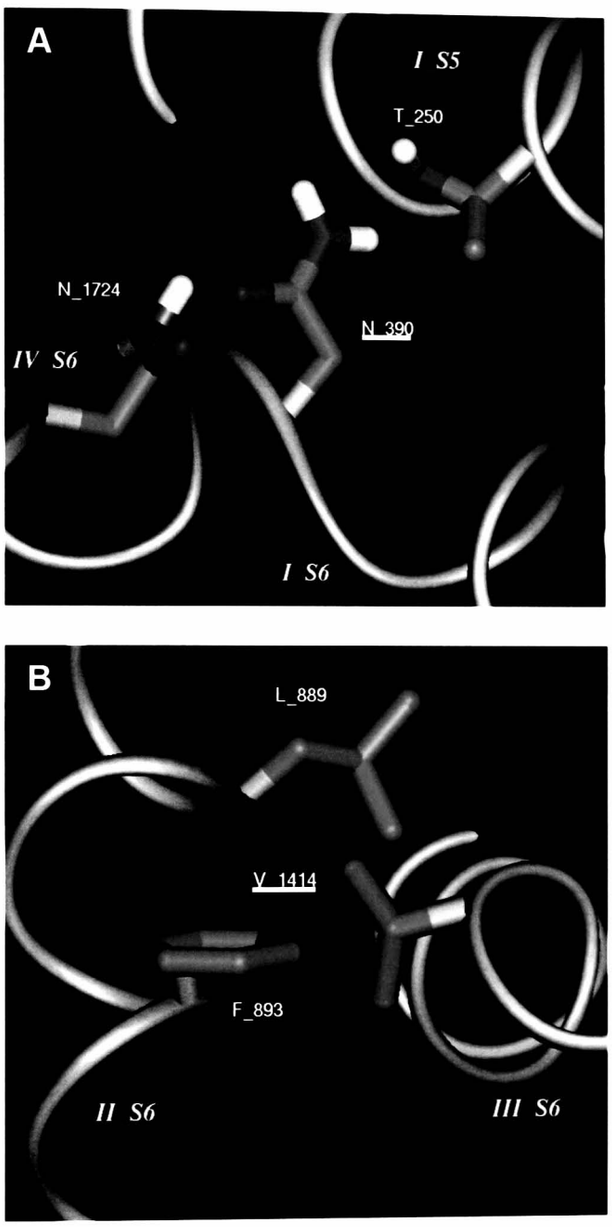

Fig. 6.15. Local environment around residues N390 and V1414 in the open human $Na_V1.8$ molecular model. A) Residue N390 (IS6) hydrogen bonds with N1724 (IVS6) and T250 (IS5). **B)** Residue V1414 (IIIS6) makes hydrophobic interactions with L889 (IIS6) and F893 (IIS6). These interactions occur at the cytoplasmic side of the transmembrane bundle in the open state. This work was carried out by Frank Blaney.

Electrophysiological recordings also showed that the hyperpolarising shift in the activation curve observed for human $Na_V1.8$ mutations I381A and F1710A was not observed for the corresponding mutations in rat $Na_V1.8$ channel. The corresponding mutations in the rat $Na_V1.2$ channel also did not show hyperpolarising shifts in previous studies (McPhee et al., 1995; Yarov-Yarovoy et al., 2002). Furthermore, in contrast to the lack of shifts for human $Na_V1.8$ mutations L1410A and I1706A, the homologous rat $Na_V1.8$ mutations showed positive shifts here, as did the corresponding rat $Na_V1.2$ mutations in previous work (Yarov-Yarovoy et al., 2001).

Therefore, almost all of the rat $Na_V1.8$ mutations showed shifts in the activation curve similar to $rNa_V1.2$, whereas, in contrast to these channels, the human $Na_V1.8$ mutations I381A and F1710A showed hyperpolarising shifts, and mutation L1410A and I1706A did not show shifts. Thus, the S6 segment residues play an important role in stabilisation and/or destabilisation of states during the activation process and this role for some of the residues appears to be different for the human $Na_V1.8$ channel than other subtypes.

The involvement of native residues in the activation process may also be considered from the effect of the point mutations on the activation curve slope. The altered slope can be taken to indicate that changes in the electric field induce movement in an altered relative valence of charges. An altered slope factor suggests that the mutated residue may also be involved in the activation process. However, only a small decrease in the slope factor (steeper slope) was observed for human $Na_V1.8$ mutations N390A and F1710A, and a small increase in the slope factor (less steep slope) was shown for rat $Na_V1.8$ mutations L1411A and I1707A.

Complex subtype-specific effects on the slope of the activation curve have been described in the literature for the corresponding S6 segment mutations. For example, the steeper slope for human $Na_V1.8$ mutation N390A described here was also described for the corresponding mutation in rat $Na_V1.2$ in previous work (Yarov-Yarovoy et al., 2002), but contrasts with the corresponding mutation in rat $Na_V1.4$ (Wang and Wang, 1997) and also the result here for rat $Na_V1.8$. Further, the steeper slope observed for human $Na_V1.8$ mutation F1710A was not described for rat $Na_V1.2$ (McPhee et al., 1995) or here for rat $Na_V1.8$, while the homologous mutation of human $Na_V1.5$ also gave a steeper slope (Carboni et al., 2005).

6.3.2 Effects on the inactivation properties by $Na_V1.8$ channel mutations in the S6 segments

For the voltage-dependence of steady-state inactivation, almost all human $Na_V1.8$ mutations and some of the rat $Na_V1.8$ mutations showed strong hyperpolarised shifts in the curve. For

example, human $Na_V1.8$ mutations I381A, N390A, L1410A, V1414A, I1706A and Y1717A, and rat $Na_V1.8$ mutations I380A, L1411A, I1707A and Y1718A all exhibited more hyperpolarised inactivation compared to the wild type channels. The shifts in the inactivation curve might possibly be explained by the shifts in the activation curves. However, the voltage-dependence of inactivation does not appear to be simply coupled to the voltage-dependence of activation since $Na_V1.8$ activation showed both negative and positive shifts depending on the mutation studied, as already noted for $Na_V1.4$ (Kondratiev and Tomaselli, 2003). Since the steady-state inactivation curves studied here were obtained over potentials where very little activation occurred, these curves represent mainly inactivation from closed states (Yarov-Yarovoy et al., 2001). All of the human $Na_V1.8$ mutations (except F1710A) and most of the rat $Na_V1.8$ mutations (I380A, L1411A, I1707A and Y1718A) shifted the inactivation to more hyperpolarising potentials, indicating the amount of closed-state inactivation is greater than for the wild type channel. The human $Na_V1.8$ mutations N390A and V1414A both showed a depolarising shift in the activation curve and a hyperpolarised shift in the inactivation curve, and a similar effect was also observed for the rat $Na_V1.8$ mutations L1411A, I1707A and Y1718A. This suggests that the native residues at these positions may play a role in coupling activation to channel opening, enabling closed-state inactivation but not channel opening. Interestingly, human $Na_V1.8$ mutation F1710A only showed a hyperpolarising shift in the activation curve and human $Na_V1.8$ mutations L1410A, I1706A and Y1717A only showed hyperpolarising shifts in the inactivation curve. Therefore, it is possible that these residues (L1410, I1706, F1710 and Y1717) are involved in the coupling of the activation to the inactivation process, and residue F1710 favours closed-state inactivation while residues L1410, I1706 and Y1717 do not favour closed-state inactivation. For rat $Na_V1.8$, mutations N389A and V1415A showed a depolarising shift in the activation curve, while the inactivation curve was unaffected, suggesting the native residues at these positions perhaps do not favour closed-state inactivation and are involved in the coupling of the activation to the inactivation process. Thus, many of the native residues at these positions appear to play different roles in the voltage-dependent gating processes between the human and rat $Na_V1.8$ channels.

It is also of interest to compare the effects of mutations on inactivation for $Na_V1.8$ channels with data in the literature for the corresponding alanine mutations in other Na_V channel subtypes. The inactivation curve for human and rat $Na_V1.8$ mutations L1410A and I1706A was shifted to a similar extent by the corresponding mutations of $rNa_V1.2$. In contrast, the lack of a shift in the $V_{1/2}$ for inactivation by the F1710A mutation in both human and rat $Na_V1.8$ channels here contrasts with the appreciable shift described for $Na_V1.2$ and $Na_V1.5$ (Carboni et al., 2005; McPhee et al., 1995). The Y1717A mutation showed depolarising shifts greater in magnitude for human and rat $Na_V1.8$ channels than for both $Na_V1.2$ and $Na_V1.4$ channels (McPhee et al., 1995; O'Reilly et al., 2000). Furthermore, the human $Na_V1.8$ channel mutation N390A showed a

similar strong negative shift to the corresponding mutation in the $Na_V1.4$ channel following a long prepulse inactivation (Nau et al., 1999; Wang and Wang, 1997). However, the latter mutation in the rat $Na_V1.8$ channel did not significantly alter the inactivation curve, and the corresponding mutation in the $Na_V1.2$ channel showed a small positive shift (Yarov-Yarovoy et al., 2002). This residue has been shown to be essential for slow inactivation in $Na_V1.4$ channels (Wang and Wang, 1997). The human $Na_V1.8$ channel I381A and V1414A mutations showed hyperpolarising shifts, which contrast with the depolarising shifts reported for the corresponding mutations of the rat $Na_V1.2$ channel (Yarov-Yarovoy et al., 2001; Yarov-Yarovoy et al., 2002). For the rat $Na_V1.8$ channel, mutation of the corresponding I381 residue also showed a hyperpolarising shift, while the corresponding V1415A mutation showed a similar inactivation curve to the wild type channel. These results suggest that the phenylalanine (corresponding to F1710 in human $Na_V1.8$ channel) residue plays a lesser role in the voltage-dependence of inactivation of human and rat $Na_V1.8$ channels. Moreover, human $Na_V1.8$ residues I381, N390, V1414 and Y1717, and rat $Na_V1.8$ residues I380 and Y1718 favour more depolarised inactivation than other Na_V subtypes.

For human $Na_V1.8$, mutations I1706A, F1710A and Y1717A showed a significant increase in the non-inactivating current component during strong depolarisation. The residues at these positions are all located in the fourth domain, and this effect was the most pronounced for Y1717A, which is proposed to be located near the intracellular mouth of the pore (I1706A and F1710A are located in the middle of the S6 segment) (Fig. 6.2). The intracellularly located fast inactivation gate (DIII-IV linker) is thought to interact with a receptor site within or close to the intracellular mouth of the pore. Mutation of these residues to alanine decreases the extent of inactivation, suggesting these mutations are somehow involved in the fast inactivation gate mechanism. Consistent with the results shown here, significantly more sustained currents at the end of a 30ms depolarising pulse were reported for the alanine mutations of the corresponding F1710A and Y1717A mutations in $rNa_V1.2$ (McPhee et al., 1995). However, in contrast to the results for human and rat $Na_V1.8$ channels, incomplete inactivation was also exhibited by $rNa_V1.4$ glutamate mutation of N434 (corresponding to human $Na_V1.8$ residue N390) (Nau et al., 2003).

The time course for open-state inactivation at 0mV was significantly faster for almost all human $Na_V1.8$ mutations; indeed only mutation N390A showed an unaltered time constant at 0mV. For rat $Na_V1.8$, mutations I1707A and Y1718A also showed significantly faster inactivation. Thus the reduced time to inactivate from open states suggests that the native residues at these positions do not favour inactivation from open states. Conversely, rat $Na_V1.8$ mutation N389A showed slower inactivation, indicating the native residue favours inactivation from open states.

Comparing the results here with the corresponding mutations of other Na_V subtypes in the literature, the effects on the time course for inactivation appear to be subtype-specific. For example, compared to $Na_V1.4$, the corresponding I1706A and Y1717A mutations did not affect the rate of inactivation, while the corresponding F1710A mutation showed a longer time to inactivate (Kimura et al., 2000). Furthermore, corresponding mutations of $Na_V1.2$ did not alter the rate of inactivation. The underlying reason for these differences is not understood, but may be related to the slower inactivation characteristic for $Na_V1.8$ channels compared to other Na_V subtypes.

In this thesis, the recovery from inactivation was only studied in the human form of the $Na_V1.8$ channel. The S6 segment mutations I381A, L1410A, I1706A and Y1717A mainly affected the first component of recovery, increasing the time constant. For the second component, only I1706A increased the time constant. Therefore these results suggest that perhaps the fast inactivation state is more favoured for the native residues at these positions.

Taken together, the results described in this chapter support the involvement of the S6 segment residues in both activation and inactivation gating mechanisms, and the coupling of activation to channel opening. It appears that the native S6 segment residues play an important role in producing the slower inactivation kinetics characteristic for the $Na_V1.8$ channel. Indeed, a number of key S6 residues are involved in the voltage-dependent inactivation properties of human and rat $Na_V1.8$ channels in a distinct manner to other voltage-gated Na^+ channel subtypes.

CHAPTER 7

STRUCTURAL DETERMINANTS OF DRUGS ACTING ON THE $Na_V1.8$ SODIUM CHANNEL

7.1 Introduction

The S6 segments of the $Na_V1.8$ channel and other voltage-gated Na^+ channel subtypes are highly homologous. However, differences in drug action between subtypes have been reported (see *Chapter 5*). For instance, inactivated state block by compound A-803467 is more than 100-fold more selective for $Na_V1.8$ than for several other Na_V channel subtypes (Jarvis et al., 2007). These properties have led to the speculation that compound A-803467 might bind elsewhere on the channel rather than the usual local anaesthetic binding site (Cummins and Rush, 2007). Furthermore, compound A-803467 showed an unusual removal of resting block ("disinhibition") for the human $Na_V1.8$ channel during repetitive stimulation or recovery from inactivation (*Chapter 5*), an effect which had never been previously described for voltage-gated Na^+ channel blocking drugs.

The role of S6 transmembrane segments in voltage-gated Na^+ channel functional properties and drug action is well established for other subtypes. The functional properties of human $Na_V1.8$ channel S6 segment mutations were studied for the first time in *Chapter 6*. Here in this chapter, the effect of the human $Na_V1.8$ channel mutations on the action of highly selective compound A-803467 was examined, and compared with the action of local anaesthetic tetracaine. This was carried out in order to understand the action of A-803467 as a selective blocker acting on a promising therapeutic target for anti-nociceptive drugs, $Na_V1.8$.

7.2 Results

7.2.1 Affinity of tetracaine and A-803467 for resting and inactivated mutant $Na_V1.8$ channels

Tetracaine and compound A-803467 were shown to preferentially bind to inactivated rather than resting $Na_V1.8$ channels in *Chapter 5*. In *Chapter 6* the effects of S6 mutations on the functional properties of the $Na_V1.8$ channel were studied. In order to determine the effects of the same human $Na_V1.8$ channel S6 segment amino acid substitutions on tetracaine and A-803467 block, the resting and inactivated state affinities were first examined.

The affinity for the resting state (calculated as the dissociation constant, K_r) was obtained as in *Chapter 5*, where a depolarising test pulse was used before and after the application of drug from a holding potential of -120mV (Fig. 7.1A). All human $Na_V1.8$ channel mutations (except Y1717A) were in the resting state at this holding potential (*Chapter 6*), and the reduction in current amplitude gives a measure of the affinity for resting channels (*Chapter 2*). However,

since mutation Y1717A showed a very strong hyperpolarising shift in the inactivation curve (see *Chapter 6*), it was partially inactivated at -120mV and consequently the resting state affinity was not calculated. Furthermore, somewhat surprisingly, the mutation L1410A showed a complete block of test pulse current at very low concentrations of tetracaine or A-803467, and thus the unusual effects of drugs on mutant L1410A will be considered separately in the next section.

For tetracaine, mutations I381A and F1710A both gave a significant reduction in the affinity (2.4- and 2.7-fold increases in the K_r, respectively), while mutations N390A, V1414A and I1706A did not significantly alter the affinity for resting channels (Fig. 7.1B, Table 7.1). For compound A-803467, mutation F1710A showed a significant reduction in the affinity for resting states (6.2-fold increase in the K_r; Fig. 7.1C, Table 7.1), while the affinity of compound A-803467 for the remaining mutations was comparable to the wild type $Na_V1.8$ channel. Therefore, these results suggest that residues I381 and F1710 are involved in the resting state binding of tetracaine to $Na_V1.8$ channels, while only residue F1710 is involved in resting state binding of compound A-803467.

The affinity for the inactivated state (calculated as the dissociation constant, K_i) was obtained as in *Chapter 5*, where channels were inactivated by 60-80% with a 4 second prepulse and the effect of the drug on a following test pulse before and after drug application was studied (Fig. 7.2A). The potential to be used for the 4 second conditioning pulse was chosen knowing the effect of each mutation on steady-state inactivation (*Chapter 6*, as to produce 60-80% inactivation). In the case of mutation Y1717A, since some inactivation is already present at the -120mV holding potential this was taken into account with the *h* value. The *h* value was calculated by determining the extent of inactivation at -120mV from the steady state inactivation curves (23.1±2.4%), which was used to adjust the control pulse current amplitude in the absence of drug. The $Na_V1.8$ channel mutations I381A, F1710A and Y1717A significantly reduced the inactivated state affinity for tetracaine, showing increases in the K_i value by 6-, 6- and 3-fold, respectively (Fig. 7.2B, Table 7.2). Mutations N390A, V1414A and I1706A did not alter the affinity for tetracaine. For compound A-803467, only mutation F1710A reduced the affinity, showing a 6-fold increase in the K_i. The other $Na_V1.8$ mutations examined here gave a similar inactivated state affinity for compound A-803467 as for the wild type channel (Fig. 7.2C, Table 7.2). These results indicate that the F1710 residue in an important molecular determinant for the inactivated state affinity of tetracaine and compound A-803467, in addition, residues I381 and Y1717 are important for tetracaine but not for A-803467.

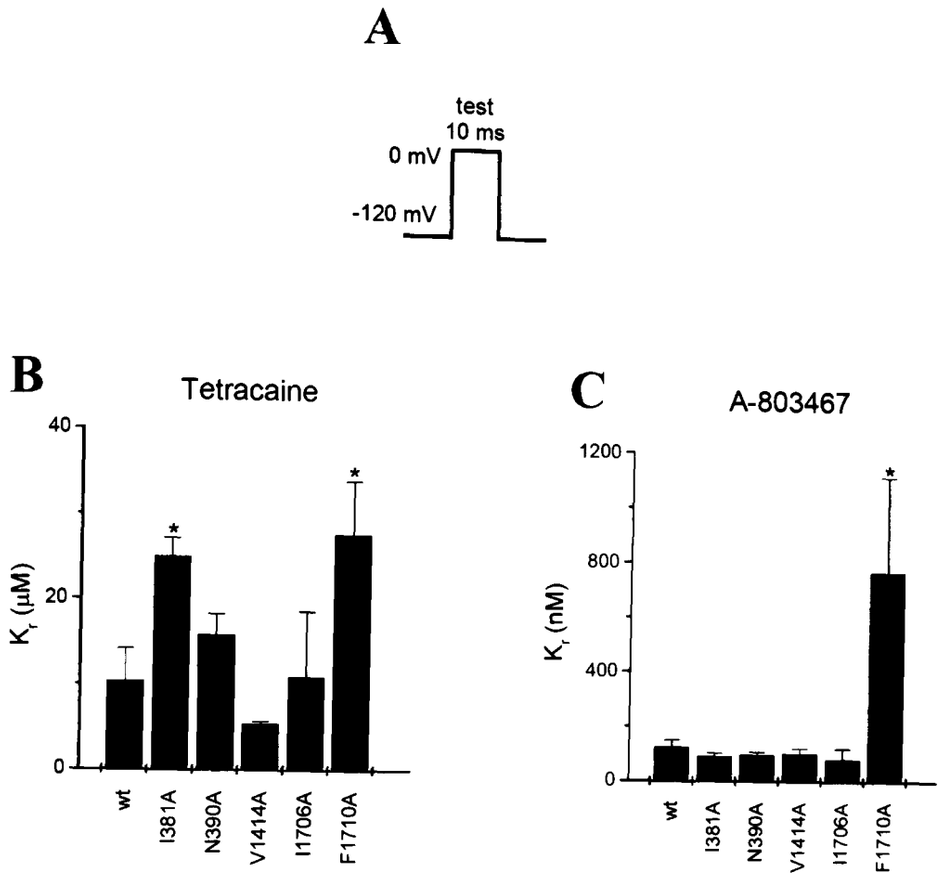

Fig. 7.1. Dissociation constants for resting state of tetracaine and A-803467 for mutant human $Na_V1.8$ channels. A) The pulse protocol shown was used in the absence and presence of drug to determine resting state dissociation constants (K_r). **B)** The bar diagram shown represents the K_r values for tetracaine for wild type and mutant $hNa_V1.8$ channels. **C)** The bar diagram shown represents the K_r values for A-803467 for wild type and mutant $hNa_V1.8$ channels. The concentrations used and n numbers are shown in Table 7.1.

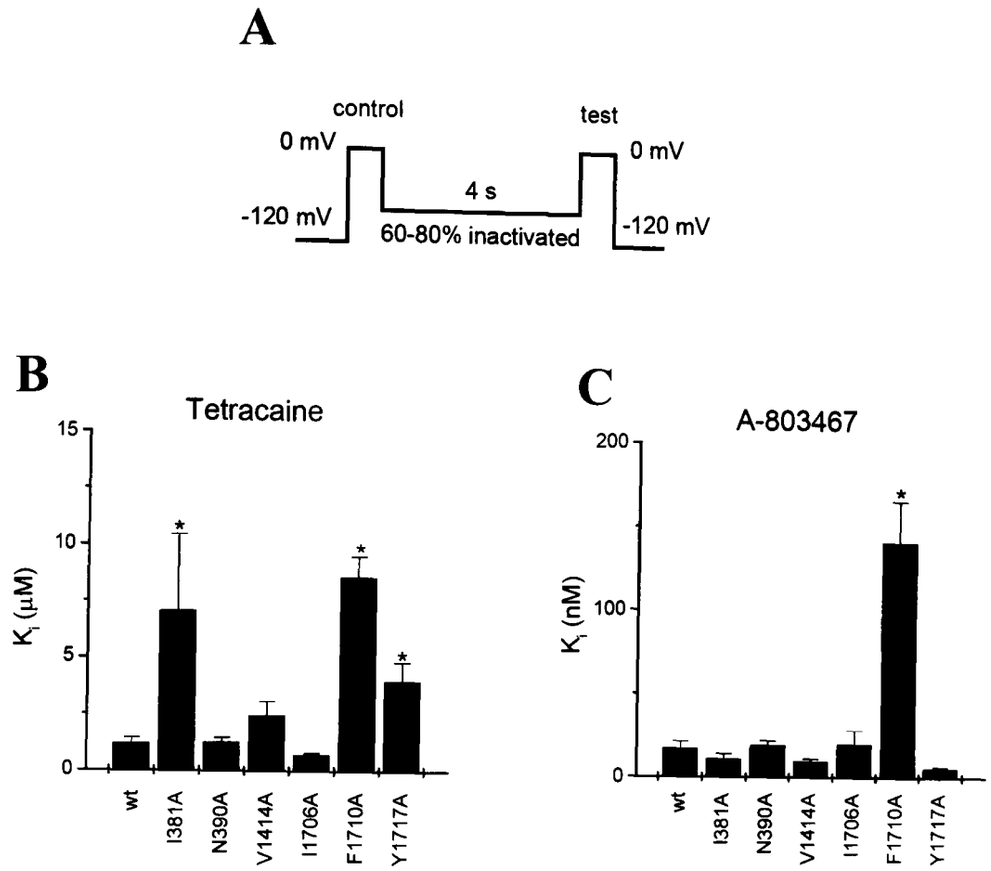

Fig. 7.2. Dissociation constants for inactivated states of tetracaine and A-803467 for mutant human $Na_V1.8$ channels. A) The pulse protocol shown was used in the absence and presence of a drug to determine inactivated state dissociation constants (K_i), where the 4 second pulse indicated was taken at membrane potentials such that 60% to 80% inactivation occurred. **B)** The bar diagram shown represents the K_i values for tetracaine for human wild type and mutant $Na_V1.8$ channels. **C)** The bar diagram shown represents the K_i values for A-803467 for human wild type and mutant $Na_V1.8$ channels. The concentrations used and n numbers are shown in Table 7.2.

TABLE 7.1

Dissociation constants for block of resting $Na_V1.8$ channel S6 mutations

$Na_V1.8$ channel	Drug	Concentration (μM)	I_{Dr}	K_r (μM)	n
$hNa_V1.8$ WT	Tetracaine	10	0.44 ± 0.07	10.3 ± 3.9	6
$hNa_V1.8$ I381A	Tetracaine	10	0.71 ± 0.02	24.9 ± 2.2	7
$hNa_V1.8$ N390A	Tetracaine	10	0.62 ± 0.05	15.8 ± 2.5	8
$hNa_V1.8$ L1410A	Tetracaine	-	-	-	-
$hNa_V1.8$ V1414A	Tetracaine	10	0.35 ± 0.02	5.34 ± 0.37	5
$hNa_V1.8$ I1706A	Tetracaine	10	0.34 ± 0.10	10.9 ± 7.7	6
$hNa_V1.8$ F1710A	Tetracaine	10	0.72 ± 0.04	27.7 ± 6.3	4
$hNa_V1.8$ Y1717A	Tetracaine	-	-	-	-
$hNa_V1.8$ WT	A-803467	0.1	0.51 ± 0.09	0.13 ± 0.03	5
$hNa_V1.8$ I381A	A-803467	0.1	0.47 ± 0.04	0.091 ± 0.012	4
$hNa_V1.8$ N390A	A-803467	0.1	0.48 ± 0.03	0.097 ± 0.010	9
$hNa_V1.8$ L1410A	A-803467	-	-	-	-
$hNa_V1.8$ V1414A	A-803467	0.1	0.48 ± 0.04	0.102 ± 0.020	6
$hNa_V1.8$ I1706A	A-803467	0.1	0.42 ± 0.13	0.081 ± 0.039	2
$hNa_V1.8$ F1710A	A-803467	0.1	0.81 ± 0.03	0.77 ± 0.35	7
$hNa_V1.8$ Y1717A	A-803467	-	-	-	-

TABLE 7.2

Dissociation constants for block of inactivated $Na_V1.8$ channel S6 mutations

$Na_V1.8$ channel	Drug	Concentration (μM)	I_{Di}	h	K_i (μM)	n
$hNa_V1.8$ WT	Tetracaine	1	0.62 ± 0.05	0.28 ± 0.05	1.12 ± 0.31	7
$hNa_V1.8$ I381A	Tetracaine	1	0.78 ± 0.07	0.34 ± 0.02	5.69 ± 2.29	6
$hNa_V1.8$ N390A	Tetracaine	1	0.62 ± 0.04	0.27 ± 0.04	1.27 ± 0.19	6
$hNa_V1.8$ L1410A	Tetracaine	-	-	-	-	-
$hNa_V1.8$ V1414A	Tetracaine	1	0.76 ± 0.04	0.39 ± 0.03	2.42 ± 0.64	6
$hNa_V1.8$ I1706A	Tetracaine	1	0.59 ± 0.06	0.37 ± 0.03	0.71 ± 0.08	5
$hNa_V1.8$ F1710A	Tetracaine	10	0.56 ± 0.03	0.35 ± 0.03	8.59 ± 0.92	4
$hNa_V1.8$ Y1717A	Tetracaine	1	0.83 ± 0.03	0.37 ± 0.02	4.00 ± 0.83	7
$hNa_V1.8$ WT	A-803467	0.01	0.63 ± 0.06	0.34 ± 0.03	0.015 ± 0.004	7
$hNa_V1.8$ I381A	A-803467	0.01	0.62 ± 0.06	0.34 ± 0.03	0.011 ± 0.003	6
$hNa_V1.8$ N390A	A-803467	0.01	0.73 ± 0.03	0.35 ± 0.05	0.019 ± 0.003	7
$hNa_V1.8$ L1410A	A-803467	-	-	-	-	-
$hNa_V1.8$ V1414A	A-803467	0.01	0.68 ± 0.08	0.40 ± 0.03	0.0105 ± 0.0025	5
$hNa_V1.8$ I1706A	A-803467	0.01	0.64 ± 0.08	0.37 ± 0.02	0.020 ± 0.0086	6
$hNa_V1.8$ F1710A	A-803467	0.1	0.65 ± 0.03	0.31 ± 0.01	0.141 ± 0.025	7
$hNa_V1.8$ Y1717A	A-803467	0.01	0.42 ± 0.03	0.28 ± 0.01	0.0056 ± 0.0009	7

7.2.2 Tetracaine and A-803467 drug block for $Na_V1.8$ mutation L1410A

While mutation L1410A did not show any unusual functional properties (*Chapter 6*), complete inhibition of test pulse current was observed following the application of tetracaine or A-803467 at concentrations even 1000 times smaller than used in the previous section to

measure resting block (i.e. 10nM tetracaine or 100pM A-803467). Since currents were not observed in the presence of drug, the resting and inactivated dissociation constants could not be readily determined for mutation L1410A using the above protocols.

Since virtually all L1410A channels are in the resting state at a holding potential of -120mV (*Chapter 6*), the complete inhibition by these drugs suggests the affinity for resting states is much larger than for wild type human $Na_V1.8$ channels. If the resting state affinity of L1410A channels is greater than the affinity for the open or inactivated state, depolarisation will cause drug dissociation. Indeed, as can be seen from Figure 7.3A, in the continual presence of tetracaine (10nM) or A-803467 (100pM), trains of depolarising pulses at 10Hz led to a marked increase in the current amplitude from very low values to 70% of the current amplitude before drug application. Furthermore, in comparison with intermediate stimulation frequencies (10-20Hz), the amplitude of the final pulse in the train was less at relatively lower (2Hz) and higher (50Hz) stimulation frequencies for both tetracaine and compound A-803467 (Fig. 7.3B). These findings show that the extensive resting block of this mutant was removed by repetitive depolarisation in a frequency-dependent manner. Indeed, it was previously shown in *Chapter 5* that in the presence of compound A-803467 (using a concentration of 100nM which gave 49% inhibition of resting channels) a train of depolarising pulses at 10Hz causes a "disinhibition" of wild type human $Na_V1.8$ channel current, which was proposed to be the result of removal of resting block. For human $Na_V1.8$ mutation L1410A, the removal of high-affinity block of A-803467 and also tetracaine appears to be a similar disinhibitory effect, with removal of resting block.

In order to determine whether the high-affinity resting block of mutant L1410A channels is removed by the induction of inactivated states, sustained depolarisation was used to inactivate channels. Using a 600ms conditioning depolarising pulse (the sum of 60, 10ms pulses used above for use-dependent inhibition) to inactivate channels and a 100ms recovery period (to allow inactivated channels to recover from inactivation), the current amplitude at a test pulse to 0mV was measured (Fig. 7.3C). Comparing the test current amplitude before and after the application of the same low concentrations of tetracaine (10nM) and A-803467 (100pM), practically complete removal of resting block was observed by this protocol. Thus it appears that sustained depolarisation removes the extensive block of resting channels, in fact even more effectively than repetitive stimulation.

Overall, these results suggest mutation of residue L1410 causes a dramatic increase in resting state block, and frequent stimulation and sustained depolarisation reduce this block. Furthermore, these data support the hypothesis that this disinhibition occurs by the removal of resting block.

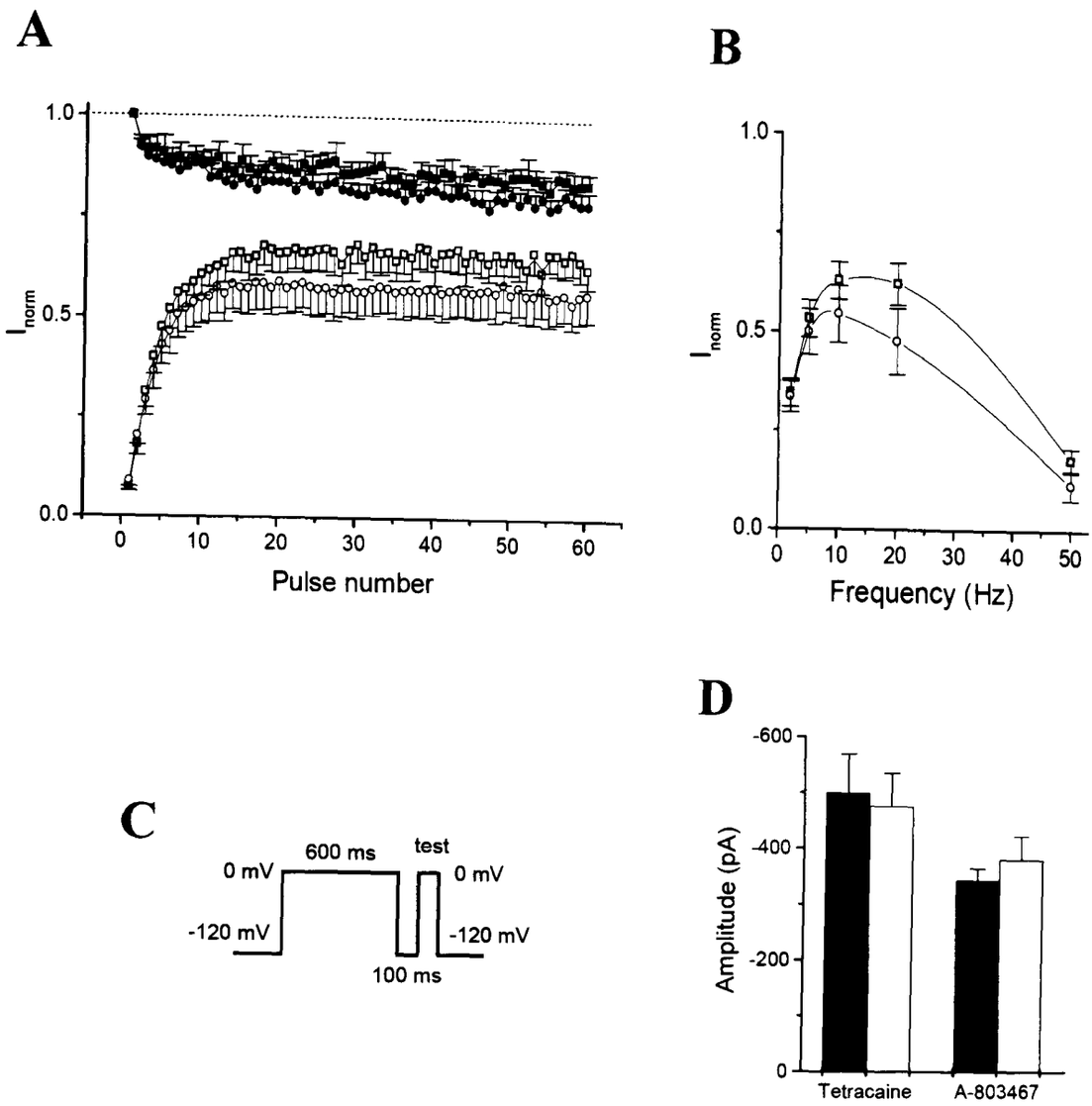

Fig. 7.3. Disinhibition of resting block for human $Na_V1.8$ mutation L1410A. A) Currents, I_{norm}, for mutant L1410A are shown during a 10Hz train of pulses (10ms duration to 0mV from a holding potential of -120mV), plotted against pulse number and normalised to the first pulse of the untreated cell. The currents are shown before the application of tetracaine (■, n=6) or A-803467 (●, n=8) and after tetracaine (10nM, □) or A-803467 (100pM, ○) in paired cells. **B)** The current amplitude elicited at the end of different frequency trains is shown for current normalised to the first pulse of the train. **C)** The pulse protocol shown was used in the absence and presence of drug to determine the effect sustained depolarisation on L1410A currents. **D)** The bar diagram shows the effect of sustained depolarisation on L1410A currents before (*filled* bars) and after (*unfilled* bars) the application of tetracaine (10nM, n=5) or compound A-803467 (100pM, n=6) in paired cells. The protocol in C was used to obtain the test current value shown.

7.2.3 The effect of A-803467 and tetracaine on the recovery from inactivation of S6 segment mutations

The recovery from inactivation was studied using the protocol shown inset in Fig. 7.4A before and after the application of drug. In Figure 7.4 and 7.5, the currents during recovery are expressed as a fraction of the control pulse amplitude in the absence of the compound. It can be seen that in the absence of drug the human $Na_V1.8$ channel current eventually recovers to similar values to the control pulse amplitude. As shown in *Chapter 5*, resting wild type human $Na_V1.8$ channel currents were reduced approximately 50% in the continual presence of compound A-803467 (100nM), and the time course of recovery from inactivation showed an increase in current above the control pulse amplitude (disinhibition). This can be seen in Figure 7.4A, in the presence of A-803467 the human $Na_V1.8$ channel current tends towards the level of resting block at longer recovery periods (approximately 50%, indicated with a dotted line). The increase in current above the control value in the presence of A-803467 was proposed to be the result of a partial removal of resting block, where the additional slow component of recovery represents the reinstatement of the resting block (*Chapter 5*). The extent for which the currents increase above the resting block level can be measured by expressing the amplitude of the additional slow component (I_3) as a fraction of resting block; termed the amplitude of disinhibition, I_{dis}. For the human $Na_V1.8$ channel the additional slow component was 26% of the magnitude of the resting block by A-803467. Therefore the amplitude of disinhibition (I_{dis}) is 26%, which may be seen from Figure 7.4A.

For the mutations in the S6 segments examined here, quite unexpectedly, I_{dis} was significantly larger for all mutations than for the wild type channel in the presence of A-803467 (Fig. 7.6A). Only small effects were apparent on the first and second components of recovery from inactivation (Table 7.3). The time courses for recovery from inactivation are shown in Figures 7.4 and 7.5, and the fit parameters are shown in Table 7.3. For mutation L1410A, there was complete resting block following the application of A-803467 (100pM) (Fig. 7.4D). For this mutant, marked disinhibition was observed during the time course of recovery from inactivation, corresponding to the removal of the high-affinity resting block during depolarisation (Fig. 7.4D). Mutations I381A, N390A, V1414A and I1706A all showed a similar extent of resting A-803467 block to wild type human $Na_V1.8$ channels (Fig 7.1C), but showed larger disinhibitory components (Figs. 7.4-7.6). For mutation F1710A, the resting block was reduced (Fig. 7.1C), but the disinhibitory component expressed as a fraction of the resting block (I_{dis}), is larger than for wild type channels (Fig. 7.6A). For mutation Y1717A, currents were too small to be measured accurately in the presence of 100nM A-803467, however even at 10nM (Fig. 7.5D), A-803467 caused a larger disinhibitory component (35.2±7.4%, n=5) compared to the very small disinhibitory component observed for wild type at the same concentration (n=9).

The time constant of recovery for the disinhibitory component was similar for all mutations studied here, except for I1706A, as compared to the wild type human $Na_V1.8$ channel (Fig. 7.6B). These results suggest that relative to the resting state, disinhibition of compound A-803467 is generally markedly increased by mutation of the S6 segment residues.

However, in contrast to compound A-803467, the time course of recovery from inactivation for tetracaine did not show disinhibition for wild type human $Na_V1.8$ channels (see *Chapter 5*). Unexpectedly, in the presence of tetracaine disinhibition was observed for all studied mutations, except I381A (Fig. 7.7-7.9). For these mutations, the recovery from inactivation was fitted with three components. The values for the fits are shown in Table 7.3. For mutation L1410A, the additional slow component expressed as a fraction of the resting block (I_{dis}) by tetracaine was 68% (Figs. 7.7D and 7.9A). For mutation F1710A, a striking disinhibition of tetracaine was also observed (Fig. 7.8C), particularly when the disinhibitory component was expressed as a fraction of resting block (Fig. 7.9A). While the L1410A and F1710A mutations showed striking disinhibitory components, the other mutations showed a disinhibitory component that was small relative to the extent of resting block (Fig. 7.9A). Following the application of tetracaine, the time constants of the additional slow component are shown in Figure 7.9B. These time constants for the human $Na_V1.8$ channel mutations could not be compared to the wild type channel since it did not show this additional component in the presence of tetracaine.

Overall these results suggest that mutation of the S6 segment residues L1410 and F1710 induced marked disinhibition by tetracaine, and mutation of all residues studied here led to pronounced disinhibition by A-803467.

TABLE 7.3

Effects of drugs on recovery from inactivation and use-dependent block of hNa $_V$1.8 channel S6 mutations

$Na_V1.8$ channel	Drug	Concentration (μM)	Recovery from inactivation							UD block	
			τ_{fast} norm	I_{fast} norm	τ_{slow} norm	I_{slow} norm	τ_3 (ms)	I_{dis} (%)	n	10Hz	n
$hNa_V1.8$ WT	Tetracaine	10	1.74 ± 0.20	0.90 ± 0.07	5.46 ± 1.80	1.24 ± 0.20	-	-	6	0.75 ± 0.05	20
$hNa_V1.8$ I381A	Tetracaine	10	1.84 ± 0.40	1.02 ± 0.10	4.62 ± 1.48	0.96 ± 0.21	-	-	6	0.75 ± 0.05	11
$hNa_V1.8$ N390A	Tetracaine	10	1.23 ± 0.31	0.87 ± 0.09	1.15 ± 0.09	1.12 ± 0.10	2639 ± 740	26.6 ± 16.6	4	0.75 ± 0.05	10
$hNa_V1.8$ L1410A	Tetracaine	0.01	1.10 ± 0.19	0.96 ± 0.11	1.16 ± 0.50	1.20 ± 0.57	1801 ± 361	67.7 ± 3.7	7	-	-
$hNa_V1.8$ V1414A	Tetracaine	10	1.73 ± 0.32	0.82 ± 0.21	4.38 ± 2.50	1.38 ± 0.57	1032 ± 575	16.2 ± 6.6	3	0.75 ± 0.05	4
$hNa_V1.8$ I1706A	Tetracaine	10	4.27 ± 2.7	0.68 ± 0.50	1.55 ± 1.38	1.51 ± 0.88	1523 ± 767	3.2 ± 1.0	3	0.75 ± 0.05	5
$hNa_V1.8$ F1710A	Tetracaine	10	1.91 ± 0.56	1.12 ± 0.23	2.39 ± 1.24	0.74 ± 0.39	2175 ± 962	63.7 ± 28.1	4	0.75 ± 0.05	16
$hNa_V1.8$ Y1717A	Tetracaine	10	0.65 ± 0.30	0.55 ± 0.19	0.41 ± 0.21	2.09 ± 0.56	4858 ± 536	18.9 ± 3.9	6	0.75 ± 0.05	13
$hNa_V1.8$ WT	A-803467	0.1	0.90 ± 0.20	1.06 ± 0.11	0.50 ± 0.27	1.92 ± 0.41	1668 ± 183	25.6 ± 3.9	5	0.75 ± 0.05	12
$hNa_V1.8$ I381A	A-803467	0.1	1.13 ± 0.3	0.85 ± 0.17	0.29 ± 0.09	1.39 ± 0.58	1479 ± 143	62.7 ± 8.9	7	0.75 ± 0.05	7
$hNa_V1.8$ N390A	A-803467	0.1	1.21 ± 0.3	0.99 ± 0.16	1.71 ± 0.76	1.01 ± 0.25	1347 ± 173	46.0 ± 12.0	7	0.75 ± 0.05	7
$hNa_V1.8$ L1410A	A-803467	0.0001	0.04 ± 0.02	-	0.30 ± 0.19	2.03 ± 0.55	1658 ± 60	58.8 ± 5.0	5	0.75 ± 0.05	-
$hNa_V1.8$ V1414A	A-803467	0.1	2.34 ± 0.81	1.00 ± 0.00	-	-	1628 ± 64	66.6 ± 9.0	6	0.75 ± 0.05	6
$hNa_V1.8$ I1706A	A-803467	0.1	0.71 ± 0.58	0.57 ± 0.23	0.09 ± 0.04	3.72 ± 2.15	751 ± 150	70.3 ± 26.5	2	0.75 ± 0.05	2
$hNa_V1.8$ F1710A	A-803467	0.1	1.24 ± 0.36	1.05 ± 0.18	0.28 ± 0.13	0.89 ± 0.36	1687 ± 223	73.5 ± 15.9	7	0.75 ± 0.05	7

UD block is use-dependent block. NB: The I_{fast} could not be obtained for mutation L1410A in the presence of A-803467 as this component was too small. For mutation V1414A the The I_{slow} could not be obtained in the presence of A-803467 as this component was also too small.

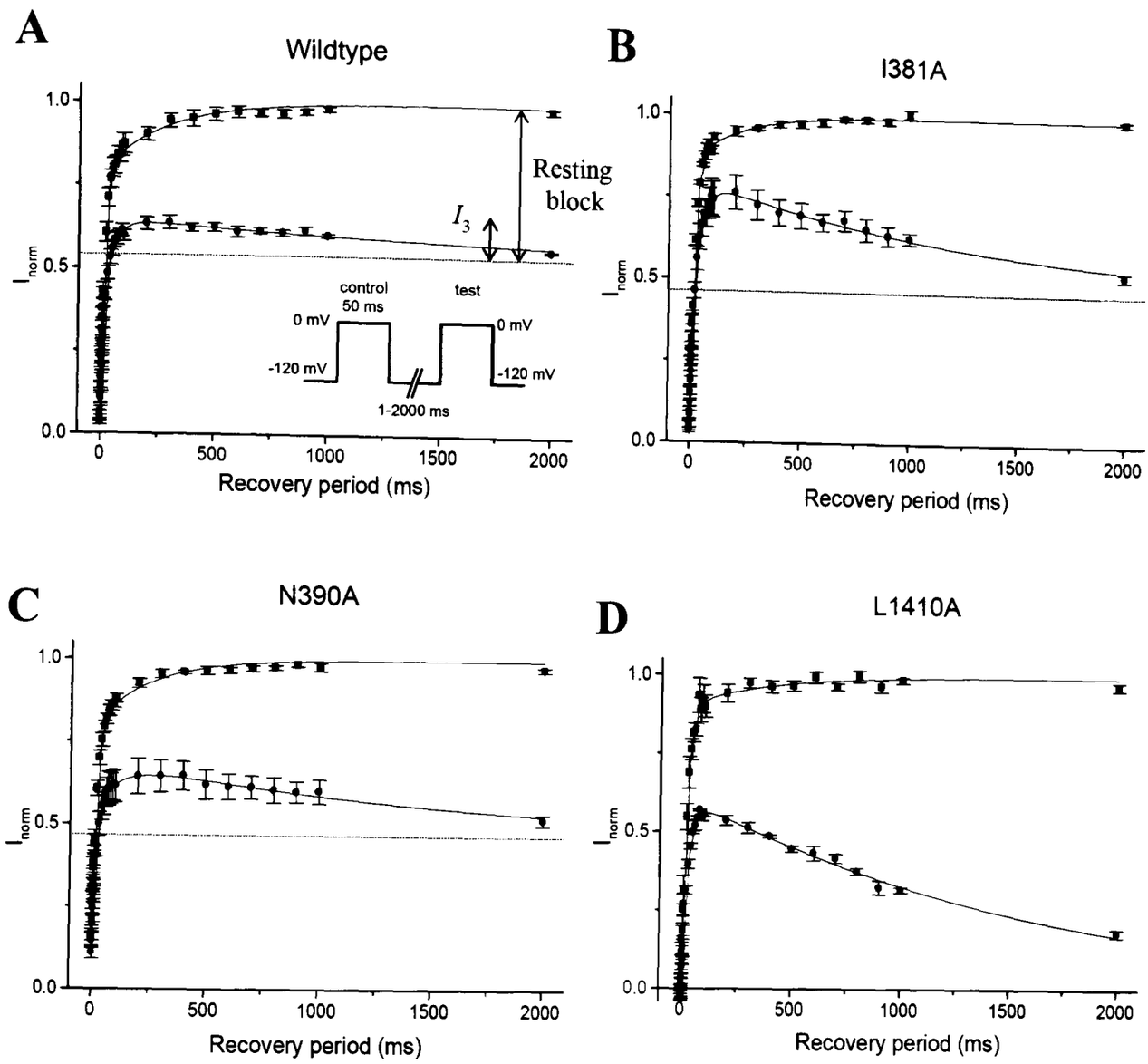

Fig. 7.4. The effects of A-803467 on the time course of recovery from inactivation for mutant human $Na_V1.8$ channels. Time courses of recovery from inactivation are shown for wild type (**A**), I381A (**B**), N390A (**C**) and L1410A (**D**) $Na_V1.8$ channels, before (■) and after (●) the application of A-803467 in paired cells. The curves for were fit with three exponential components. The pulse protocol is shown in the inset of A. The *dotted* line represents the extent of resting block. The resting block and the amplitude of the addition slow component (I_3) are illustrated with arrows in A. The concentrations used and n numbers are shown in Table 7.3.

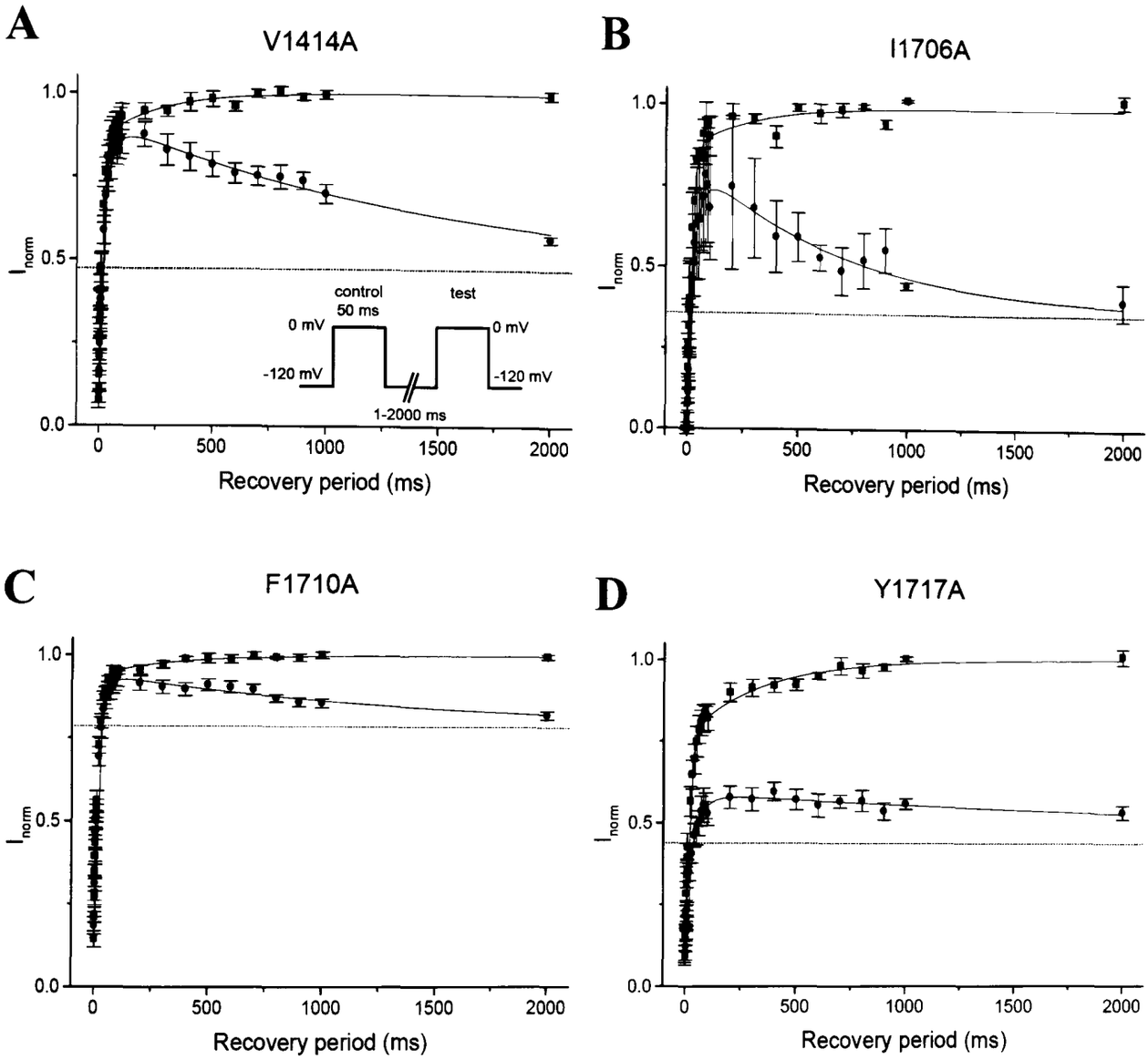

Fig. 7.5. The effects of A-803467 on the time course of recovery from inactivation for mutant human $Na_V1.8$ channels. Time courses of recovery from inactivation are shown for V1414A (**A**), I1706A (**B**), F1710A (**C**) and Y1717A (**D**) $Na_V1.8$ channels, before (■) and after (●) the application of A-803467 in paired cells. The pulse protocol is shown in the inset of A. The curves fwere fit with three exponential components. The *dotted* line represents the extent of resting block. The concentrations used and n numbers are shown in Table 7.3.

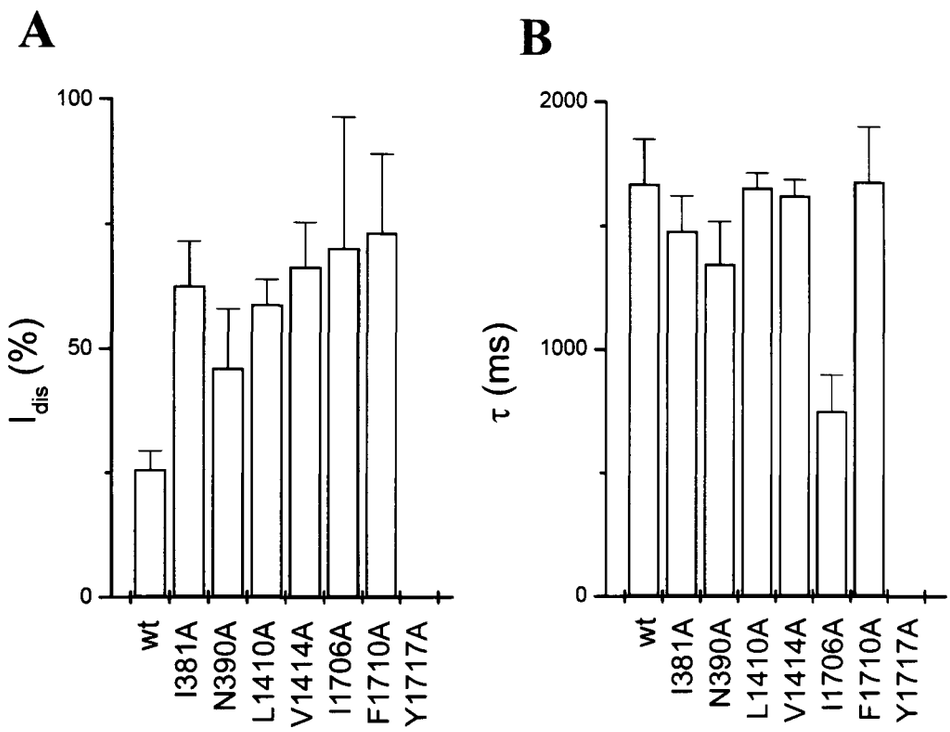

Fig. 7.6. The effects of A-803467 on the parameters of the disinhibitory component of recovery. A) The bar diagram shows the amplitude (I_{dis}, which is I_3 expressed as a fraction of the resting channel block) of the disinhibitory component from the time course of recovery from inactivation for wild type, and mutant $Na_V1.8$ channels. **B)** The bar diagram shows the time constant, τ, of the disinhibitory component for wild type, and mutant $Na_V1.8$ channels. The n numbers are shown in Table 7.3.

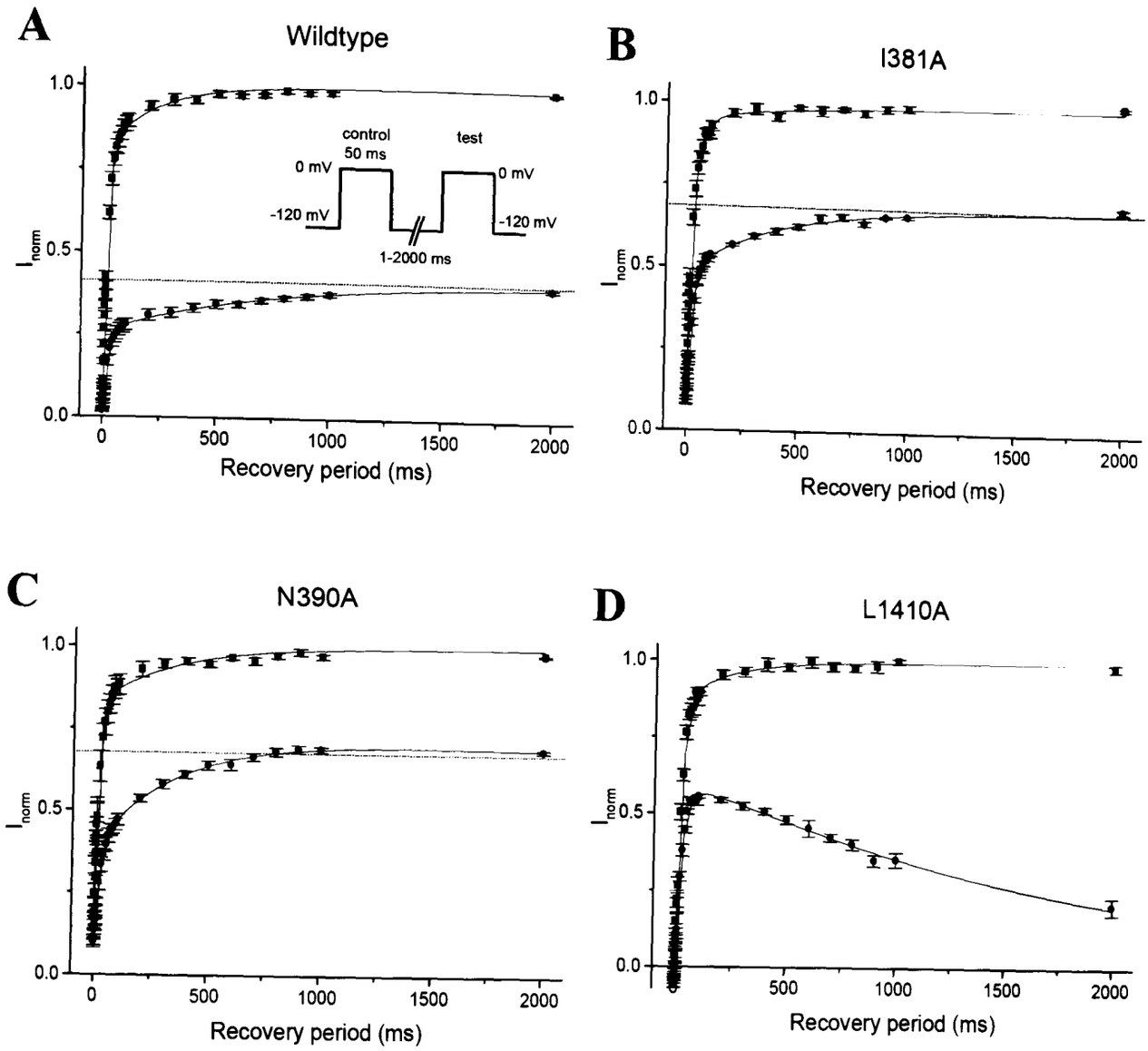

Fig. 7.7. The effects of tetracaine on the time course of recovery from inactivation for mutant human $Na_v1.8$ channels. Time courses of recovery from inactivation are shown for wild type (**A**), I381A (**B**), N390A (**C**) and L1410A (**D**) $Na_v1.8$ channels, before (■) and after (●) the application of tetracaine in paired cells. The pulse protocol is shown in the inset of A. The curves for wild type and I381A were fit with two exponential components, while the curves for N390A and L1410A were fit with three. The *dotted* line represents the extent of resting block. The concentrations used and n numbers are shown in Table 7.3.

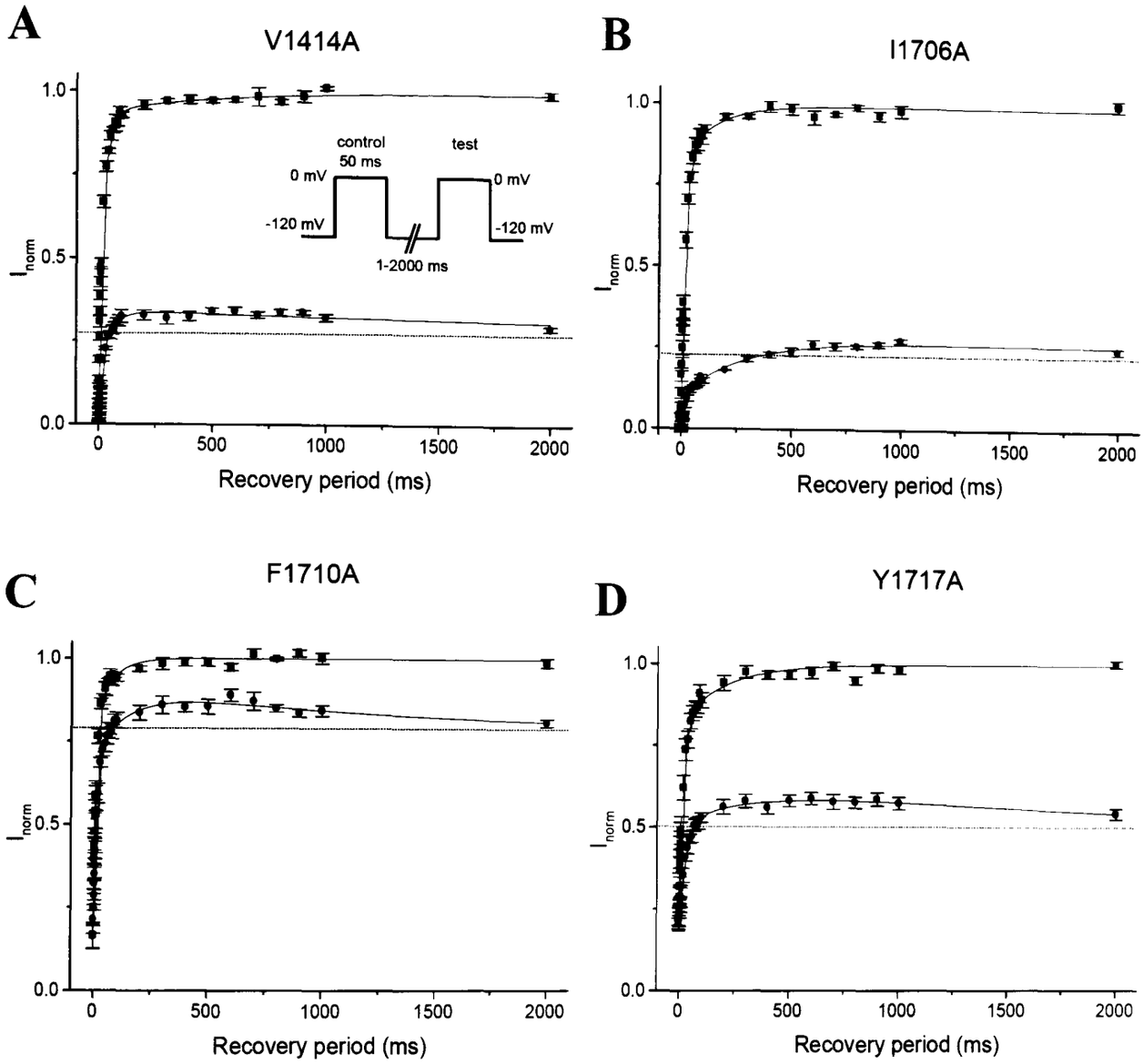

Fig. 7.8. The effects of tetracaine on the time course of recovery from inactivation for mutant human $Na_V1.8$ channels. Time courses are for V1414A (**A**), I1706A (**B**), F1710A (**C**) and Y1717A (**D**) $Na_V1.8$ channels, before (■) and after (●) the application of tetracaine in paired cells. The pulse protocol is shown in the inset of A. The curves for were fit with three exponential components. The *dotted* line represents the extent of resting block. The concentrations used and n numbers are shown in Table 7.3.

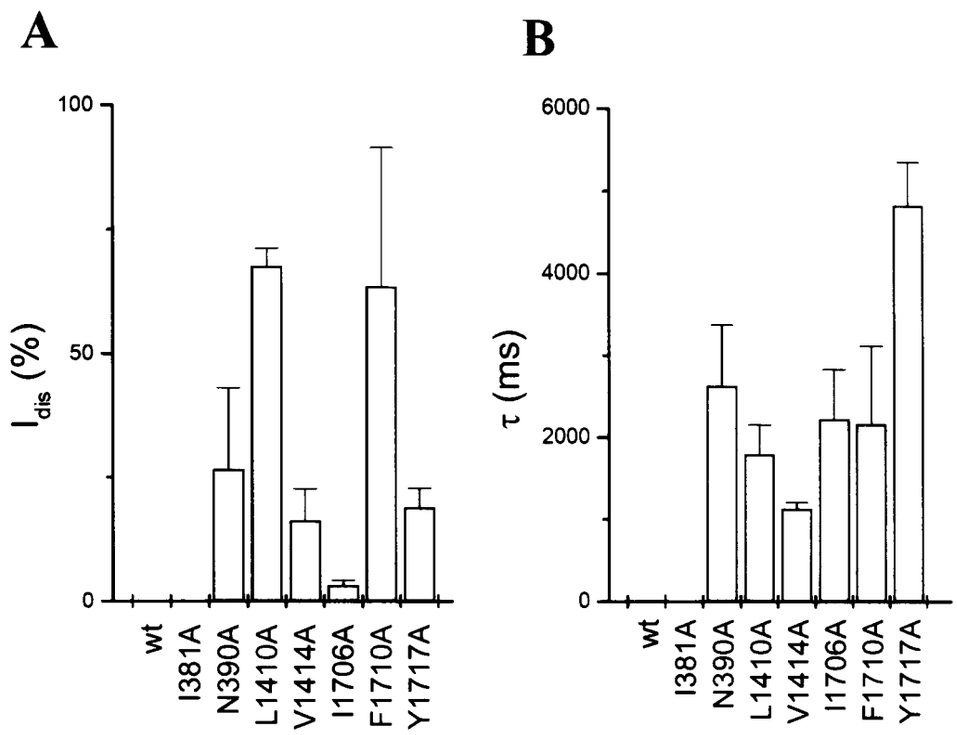

Fig. 7.9. The effects of tetracaine on the parameters of the disinhibitory component of recovery. A) The bar diagram shows the amplitude (I_{dis}, which is I_3 expressed as a fraction of the resting channel block) of the disinhibitory component from the time course of recovery from inactivation for wild type, and mutant $Na_V1.8$ channels. **B)** The bar diagram shows the time constant, τ, of the disinhibitory component for wild type, and mutant $Na_V1.8$ channels. The n numbers are shown in Table 7.3.

7.2.4 The effect of S6 segment mutations on use-dependent block of A-803467 and tetracaine

Since most of the S6 mutations showed an altered time course of recovery from inactivation time course in the presence of drug, it would be expected that this property would also be observed during trains of depolarising pulses. Indeed, use-dependent block of 1μM tetracaine at 10Hz (example mean currents are shown in Fig. 7.10A) was no longer observed for mutations I381A, N390A, V1414A or F1710A (Fig. 7.10A,B). Furthermore, mutant Y1717A showed the disinhibition of tetracaine (Fig. 7.10B). In contrast, mutation I1706A showed a similar extent of use-dependent block compared to wild type human $Na_V1.8$ channels (Fig. 7.10B).

For compound A-803467 (10nM), 10Hz stimulation showed a greater extent of disinhibition (example mean currents are shown in Fig. 7.10C) for mutations I381A, N390A, V1414A, I1706A and Y1717A compared to wild type channels (Fig. 7.10C,D). Only mutation F1710A did not alter the extent of use-dependent disinhibition (Fig. 7.10D).

Taken together, the results show that mutations of the S6 segments induced disinhibitory components for both tetracaine and A-803467.

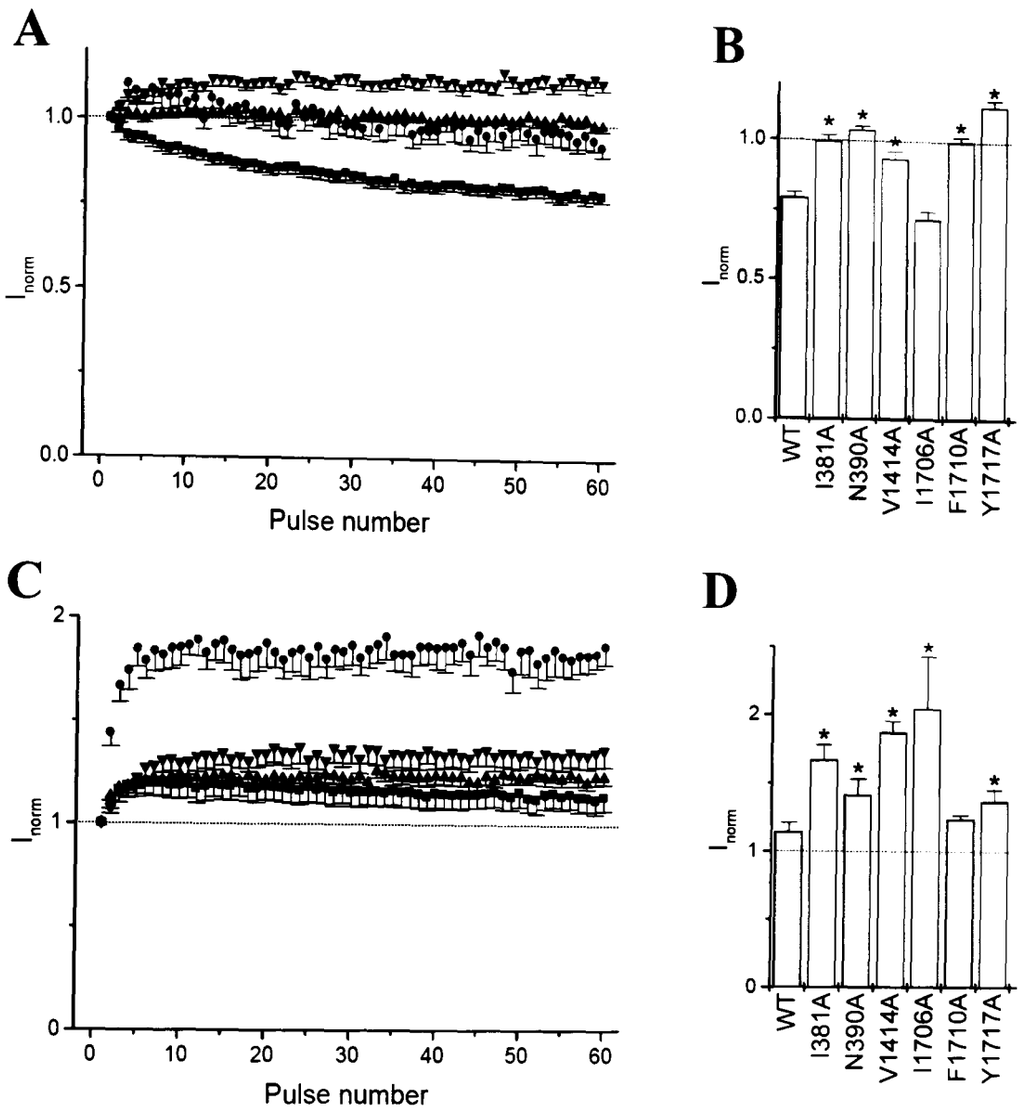

Fig. 7.10. Effect of mutant human $Na_V1.8$ channels on the use-dependent block by tetracaine and A-803467. A) Normalised mean currents are shown plotted against pulse number during stimulation at 10Hz (pulses to 0mV of 10ms duration from a holding potential of -120mV) in the continual presence of tetracaine (1μM). Curves are for wild type (■), V1414A (●), F1710A (▲), and Y1717A (▼). **B)** The bar diagram shows the extent of use-dependent block by tetracaine at the 60th pulse of a 10Hz train for wild type and mutant $hNa_V1.8$ channels. **C)** Normalised example mean currents are shown plotted against pulse number during stimulation at 10Hz in the continual presence of A-803467 (10nM). Curves are for wild type (■), V1414A (●), F1710A (▲), and Y1717A (▼). **D)** The bar diagram shows the extent of use-dependent block by A-803467 at the 60th pulse of a 10Hz train for wild type and mutant $hNa_V1.8$ channels. In A-D, currents were first expressed as a fraction of the first pulse and then expressed as a fraction of their respective control pulses before the application of drug, as shown in Figure 5.6. * $p<0.05$, compared to the first pulse. The n numbers are shown in Table 7.3.

7.3 Discussion

7.3.1 Effects of S6 segment mutations on the tonic block of tetracaine and A-803467

In this chapter, the effects of $Na_V1.8$ channel S6 segment mutations on the action of local anaesthetic, tetracaine, and the highly $Na_V1.8$-selective compound, A-803467, were studied. These mutations have all been shown to affect the tonic and/or use-dependent properties of a number of drugs for other Na_V channel subtypes (see *Chapter 1*). The effect of the mutations on block by tetracaine and A-803467 was first investigated by examining the affinity for both the resting and inactivated states. For tetracaine, the affinity for the resting channel was reduced by I381A and F1710A, with 2-fold and 3-fold increases in K_r respectively (the resting state affinity was not calculated for Y1717A). The affinity for the inactivated channel was reduced by I381A, F1710A and Y1717A, with 6-fold, 6-fold and 3-fold increases in K_r respectively. For compound A-803467, mutation of the F1710 residue reduced the resting state affinity (K_r increased 6-fold), and the affinity for the inactivated channel was also reduced (K_i also increased 6-fold). In contrast to the effects of the other mutations, mutation L1410A showed a surprising increase in resting block, as currents were completely inhibited even by 1000-fold lower concentrations of tetracaine or A-803467, suggesting a greater than 1000-fold increase in affinity for resting states. These results suggest that while the role of L1410 is unknown, residues I381, F1710 and Y1717 are important for the action of tetracaine, but only residue F1710 for the action of A-803467. Thus the F1710 residue is important for the action of both tetracaine and compound A-803467, but in contrast to tetracaine, mutations I381A and Y1717A do not appear to be important for the affinity of compound A-803467 for resting or inactivated channels. Previously, mutagenesis of the drug binding sites on $Na_V1.8$ sodium channels has not been carried out. It was not understood where compound A-803467 bound in the $Na_V1.8$ channel; indeed, it was speculated that it might not bind to the local anaesthetic site (Cummins and Rush, 2007). However, these results suggest it binds to a site within the pore, which partially overlaps the local anaesthetic binding site.

As discussed in *Chapter 1*, the residue corresponding to F1710 has been found to be the most important in determining the action of voltage-dependent pore-blocking drugs; indeed, no drug tested has been shown to be unaffected by the mutation F1710A. This residue is also important for the preference of drugs for the inactivated state over the resting state (Li et al., 1999). For tetracaine, mutation F1710A reduced the affinity for inactivated states more than for resting states, in $Na_V1.3$ channels (Li et al., 1999) and in $Na_V1.8$ channels in this chapter, indicating tetracaine interacts with F1710 more effectively when the $Na_V1.8$ channel is inactivated. This property likely underlies the preference of tetracaine for the inactivated channel rather than the

resting channel. In contrast, mutation F1710A showed a practically equal effect on the resting and inactivated state binding of compound A-803467. Therefore, while F1710 appears to be important for the binding of A-803467, it does not appear to contribute to the preferential inactivated state binding of this compound. A more extensive study of mutations at other positions would be necessary to understand the selectivity of A-803467 for the inactivated state over the resting state in $Na_V1.8$, and also for the $Na_V1.8$ channel subtype over other Na_V channel subtypes.

7.3.2 Effects of A-803467 and tetracaine on the recovery from inactivation of S6 segment mutations

The effect of disinhibition, first observed in *Chapter 5*, involves the partial removal of A-803467 resting block during recovery from inactivation. The extent of disinhibition of A-803467 was more pronounced than the wild type channel for all the human $Na_V1.8$ channel S6 segment mutations examined in this chapter. A striking example of this was for mutation L1410A, where resting channels were completely inhibited in the presence of tetracaine and A-803467, but a marked disinhibition of resting block was observed during recovery from inactivation. For the other mutations, relative to the extent of resting block, the extent of A-803467 disinhibition was more pronounced for all the mutations studied than for wild type channels. Thus the native residues at all these positions appear to be involved in the disinhibitory phenomenon.

While tetracaine did not show the disinhibitory effect for wild type human $Na_V1.8$ channels, the appearance of a disinhibitory component was observed for mutations during recovery from inactivation. The time course of recovery from inactivation showed disinhibition by tetracaine of varying extents for mutations N390A, L1410A, V1414A, I1706A, F1710A and Y1717A, but not I381A. Although small effects were observed for N390A, V1414A, I1706A and Y1717A, the most marked disinhibition was shown for L1410A and F1710A. As with compound A-803467, tetracaine blocked resting L1410A mutant channels with high-affinity, and marked disinhibition of tetracaine was shown during stimulation. For mutation F1710A, tetracaine blocked resting channels with a lower affinity than wild type, but a large proportion of the blocked channels were also disinhibited by stimulation. These findings suggest that the native residues L1410 and F1710 contribute to the mechanism underlying the main disinhibitory effect on human $Na_V1.8$ channels for tetracaine.

The residues considered here have been shown to be important determinants for the action of a number of drugs in $Na_V1.2$, $Na_V1.3$, $Na_V1.4$ and $Na_V1.5$ channels (see *Chapter 1*). The effect of corresponding mutations on the action of tetracaine has so far only been studied in $Na_V1.3$,

and the effects were similar to those here in the present chapter. For $Na_V1.2$ channels, the inactivated state affinity of etidocaine was significantly reduced by corresponding mutations I381A (K_i increased 6-fold), L1410A (K_i increased 6-fold), V1414A (K_i increased 7-fold), F1710A (K_i increased 130-fold) and Y1717A (K_i increased 35-fold) (Ragdale et al., 1994; Yarov-Yarovoy et al., 2001; Yarov-Yarovoy et al., 2002). For all drugs studied to date, the corresponding F1710 residue appears to be the principal determinant for drug action in a number of Na_V channel subtypes, and is proposed to directly bind to local anaesthetics by a π-cation interaction (Ahern et al., 2008). For the human $Na_V1.8$ channel, the F1710 residue was shown in this chapter to be important for the action of both local anaesthetic tetracaine and $Na_V1.8$-selective compound A-803467. For V1414A, tetracaine does not appear to make interactions with the $Na_V1.8$ channel that were found to be important for etidocaine binding in the $Na_V1.2$ channel. For L1410A, high-affinity drug block of resting channels was not observed in the corresponding mutations of $Na_V1.2$ or $Na_V1.4$ (Wang et al., 2004; Wang et al., 2000; Yarov-Yarovoy et al., 2001), or indeed any mutation of a Na_V channel.

While it is possible that the substitution of the leucine to an alanine residue at position 1410 might cause the marked increase in resting block by direct interactions, the notable magnitude of this effect suggests that this is unlikely. The hydrophobic pathway (see *Section 1.3.3*) has been suggested to exist at the interface between the IIIS6 and IVS6 segments (Bruhova et al., 2008), and since the L1410 residue is located on the IIIS6 segment perhaps its mutation alters this pathway. Perhaps the drugs become trapped in the resting state, although it is difficult to understand how mutation to a smaller alanine residue might enhance trapping. The mutation did not show unusual functional properties in the absence of drug (*Chapter 5*), thus it is unlikely that the mutation caused severe distortion of the molecular structure.

7.3.3 Effects of mutations of S6 segments on the use-dependent block of tetracaine and A-803467

It was observed in *Chapter 5*, that the disinhibition observed during frequent stimulation correlated with the effects on the time course of recovery from inactivation. As expected from the time course of recovery from inactivation showing marked disinhibition by tetracaine, mutations N390A, V1414A, F1710A and Y1717A caused a reduction in use-dependent block by tetracaine. For tetracaine acting on $Na_V1.8$, the N390A mutation showed a similar effect for etidocaine acting on the corresponding mutation of $rNa_V1.2$; while the binding affinities were unaffected, the extent of use-dependent block was reduced (Yarov-Yarovoy et al., 2002).

Despite not showing disinhibition during recovery from inactivation in the presence of tetracaine, mutation I381A did not display use-dependent block by tetracaine, and vice versa,

mutation I1706A showed use-dependent block despite showing disinhibition during recovery from inactivation. The corresponding I1706A mutation in $rNa_V1.2$ channel was shown to reduce the use-dependent block by etidocaine while the binding affinities were not affected (Ragsdale et al., 1994; Wang et al., 1998a). The latter mutation in the $rNa_V1.4$ channel was also shown to reduce the use-dependent block by etidocaine, however, use-dependent block by benzocaine was shown to be more pronounced for this mutation (Wang et al., 1998a). Using quaternary local anaesthetics it was proposed that this mutation created another pathway for local anaesthetics to dissociate from, and is perhaps not directly involved in the local anaesthetic binding site (Ragsdale et al., 1994; Wang et al., 1998a).

For compound A-803467, all mutations showed more pronounced disinhibition (except F1710A) than wild type $Na_V1.8$ channels at 10Hz. These results suggest these native residues at these positions do not affect the affinity for the inactivated state, but somehow contribute to reducing the disinhibitory effect. Taken together, the S6 segment mutations generally abolished the use-dependent block by tetracaine and showed more pronounced use-dependent disinhibition of compound A-803467.

7.3.4 Homology models for the binding of tetracaine and A-803467

Based on the mutagenesis data in this thesis, Frank Blaney constructed a (unpublished) model of the human $Na_V1.8$ channel using homology with the crystal structure of the open rat $K_V1.2$ channel (Long et al., 2005) and carried out docking studies with tetracaine and A-803467. Figure 7.11A,B shows tetracaine docked into the open human $Na_V1.8$ channel, and Figure 7.11C,D shows A-803467. These models suggest that the protonated nitrogen of tetracaine and the amide NH of A-803467 interacts with D356 (i.e. the D of the DEKA motif). The F1710 residue interacts with the aromatic ring of both compounds by π-π stacking, and L1410 forms a hydrophobic interaction with both drugs. The diethyl amino group of tetracaine is able to form a hydrophobic interaction with I381. In contrast, the methoxy groups of A-803467 form hydrogen bonds with T354 and S1660 (in the P loops), which lock A-803467 in a position where the substituted ring of A-803467 cannot interact with I381. The Y1717 residue can hydrogen bond to the ester carbonyl of tetracaine, but it cannot interact with A-803467. Furthermore, this molecular model also suggests interactions with residues not mutated in this thesis. Tetracaine might interact with F382, L882, F1713, L1711 and V1714, and A-803467 might interact with S385, L882 and V1714. All these residues are conserved between all Na_V channel subtypes. Overall, the experimentally obtained affinities for both compounds support this molecular model. However, the selectivity of A-803467 for $Na_V1.8$ channels is not easily understood from the molecular model, nor is the unusual effect of disinhibition.

In summary, some of the human $Na_V1.8$ channel S6 segment residues involved in the resting and inactivating state block by tetracaine and A-803467 have been identified. Residues I381, L1410, F1710, and Y1717 are involved in the action of tetracaine while only L1410 and F1710 were found to be involved in the action of A-803467, indicating differing but partially overlapping areas of binding within the pore. For tetracaine, mutation F1710A gave a greater percentage reduction in the inactivated state compared to the resting state affinity, while compound A-803467 gave similar percent reductions, suggesting that residue F1710 does not underlie the preference of compound A-803467 for the inactivated state. For both tetracaine and A-803467, mutation L1410A showed a striking increase in the affinity for the resting channel, and depolarisation was found to cause a "disinhibition" of channel current, supporting the idea that disinhibition is the removal of resting block. Furthermore, all mutations studied increased the extent of disinhibition of A-803467, some also caused the disinhibition of tetracaine. Overall it is surprising that compound A-803467 is selective for $Na_V1.8$, since alignment with other human voltage-gated Na^+ channel subtype protein sequences (Fig. 7.12) show that the S6 residues implicated in drug binding (whether by the mutational study or by modelling) are almost completely conserved between different voltage-gated Na^+ channel subtypes.

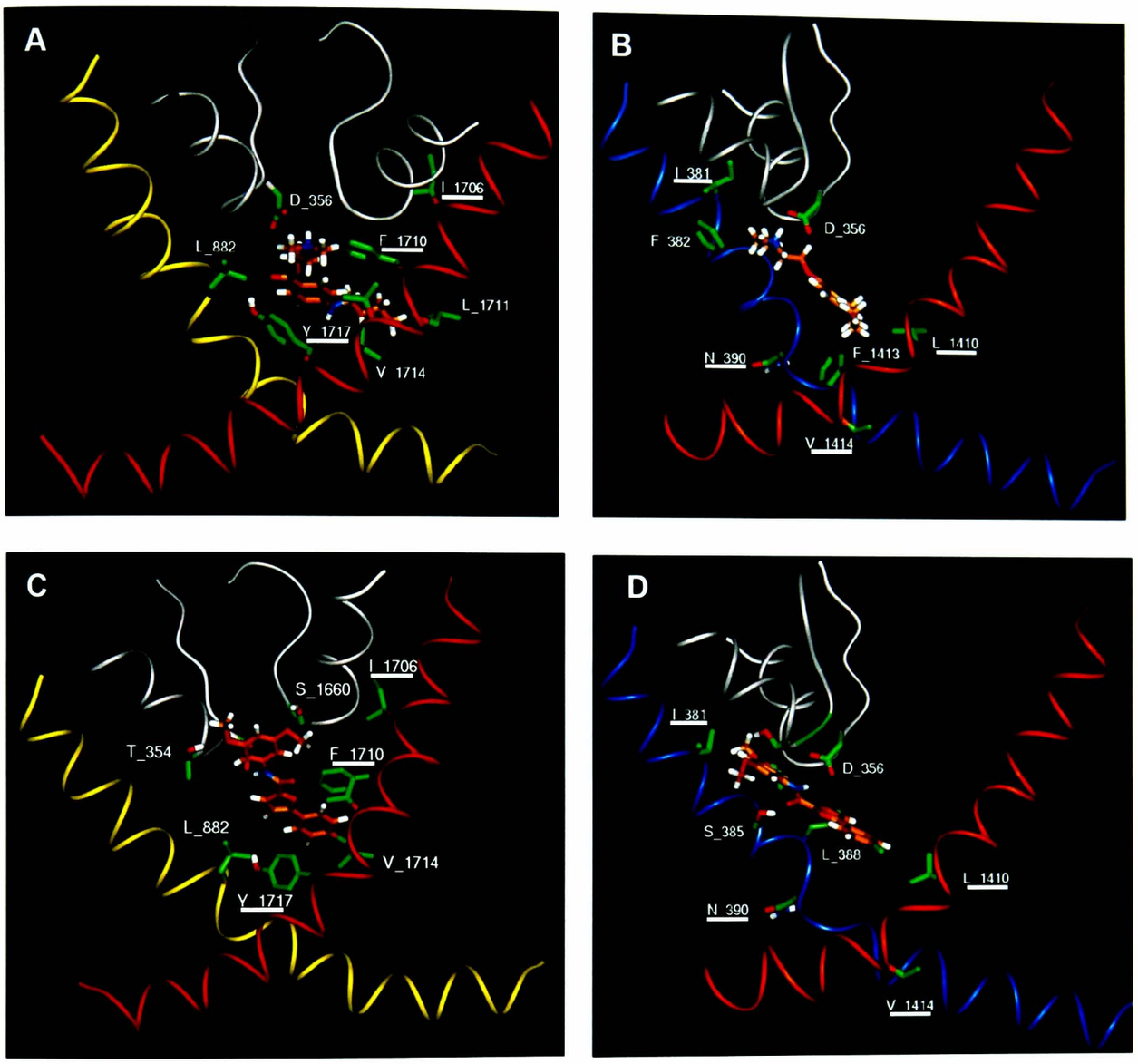

Fig. 7.11. Docking of tetracaine and A-803467 in the human $Na_V1.8$ channel model. The figures show P-loops for domains I and IV and S6 helices for all four domains. The alpha carbon ribbons are for pore loops (*grey*), IS6 (*blue*), IIS6 (*yellow),* IIIS6 (*orange*), IVS6 (*red*). The residues underlined were mutated. **A)** The figure shows docking of tetracaine to IIS6, IVS6 and P-loops, with π-π stacking with F1710 (IVS6) and Y1717 (in IVS6), while the latter residue also forms a hydrogen bond with tetracaine. Tetracaine also made hydrophobic interactions with L882 (IIS6) and L1711 (IVS6). **B)** Docking is shown for tetracaine to IS6, IIIS6 and P-loops, with a salt bridge between D356 (P-loop) and the protonated amino group of tetracaine. The amino-methyl groups of tetracaine has hydrophobic interactions with I381 (IS6) and F382 (IS6), and the butyl group also interacting hydrophobically with L1410 (IIIS6) and F1413 (IIIS6). **C)** Docking of A-803467 is shown to IIS6, IVS6 and P-loops, with π-π stacking F1710 (IVS6) and with hydrogen bonding T354 and S1660 (P-loop). Compound A-803467 also made hydrophobic interaction with L882 (IIS6) and V1714 (IVS6). **D)** Docking is shown for A-803467 to IS6, IIIS6 and P-loops, with D356 (P-loop) and L1410 (IIIS6) in the proximity of the chlorophenyl ring of the compound. Compound A-803467 also hydrogen bonds with S385 (IS6). Residues N390 (IS6) and V1414 (IIIS6) do not interact with either compound. This work was carried out by Frank Blaney (GlaxoSmithKline, Harlow).

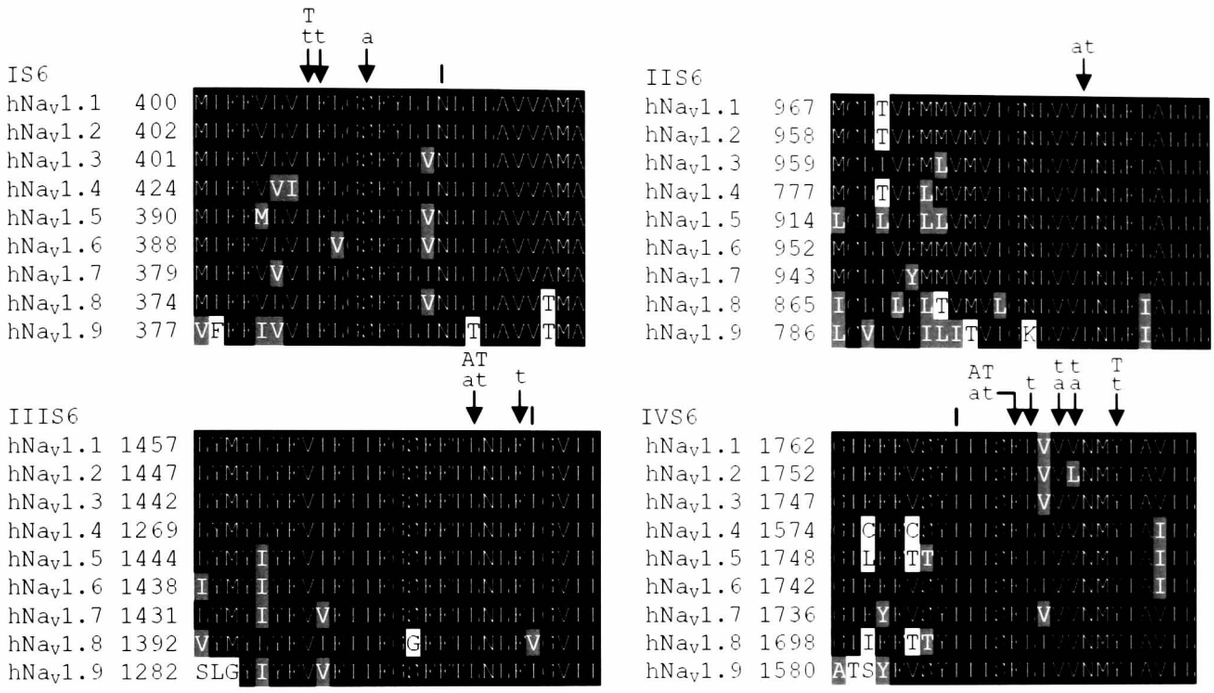

Fig. 7.12. Amino acid sequence similarity between human Na_V channel S6 segments from domains I-IV with structural determinants of drug action indicated. The residues shown to be involved for the affinity of tetracaine (*T*) and A-803467 (*A*) using mutagenesis, or tetracaine (*t*) and A-803467 (*a*) using computational modelling are shown. Residues indicated (I) were mutated but did not alter the affinity of either test compound, and were not involved in interactions in the molecular model. Sequences were aligned using ClustalW and visualised using BoxShade.

7.4 Future work

In this thesis, wild type and mutant $Na_V1.8$ sodium channels were expressed in mammalian sensory neuron-derived ND7/23 cells and the functional properties and drug binding sites were studied using whole-cell patch clamp.

In chapter 4, the functional properties were shown to be different between wild type human and rat $Na_V1.8$ channels. To study the difference between the two $Na_V1.8$ channels further, electrophysiological recordings could be made from adult human and rat dorsal root ganglion cells, and from human and rat $Na_V1.8$ channels expressed in different mammalian cell lines. The generation of human and rat $Na_V1.8$ channel chimeras and eventually point mutations could be used to study the molecular determinants responsible for the different functional properties between these two channels.

In chapter 5, the action of various drugs on wild type human and rat $Na_V1.8$ channels were studied and potent compounds V102862 and A-803467 showed a novel "disinhibition" during recovery from inactivation. The mechanism underlying this effect may be understood further by recording from single channels.

In chapter 6, the functional properties of human and rat $Na_V1.8$ channels were altered by alanine mutations in the S6 segments. By substituting these residues for residues with different properties (size, hydrophobicity, aromaticity and charge) it should be possible to determine the role of the native amino acid residue side chain. It was proposed here that the two residues (N390 and V1414) stabilise the activated state by interating with other residues in other transmembrane segments; mutation the binding partners might determine whether this is the case.

In chapter 7, some of the pore-lining S6 segment mutations were shown to reduce the sensitivity of the human $Na_V1.8$ channel to tetracaine and compound A-803467, suggesting that both drugs act on a differing but partially overlapping area within the pore. The selectivity of A-803467 for the $Na_V1.8$ channel over other voltage-gated Na^+ channel subtypes is therefore surprising since the pore lining S6 residues are well conserved. It would be relatively easy to substitute all of the $Na_V1.8$ channel S6 segment residues to the $Na_V1.2$ channel S6 segment residues to assertain whether selectivity of compound A-803467 is determined by the S6 segements. For mutation L1410A both compounds caused complete resting block at very low concentrations; block was disinhibited after depolarisation. Mutation of the L1410 residue to residues with different properties might explain the greatly increased resting state binding affinity shown with mutation L1410A. Furthermore, single channel recording of mutation L1410A might also provide a better understanding of the disinhibition effect.

REFERENCES

Abrahamsen, B., Zhao, J., Asante, C. O., Cendan, C. M., Marsh, S., Martinez-Barbara, J. P., Nassar, M. A., Dickenson, A. H., Wood, J. N. (2008). The cell and molecular basis of mechanical, cold, and inflammatory pain. *Science* **321**, 702-705.

Ahern, C. A., Eastwood, A. L., Dougherty, D. A., Horn, R. (2008). Electrostatic contributions of aromatic residues in the local anesthetic receptor of voltage-gated sodium channels. *Circ Res* **102**, 86-94.

Ahmad, S., Dahllund, L., Eriksson, A. B., Hellgren, D., Karlsson, U., Lund, P. E., Meijer, I. A., Meury, L., Mills, T., Moody, A., Morinville, A., Morten, J., O'Donnell, D., Raynoschek, C., Salter, H., Rouleau, G. A., Krupp, J. J. (2007). A stop codon mutation in SCN9A causes lack of pain sensation. *Hum Mol Genet* **16**, 2114-2121.

Akiba, I., Seki, T., Mori, M., Iizuka, M., Nishimura, S., Sasaki, S., Imoto, K., Barsoumian, E. L. (2003). Stable expression and characterization of human PN1 and PN3 sodium channels. *Receptors Channels* **9**, 291-299.

Akopian, A. N., Sivilotti, L., Wood, J. N. (1996). A tetrodotoxin-resistant voltage-gated sodium channel expressed by sensory neurons. *Nature* **379**, 257-262.

Akopian, A. N., Souslova, V., England, S., Okuse, K., Ogata, N., Ure, J., Smith, A., Kerr, B. J., McMahon, S. B., Boyce, S., Hill, R., Stanfa, L. C., Dickenson, A. H., Wood, J. N. (1999). The tetrodotoxin-resistant sodium channel SNS has a specialized function in pain pathways. *Nat Neurosci* **2**, 541-548.

Armstrong, C. M. (1981). Sodium channels and gating currents. *Physiol Rev* **61**, 644-683.

Armstrong, C. M., Bezanilla, F., Rojas, E. (1973). Destruction of sodium conductance inactivation in squid axons perfused with pronase. *J Gen Physiol* **62**, 375-391.

Bai, C. X., Glaaser, I. W., Sawanobori, T., Sunami, A. (2003). Involvement of local anesthetic binding sites on IVS6 of sodium channels in fast and slow inactivation. *Neurosci Lett* **337**, 41-45.

Beacham, D., Ahn, M., Catterall, W. A., Scheuer, T. (2007). Sites and molecular mechanisms of modulation of $Na_V1.2$ channels by Fyn tyrosine kinase. *J Neurosci* **27**, 11543-11551.

Bennett, P. B., Valenzuela, C., Chen L. Q., Kallen R. G. (1995a). On the molecular nature of the lidocaine receptor of cardiac Na^+ channels. Modification of block by alterations in the alpha-subunit III-IV interdomain. *Circ Res* **77**, 584-92.

Bennett, P. B., Yazawa, K., Makita, N., George, A. L., Jr. (1995b). Molecular mechanism for an inherited cardiac arrhythmia. *Nature* **376**, 683-685.

Blair, N. T., Bean, B. P. (2002). Roles of tetrodotoxin (TTX)-sensitive Na^+ current, TTX-resistant Na^+ current, and Ca^{2+} current in the action potentials of nociceptive sensory neurons. *J Neurosci* **22**, 10277-10290.

Blair, N. T., Bean, B. P. (2003). Role of tetrodotoxin-resistant Na^+ current slow inactivation in adaptation of action potential firing in small-diameter dorsal root ganglion neurons. *J Neurosci* **23**, 10338-10350.

Bruhova, I., Tikhonov, D. B., Zhorov, B. S. (2008). Access and binding of local anesthetics in the closed sodium channel. *Mol Pharmacol* **74**, 1033-1045.

Cahalan, M. D., Almers, W. (1979). Block of sodium conductance and gating current in squid giant axons poisoned with quaternary strychnine. *Biophys J* **27**, 57-73.

Campos, F. V., Coronas, F. I., Beirao, P. S. (2004). Voltage-dependent displacement of the scorpion toxin Ts3 from sodium channels and its implication on the control of inactivation. *Br J Pharmacol* **142**, 1115-1122.

Cantrell, A. R., Tibbs, V. C., Yu, F. H., Murphy, B. J., Sharp, E. M., Qu, Y., Catterall, W. A., Scheuer, T. (2002). Molecular mechanism of convergent regulation of brain Na^+ channels by protein kinase C and protein kinase A anchored to AKAP-15. *Mol Cell Neurosci* **21**, 63-80.

Carboni, M., Zhang, Z. S., Neplioueva, V., Starmer, C. F., Grant, A. O. (2005). Slow sodium channel inactivation and use-dependent block modulated by the same domain IV S6 residue. *J Membr Biol* **207**, 107-117.

Cardenas, C. A., Cardenas, C. G., de Armendi, A. J., Scroggs, R. S. (2006). Carbamazepine interacts with a slow inactivation state of $Na_V1.8$-like sodium channels. *Neurosci Lett* **408**, 129-134.

Carter, A. J., Grauert, M., Pschorn, U., Bechtel, W. D., Bartmann-Lindholm, C., Qu, Y., Scheuer, T., Catterall, W. A., Weiser, T. (2000). Potent blockade of sodium channels and protection of brain tissue from ischemia by BIII 890 CL. *Proc Natl Acad Sci U S A* **97**, 4944-4949.

Casula, M. A., Facer, P., Powell, A. J., Kinghorn, I. J., Plumpton, C., Tate, S. N., Bountra, C., Birch, R., Anand, P. (2004). Expression of the sodium channel beta3 subunit in injured human sensory neurons. *Neuroreport* **15**, 1629-1632.

Catterall, W. A. (1992). Cellular and molecular biology of voltage-gated sodium channels. *Physiol Rev* **72**, S15-48.

Catterall, W. A. (2000). From ionic currents to molecular mechanisms: the structure and function of voltage-gated sodium channels. *Neuron* **26**, 13-25.

Catterall, W. A. (2002). Molecular mechanisms of gating and drug block of sodium channels. *Novartis Found Symp* **241**, 206-218; discussion 218-232.

Catterall, W. A., Goldin, A. L., Waxman, S. G. (2005). International Union of Pharmacology. XLVII. Nomenclature and structure-function relationships of voltage-gated sodium channels. *Pharmacol Rev* **57**, 397-409.

Chahine, M., Ziane, R., Vijayaragavan, K., Okamura, Y. (2005). Regulation of Na_V channels in sensory neurons. *Trends Pharmacol Sci* **26**, 496-502.

Chanda, B., Bezanilla, F. (2002). Tracking voltage-dependent conformational changes in skeletal muscle sodium channel during activation. *J Gen Physiol* **120**, 629-645.

Chen, J., Seebohm, G., Sanguinetti, M. C. (2002). Position of aromatic residues in the S6 domain, not inactivation, dictates cisapride sensitivity of HERG and eag potassium channels. *Proc Natl Acad Sci U S A* **99**, 12461-12466.

Chen, Q., Kirsch, G. E., Zhang, D., Brugada, R., Brugada, J., Brugada, P., Potenza, D., Moya, A., Borggrefe, M., Breithardt, G., Ortiz-Lopez, R., Wang, Z., Antzelevitch, C., O'Brien, R. E., Schulze-Bahr, E., Keating, M. T., Towbin, J. A., Wang, Q. (1998). Genetic basis and molecular mechanism for idiopathic ventricular fibrillation. *Nature* **392**, 293-296.

Choi, J. S., Hudmon, A., Waxman, S. G., Dib-Hajj, S. D. (2006). Calmodulin regulates current density and frequency-dependent inhibition of sodium channel $Na_V1.8$ in DRG neurons. *J Neurophysiol* **96**, 97-108.

Choi, J. S., Tyrrell, L., Waxman, S. G., Dib-Hajj, S. D. (2004). Functional role of the C-terminus of voltage-gated sodium channel $Na_V1.8$. *FEBS Lett* **572**, 256-260.

Clare, J. J., Tate, S. N., Nobbs, M., Romanos, M. A. (2000). Voltage-gated sodium channels as therapeutic targets. *Drug Discov Today* **5**, 506-520.

Condreay, J. P., Witherspoon, S. M., Clay, W. C., Kost, T. A. (1999). Transient and stable gene expression in mammalian cells transduced with a recombinant baculovirus vector. *Proc Natl Acad Sci U S A* **96**, 127-132.

Cox, J. J., Reimann, F., Nicholas, A. K., Thornton, G., Roberts, E., Springell, K., Karbani, G., Jafri, H., Mannan, J., Raashid, Y., Al-Gazali, L., Hamamy, H., Valente, E. M., Gorman, S., Williams, R., McHale, D. P., Wood, J. N., Gribble, F. M., Woods, C. G. (2006). An SCN9A channelopathy causes congenital inability to experience pain. *Nature* **444**, 894-898.

Cummins, T. R., Dib-Hajj, S. D., Black, J. A., Akopian, A. N., Wood, J. N., Waxman, S. G. (1999). A novel persistent tetrodotoxin-resistant sodium current in SNS-null and wild-type small primary sensory neurons. *J Neurosci* **19**, RC43.

Cummins, T. R., Rush, A. M. (2007). Voltage-gated sodium channel blockers for the treatment of neuropathic pain. *Expert Rev Neurother* **7**, 1597-1612.

Cummins, T. R., Waxman, S. G. (1997). Downregulation of tetrodotoxin-resistant sodium currents and upregulation of a rapidly repriming tetrodotoxin-sensitive sodium current in small spinal sensory neurons after nerve injury. *J Neurosci* **17**, 3503-3514.

Cusdin, F.S., Clare, J.J., Jackson, A.P. (2008) Trafficking and cellular distribution of voltage-gated sodium channels. *Traffic* **9**, 17-26.

De Col, R., Messlinger, K., Carr, R. W. (2008). Conduction velocity is regulated by sodium channel inactivation in unmyelinated axons innervating the rat cranial meninges. *J Physiol* **586**, 1089-1103.

Dekker, L. V., Daniels, Z., Hick, C., Elsegood, K., Bowden, S., Szestak, T., Burley, J. R., Southan, A., Cronk, D., James, I. F. (2005). Analysis of human $Na_V1.8$ expressed in SH-SY5Y neuroblastoma cells. *Eur J Pharmacol* **528**, 52-58.

Dib-Hajj S. D., Ishikawa K., Cummins T. R., Waxman S. G. (1997). Insertion of a SNS-specific tetrapeptide in S3-S4 linker of D4 accelerates recovery from inactivation of skeletal muscle voltage-gated Na channel mu1 in HEK293 cells. *FEBS Lett* **416**, 11-14.

Dib-Hajj, S. D., Tyrrell, L., Black, J. A., Waxman, S. G. (1998). NaN, a novel voltage-gated Na channel, is expressed preferentially in peripheral sensory neurons and down-regulated after axotomy. *Proc Natl Acad Sci U S A* **95**, 8963-8968.

Dong, X. W., Goregoaker, S., Engler, H., Zhou, X., Mark, L., Crona, J., Terry, R., Hunter, J., Priestley, T. (2007). Small interfering RNA-mediated selective knockdown of $Na_V1.8$ tetrodotoxin-resistant sodium channel reverses mechanical allodynia in neuropathic rats. *Neuroscience* **146**, 812-821.

Doyle, D. A., Morais Cabral, J., Pfuetzner, R. A., Kuo, A., Gulbis, J. M., Cohen, S. L., Chait, B. T., MacKinnon, R. (1998). The structure of the potassium channel: molecular basis of K^+ conduction and selectivity. *Science* **280**, 69-77.

Dudley, S. C., Jr., Chang, N., Hall, J., Lipkind, G., Fozzard, H. A., French, R. J. (2000). mu-conotoxin GIIIA interactions with the voltage-gated Na^+ channel predict a clockwise arrangement of the domains. *J Gen Physiol* **116**, 679-690.

Eaholtz, G., Scheuer, T., Catterall, W. A. (1994). Restoration of inactivation and block of open sodium channels by an inactivation gate peptide. *Neuron* **12**, 1041-1048.

Ekberg, J., Jayamanne, A., Vaughan, C. W., Aslan, S., Thomas, L., Mould, J., Drinkwater, R., Baker, M. D., Abrahamsen, B., Wood, J. N., Adams, D. J., Christie, M. J., Lewis, R. J. (2006). muO-conotoxin MrVIB selectively blocks $Na_V1.8$ sensory neuron specific sodium channels and chronic pain behavior without motor deficits. *Proc Natl Acad Sci U S A* **103**, 17030-17035.

Elliott, A. A., Elliott, J. R., 1993. Characterization of TTX-sensitive and TTX-resistant sodium currents in small cells from adult rat dorsal root ganglia. *J Physiol* **463**, 39-56.

Errington, A. C., Stohr, T., Heers, C., Lees, G. (2008). The investigational anticonvulsant lacosamide selectively enhances slow inactivation of voltage-gated sodium channels. *Mol Pharmacol* **73**, 157-169.

Escayg, A., MacDonald, B. T., Meisler, M. H., Baulac, S., Huberfeld, G., An-Gourfinkel, I., Brice, A., LeGuern, E., Moulard, B., Chaigne, D., Buresi, C., Malafosse, A. (2000). Mutations of SCN1A, encoding a neuronal sodium channel, in two families with GEFS+2. *Nat Genet* **24**, 343-345.

Favre, I., Moczydlowski, E., Schild, L. (1996). On the structural basis for ionic selectivity among Na^+, K^+, and Ca^{2+} in the voltage-gated sodium channel. *Biophys J* **71**, 3110-3125.

Fitzgerald, E. M., Okuse, K., Wood, J. N., Dolphin, A. C., Moss, S. J. (1999). cAMP-dependent phosphorylation of the tetrodotoxin-resistant voltage-dependent sodium channel SNS. *J Physiol* **516 (Pt 2)**, 433-446.

Foulkes, T., Nassar, M. A., Lane, T., Matthews, E. A., Baker, M. D., Gerke, V., Okuse, K., Dickenson, A. H., Wood, J. N. (2006). Deletion of annexin 2 light chain p11 in nociceptors causes deficits in somatosensory coding and pain behavior. *J Neurosci* **26**, 10499-10507.

Fozzard, H. A., Hanck, D. A. (1996). Structure and function of voltage-dependent sodium channels: comparison of brain II and cardiac isoforms. *Physiol Rev* **76**, 887-926.

Fraceto, L. F., Oyama, S., Jr., Nakaie, C. R., Spisni, A., de Paula, E., Pertinhez, T. A. (2006). Interaction of local anesthetics with a peptide encompassing the IV/S4-S5 linker of the Na^+ channel. *Biophys Chem* **123**, 29-39.

Frazier, D. T., Narahashi, T., Yamada, M. (1970). The site of action and active form of local anesthetics. II. Experiments with quaternary compounds. *J Pharmacol Exp Ther* **171**, 45-51.

Fujiwara, T., Sugawara, T., Mazaki-Miyazaki, E., Takahashi, Y., Fukushima, K., Watanabe, M., Hara, K., Morikawa, T., Yagi, K., Yamakawa, K., Inoue, Y. (2003). Mutations of sodium channel alpha subunit type 1 (SCN1A) in intractable childhood epilepsies with frequent generalized tonic-clonic seizures. *Brain* **126**, 531-546.

Gauthereau, M. Y., Salinas-Stefanon, E. M., Cruz, S. L. (2005). A mutation in the local anaesthetic binding site abolishes toluene effects in sodium channels. *Eur J Pharmacol* **528**, 17-26.

Gold, M. S., Weinreich, D., Kim, C. S., Wang, R., Treanor, J., Porreca, F., Lai, J. (2003). Redistribution of $Na_V1.8$ in uninjured axons enables neuropathic pain. *J Neurosci* **23**, 158-166.

Goldberg, Y. P., MacFarlane, J., MacDonald, M. L., Thompson, J., Dube, M. P., Mattice, M., Fraser, R., Young, C., Hossain, S., Pape, T., Payne, B., Radomski, C., Donaldson, G., Ives, E., Cox, J., Younghusband, H. B., Green, R., Duff, A., Boltshauser, E., Grinspan, G. A., Dimon, J. H., Sibley, B. G., Andria, G., Toscano, E., Kerdraon, J., Bowsher, D., Pimstone, S. N., Samuels, M. E., Sherrington, R., Hayden, M. R. (2007). Loss-of-function mutations in the $Na_V1.7$ gene underlie congenital indifference to pain in multiple human populations. *Clin Genet* **71**, 311-319.

Goldin, A. L. (2002). Evolution of voltage-gated Na^+ channels. *J Exp Biol* **205**, 575-584.

Goldin, A. L., Barchi, R. L., Caldwell, J. H., Hofmann, F., Howe, J. R., Hunter, J. C., Kallen, R. G., Mandel, G., Meisler, M. H., Netter, Y. B., Noda, M., Tamkun, M. M., Waxman, S. G., Wood, J. N., Catterall, W. A. (2000). Nomenclature of voltage-gated sodium channels. *Neuron* **28**, 365-368.

Grant, A. O., Chandra, R., Keller, C., Carboni, M., Starmer, C. F. (2000). Block of wild-type and inactivation-deficient cardiac sodium channels IFM/QQQ stably expressed in mammalian cells. *Biophys J* **79**, 3019-3035.

Grant, A. O., John, J. E., Nesterenko, V. V., Starmer, C. F., Moorman, J. R. (1996). The role of inactivation in open-channel block of the sodium channel: studies with inactivation-deficient mutant channels. *Mol Pharmacol* **50**, 1643-1650.

Haeseler, G., Bufler, J., Merken, S., Dengler, R., Aronson, J., Leuwer, M. (2002). Block of voltage-operated sodium channels by 2,6-dimethylphenol, a structural analogue of lidocaine's aromatic tail. *Br J Pharmacol* **137**, 285-293.

Harty, P. T., Waxman, S. G. (2007). Inactivation properties of sodium channel $Na_V1.8$ maintain action potential amplitude in small DRG neurons in the context of depolarization. *Mol Pain* **3**, 12.

Heinemann, S. H., Terlau, H., Stuhmer, W., Imoto, K., Numa, S. (1992). Calcium channel characteristics conferred on the sodium channel by single mutations. *Nature* **356**, 441-443.

Hille, B. (1967). The selective inhibition of delayed potassium currents in nerve by tetraethylammonium ion. *J Gen Physiol* **50**, 1287-1302.

Hille, B. (1971). The permeability of the sodium channel to organic cations in myelinated nerve. *J Gen Physiol* **58**, 599-619.

Hille, B. (1977). Local anesthetics: hydrophilic and hydrophobic pathways for the drug-receptor reaction. *J Gen Physiol* **69**, 497-515.

Hille, B. (2001). Ionic channels of excitable membranes. *Sinauer*, Sunderland, MA.

Hockerman, G. H., Peterson, B. Z., Sharp, E., Tanada, T. N., Scheuer, T., Catterall, W. A. (1997). Construction of a high-affinity receptor site for dihydropyridine agonists and antagonists by single amino acid substitutions in a non-L-type Ca^{2+} channel. *Proc Natl Acad Sci U S A* **94**, 14906-14911.

Hodgkin, A. L., Huxley, A. F. (1952). A quantitative description of membrane current and its application to conduction and excitation in nerve. *J Physiol* **117**, 500-544.

Hondeghem, L. M., Katzung, B. G. (1977). Time- and voltage-dependent interactions of antiarrhythmic drugs with cardiac sodium channels. *Biochim Biophys Acta* **472**, 373-398.

Horn, R., Ding, S., Gruber, H. J. (2000). Immobilizing the moving parts of voltage-gated ion channels. *J Gen Physiol* **116**, 461-476.

Hudmon, A., Choi, J. S., Tyrrell, L., Black, J. A., Rush, A. M., Waxman, S. G., Dib-Hajj, S. D. (2008). Phosphorylation of sodium channel $Na_V1.8$ by p38 mitogen-activated protein kinase increases current density in dorsal root ganglion neurons. *J Neurosci* **28**, 3190-3201.

Ilyin, V. I., Hodges, D. D., Whittemore, E. R., Carter, R. B., Cai, S. X., Woodward, R. M. (2005). V102862 (Co 102862): a potent, broad-spectrum state-dependent blocker of mammalian voltage-gated sodium channels. *Br J Pharmacol* **144**, 801-812.

Isom, L. L. (2001). Sodium channel beta subunits: anything but auxiliary. *Neuroscientist* **7**, 42-54.

Isom, L. L. (2002). The role of sodium channels in cell adhesion. *Front Biosci* **7**, 12-23.

Isom, L. L., Catterall, W. A. (1996). Na^+ channel subunits and Ig domains. *Nature* **383**, 307-308.

Isom, L. L., De Jongh, K. S., Patton, D. E., Reber, B. F., Offord, J., Charbonneau, H., Walsh, K., Goldin, A. L., Catterall, W. A. (1992). Primary structure and functional expression of the beta 1 subunit of the rat brain sodium channel. *Science* **256**, 839-842.

Isom, L. L., Ragsdale, D. S., De Jongh, K. S., Westenbroek, R. E., Reber, B. F., Scheuer, T., Catterall, W. A. (1995a). Structure and function of the beta 2 subunit of brain sodium channels, a transmembrane glycoprotein with a CAM motif. *Cell* **83**, 433-442.

Isom, L. L., Scheuer, T., Brownstein, A. B., Ragsdale, D. S., Murphy, B. J., Catterall, W. A., (1995b). Functional co-expression of the beta 1 and type IIA alpha subunits of sodium channels in a mammalian cell line. *J Biol Chem* **270**, 3306-3312.

Jarvis, M. F., Honore, P., Shieh, C. C., Chapman, M., Joshi, S., Zhang, X. F., Kort, M., Carroll, W., Marron, B., Atkinson, R., Thomas, J., Liu, D., Krambis, M., Liu, Y., McGaraughty, S., Chu, K., Roeloffs, R., Zhong, C., Mikusa, J. P., Hernandez, G., Gauvin, D., Wade, C., Zhu, C., Pai, M., Scanio, M., Shi, L., Drizin, I., Gregg, R., Matulenko, M., Hakeem, A., Gross, M., Johnson, M., Marsh, K., Wagoner, P. K., Sullivan, J. P., Faltynek, C. R., Krafte, D. S. (2007). A-803467, a potent and selective $Na_V1.8$ sodium channel blocker, attenuates neuropathic and inflammatory pain in the rat. *Proc Natl Acad Sci U S A* **104**, 8520-8525.

Jeftinija, S. (1994). The role of tetrodotoxin-resistant sodium channels of small primary afferent fibers. *Brain Res* **639**, 125-134.

Jiang, Y., Lee, A., Chen, J., Cadene, M., Chait, B. T., MacKinnon, R. (2002). The open pore conformation of potassium channels. *Nature* **417**, 523-526.

John, V. H., Main, M. J., Powell, A. J., Gladwell, Z. M., Hick, C., Sidhu, H. S., Clare, J. J., Tate, S., Trezise, D. J. (2004). Heterologous expression and functional analysis of rat $Na_V1.8$

(SNS) voltage-gated sodium channels in the dorsal root ganglion neuroblastoma cell line ND7-23. *Neuropharmacology* **46**, 425-438.

Joshi, S. K., Mikusa, J. P., Hernandez, G., Baker, S., Shieh, C. C., Neelands, T., Zhang, X. F., Niforatos, W., Kage, K., Han, P., Krafte, D., Faltynek, C., Sullivan, J. P., Jarvis, M. F., Honore, P. (2006). Involvement of the TTX-resistant sodium channel $Na_V1.8$ in inflammatory and neuropathic, but not post-operative, pain states. *Pain* **123**, 75-82.

Kajander, K. C., Bennett, G. J. (1992). Onset of a painful peripheral neuropathy in rat: a partial and differential deafferentation and spontaneous discharge in A beta and A delta primary afferent neurons. *J Neurophysiol* **68**, 734-744.

Kamiya, K., Kaneda, M., Sugawara, T., Mazaki, E., Okamura, N., Montal, M., Makita, N., Tanaka, M., Fukushima, K., Fujiwara, T., Inoue, Y., Yamakawa, K. (2004). A nonsense mutation of the sodium channel gene SCN2A in a patient with intractable epilepsy and mental decline. *J Neurosci* **24**, 2690-2698.

Kazen-Gillespie, K. A., Ragsdale, D. S., D'Andrea, M. R., Mattei, L. N., Rogers, K. E., Isom, L. L. (2000). Cloning, localization, and functional expression of sodium channel beta1A subunits. *J Biol Chem* **275**, 1079-1088.

Kearney, J. A., Plummer, N. W., Smith, M. R., Kapur, J., Cummins, T. R., Waxman, S. G., Goldin, A. L., Meisler, M. H. (2001). A gain-of-function mutation in the sodium channel gene Scn2a results in seizures and behavioral abnormalities. *Neuroscience* **102**, 307-317.

Kerr, B. J., Souslova, V., McMahon, S. B., Wood, J. N. (2001). A role for the TTX-resistant sodium channel $Na_V1.8$ in NGF-induced hyperalgesia, but not neuropathic pain. *Neuroreport* **12**, 3077-3080.

Kimura, T., Kinoshita, E., Yamaoka, K., Yuki, T., Yakehiro, M., Seyama, I. (2000). On site of action of grayanotoxin in domain 4 segment 6 of rat skeletal muscle sodium channel. *FEBS Lett* **465**, 18-22.

Kondratiev, A., Tomaselli, G. F. (2003). Altered gating and local anesthetic block mediated by residues in the I-S6 and II-S6 transmembrane segments of voltage-dependent Na^+ channels. *Mol Pharmacol* **64**, 741-752.

Krieg, P. A., Melton, D. A. (1984). Functional messenger RNAs are produced by SP6 in vitro transcription of cloned cDNAs. *Nucleic Acids Res* **12**, 7057-7070

Kuo, C. C. (1998). A common anticonvulsant binding site for phenytoin, carbamazepine, and lamotrigine in neuronal Na^+ channels. *Mol Pharmacol* **54**, 712-721.

Kuo, C. C., Bean, B. P. (1994). Slow binding of phenytoin to inactivated sodium channels in rat hippocampal neurons. *Mol Pharmacol* **46**, 716-725.

Lai, J., Gold, M. S., Kim, C. S., Bian, D., Ossipov, M. H., Hunter, J. C., Porreca, F. (2002). Inhibition of neuropathic pain by decreased expression of the tetrodotoxin-resistant sodium channel, $Na_V1.8$. *Pain* **95**, 143-152.

Laird, J. M., Souslova, V., Wood, J. N., Cervero, F. (2002). Deficits in visceral pain and referred hyperalgesia in $Na_V1.8$ (SNS/PN3)-null mice. *J Neurosci* **22**, 8352-8356.

Leffler, A., Reiprich, A., Mohapatra, D. P., Nau, C. (2007). Use-dependent block by lidocaine but not amitriptyline is more pronounced in tetrodotoxin (TTX)-Resistant $Na_V1.8$ than in TTX-sensitive Na^+ channels. *J Pharmacol Exp Ther* **320**, 354-364.

Li, H. L., Galue, A., Meadows, L., Ragsdale, D. S. (1999). A molecular basis for the different local anesthetic affinities of resting versus open and inactivated states of the sodium channel. *Mol Pharmacol* **55**, 134-141.

Lipkind, G. M., Fozzard, H. A. (2005). Molecular modeling of local anesthetic drug binding by voltage-gated sodium channels. *Mol Pharmacol* **68**, 1611-1622.

Lipkind, G. M., Fozzard, H. A. (2008). Voltage-gated Na channel selectivity: the role of the conserved domain III lysine residue. *J Gen Physiol* **131**, 523-529.

Liu, G., Yarov-Yarovoy, V., Nobbs, M., Clare, J. J., Scheuer, T., Catterall, W. A. (2003). Differential interactions of lamotrigine and related drugs with transmembrane segment IVS6 of voltage-gated sodium channels. *Neuropharmacology* **44**, 413-422.

Long, S. B., Campbell, E. B., Mackinnon, R. (2005). Crystal structure of a mammalian voltage-dependent Shaker family K^+ channel. *Science* **309**, 897-903.

Lou, B. S., Lin, T. H., Lo, C. Z. (2005). The interactions of phenytoin and its binding site in DI-S6 segment of Na^+ channel voltage-gated peptide by NMR spectroscopy and molecular modeling study. *J Pept Res* **66**, 27-38.

Malik-Hall, M., Poon, W. Y., Baker, M. D., Wood, J. N., Okuse, K. (2003). Sensory neuron proteins interact with the intracellular domains of sodium channel $Na_V1.8$. *Brain Res Mol Brain Res* **110**, 298-304.

McClatchey, A. I., Van den Bergh, P., Pericak-Vance, M. A., Raskind, W., Verellen, C., McKenna-Yasek, D., Rao, K., Haines, J. L., Bird, T., Brown, R. H., Jr., et al. (1992). Temperature-sensitive mutations in the III-IV cytoplasmic loop region of the skeletal muscle sodium channel gene in paramyotonia congenita. *Cell* **68**, 769-774.

McNulty, M. M., Edgerton, G. B., Shah, R. D., Hanck, D. A., Fozzard, H. A., Lipkind, G. M. (2007). Charge at the lidocaine binding site residue Phe-1759 affects permeation in human cardiac voltage-gated sodium channels. *J Physiol* **581**, 741-755.

McPhee, J. C., Ragsdale, D. S., Scheuer, T., Catterall, W. A. (1995). A critical role for transmembrane segment IVS6 of the sodium channel alpha subunit in fast inactivation. *J Biol Chem* **270**, 12025-12034.

Morgan, K., Stevens, E. B., Shah, B., Cox, P. J., Dixon, A. K., Lee, K., Pinnock, R. D., Hughes, J., Richardson, P. J., Mizuguchi, K., Jackson, A. P. (2000). beta 3: an additional auxiliary subunit of the voltage-sensitive sodium channel that modulates channel gating with distinct kinetics. *Proc Natl Acad Sci U S A* **97**, 2308-2313.

Murphy, B. J., Catterall, W. A. (1992). Phosphorylation of purified rat brain Na^+ channel reconstituted into phospholipid vesicles by protein kinase C. *J Biol Chem* **267**, 16129-16134.

Narahashi, T. (1974). Chemicals as tools in the study of excitable membranes. *Physiol Rev* **54**, 813-889.

Narahashi, T. (1998). Ion Channel Pharmacology. *Oxford University Press*, Oxford.

Nassar, M. A., Levato, A., Stirling, L. C., Wood, J. N. (2005). Neuropathic pain develops normally in mice lacking both $Na_V1.7$ and $Na_V1.8$. *Mol Pain* **1**, 24.

Nau, C., Wang, G. K. (2004). Interactions of local anesthetics with voltage-gated Na^+ channels. *J Membr Biol* **201**, 1-8.

Nau, C., Wang, S. Y., Strichartz, G. R., Wang, G. K. (1999). Point mutations at N434 in D1-S6 of mu1 Na^+ channels modulate binding affinity and stereoselectivity of local anesthetic enantiomers. *Mol Pharmacol* **56**, 404-413.

Nau, C., Seaver, M., Wang, S. Y., Wang, G. K. (2000). Block of human heart hH1 sodium channels by amitriptyline. *J Pharmacol Exp Ther* **292**,1015-1023.

Nau, C., Wang, S. Y., Strichartz, G. R., Wang, G. K. (2000). Block of human heart hH1 sodium channels by the enantiomers of bupivacaine. *Anesthesiology* **93**, 1022-1033.

Nau, C., Wang, S. Y., Wang, G. K. (2003). Point mutations at L1280 in $Na_V1.4$ channel D3-S6 modulate binding affinity and stereoselectivity of bupivacaine enantiomers. *Mol Pharmacol* **63**, 1398-1406.

Noda, M., Shimizu, S., Tanabe, T., Takai, T., Kayano, T., Ikeda, T., Takahashi, H., Nakayama, H., Kanaoka, Y., Minamino, N., et al. (1984). Primary structure of Electrophorus electricus sodium channel deduced from cDNA sequence. *Nature* **312**, 121-127.

Okuse, K., Malik-Hall M., Baker, M.D., Poon, W.Y., Kong, H., Chao, M.V., Wood, J.N. (2002). Annexin II light chain regulates sensory neuron-specific sodium channel expression. *Nature* **417**, 653-6.

O'Reilly, J. P., Wang, S. Y., Wang, G. K. (2000). A point mutation in domain 4-segment 6 of the skeletal muscle sodium channel produces an atypical inactivation state. *Biophys J* **78**, 773-784.

Ong, B. H., Tomaselli, G. F., Balser, J. R. (2000). A structural rearrangement in the sodium channel pore linked to slow inactivation and use dependence. *J Gen Physiol* **116**, 653-662.

Patton, D. E., Isom, L. L., Catterall, W. A., Goldin, A. L. (1994). The adult rat brain beta 1 subunit modifies activation and inactivation gating of multiple sodium channel alpha subunits. *J Biol Chem* **269**, 17649-17655.

Perez-Ceballos, M. A., Vega-Gil, N., Sanchez, M. B., Armijo, J. A. (2006). Use of antiepileptic drugs in bipolar disorder. *Actas Esp Psiquiatr* **34**, 55-64.

Perozo, E., Cortes, D. M., Cuello, L. G. (1999). Structural rearrangements underlying K^+-channel activation gating. *Science* **285**, 73-78.

Poon, W. Y., Malik-Hall, M., Wood, J. N., Okuse, K. (2004). Identification of binding domains in the sodium channel $Na_V1.8$ intracellular N-terminal region and annexin II light chain p11. *FEBS Lett* **558**, 114-118.

Porreca, F., Lai, J., Bian, D., Wegert, S., Ossipov, M. H., Eglen, R. M., Kassotakis, L., Novakovic, S., Rabert, D. K., Sangameswaran, L., Hunter, J. C. (1999). A comparison of the potential role of the tetrodotoxin-insensitive sodium channels, PN3/SNS and NaN/SNS2, in rat models of chronic pain. *Proc Natl Acad Sci U S A* **96**, 7640-7644.

Ptacek, L. J., George, A. L., Jr., Barchi, R. L., Griggs, R. C., Riggs, J. E., Robertson, M., Leppert, M. F. (1992). Mutations in an S4 segment of the adult skeletal muscle sodium channel cause paramyotonia congenita. *Neuron* **8**, 891-897.

Ptacek, L. J., George, A. L., Jr., Griggs, R. C., Tawil, R., Kallen, R. G., Barchi, R. L., Robertson, M., Leppert, M. F. (1991). Identification of a mutation in the gene causing hyperkalemic periodic paralysis. *Cell* **67**, 1021-1027.

Rabert, D. K., Koch, B. D., Ilnicka, M., Obernolte, R. A., Naylor, S. L., Herman, R. C., Eglen, R. M., Hunter, J. C., Sangameswaran, L. (1998). A tetrodotoxin-resistant voltage-gated sodium channel from human dorsal root ganglia, hPN3/SCN10A. *Pain* **78**, 107-114.

Ragsdale, D. S., McPhee, J. C., Scheuer, T., Catterall, W. A. (1994). Molecular determinants of state-dependent block of Na^+ channels by local anesthetics. *Science* **265**, 1724-1728.

Ragsdale, D. S., McPhee, J. C., Scheuer, T., Catterall, W. A. (1996). Common molecular determinants of local anesthetic, antiarrhythmic, and anticonvulsant block of voltage-gated Na^+ channels. *Proc Natl Acad Sci U S A* **93**, 9270-9275.

Renganathan, M., Cummins, T. R., Waxman, S. G. (2001). Contribution of $Na_V1.8$ sodium channels to action potential electrogenesis in DRG neurons. *J Neurophysiol* **86**, 629-640.

Riddall, D. R., Leach, M. J., Garthwaite, J., (2006). A novel drug binding site on voltage-gated sodium channels in rat brain. *Mol Pharmacol* **69**, 278-287.

Rogawski, M. A., Loscher, W. (2004). The neurobiology of antiepileptic drugs for the treatment of nonepileptic conditions. *Nat Med* **10**, 685-692.

Rojas, C. V., Wang, J. Z., Schwartz, L. S., Hoffman, E. P., Powell, B. R., Brown, R. H., Jr. (1991). A Met-to-Val mutation in the skeletal muscle Na^+ channel alpha-subunit in hyperkalaemic periodic paralysis. *Nature* **354**, 387-389.

Roy, M. L., Narahashi, T. (1992). Differential properties of tetrodotoxin-sensitive and tetrodotoxin-resistant sodium channels in rat dorsal root ganglion neurons. *J Neurosci* **12**, 2104-2111.

Saab, C. Y., Cummins, T. R., Waxman, S. G. (2003). GTP gamma S increases $Na_V1.8$ current in small-diameter dorsal root ganglia neurons. *Exp Brain Res* **152**, 415-419.

Sangameswaran, L., Delgado, S. G., Fish, L. M., Koch, B. D., Jakeman, L. B., Stewart, G. R., Sze, P., Hunter, J. C., Eglen, R. M., Herman, R. C. (1996). Structure and function of a novel voltage-gated, tetrodotoxin-resistant sodium channel specific to sensory neurons. *J Biol Chem* **271**, 5953-5956.

Sato, C., Ueno, Y., Asai, K., Takahashi, K., Sato, M., Engel, A., Fujiyoshi, Y. (2001). The voltage-sensitive sodium channel is a bell-shaped molecule with several cavities. *Nature* **409**, 1047-1051.

Scheib, H., McLay, I., Guex, N., Clare, J. J., Blaney, F. E., Dale, T. J., Tate, S. N., Robertson, G. M. (2006). Modeling the pore structure of voltage-gated sodium channels in closed, open, and fast-inactivated conformation reveals details of site 1 toxin and local anesthetic binding. *J Mol Model* **12**, 813-822.

Schild, J. H., Kunze, D. L. (1997). Experimental and modeling study of Na^+ current heterogeneity in rat nodose neurons and its impact on neuronal discharge. *J Neurophysiol* **78**, 3198-3209.

Shanes, A. M., Freygang, W. H., Grundfest, H., Amatniek, E. (1959). Anesthetic and calcium action in the voltage-clamped squid giant axon. *J Gen Physiol* **42**, 793-802.

Sheets, M. F., Hanck, D. A. (2003). Molecular action of lidocaine on the voltage sensors of sodium channels. *J Gen Physiol* **121**, 163-175.

Sheets, M. F., Hanck, D. A. (2007). Outward stabilization of the S4 segments in domains III and IV enhances lidocaine block of sodium channels. *J Physiol* **582**, 317-334.

Sheets, P. L., Jackson, J. O., 2nd, Waxman, S. G., Dib-Hajj, S. D., Cummins, T. R. (2007). A $Na_V1.7$ channel mutation associated with hereditary erythromelalgia contributes to neuronal hyperexcitability and displays reduced lidocaine sensitivity. *J Physiol* **581**, 1019-1031.

Shiraishi, M., Harris, R. A. (2004). Effects of alcohols and anesthetics on recombinant voltage-gated Na+ channels. *J Pharmacol Exp Ther* **309**, 987-994.

Starmer, C. F., Grant, A. O., Strauss, H. C. (1984). Mechanisms of use-dependent block of sodium channels in excitable membranes by local anesthetics. *Biophys J* **46**, 15-27.

Strichartz, G. R. (1973). The inhibition of sodium currents in myelinated nerve by quaternary derivatives of lidocaine. *J Gen Physiol* **62**, 37-57.

Striessnig, J., Glossmann, H., Catterall, W. A. (1990). Identification of a phenylalkylamine binding region within the alpha 1 subunit of skeletal muscle Ca^{2+} channels. *Proc Natl Acad Sci U S A* **87**, 9108-9112.

Stuhmer, W., Conti, F., Suzuki, H., Wang, X. D., Noda, M., Yahagi, N., Kubo, H., Numa, S. (1989). Structural parts involved in activation and inactivation of the sodium channel. *Nature* **339**, 597-603.

Stummann, T. C., Salvati, P., Fariello, R. G., Faravelli, L. (2005). The anti-nociceptive agent ralfinamide inhibits tetrodotoxin-resistant and tetrodotoxin-sensitive Na^+ currents in dorsal root ganglion neurons. *Eur J Pharmacol* **510**, 197-208.

Sunami, A., Dudley, S. C., Jr., Fozzard, H. A. (1997). Sodium channel selectivity filter regulates antiarrhythmic drug binding. *Proc Natl Acad Sci U S A* **94**, 14126-14131.

Tate, S., Benn, S., Hick, C., Trezise, D., John, V., Mannion, R. J., Costigan, M., Plumpton, C., Grose, D., Gladwell, Z., Kendall, G., Dale, K., Bountra, C., Woolf, C. J. (1998). Two sodium

channels contribute to the TTX-R sodium current in primary sensory neurons. *Nat Neurosci* **1**, 653-655.

Taylor, R. E. (1959). Effect of procaine on electrical properties of squid axon membrane. *Am J Physiol* **196**, 1071-1078.

Terlau, H., Stuhmer, W. (1998). Structure and function of voltage-gated ion channels. *Naturwissenschaften* **85**, 437-444.

Tikhonov, D. B., Zhorov, B. S. (2005). Modeling P-loops domain of sodium channel: homology with potassium channels and interaction with ligands. *Biophys J* **88**, 184-197.

Tripathi, P. K., Trujillo, L., Cardenas, C. A., Cardenas, C. G., de Armendi, A. J., Scroggs, R. S. (2006). Analysis of the variation in use-dependent inactivation of high-threshold tetrodotoxin-resistant sodium currents recorded from rat sensory neurons. *Neuroscience* **143**, 923-938.

Tsang, S. Y., Tsushima, R. G., Tomaselli, G. F., Li, R. A., Backx, P. H. (2005). A multifunctional aromatic residue in the external pore vestibule of Na^+ channels contributes to the local anesthetic receptor. *Mol Pharmacol* **67**, 424-434.

Ulbricht, W. (2005). Sodium channel inactivation: molecular determinants and modulation. *Physiol Rev* **85**, 1271-1301.

Vassilev, P. M., Scheuer, T., Catterall, W. A. (1988). Identification of an intracellular peptide segment involved in sodium channel inactivation. *Science* **241**, 1658-1661.

Vijayaragavan, K., Boutjdir, M., Chahine, M. (2004a). Modulation of $Na_V1.7$ and $Na_V1.8$ peripheral nerve sodium channels by protein kinase A and protein kinase C. *J Neurophysiol* **91**, 1556-1569.

Vijayaragavan, K., Powell, A. J., Kinghorn, I. J., Chahine, M. (2004b). Role of auxiliary beta1-, beta2-, and beta3-subunits and their interaction with $Na_V1.8$ voltage-gated sodium channel. *Biochem Biophys Res Commun* **319**, 531-540.

Vora, T., Corry, B., Chung, S. H. (2005). A model of sodium channels. *Biochim Biophys Acta* **1668**, 106-116.

Wang G. K., Brodwick M. S., Eaton D. C., Strichartz G. R. (1987). Inhibition of sodium currents by local anesthetics in chloramine-T-treated squid axons. The role of channel activation. *J Gen Physiol* **89**, 645-67.

Wang, G. K., Quan, C., Wang, S. (1998a). A common local anesthetic receptor for benzocaine and etidocaine in voltage-gated mu1 Na^+ channels. *Pflugers Arch* **435**, 293-302.

Wang, G. K., Quan, C., Wang, S. Y. (1998b). Local anesthetic block of batrachotoxin-resistant muscle Na^+ channels. *Mol Pharmacol* **54**, 389-396.

Wang, G. K., Russell, C., Wang, S. Y. (2003). State-dependent block of wild-type and inactivation-deficient Na^+ channels by flecainide. *J Gen Physiol* **122**, 365-374.

Wang, G. K., Russell, C., Wang, S. Y. (2004). Mexiletine block of wild-type and inactivation-deficient human skeletal muscle $hNa_V1.4$ Na^+ channels. *J Physiol* **554**, 621-633.

Wang, Q., Shen, J., Splawski, I., Atkinson, D., Li, Z., Robinson, J. L., Moss, A. J., Towbin, J. A., Keating, M. T. (1995). SCN5A mutations associated with an inherited cardiac arrhythmia, long QT syndrome. *Cell* **80**, 805-811.

Wang, S. Y., Barile, M., Wang, G. K. (2001). Disparate role of Na^+ channel D2-S6 residues in batrachotoxin and local anesthetic action. *Mol Pharmacol* **59**, 1100-1107.

Wang, S. Y., Nau, C., Wang, G. K. (2000). Residues in Na^+ channel D3-S6 segment modulate both batrachotoxin and local anesthetic affinities. *Biophys J* **79**, 1379-1387.

Wang, S. Y., Russell, C., Wang, G. K. (2005). Tryptophan substitution of a putative D4S6 gating hinge alters slow inactivation in cardiac sodium channels. *Biophys J* **88**, 3991-3999.

Wang, S. Y., Tikhonov, D. B., Zhorov, B. S., Mitchell, J., Wang, G. K. (2007). Serine-401 as a batrachotoxin- and local anesthetic-sensing residue in the human cardiac Na^+ channel. *Pflugers Arch* **454**, 277-287.

Wang, S. Y., Wang, G. K. (1997). A mutation in segment I-S6 alters slow inactivation of sodium channels. *Biophys J* **72**, 1633-1640.

Weiser, T. (2006). Comparison of the effects of four Na^+ channel analgesics on TTX-resistant Na^+ currents in rat sensory neurons and recombinant $Na_V1.2$ channels. *Neurosci Lett* **395**, 179-184.

Weiser, T., Qu, Y., Catterall, W. A., Scheuer, T. (1999). Differential interaction of R-mexiletine with the local anesthetic receptor site on brain and heart sodium channel alpha-subunits. *Mol Pharmacol* **56**, 1238-1244.

West, J. W., Numann, R., Murphy, B. J., Scheuer, T., Catterall, W. A. (1991). A phosphorylation site in the Na^+ channel required for modulation by protein kinase C. *Science* **254**, 866-868.

West, J. W., Patton, D. E., Scheuer, T., Wang, Y., Goldin, A. L., Catterall, W. A. (1992). A cluster of hydrophobic amino acid residues required for fast Na^+-channel inactivation. *Proc Natl Acad Sci U S A* **89**, 10910-10914.

Wollner, D. A., Messner, D. J., Catterall, W. A. (1987). Beta 2 subunits of sodium channels from vertebrate brain. Studies with subunit-specific antibodies. *J Biol Chem* **262**, 14709-14715.

Wood, J. N., Bevan, S. J., Coote, P. R., Dunn, P. M., Harmar, A., Hogan, P., Latchman, D. S., Morrison, C., Rougon, G., Theveniau, M., et al. (1990). Novel cell lines display properties of nociceptive sensory neurons. *Proc Biol Sci* **241**, 187-194.

Wright, S. N., Wang, S. Y., Wang, G. K. (1998). Lysine point mutations in Na^+ channel D4-S6 reduce inactivated channel block by local anesthetics. *Mol Pharmacol* **54**, 733-739.

Yang, N., George, A. L., Jr., Horn, R. (1996). Molecular basis of charge movement in voltage-gated sodium channels. *Neuron* **16**, 113-122.

Yarov-Yarovoy, V., Brown, J., Sharp, E. M., Clare, J. J., Scheuer, T., Catterall, W. A. (2001). Molecular determinants of voltage-dependent gating and binding of pore-blocking drugs in transmembrane segment IIIS6 of the Na^+ channel alpha subunit. *J Biol Chem* **276**, 20-27.

Yarov-Yarovoy, V., McPhee, J. C., Idsvoog, D., Pate, C., Scheuer, T., Catterall, W. A. (2002). Role of amino acid residues in transmembrane segments IS6 and IIS6 of the Na^+ channel alpha subunit in voltage-dependent gating and drug block. *J Biol Chem* **277**, 35393-35401.

Yellen, G. (1998). The moving parts of voltage-gated ion channels. *Q Rev Biophys* **31**, 239-295.

Yu, F. H., Catterall, W. A. (2003). Overview of the voltage-gated sodium channel family. Genome Biol. **4,** 207

Yu, F. H., Westenbroek, R. E., Silos-Santiago, I., McCormick, K. A., Lawson, D., Ge, P., Ferriera, H., Lilly, J., DiStefano, P. S., Catterall, W. A., Scheuer, T., Curtis, R. (2003). Sodium channel beta4, a new disulfide-linked auxiliary subunit with similarity to beta2. *J Neurosci* **23**, 7577-7585.

Zhang, H., Kolibal, S., Vanderkooi, J. M., Cohen, S. A., Kallen, R. G. (2000). A carboxy-terminal alpha-helical segment in the rat skeletal muscle voltage-dependent Na^+ channel is responsible for its interaction with the amino-terminus. *Biochim Biophys Acta* **1467**, 406-418.

Zhao, Y., Yarov-Yarovoy, V., Scheuer, T., Catterall, W. A. (2004). A gating hinge in Na^+ channels; a molecular switch for electrical signaling. *Neuron* **41**, 859-865.

Zimmermann, K., Leffler, A., Babes, A., Cendan, C. M., Carr, R. W., Kobayashi, J., Nau, C., Wood, J. N., Reeh, P. W. (2007). Sensory neuron sodium channel $Na_V1.8$ is essential for pain at low temperatures. *Nature* **447**, 855-858.